Dynamic Assessment and Optimization of Catalytic Hydroprocessing Process: Sensitivity Analysis and Practical Tips

By

©Abbas Azarpour Hassankiadeh

A thesis submitted to the school of Graduate Studies in partial fulfillment of the requirements for the degree of

Doctor of Philosophy

Faculty of Engineering and Applied Science

Memorial University of Newfoundland

May 2021

St. John's, Newfoundland

Canada

Abstract

Among the processes in petrochemical industry, hydroprocessing is an imperative process to produce clean fuels. This process is still being improved despite its 70-year maturity. Catalyst deactivation is a key aspect in the design and operation of catalytic processes in petrochemical industry. In this research, a dynamic heterogeneous model is presented to evaluate the performance of an industrial hydropurification/hydrotreating process in the purified terephthalic acid (PTA) production plant. This process includes a trickle-bed reactor (TBR) packed with palladium supported on carbon (0.5wt.% Pd/C) catalyst. In fact, this chemical production unit represents a three-phase catalytic system where some chemical reactions take place. Therefore, an accurate and meticulous analysis is required to develop a proper mathematical model, taking into account all transport phenomena occurring in the system. The model considers the axial back-mixing, flow non-ideality, and the catalyst deactivation. Model development leads to a set of partial differential equations consisting of nonlinear equations of the reaction rates, nonlinear expression of the catalyst deactivation rate, mass balance of each component in the reaction mixture, and energy balance of each phase. The model parameters are calculated using suitable correlations. The set of partial differential equations is solved using proper numerical techniques, including method of lines and finite difference method, in MATLAB software environment. First, the model reliability is assessed through the comparison of the model results with the industrial data. The validation phase confirms that the model results are accurate, and the developed model can be used for further process evaluation. A sensitivity analysis is then implemented to assess the effects of different operating parameters on the performance of the hydropurification/hydrotreating process. The results reveal that axial dispersion model is more accurate than the plug flow model. Moreover, 4-carboxybenzaldehyde (4-CBA) impurity in the reactor feed is the most detrimental parameter, affecting the catalytic performance. It is found that reduction in the catalyst particle size can improve the catalyst performance by about 16%, and an increase in the catalyst particle porosity can enhance the catalyst lifetime by around 8%. In this condition, the catalyst bed pressure drop is maintained at an acceptable level. In addition, 13% increase in the hydrogen partial pressure enhances the catalyst lifetime by about 20%. It should be noted that pressure increase might lead to the reactor pressure fluctuation, leading to an increase in the PTA powder turbidity. Therefore, reactor operation control is a critical factor. Considering other hydrodynamic parameters, a decrease in liquid hourly space velocity and the catalyst bed porosity improves the system performance in terms of catalyst lifetime and product quality. An increase in the liquid-solid mass transfer and contacting efficiency has a slight positive impact on the catalytic system performance. Product quality control can be carried out more properly if the feed impurity concentration is managed/controlled efficiently. In this research, a practical strategy is presented to effectively mix the feed streams having varying concentrations of the impurities (e.g., high and low concentrations of 4-CBA). This can be achieved by suggesting a proper ratio control, keeping the feed composition and flowrate at normal operating conditions. This strategy can also be employed to deal with the off-spec PTA powder product. In addition, the effect of temperature on the sintering mechanism of the Pd/C catalyst deactivation is investigated. The results reveal that temperature increase can accelerate the decline rate of the Pd/C catalyst surface area. The reduced activity of Pd/C catalyst is in an acceptable agreement with the normalized ratio of reduction in the surface area of pure Pd with increasing temperature. In the last phase, an efficient methodology is proposed to assess the hydroprocessing process in terms of energy and exergy performance. The process simulation and exergy analysis are conducted using Aspen Plus® and MATLAB software packages. The results are in a satisfactory agreement with the industrial data. It is concluded that the optimal operating conditions result in 15% reduction in the exergy destruction; the optimal scenario can also reduce the operation costs and the carbon tax at 9.96% ($20.5/h) and 14.75% ($14.54/h), respectively.

Acknowledgements

I would like to acknowledge those who supported me to successfully complete this research. Firstly, I declare my genuine appreciation to Dr. Sohrab Zendehboudi as my supervisor for his exceptional guidance through all endeavors of this research accomplishment. He is insightful, supportive, and encouraging. Also, I would like to thank Dr. Kelly Hawboldt and Dr. Yahui Zhang as my committee members for their invaluable inputs on my PhD proposal and thesis. Furthermore, I am grateful to Dr. Nima Rezaei for offering great comments on the different phases of this research. Moreover, I thank Dr. Mohamad Mohamadi-Baghmolaei and Abdollah Hajizadeh to help me carry out the last phase of this research. Finally, I highly appreciate the financial support of Memorial University (Canada) and the Natural Sciences and Engineering Research Council of Canada (NSERC).

Table of Contents

List of Tables

List of Figures

1 CHAPTER ONE: Introduction and Overview

1.1 Motivation

There are many chemical and petrochemical plants that produce numerous products. These plants face many challenges, including operational problems and the negative impacts of their processes on the environment. Hydroprocessing processes are extensively used in the industrial plants, producing several important chemicals. One of the highly consumed chemicals is purified terephthalic acid (PTA). This chemical is used as a raw material for the production of several polymer products (e.g., bottle and textile grades) [1, 2]. In the process of PTA production, its final quality has a key role in the sale of the product and in the polymerization process. PTA production is carried out in two different process units. In the first unit, para-xylene is oxidized in a CSTR using air in the mixture of catalyst (usually Mn, Co, and Br) and acetic acid as the solvent. The final product of this unit is a lightly yellowish powder containing some impurities, which is not suitable to be processed in a polymer plant. This powder is called crude terephthalic acid (CTA). In the second unit, CTA is purified in the hydropurification process [2, 3]. This unit includes pumps, heat exchangers, a trickle-bed reactor (TBR), crystallizers, centrifuges, a rotary vacuum filter, a dryer, and other process equipment (e.g., compressor, blower, and scrubber) [4].

Hydropurification process encounters some problems such as product quality fluctuation, operational concerns (e.g., power failure and emergency shutdown), high costs of operation, and environmental issues. Low product quality can lead to the reduction of the selling price and low quality of the produced polymer, resulting in the human's health and environment problems since it is sometimes dumped in the environment. To name the operational problems, the hydropurification unit encounters the transfer lines blockage, equipment low function, fast deactivation of the catalyst, high consumption of chemicals (e.g., caustic soda), excessive utilization of demineralized water, and unsafe high pressure and temperature conditions in the reactor and furnace. High operational cost is another issue in this process. This chemical plant uses a very expensive catalyst, a costly oil (as the heat transfer medium), hydrogen, high pressure steam, and other utilities (e.g., nitrogen). This process uses a hot oil system for preheating the reactor feed mixture [4]. In the hot oil system, there is a risk of oil leakage, which is discharged into the environment. Other problems are the powder leakage and the drain of slurry into ditches under abnormal operating conditions. Therefore, a high acidic and sometimes oily water are transferred to the waste water treatment plant (WWTP). The CO_2 emissions also cause environmental concerns.

The above problems/concerns can be addressed by advanced theoretical assessment and properly planned practical approaches. The process performance can be analyzed by the development of a reliable and accurate mathematical model, which involves the vital operating parameters and the transport phenomena taking place in the process. The process modeling can give the detailed knowledge, and provide a suitable platform for the determination of the optimal operating conditions. The process improvement can reduce the chemical usage, lengthen the catalyst lifetime, decrease the energy consumption, increase the operation safety, and mitigate the negative environmental impacts. The process optimization can be accomplished through employing an effective strategy, which comprises the most suitable mathematical model, an appropriate optimization technique, and a systematic approach for the results analysis. An extensive knowledge on the mathematical modeling, simulation, and optimization, importance of hydroprocessing process in petrochemical industry, various theoretical and practical challenges in the process, and a practical experience in the environment of chemical plants provide a high motivation to carry out this research work on the industrial process.

1.2 Problem Statement

The operating problems of the PTA hydropurification process are addressed in this research. The followings are some of the process difficulties:

- Product quality: One of the concerns of the hydropurification process is to maintain the product quality at an acceptable level, and continue the on-spec product production. There are some criteria that need to be met for considering the PTA powder produced as the on-spec product. For instance, the concentration of 4-carboxybenzaldehyde (4-CBA) should be less than 25 ppm [5]. High concentration of 4-CBA decreases the polymer molecular weight, hinders the polymer chain [6], and strengthens the yellowish appearance of the powder [7]. Other criterion is the appearance of the powder. Its turbidity needs to be controlled (Δy), and its yellowish appearance should be less than a certain value (b-value). The transparency of the powder is another quality specification, since it considerably impacts the appearance of the polymer product (e.g., plastic bottle). Volatility and acidity of the PTA powder are other vital specifications, which are influenced by the organic contents in the powder and the chemicals used in the production process, especially in the production of CTA. The moisture (as a quality criterion) is affected by the process of filtration and drying. High moisture can cause a tremendous operational problem in the powder conveying system. The content of the metals (e.g., Mn and Co) should be analyzed in the industrial laboratory to determine the quality of the powder. High concentration of the metals reveals the improper control of the CTA production process and high risk of corrosion in the involved equipment. The crystal size distribution (CSD) is another product quality criterion, which determines the degree of solubility of the powder in the polymerization reaction [4]. This characteristic can be influenced by the crystallization pressure, crystallizers' level, and the production rate (production rate fluctuation).

- Operational difficulties: The operation of PTA hydropurification process is a relatively challenging task due to the presence of the slurry phase. This process is operated under high pressure and temperature conditions; therefore, it requires a reliable and accurate control system. The slurry phase might cause particles settlement in the heat exchangers, blockage of crystallizers' transfer lines, possible crystallization of terephthalic acid (TA) in the catalytic reaction bed, and inefficient separation of TA cake in the rotary vacuum filter. Another issue is the degradation of the expensive oil (e.g., Therminol® 66) used in the furnace. This oil is utilized as the heat transfer medium in the reactor feed preheaters. The oil degradation can be worsened due to the improper control of operating parameters, such as composition and flow rate of the reactor feed.

- Catalyst deactivation: The hydropurification process uses the expensive Pd catalysts (palladium supported on carbon; Pd/C) packed in a TBR. This catalyst encounters the adverse phenomenon of deactivation over the process [1, 2]. The change of the catalytic activity generally influences the final product quality. Therefore, its lifetime plays a critical role in the process efficiency and the operational costs. The catalyst deactivation can be accelerated due to the improper control of key operating parameters (e.g., composition, flow rate, and pressure of reactor feed, and concentration of impurities). Determination of the catalyst deactivation rate is a challenging task that needs systematic experimental and modeling research investigations. It should be noted that each catalyst experiences specific deactivation mechanisms, which adds further complexities to planned research work.
- Operating cost: one of the serious issues in the hydropurification process is high operational costs. An inaccurate and inefficient control of the operation can result in the fast deactivation of the catalyst, high degradation rate of the hot oil, massive consumption of the chemicals (e.g., caustic soda, demineralized water, hydrogen, and nitrogen), and high-pressure steam. Moreover, the process is energy-intensive since it is operated under high temperature and pressure conditions.
- Environmental concerns: The hydropurification process could result in several pollutant materials. The PTA powder leakage from the dryer and the powder conveying system, oil leakage from the hot oil system, CO_2 emissions (e.g., furnace), highly acidic wastewater, and oil leakage

from the centrifuges and other equipment are the examples that require careful process control and detailed operation procedures to avoid the pollution and negative environmental impacts.

In order to adequately address the mentioned concerns, the process analysis should be systematically conducted, considering the most critical operating parameters. The process is strongly affected by the reactor feed characteristics (e.g., temperature, pressure, flow rate, composition, and impurity concentration), and the hydrogen partial pressure. In addition, the hydrodynamic parameters, such as phase holdup, wetting efficiency, flow regime, catalyst particle size, catalyst particle porosity, reactor bed porosity, and mass transfer coefficients are important, affecting the process performance. The developed model should thus include all key factors and involved transport phenomena so that the modeling and simulation phase can determine the optimal operating conditions of the process. Moreover, the product quality can be efficiently controlled by proposing an advanced strategy to minimize the negative impacts of the feed impurities. Also, an energy-exergy model can be employed to obtain the energy consumption and exergy destruction of the process; optimization/minimization of these key parameters can appreciably increase the system efficiency. Therefore, development of sophisticated models can propose proper operational approaches towards reduction of operating expenses and CO_2 emissions.

This research develops a dynamic heterogeneous three-phase model including the multiple reactions and the deactivation mechanism to more accurately represent the complicated catalytic reaction systems. The deactivation model is examined under the various changes in the operating parameters to validate the deactivation rate, which is one of the most significant parameter in the developed model. The model is validated with the real industrial data for practical implementation. Moreover, the model investigates the effects of the catalyst specifications (e.g., particle size and porosity) and vital operating parameters (e.g., liquid hourly space velocity) on a hydroprocessing unit considering the dynamic nature of the process. In addition, this study proposes a strategy to utilize the feedstock having different concentrations of impurities without any detrimental impact on the process efficient performance. Furthermore, this investigation develops a thermodynamic model for the energy and exergy analysis of the process, which is usually operated under high temperature and pressure conditions, to decrease the costly energy utilization. More importantly, the research suggests practical solutions to the hydroprocessing units to improve their operations in terms of product quality (e.g., longer production time), catalyst lifetime (higher lifetime of the expensive catalysts), operation cost (e.g., deceleration of the oil degradation), and environmental impact (e.g., CO_2 emission).

1.3 Thesis Structure

The structure of the thesis is described as follows:

Chapter 1 includes the motivation of the study, process challenges, and the thesis structure.

Chapter 2 was submitted to the Journal of Industrial and Engineering Chemistry (Elsevier Publication). It presents a detailed review on the hydroprocessing process that includes three-phase trickle-bed reactors. It discusses the advancements and challenges in the hydroprocessing systems, and suggests the practical solutions and theoretical guidelines for improving the process performance.

Chapter 3 was published in the Journal of Industrial and Engineering Chemistry Research (ACS Publication). This chapter includes the development of a dispersion model for the catalytic hydropurification system, and sensitivity analysis to explore the effects of catalyst particle size and porosity on the system performance. It also investigates the influences of the hydrogen partial pressure and system temperature on the product quality and the catalyst lifetime.

Chapter 4 was published in the Journal of Industrial and Engineering Chemistry research (ACS Publication). This chapter focuses on the impacts of hydrodynamic parameters on the industrial hydropurification process performance. It also discusses about the effects of liquid hourly space velocity, catalyst bed porosity, and mass transfer coefficients on the product quality and catalyst lifetime.

Chapter 5 was published in the Journal of Industrial and Engineering Chemistry (Elsevier Publication). This research phase introduces a systematic strategy to effectively use the feed streams with low and high concentration of impurities without affecting the final product quality and catalyst lifetime. It also investigates the impact of temperature on the Pd distribution in the Pd/C catalyst and the sintering mechanism of deactivation.

Chapter 6 was prepared for submission to Energy Journal (Elsevier Publication). The main objectives of this chapter are to develop a proper energy-exergy model for the hydropurification process, and consequently present the optimal operating conditions toward achieving lower energy consumption, less operational expenses, and smaller amount of CO_2 emissions based on energy and exergy analysis. This research phase also identifies the units/equipment with the minimum and maximum exergy destruction.

Chapter 7 contains a summary of the thesis, conclusions, and recommendations for further research investigations on the targeted process.

2 CHAPTER TWO: Performance Analysis and Modeling of Catalytic Trickle-Bed Reactors: A Comprehensive Review

Preface

A version of this chapter was accepted to the Journal of Industrial and Engineering Chemistry. I am the primary author of this manuscript. I did most of the literature review, data collection, and the critical analysis of the research papers and reports published on the subject so far. I prepared the first draft of the manuscript, and then revised the manuscript based on the co-authors' comments as well as reviewers' feedback. Nima Rezaei as the second author helped in reviewing the manuscript. Sohrab Zendehboudi contributed by giving the manuscript's outlines, comments on the different sections of the manuscript, and technical critiques on the previous relevant works. Sohrab Zendehboudi also assisted in reviewing/revising the manuscript.

Abstract

Trickle-bed reactors (TBRs) are extensively used in industry. There have been great progresses in the design and control of TBRs. However, there are rooms for the improvement in the performance/operation of TBRs. These improvements can lead to more efficient process control and further reduction of the operation costs. In terms of process efficiency, the product quality can be improved since a large number of the TBRs is used in purification processes. In terms of operation costs, the process improvement can result in longer utilization of the catalysts used because the catalytic TBRs' operations usually suffer from the deactivation phenomenon for expensive catalysts. Hydrodynamic parameters play a significant role in the control and operation of TBRs. We provide comprehensive information on TBRs application and hydrodynamic characteristics. Moreover, a systematic methodology is proposed to develop a TBR mathematical model. A detailed review on the TBRs studies is presented, and technical issues in their design and operation are discussed. In addition, current challenges in TBRs modeling are summarized, and the chances for further research are suggested. This review provides an exhaustive knowledge and links to references that can be employed to more efficaciously model targeted TBR processes, leading to better understanding of the process behaviours, and more efficient operation of the relevant industry.

2.1 Introduction

Catalytic gas-liquid-solid reactions are extensively used in industrial applications [8]. Multiphase reactors are generally utilized for a broad class of catalytic reactions encompassing hydrogenation, oxidation, alkylation, and halogenation [9]. Numerous factors contribute to the selection of multiphase reactors, such as various physical properties of the phases, presence of multi-phases, reactants stoichiometry, adiabatic/isothermal modes of operation, intrinsic reaction rate, downstream separation process, residence time, and the reactor heat and mass transfer specifications [10]. Three-phase catalytic reactors are chosen when a high ratio of catalyst-to-liquid volume is required, the reactions rate is not very high, and the catalyst deactivation is negligible or very slow [11]. Three-phase fixed-bed catalytic reactors operation configuration is chosen based on the mass-transfer limiting steps. Liquid phase is distributed by trickle operation (a continuous gas and a distributed liquid phase) over the catalyst bed, and gas phase is distributed under a bubble operation condition corresponding to a distributed gas and a continuous liquid phase [11]. The flow direction of gas and liquid is determined based on some criteria, such as pressure drop, equilibrium limitations, flowrate constraints for flooding, required conversion, heat recovery, and limiting reactant; upflow operation is followed when the limiting reactant is in the liquid phase and downflow operation is used when the limiting reactant is in the gas phase [11].

Trickle-bed reactors (TBRs) are the most common utilized reactors among the three-phase reaction systems in industry. They are used in chemical, petrochemical, petroleum, waste treatment, electrochemical, and biochemical processes [12]. The products processed using TBRs is globally estimated at 1.6 billion t/y, and their value is around $300 billion/y [13]. In a TBR, gas and liquid flow downward concurrently containing both reactants and products through randomly packed bed of catalyst particles [14]. In a TBR, the liquid trickles down the catalyst particles as films or rivulets, while the gas is distributed as a continuous phase downward or upward based on its most efficient configuration [13, 14]. The upward concurrent flows of gas and liquid through the catalyst bed are configured in a flooded-bed reactor, which is scarcely employed in industrial applications compared to the TBRs [12]. Since the plug flow mechanism is established in TBRs due to the fixed catalyst bed, their utilization is more preferred than fluidized or slurry reactors [12]. However, being unsuitable for the processes with fast catalyst deactivation (e.g., heavy oil hydrotreating) and the chance of poor liquid distribution, which might lead to the formation of hotspots and reactor runaway, are the pitfalls of TBRs utilization [12]. Industrial TBRs are usually operated at high pressures and temperatures under adiabatic operation mode [12]. Most TBRs are run under the operating pressure range of 20–30 bar. The use of high pressure improves the gaseous reactant solubility, facilitates the mass and heat transfer, and slows down the adverse phenomenon of catalyst deactivation [15, 16]. The interrelationship of reaction kinetics and mass transfer makes the analysis of TBRs performance complicated [12]. Unrealistic mathematical expressions and lack of proper experimental data, which are used to formulate the correlations, are the most important concerns of appropriate design of TBRs [17].

Hydrodynamic parameters play a critical role in the operation of TBRs. For instance, liquid holdup, gas holdup, liquid distribution, catalyst particle size, particle porosity, and bed porosity are the parameters that have significant impact on the TBRs performance. In this review paper, the works accomplished on the TBRs with focus on the effects of hydrodynamic parameters are discussed thoroughly. We discuss mainly about the modeling investigations that are available in the literature. Understanding the complex hydrodynamic behavior of the TBRs is required to systematically analyze the process for the determination of optimal operating conditions.

2.2 TBRs Structure and Applications

Hydrodynamics of TBRs is governed by the complicated internal structure of the catalyst bed and the interactions between available phases, flowing in the reactor. The bed structure could affect the transition of the trickling flow regime to other types of flow regimes. Packing characteristics and interactions of the catalyst particles properties can appreciably influence the TBRs hydrodynamics. Bed structure also impacts the pressure drop, residence time distribution (RTD), liquid holdup, and heat and mass transfer rates.

2.2.1 TBRs Structure

In TBRs, catalyst loading is higher than that in other multiphase reactors. Also in the TBRs, the catalyst particles are usually porous, having various shapes, such as spherical, extrudates, cylindrical, trilobe, and multilobe [13]. As most reactions taking place in TBRs are exothermic, handling the liberated energy is a critical task that requires optimal process design. Catalyst bed specifications (e.g., particle size and porosity), flow distribution, catalyst wetting characteristic, interphase and interparticle heat and mass transfer, bed to wall heat transfer, reaction kinetics are among the most critical issues affecting the performance of TBRs. The specifications and configuration of the catalyst bed considerably impact the fluid dynamics, and consequently influencing catalyst wetting, local heat and mass transfer rates, and gas and liquid mixing in TBRs. The advancement of experimental, analytical, and computational techniques have provided the opportunity to better understand the TBRs operation and their complexities. For instance, magnetic resonance imaging and computed tomography can present detailed information on gas-liquid distribution and catalyst bed porosity under real operating conditions of a TBR. Moreover, gas and liquid flows and their distributions can be simulated due to the advances in numerical techniques and computational software, reducing the experimental costs [13].

The configurations of TBRs can be categorized as follows [13]:

a) Conventional TBRs (Figure 2-1): The porous catalyst particles are packed randomly. The catalyst is supported on inert material to provide mechanical strength for the catalyst bed. For highly exothermic reactions, the particle outer layer is impregnated with an active catalytic material (on an inert support) to prevent high temperature shocks inside the particle. The particles are usually loaded on a wire mesh sieve plate. Gas and liquid phases are introduced to the TBRs using flow distributors such as nozzles with various openings design. Sieve plate distributor and bubble cap distributor can also be employed at the top of TBR to establish uniform flow distribution. Redistribution of the reactant phases might be required in large TBRs to avoid the formation of hotspots. The bed temperature control as one of the main issues in TBRs can be handled by internal cooling coils or external jackets as intermediate quenching.

b) Semi-structured TBRs (Figure 2-2 (a)): The porous catalyst particles are packed non-randomly. Non-random load of catalysts is considered when a significant amount of catalysts is not required, or when the catalyst mechanical strength is not high. Lower pressure drop is expected for the structured packing, compared to a random one. Coated structured packings and monolith channels are the examples of structured packings. Redistribution and intermediate quenching can be applied when using the structured packing reactors. Liquid maldistribution is minimum for monolith reactors including a single monolith even though the distribution of liquid at the entrance is troublesome. Other than liquid distribution, there are some concerns related to the monolith reactors partial channel surface wetting and the chance for evaporation (and potentially dry out) from solid surface because of the heat released by the chemical reaction.

c) Micro-TBRs (Figure 2-2 (b)): The porous catalyst particles are packed in micro-channels. Their function is similar to TBRs; however, their size is much smaller than the conventional TBRs.

They contain several small channels where the catalyst is loaded as very small particles; alternatively, the catalyst is impregnated over the channel wall. In these reactors, heat removing fins might be considered for the bed cooling. Higher rates of mass and heat transfer can be obtained with these reactors because of their very pact/small in size, large surface area-to-volume, and more precise control of flow distribution. Thus, for very fast and exothermic reactions encountering considerable mass transfer limitations, this type of reactors is a good choice. Even though temperature can be controlled properly, operational problems, such as cleaning and clogging, and initial capital cost are their drawbacks compared to conventional TBRs.

Regarding the TRBs temperature control as a significant issue, it should be noted that internal coils or external jackets could be utilized only in small-scale laboratory reactors. Since they have a considerable impact on the flow field, the measured data are not suitable for reactor scale-up. In a practical approach, the temperature control is more likely accomplished by splitting TBR reactor into two or more sections/beds with intermediate heat exchangers followed by a flow redistribution unit before each additional section of the segmented TBR reactor.

Microstructured reactors might be usually preferred to conventional reactors in some scenarios, such as strong limitations in heat or mass transfer, production of considerable waste by multiple reactions, low yield, improper control of reaction variables, high dilutions with solvent or inert for safety purpose, and not meeting the market required quality [10].

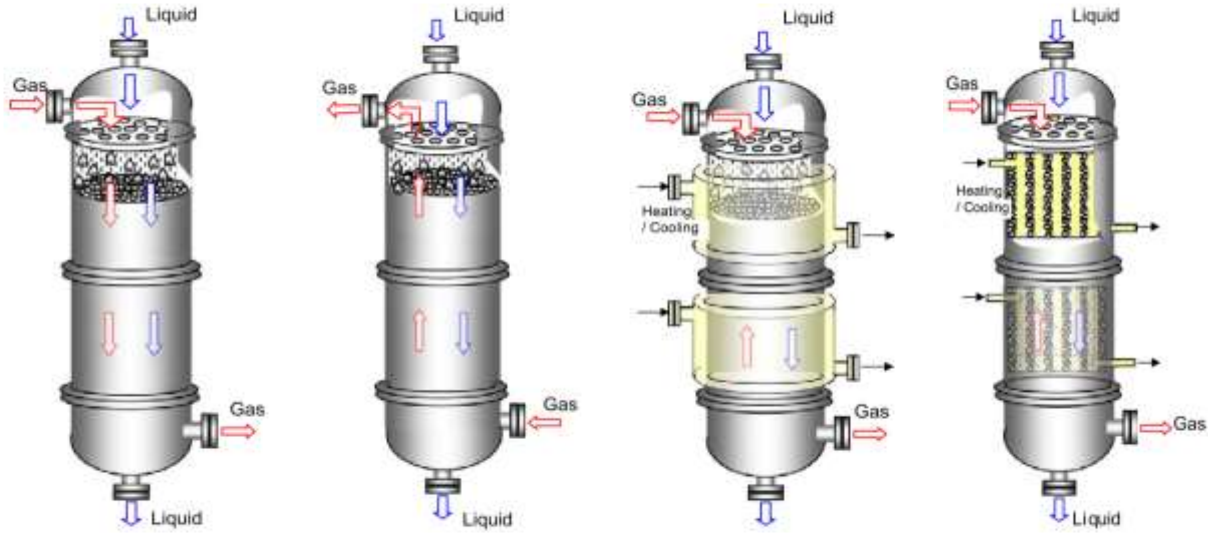

(a) (b) (c) (d)

Figure 2-1: Different configurations of TBRs considering the mode of operation: (a) Concurrent TBR; (b) Countercurrent TBR; (c) Jacketed TBR; and (d) Internally cooled TBR [13].

(a) (b)

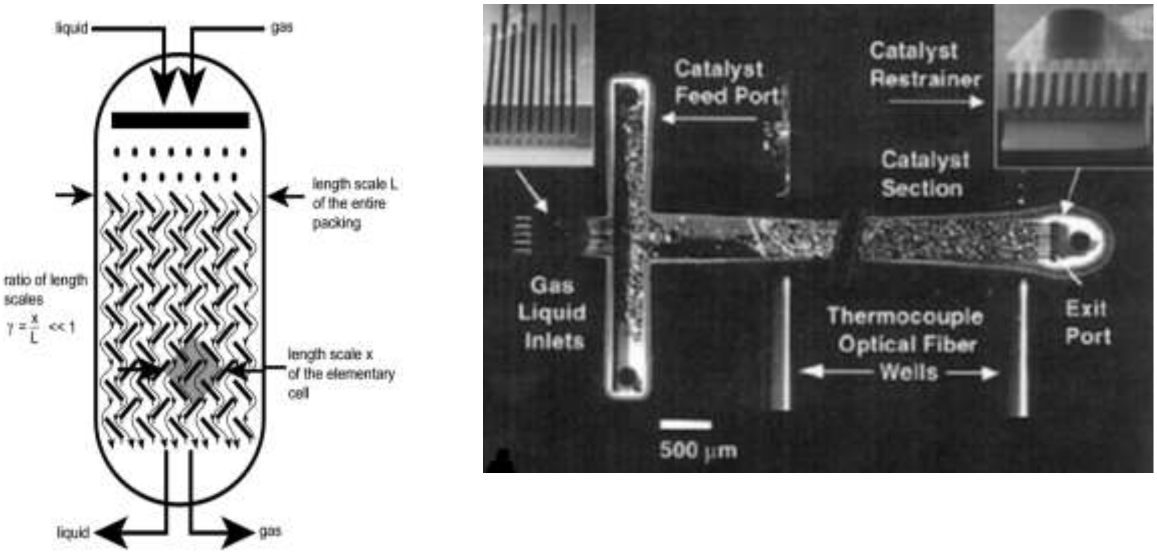

Figure 2-2: Schematics of different TBRs: (a) structured [18], and (b) micro-reactor [19].

2.2.2 TBRs Applications

A TBR might be 10-30 m high, assembled with one or a number of fixed-bed sections of catalyst particles [20]. Due to the lower severe limitations in throughput, the cocurrent operation mode is preferred to countercurrent and cocurrent upflow modes [11]. Moreover, downward operation is preferred for gas-limited reactions and partial wetting conditions since it promotes the gas reactant transport to the catalyst surface [20]. When there is vaporization of reactants in the reaction mixture, TBR might be suitable in terms of energy costs saving [11]. A TBR can also be employed for the absorption of gas into the reacting liquid when there is either very high or very low ratio of liquid-to-gas flowrates. However, low liquid flowrate creates the catalyst partial wetting, leading to the conversion reduction for the limiting reactant [11]. Table 2-1 includes some of the applications of TBRs based on the literature [13].

Table 2-1: Some of TBRs applications [13].

Reaction type	**Reactant**	**Catalyst**	**P (MPa)**	**T (K)**
Oxidation	ethanol	Pd/Al	2	343–373
	phenol	Pt/Al_2O_3	3–10	373–473
	formic acid, phenol, and organic material (in wastewater)	Co/SiO_2-AlO_2, CuO	0.1–1.5	300–403
Petroleum processing	reservoir fluids, and its fractions	Mo-Ni	20–80	593–653
Hydrogenation	petroleum fractions, nitro compounds, carbonyls, and carboxylic acids (→alcohols)	Pd, Pt, Ni, Cu	3–10	323–423
	acetylene (in the presence of butadiene)	Au/Al, Pd/Al_2O_3	0.1–2.5	313–523
	crotonaldehyde and α-methylstyrene (→cumene)	Pd/Al_2O_3	0.1–5	373–773
	2-butyne-1,4-diol	Ni	10–30	350–450
	caprolactone and adipic acid	Cu	15–25	450–550
	aniline (→cyclohexyaniline)	Pd/Al_2O_3	3–20	298–313
	glucose (→sorbitol)	Ru/C	8	373–393
	maleic anhydride acid esters (→alcohols)	Raney Ni, Pt/C	1–5	200–400
	coal liquefaction extracts	Ni-Mo/Al_2O_3	7	593–623
Esterification	acetone and butanol	ion exchange resin (acidic)		
	acetone and butanol (FT synthesis)	Co/TiO_2	10–50	450–650

The major advantages and disadvantages of the conventional TBRs are listed in Table 2-2, revealing the wide applications of the TBRs due to their high productivity and selectivity [11].

Table 2-2: Advantages and disadvantages of cocurrent downflow TBR [11, 20].

Attributes	**Advantages**	**Disadvantages**
Catalyst	• low catalyst loss	• low catalyst effectiveness • slow catalyst deactivation by depositions • catalyst replacement requires reactor dismantling • catalyst particle size >1 mm
Process design	• simple equipment design • no moving parts	• large reactor size
Operation	• easy operation • low Δ*P* and pumping costs • low operating and capital costs • safe operation under high *T* and *P* • flexible controllability • low chance of flooding, compared to countercurrent flow system • improved liquid distribution by controlling gas flow	• no foaming or viscous liquids • partial wetting of catalyst is possible • sensitivity to thermal effects • low liquid holdup compared to concurrent gas-liquid upflow • possibility of catalyst cementation • chance of fouling • bypassing and channelling are possible • non-ideal flow distribution • consistent heat removal is challenging
Reaction	• low chance of homogeneous reactions • high conversion due to plug flow • applicable for gas-limited reactions • suitable for slow reactions	• low conversion for equilibrium-limited reactions • not suitable for moderately fast reactions

2.3 Hydrodynamics

The flow phenomena taking place in TBRs are similar to those happening in pipes to some extent. The main difference is that the random pore structure of the TBRs makes it much more complicated [21]. Mass and heat transfer rates, pressure drop, and phase holdup fluctuate due to the significant difference in the characteristics of the flow regimes. Therefore, the prediction of the flow regime type, considering the reaction system and operating conditions is elemental to design and scale-up of TBRs [21-23]. Knowledge on the hydrodynamics parameters is critical to avoid hotspots formation and potentially, reactor runaway condition in TBRs [24]. Utilizing pilot plant and laboratory experiments for the development of processes or operation optimization requires obtaining accurate results. Fundamental knowledge of small scale TBRs can help to develop industrial reactors [12, 25]. The hydrodynamics of

TBRs depends on the catalyst particle size and surface specifications, fluids physical properties, and reactor diameter [26].

2.3.1 Flow Patterns and Their Deviations

Industrial TBRs are operated at high temperatures and pressures. Hence, understanding the characteristics and the nature of the flow regimes/patterns hydrodynamics is crucial. The existence of different flow regimes in TBRs was initially explored by McIlvried [27] and Larkins [28] in their first experiments [29].

Although there are different flow regimes that can be recognized in TBRs, they are generally classified into two wider regimes of low interaction regime (LIR: trickle flow) and high interaction regime (HIR: bubble, pulse, spray, and dispersed flows). The LIR is achieved at low gas and liquid flowrates, and it is distinguished by a weak interfacial activity between the gas and liquid phases and the flow of liquid driven by the gravity. At elevated pressures and high gas and liquid flowrates, the interactions between the gas and liquid increase, which brings the system near the HIR transition. In the LIR, the liquid (foaming or nonfoaming) trickles down the particles' surface in the fashions of films, droplets, and rivulets, while the continuous gas phase flows independently, filling the remaining of the porous spaces. The HIR is identified by an average to high gas-liquid shear because of a moderate to large flowrates for one or both phases. This leads to the formation of different flow regimes based on gas-to-liquid holdup ratio and liquid proneness to produce foam. At high liquid flowrates and low gas flowrates, bubble flow regime is formed where the liquid flows continuously, containing small spherical bubbles. Maintaining the liquid flowrate at high values and increasing the gas flowrate (up to average level) results in the coalescence of the gas bubbles, making the gas phase to flow in the form of extended bubbles or slug flow bubbles [30]. This flow pattern is called dispersed bubble flow. Pulsing flow regime occurs under average to large gas flowrates and average liquid flowrates. This pattern can be macroscopically pictured as a combination of trickle flow regime (gas-rich slugs) and dispersed bubble flow regime (liquid-rich slugs). Mist or spray flow regime is obtained by increasing the gas flowrate so that the gas phase becomes continuous, and liquid phase appears in the form of droplets. The described flow regimes are for coalescing (non-foaming) liquids. There are two flow regimes for non-coalescing (foaming) liquids, which are foaming flow and foaming-pulsing flow [12, 21, 31]. It is commonly accepted that there are four flow regimes taking place in cocurrent downward gas-liquid flow in packed beds: 1) trickling regime, 2) spray regime, 3) pulsing regime, and 4) dispersed bubble regime [29]. Figure 2-3 illustrates the flow regimes discussed above [32].

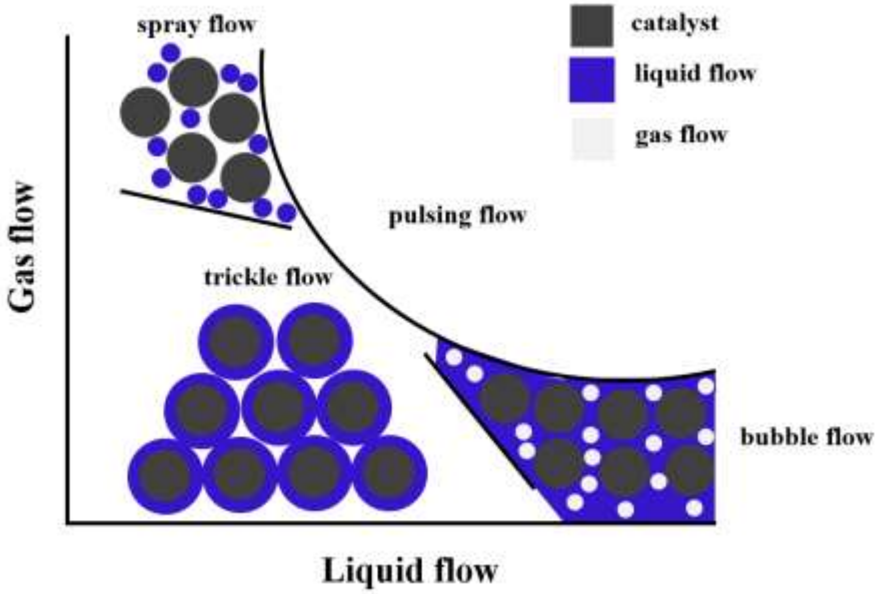

Figure 2-3: Flow patterns of trickle, spray, bubble, and pulse in cocurrent downflow packed bed reactors [32].

For industrial TBRs, trickle flow regime, pulse flow regime, and the transition between them are plausible [24]. The dominant flow regime in the industrial TBRs is trickling (e.g., hydrogenation process) and/or pulsing (e.g., hydrotreating process) regimes because of the vigorous interactions among phases [22, 24]. Even though the industrial TBRs are operated in trickling flow regime, the pulsing flow regime is also observed for petrochemical reactions, such as hydrotreating and hydrodesulfurization [33].

2.3.2 Pressure Drop

Pressure influences the gas and liquid physiochemical properties, affecting the heat and mass transfer, and fluid dynamics in catalytic reactors. Density, diffusivity, thermal conductivity, dynamic viscosity, heat capacity, gas solubility, surface tension, and Henry's constant are significantly affected by pressure. Gas diffusivity and density, solubility of gas in the liquid, and Henry's constant are significantly affected by pressure [12]. The Henry's law has broad applications in chemical and environmental engineering processes. In fact, the Henry's law relates the equilibrium vapor phase and liquid phase concentrations of a solute in a dilute solution at constant temperature and moderate pressures. The amount of a gas dissolved in a specific volume of a liquid to form an ideal mixture is directly proportional to the partial pressure of the gas in equilibrium with the liquid. The corresponding constant is called the Henry's law constant [34]. Since the Henry's constant is defined at infinite dilution conditions, the most conventional methods for determination of the Henry's constant are measuring the solvent vapor pressure considering a pressure correction, obtaining the VLE data as a function of both temperature and pressure, and deduction of a reference state model (e.g., Shock and Helgeson equation) [35]. The experimental techniques of the Henry's constant measurement are phase ratio variation, differential headspace method, modified headspace technique, and headspace gas chromatography [34]. Thus, the Henry's constant is dependent on temperature and pressure since the solute fugacity in the liquid phase is dependent on temperature and pressure, though the effect of pressure on liquid fugacity is not important in some cases [36]. Henry's constant for aqueous solutions depends on the solution composition (e.g., ionic strength and the dissolved organics) [37]. The Henry's constant is also a function of the solvent-solvent and the solute-solvent interactions [38]. To extend Henry's law to greater concentrations, a correction term incorporating the activity coefficient needs to be considered. To cover both high concentrations and high pressures, Krichevski-Kasarnovsky-Ilinskaya model is frequently employed [36].

Dissipation of mechanical energy because of two-phase flow through the fixed-bed solid particles causes pressure drop [23]. Pressure drop is one of the most critical parameters in the design, scale-up, and operation of TBRs. It provides the required energy to drive the fluid through the catalyst bed [39]. Pressure drop is a critical parameter to assess mechanical energy loss, to size equipment for fluid pumping and compression, and to correlate gas-liquid and liquid-solid mass transfer [23]. It is also used to predict the mass transfer rates among the phases. In porous media, flow resistance in a gas-liquid system is established by friction forces at gas-liquid, gas-solid, and liquid-solid interfaces; turbulence is caused by local velocity of gas and liquid phases; and the inertial forces are resulted from acceleration and deceleration of the fluids and capillary forces. In trickling flow pattern, the capillary forces and shear forces are the major causes for the resistance to flow [39]. Knowledge of the single-phase pressure drop is critical in the development of separated flow models to quantify two-phase pressure drop and liquid holdup in TBRs [12]. Pressure drop is low in trickling flow regime, and it is high in HIR. For HIR, empirical correlations are used to predict the pressure drop, while Ergun equation is usually used to predict the pressure drop in LIR [40]. The pressure drop is dependent on the gas and liquid flowrates as well as the bed specifications (e.g., catalyst shape and size). This important parameter also varies with the bed porosity, porosity distribution, and the particles' contact points, which rely on the catalyst shape and packing method (particles orientation) [41]. A recent study claims that the pressure drop for the spherical particles is lower than that for the other particle shapes such as cylindrical and trilobe [41]. Packing pattern/structure is one of the major causes of pressure drop in all flow regimes. Liquid presence in the bed can restrict the pressure drop by the gas flow in the poor interaction regime. Moreover, a higher pressure drop is attained in foaming systems compared to non-foaming ones. In two-phase flow systems, an increase in the pressure drop is more noticeable since the availability of void space for the gas phase is decreased by an increase in liquid holdup. In addition, void space blockage by high liquid holdup forms large gas-liquid interfacial frictions, leading to a high pressure drop. Pressure reduction improves the fluid-mechanical efficiency, and it can be fulfilled by increasing the operating temperature, improving the catalyst bed porosity by effectual packing, and utilizing pressure decreasing agent, such as surfactant. Pressure reduction is beneficial to the design of reactor and operation cost effectiveness [39]. In high pressure TBRs, the gas phase properties are mainly affected by pressure, while the liquid phase properties are only influenced by temperature [12]. A majority of the models available for the pressure drop estimation show significant deviation, leading to errors/uncertainties in the corresponding calculations. In a recent study, Qi et al. [42] introduced a new equation based on the volume average two-phase transport equations using the model originally developed by Whitaker [43], as given below:

$$\frac{\Delta\langle P\rangle}{\rho_l g L} = (\varepsilon_B - \varepsilon_l)\left[\frac{\mu_g(J_{gl}-1)}{I_g\rho_l g}\langle u_g\rangle_0 + \frac{\rho_g}{\rho_l}\right] + \varepsilon_l\left[\frac{\mu_l(J_{lg}-1)}{I_l\rho_l g}\langle u_l\rangle_0 + 1\right] \tag{2-1}$$

where $\langle P\rangle$ is the intrinsic average pressure in Pa; ρ denotes the phase density in kg/m^3; ε_B refers to the bed porosity; μ signifies the phase viscosity in Pa.s; *J* indicates the viscous drag tensor; *g* stands for the gravitational acceleration constant in m/s^2; I symbolizes the phase permeability tensor in m^2; $\langle u\rangle$ introduces the superficial average velocity vector in m/s; and subscripts *g*, *l*, and *0* represent the gas phase, liquid phase, and reactor inlet condition, respectively.

2.3.3 Liquid Holdup

Liquid holdup is a crucial parameter in the TBR design and its safe operation, especially for highly exothermic reactions [33, 44]. It is the major parameter, contributing to the transition from trickling flow regime to the pulsing regime [45]. The liquid hold up depends on the liquid residence time and pressure drop [33, 46]. Particle wetting and thickness of the liquid film reflect the holdup value, affecting the gaseous component mass transfer through the liquid film and into the catalyst particles [33, 44, 47-49]. The liquid hold up value changes with time and spatial location in the reactor. For a given gas superficial velocity, increasing the liquid superficial velocity increases the liquid holdup [26, 33, 49, 50]. Moreover, the liquid hold up decreases with increasing the gas flowrate [15, 26, 49, 50]. The major impacts of the gas flow is ascribed to its interaction with the liquid phase, especially at high gas flowrates [46]. Liquid viscosity has only a small effect on the liquid holdup under pulsing flow regime since inertia force is the dominant force influencing the liquid behavior. In the trickling flow regime, the liquid superficial velocity has a strong impact on the liquid holdup while the influence of gas superficial velocity is minimal [33]. In TBRs, the ratio of reactor diameter to particle diameter ratio, and Reynolds number greatly influence the liquid holdup [44, 46, 47]. Moreover, the liquid holdup when using spherical and cylindrical catalysts can be influenced by inconsistencies in the bed porosities and the particle shape factor [46, 47]. Spherical particles have considerable benefits over cylindrical extrudates of comparable size [50]. In industrial TBRs, the catalysts are packed by sock method (random introduction of particles) or dense method (particles introduction is performed to accomplish a maximum horizontality). It was extensively reported that there is a pressure drop increase and dynamic liquid holdup decrease in TBRs packed with sock method in which the number of contact points is high [47]. Smaller particle size and higher liquid viscosity lead to a larger total liquid holdup [48]. Decreasing the particle size increases the bed specific surface area, and consequently, liquid holdup because the liquid phase cannot easily flow downwards through the bed at a specified gas and liquid flowrate [46]. To evaluate the effect of pressure on liquid holdup, the combined effects of pressure and gas flowrate should be considered. Moreover, it has been reported that considering the gas density as an independent variable to evaluate the liquid holdup in TBRs (instead of pressure) has a small deviation from the evaluation made by the combined impacts of pressure and gas flowrate (García-Serna et al. 2017; Fu and Tan 1996). Increasing temperature reduces the gas density, which pushes out the liquid because of increased gas buoyancy, leading to the liquid holdup reduction [26].

To measure liquid holdup in a laboratory TBR, analytical techniques such as tracer, weighing, and drainage are applied [47]. Although the methods of tracer and drainage (stop flow) are very reliable, they are time-consuming. However, weighing (gravimetric) method is reliable and fast under atmospheric pressure. Tomographic methods, such as gammametry, might be used for high pressure operations. Although accurate and on-line (continuous) measurements of liquid holdup are among the advantages of these techniques, their high equipment cost and safety risks are the critical issues in employing these analytical techniques [51].

There are different definitions for the description of liquid holdup in the literature. Total liquid holdup is the total amount of liquid in the bed during steady-state operation. Static liquid (internal) holdup is the amount of liquid remained in the bed after stopping the liquid feed and allowing the bed to drain freely. Furthermore, dynamic liquid (external) holdup is the amount of liquid drained from the bed after stopping the liquid feed [44, 47, 48].

The correlations available for the prediction of liquid holdup are constrained to the proposed systems and the range of used process conditions. Thus, it is critical to estimate the liquid holdup as a function of the system physical properties and operating conditions [44]. To accurately predict the liquid holdup and pressure drop, velocity and shear-based correction factors are required to be included into the correlations-especially for the trickling flow regime [15].

2.3.4 Liquid Distribution Homogeneity

One of the most important factors in the operation, design, and scale-up of the TBRs is liquid phase distribution [52]. Reactor maldistribution depends on reactor diameter to particle diameter ratio, liquid physicochemical properties, flowrates of liquid and gas, wetting efficiency, and the catalyst particle shape and orientation [53]. The liquid phase might channel because of inefficient inlet liquid distributor, packing anisotropy, catalyst fines, change in the liquid physical properties, and physical obstructions.

These problems can be avoided by an efficient design for liquid distributor, and liquid redistribution system. Although the liquid distribution is established at the top of the TBR, formation of rivulets at downstream can occur because of capillary pressure and heterogeneities in the bed porosity. The chance of rivulets formation increases with increasing the liquid flowrate [54]. Liquid maldistribution adversely affects the gas-liquid phases contact over the surface of the catalyst and causes flow channelling. Local flow maldistribution and gross maldistribution are two categories for liquid flow distribution in TBRs. The local maldistribution can be resulted from particle shape and size, its surface roughness, particles arrangement, bed porosity, and properties of the gas and liquid phases. The gross maldistribution can be caused by improper distribution of the liquid at the reactor inlet [13]. Proper distribution of the liquid at the top layers of the TBR catalyst bed does not guarantee its uniform distribution through the bed, and the liquid maldistribution might take place across the remaining layers/length of the catalyst bed. Therefore, liquid redistribution in the reactor is required to efficiently control the liquid distribution. It should be noted that the catalyst porous bed itself eases the liquid distribution to some extent. The requirements to satisfy an efficient liquid distributor are low pressure drop, ability to operate within a wide range of flowrates, less proneness to fouling and blockage, ease of operation, and ease of maintenance and installation. Types of liquid distributors, which are commonly used in TBRs, are weir channel, nozzle, shower, sieve tray, down-comer tube, bubble cap, and vapor lift tray. The factors affecting the selection of distributor type are reactor dimension, flowrate, fluid properties (foaming, viscous, and fouling), and pressure drop [13]. Based on the experimental and modeling studies, the effects of liquid distribution on TBR performance are greater than those of the wetting efficiency. Quantifying maldistribution is a difficult task, and it is usually inferred from liquid distribution at the reactor outlet. It is important to note that this technique is limited to small size reactors. Knowledge on liquid distribution through the reactor bed is fundamental for the development of any model, representing the reactor performance. Packing structure complexity and fluids interaction with the packing structures make the liquid distribution modeling difficult. Computational fluid dynamics (CFD) can help understand the liquid distribution in the TBRs (e.g., discrete cell modeling approach to predict the liquid distribution for single, two, and uniform inlets). Computer-assisted tomographic is an analytical technique to observe the different features of trickling flow regime. Figure 2-4 shows various liquid flow patterns [13].

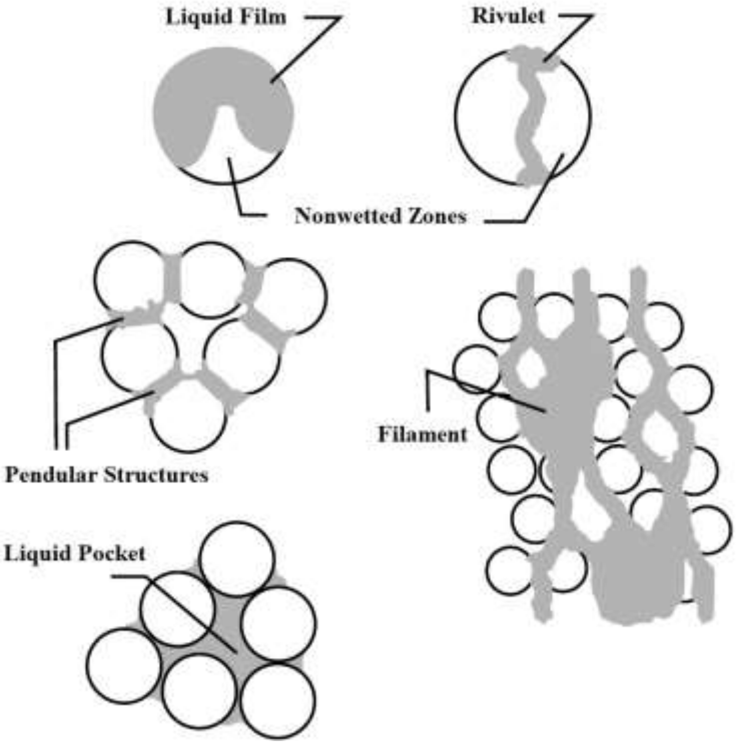

Figure 2-4: Different patterns of liquid flow [55].

Impulse tracer response is another technique to evaluate the flow distribution in a reactor [56]. The phases' flowrates, fluids properties, and catalyst particle properties determine the shapes of liquid formation in the bed void as films, rivulets, filaments, pendular, and/or stagnant pockets. The formation of films and rivulets occur in a single particle while filaments, pendular, and stagnant liquid pockets are observed in a multiparticle system. Capillary pressure crevices at the contact points and between the particles produce stagnant liquid pockets and pendular structure. Filament is a continuous liquid flow over the particles that can be formed as films or rivulets. The film flow and filament flow are expected to form in prewetted and non-prewetted beds, respectively [13]. The bed prewetting is a crucial parameter to improve the liquid distribution during the operation [54]. In case of liquid maldistribution, poor wetting results in liquid segregation, and consequently, catalyst underutilization [13, 53, 57, 58]. Also, hotspot formation is possible when the liquid maldistribution occurs [13, 52, 53, 57-59]. Hotspots can increase the chance for catalyst sintering, leading to reduction in the catalyst activity and surface area; consequently, the catalyst lifetime is shortened, and the operating cost is increased by sintering. In addition, reactor may encounter runaway condition upon the formation of hotspots, which is considered as an unsafe operation [54]. Liquid channeling happens by merging the filaments as a dominant flow type [13]. Non-uniform catalyst packing, uneven liquid inlet distribution, and large particles enhance the channeling phenomenon [54].

2.3.5 Wetting Efficiency

In hydrotreating processes, hydrodynamic parameters influencing the rate of mass transfer in the liquid phase are of critical significance. The mass transfer rate is greatly affected by the liquid-solid mass transfer coefficient and the catalyst wetting efficiency [60]. Partial vaporization of the liquid feed may occur in TBRs, operating at high pressures and temperatures [61]. Moreover, in TBRs operating at low liquid flowrates (<0.01 m/s [62], part of the catalyst surface is covered by gas [13, 63-65]. Hence, incomplete surface wetting is a fundamental feature of the TBRs operating at low liquid mass flow rates [13, 64, 66].

In a trickling flow regime, a catalyst particle external surface is either fully- or partially-wetted [67]. Figure 2-5 illustrates possible scenarios for catalyst particle wetting conditions [32].

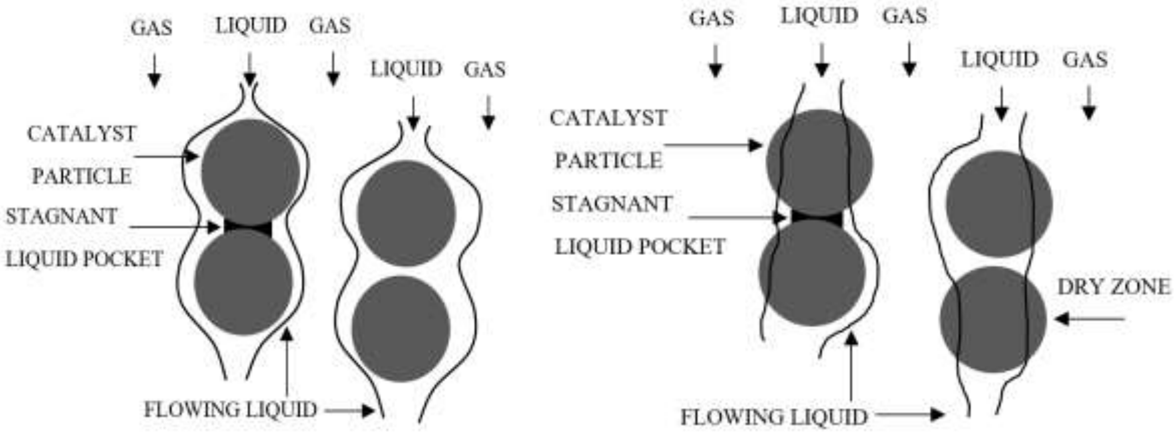

Figure 2-5: Catalyst particle wetting conditions: (a) fully externally wetted; and (b) partially externally wetted [32].

Partial wetting is a key concern in the development and operation of industrial TBRs. The main reasons for this concern are: continuous reduction in the sulfur content dictated by the environmental regulations (greater residence time/lower liquid flowrate); higher conversion of heavier feedstocks/oils, which require higher residence time; and drastic changes in the operating conditions and the amounts of catalyst used due to transformation of lab-scale reactor to the commercial level [66]. At high liquid flowrates, the catalyst internal pores are completely saturated by the liquid due to the capillary force [61]. Different conversions result from the external mass transfer resistance on the wet and dry catalyst regions [61, 62, 64]. A direct relation between the external wetting efficiency and reaction rate is required for the volatile reactants [64, 68]. The wetting efficiency is affected by the effective diffusivity and mass transfer coefficient [68]. Although catalyst pores might be entirely wetted because of the capillary force, wet and dry zones of catalyst might not be sufficiently explained by the flash calculations (employing various equations of state and Gibbs free energy minimization techniques) [61].

There are different methods to measure the wetting efficiency in a TBR, including, residence time distribution (RTD), pressure drop, computed tomography, calorimetry, and dye absorption [62]. Magnetic resonance imaging (MRI) is another direct technique to measure the catalyst wetted surface during the trickling flow regime at 2D and 3D [62, 66, 69]. However, ferromagnetic material and liquids, consisting of a considerable amount of paramagnetic components, cannot be analyzed using the MRI technique [69]. The most common approach to measure the wetting efficiency is tracer technique, which is an indirect analytical method. In this approach, an impulse or step concentration of tracer (in the liquid) is introduced in the TBR feed. The tracer concentration distribution is tracked at the reactor outlet [62, 65, 66]. Another indirect measurement technique for the wetting efficiency is reaction method [13, 66, 68]. The tracer and reaction techniques are costly, and can be applied to the industrial processes [13]. In the reaction method, chemically active area in the catalyst bed is determined as an fundamental parameter for the prediction of a TBR performance [68]. In this method, reaction conversion data under varying wetting conditions is employed to predict the wetting efficiency [65]. Most of the methods, which use kinetic data to calculate the wetting efficiency, can be only applied for the first order reactions. Since the data analysis and introduction of an analytical solution for the effectiveness factor are complicated, use of non-linear kinetics for the wetting efficiency estimation is avoided. Some theoretical models, which are presented for non-linear kinetics, lack experimental data for validation [68].

The internal catalyst wetting efficiency is commonly equal to unity because of the capillary effects [67], except for the volatile liquid reactants and extremely exothermic reactions [65]. The external catalyst wetting efficiency increases with increasing liquid flowrate [66, 67, 69], and it is unity for high liquid flowrates [67]. Fluctuations of liquid flowrate have a significant impact on the liquid holdup and the wetting efficiency [60]. The catalyst external wetting efficiency is a critical parameter in designing a TBR, which determines the degree of catalyst utilization in a TBR [67]. Depending on the phase in which the limiting reactant resides, the reaction rate over an incompletely wetted catalyst can be smaller or larger than that over a completely wetted catalyst [67]. If the limiting reactant is in the liquid phase (e.g., hydrodesulfurization), the surface area available for effective mass transfer between the catalyst and the reactant is not sufficient to have a complete reaction when the catalyst surface is not completely wet [13, 62, 64, 67]. If the limiting reactant is in the gas phase, it can have easy access to the catalyst pores in an incompletely wetted catalyst, leading to the reaction rate enhancement [13, 62, 64, 67, 70]. Therefore, the knowledge on the wetting efficiency and the effectiveness factor for the partly wetted catalyst is necessary to predict the performance of a TBR [67]. Since at high pressures, the catalyst wetting efficiency might enhance in a TBR, using the correlations and experimental data from atmospheric operating conditions cannot capture the physics of wetting that may lead to unreliable results for TBRs operating at high pressures. Most of the correlations for the calculation of the wetting efficiency were derived under atmospheric conditions. One of the reasons is that the degree of effect of pressure on the wetting efficiency cannot be effectively measured [64, 67, 68]. The liquid wetting efficiency is affected by both liquid holdup and pressure drop. For a constant liquid flowrate, the wetting efficiency increases at high gas flowrate and high pressure. A decrease in holdup and an increase in pressure drop take place at high gas flowrate and high pressure. When the liquid flowrate increases, the wetting efficiency improves due to an increase in both liquid holdup and pressure drop [67]. Gas flowrate can have different effects on the wetting efficiency. When the gas flowrate increases, wetting efficiency might increase due to the improvement in gas-liquid shear, and it might decrease due to the reduction in liquid holdup [13]. The effect of gas flowrate on wetting efficiency, liquid holdup, and pressure drop is more noticeable at high pressure conditions [64, 67]. This improved wetting efficiency results from enhanced spreading of the liquid over the external catalyst surface due to increased shear stress on the interfaces between the gas and liquid phases at a higher pressure (gas density) or a higher gas flowrate [13, 64, 66, 67].

The liquid viscosity can also affect the wetting efficiency. Multiplying the liquid viscosity by 8.5 is found to slightly increase the wetting efficiency (by <10%). This can be justified by an increase in liquid holdup [62]. Reactor and catalyst specifications, such as bed porosity and particle diameter, have considerable influences on the wetting efficiency. Another parameter, which indirectly affects the wetting efficiency, is liquid distributor. This parameter has its most negative effect at the zone close to the reactor inlet nozzle [13]. Wetting efficiency decreases when the particle size increases, especially for liquid velocities higher than 1×10^{-3} m/s [13]. This trend can be explained by the effects of liquid holdup and capillary pressure. Higher wetting efficiency can be achieved by greater solid-liquid interactions for smaller particle sizes. However, decreasing the particles size results in higher pressure drop [13]. The wetting efficiency also decreases when the bed porosity increases due to the less contact points among the particles, and, therefore, a less number of liquid menisci to push the liquid rivulets [62, 66]. Particle shape has a negligible effect on the wetting efficiency (for dense packing bed and liquid velocities more than 0.002 m/s) [62, 66]. Adding no-porous fines (e.g., SiC/inert fines) can improve the wetting efficiency [13, 62].

2.3.6 Mass Transfer Coefficients

As there is no rigorous mixing mechanism in the trickle flow operation (unlike other multiphase reaction systems, such as stirred tank reactors and slurry bubble column reactors), the rate of mass transfer is low and often becomes rate-limiting in the TBRs performance. Gas-liquid, liquid-solid, and gas-solid mass transfer rates are important in TBRs [13]. The flow regime has a significant impact on the mass transfer rate [71]. Figure 2-6 illustrates the mechanism of mass transfer for the hypothetical gas reactant *A* and hypothetical liquid reactant *B* in a three-phase catalytic reaction system [72].

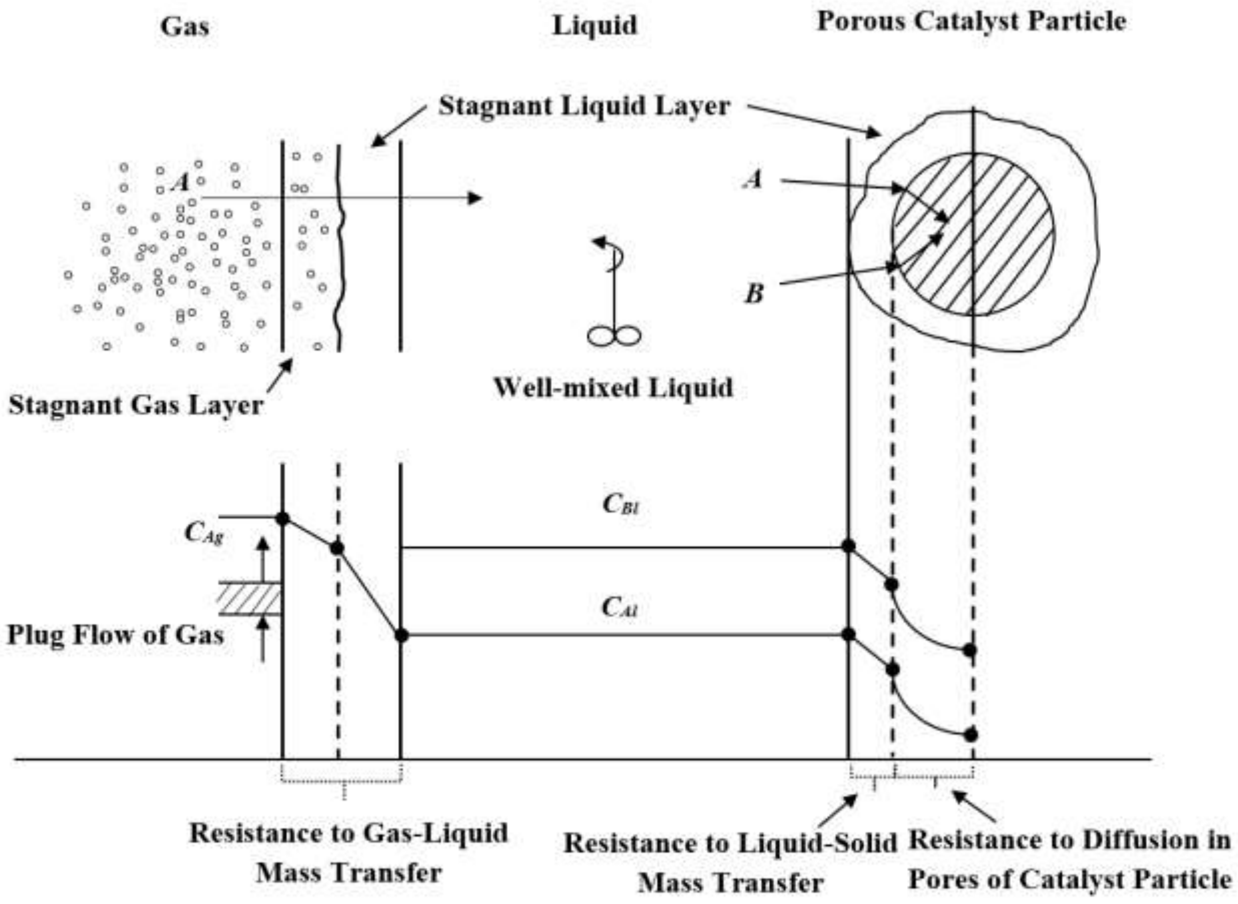

Figure 2-6: Profiles of concentration in a catalytic three-phase reactor [72].

2.3.6.1 Gas-liquid mass transfer

In a TBR, the gas-liquid mass transfer resistance has a significant impact on the reaction rate. Hence, evaluating the gas-liquid mass transfer is critical to properly design and scale a TBR [73, 74]; it is also important in assessing the overall conversion rate for moderately fast chemical reactions [75].

There are two general techniques to measure the mass transfer rate in TBRs that are based on measurements of dissolution rate from a packing (packed with soluble solids), and electrochemical redox reaction rate. The electrochemical method has the advantage of online measurements and convenient mass transfer rate measurement under dynamic conditions [54].

The liquid side mass transfer is often rate-limiting in gas-liquid mass transfer processes. The gas-liquid mass transfer rate depends on the gas and liquid flowrates, particle diameter, fluids' properties, and the system operating conditions. The reactor height and diameter have a limited effect on the rates of gas-liquid mass transfer in comparison with the particle size. Reduction in particle size improves the gas-liquid mass transfer rate. Two-phase pressure represents the interaction among the flowing phases. This interaction is more significant for smaller particles, demonstrating higher rates of gas-liquid mass transfer [13]. Gas and liquid flowrates have considerable influences on the gas-liquid mass transfer coefficient [13, 74, 75]. Increasing the gas and liquid flow rates increases the interactions between these phases and the liquid spreading, leading to an enhancement in gas-liquid interfacial area [13, 74]. However, the study carried out by Goto and Smith [76] claims that the mass transfer coefficient (k_{gl}) is not affected by the gas flowrate. Moreover, mass transfer data analysis can be made without considering the axial dispersion [76]. Physical properties, such as liquid surface tension, liquid viscosity, gas density, and diffusion coefficients significantly affect the gas-liquid mass transfer rates [13]. For viscous systems, the interfacial area considerably increases at low liquid flowrates, possibly upon an appreciable increase in the liquid holdup [77]. Liquid density and gas viscosity do not affect the gas-liquid mass transfer rates significantly. Higher pressure results in lower mass transfer rate in a foaming liquid system while it has a minor influence on the mass transfer rate in non-foaming liquid systems [13]. An increase in gas density or operating pressure improves the mass transfer rate due to the increase in the interfacial area and gas holdup [12, 13, 73-75, 77]. Interfacial area is not considerably affected by pressure at very low gas and liquid flowrates. However, the interfacial area improves by an increase in pressure at higher liquid flowrates for gas flowrate above a threshold level. The impact of pressure can be due to either an increase in interfacial area, or gas-liquid mass transfer coefficient, or both. Some studies revealed that the mass transfer coefficient (k_{gl}) is independent of pressure. Therefore, volumetric mass transfer coefficient (k_{gl} a) should change with pressure because of the interfacial area effect [73]. The gas diffuses into the liquid film, and small bubbles are formed at moderate gas flowrates and high pressures; this increases gas-liquid interfacial area and gas holdup [12, 13, 73]. Under such operating conditions, the liquid spreading also improves, which leads to higher gas-liquid interfacial area and wetting efficiency [12, 13]. Research studies with focus on the interfacial area and volumetric liquid-side mass transfer coefficient at high pressures are scarce [73]. At very low gas flowrates, pressure has a negligible effect on the gas-liquid mass transfer [74]. Some studies show that the gas-liquid mass transfer rate and the gas-liquid interfacial area are strongly dependent on the hydrodynamics of flow patterns. Mass transfer resistances in trickling flow regime are higher compared to those in bubble flow regime, pulse flow regime, and spray flow regime [77].

2.3.6.2 Liquid-solid mass transfer

The liquid-solid mass transfer coefficient is one of the most vital parameters for TBRs' design, scale up, and performance analysis [71]. Various studies have been conducted to determine liquid-solid mass transfer coefficients. The majority of the studies have been focused on the electrochemical and dissolution techniques [78]; however, other methods, such as chemical reaction and activated carbon absorption, have also been employed [79]. The electrochemical method measures the liquid-solid mass transfer coefficient for a single particle in the bed (local measurement), while the dissolution method measures the average volumetric liquid-solid mass transfer coefficient ($k_{ls}\ a$) for a short portion of the bed or entire bed [71]. Liquid-solid mass transfer rates depend on the extent of liquid-solid contact. This is the reason that many correlations incorporate wetting efficiency into the liquid-solid mass transfer coefficient [13].

The liquid-solid mass transfer rate increases when the liquid flowrate increases [13, 71, 78]. However, it was reported that the liquid-solid mass transfer coefficient does not depend on the liquid flowrate in pulsing flow regime [71]. Some studies showed that the gas flowrate has no effect on the liquid-solid mass transfer coefficient, while others reported that the liquid-solid mass transfer rate increases with an increase in the gas flowrate, which might be affected by the type of the flow regime [71]. Volumetric liquid-solid mass transfer decreases upon an increase in the catalyst particle diameter [71]. At a constant pressure, the liquid-solid mass transfer coefficient increases with an increase in gas and liquid flowrates [71]. At high gas and liquid flowrates, the liquid-solid mass transfer is greatly affected by the reactor pressure. For a given gas flowrate and pressure, the liquid-solid mass transfer increases with an increase in the liquid flowrate [71]. The empirical correlations resulted from the atmospheric systems cannot accurately determine the liquid-solid mass transfer coefficients and the pressure effect [71]. The effect of gas flowrate on k_{ls} is more noticeable when the trickling flow regime changes to pulsing flow regime. There is a considerable increase in k_{ls} when gas flowrate increases, which might be influenced by the extent of energy dissipation in turbulent flow [78, 80]. Referring to the impact of the particle size on the mass transfer, Goto and Smith [76] concluded that $k_{ls}\ a$ in TBRs can change for the particles with a diameter smaller than 0.2 cm.

2.3.7 Packing Structure

Catalyst loading into the reactor bed is a critical task in the operation of TBRs. The most utilized practice is to house the catalyst particles randomly inside the bed. Semi-structured and structured packing of catalyst particles are also proposed.

2.3.7.1 Randomly packed bed

Randomly packed beds are mostly used in industrial TBRs operation due to their simple construction and loading procedure. The most common shapes of the catalyst particles are spherical, extrudates, cylindrical, trilobes, and quadrilobes. The desired pressure drop and intraparticle and external heat and mass transfer determine the choice of particle shape and size. In addition, particles’ durability and attrition are important selection criteria for the catalysts. Packing characteristics are considerably dependent on the ratio of particle diameter to bed diameter and on the particle shape if the particles are randomly packed in a cylindrical reactor vessel. The bed porosity can be higher in regions near the wall, due to straight and smooth solid boundary. It was experimentally verified that porosity follows a Gaussian distribution on the particles cluster scale. Porosity has a bi-modal distribution at a very smaller scale. Fluctuations in porosity with the spherical particles are higher than those noticed with the trilobes [13].

2.3.7.2 Structured packed bed

Application of semi-structured or fully-structured packed beds for TBRs is to prevent high pressure build up that is involved with the random packing. This idea stemmed from successful utilization in the distillation columns. The main advantages of structured packings are less pressure drop, increased surface area per unit volume, and simple scale up. However, the structured packings are more expensive than the randomly packed beds since they need some extra internal installations. Some types of structured packings that are utilized in TBRs are corrugated sheet packing, Gauze packing, mesh-type packing, three-layer packing, and monoliths [13]. The packing porosity can considerably influence the RTD and the axial dispersion coefficient [81].

2.3.8 Particle Shape and Porosity

The particle shapes with a higher hydraulic diameter and larger void fractions impose less pressure drop [82]. Smaller catalyst particles increase the surface area, leading to a higher catalytic reaction rate. Therefore, the catalyst size needs careful optimization [82]. For example, the size and shape of hydrotreating (HDT) catalysts are factors that should be closely chosen in accordance with the reactor technology and the feed type for optimal operation of the reactor. The conventional shapes of catalysts like spheres and pellets are suitable for distillate HDT. These shapes are not suitable for feed streams containing heavy molecules, since the large molecules are not able to reach the internal parts of the particles. Particle size reduction usually leads to the higher pressure drop in the fixed-bed reactors. A practical solution to this problem is the utilization of other shapes, such as trilobules and tetralobules, which have extensive surface area to significantly decrease the diffusion path. Particle shape affects the void fraction, therefore, influencing liquid holdup; it also affects the fluid dynamics, and eventually the Peclet number [82]. Catalyst particles have chemical and physical impacts on reaction (s). For instance, catalyst particle porosity might cause diffusional restrictions for both the product selectivity and reaction rate [82]. Catalyst particles are designed to enhance external surface area (better catalytic activity) as effectiveness factors are low. Less tube wall temperature is achieved for the multi-holed particles (structural integrity reduction) for similar pressure drop amounts due to the bed voidage increase and velocity decrease [13].

2.4 Catalytic Reactor Mathematical Modeling Framework

A mathematical model represents a given system at some certain points in time and /or space. It improves the understanding of the real system. A system usually includes interconnected elements or components to provide the fluid flow of information (e.g., mass, momentum, or energy) [83]. The mathematical model development is intended to describe the performance of a process of interest, which can be physical, conceptual, and mathematical [84]. A process model consists of a set of equations, which can estimate the chemical process dynamics/performance. A mathematical model typically specifies a system by a set of equations which involves several variables. The main categories of variables are input variables, output variables, state variables, decision variables, random variables, and exogenous variables (parameters such as density, heat capacity, and viscosity). All process variables are dependent on time or/and spatial position. Hence, all variables are dependent on each other whereas time and spatial coordinate variables are independent [83]. A mathematical formulation of a process can predict its physical performance. The classification of mathematical models is complicated since their characterization is complicated by time, space, subject, continuity, and computational aspects [84]. Mathematical models have various engineering applications in design, control, estimation, and monitoring [84]. All industrial chemical processes are designed to transform inexpensive raw materials to value-added products. These chemical transformations occur in a reactor, which facilitates numerous functions such as, contacting the reactants of the reaction mixture, giving a suitable environment (e.g., pressure, temperature, and catalyst) for a sufficient time, and providing the products removal [85]. The chemical reactor engineering involves the interrelated categories of reactor performance and reactor hardware and operating procedure. Reactor performance deals with conversion, selectivity, stability, operability, product quality, environmental effects, cost, and safety. Reactor hardware and operating procedure include reactor configuration (e.g., size and nozzles), operation mode (e.g., batch or continuous), start up and shut down procedures, operating conditions (e.g., temperature and pressure), and reactor internals (e.g., baffles and distributors) [85].

Considering the requirements of process knowledge and availability of the process data, there are three types of models as white-box model (WBM) or first principle model (FPM), black-box model (BBM), and hybrid model or gray-box model. FPM development significantly depends on the process knowledge whereas BBM largely relies on the data of the process. Hybrid model is a combination of FPM and BBM. FPM is developed by the first principles relevant to the base of engineering and science laws. BBM is based on mapping input-output data instead of using the process mechanism. Hybrid models can be structured by a serial, parallel, or serial-parallel integration of different mathematical sub models. Hybrid models are broadly used in the chemical processes to study the reaction mechanisms. Usually the hybrid models are used for a process (or, a part of the process) for which there is not enough knowledge about its mechanism. Hybrid models can be constructed by the utilization of fuzzy logic (FL), artificial neural network (ANN), lattice Boltzmann method, support vector machine, molecular dynamic (MD) simulation, and Kalman filter [84]. Figure 2-7 shows the reactor engineering methodology [85].

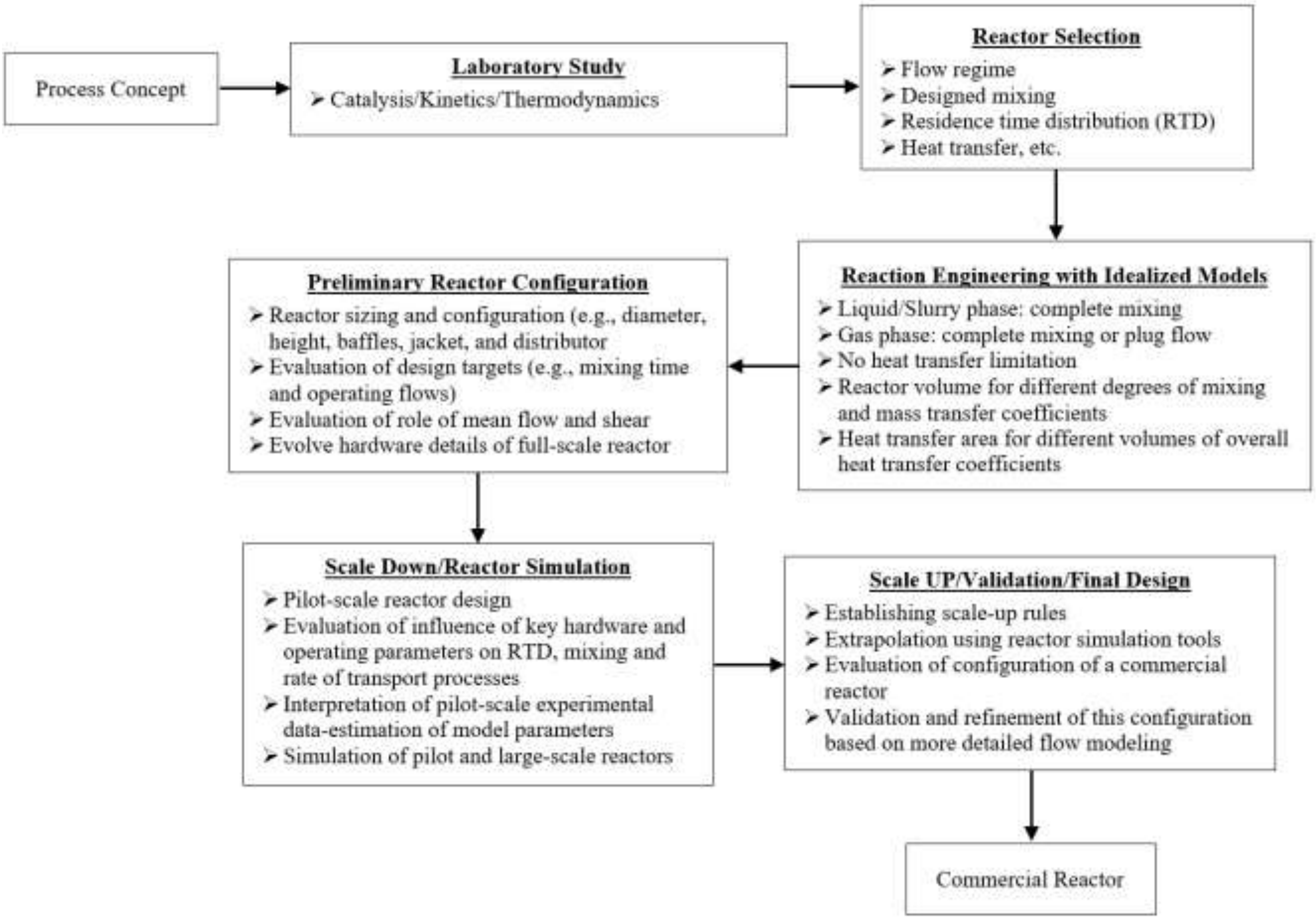

Figure 2-7: Reactor engineering methodology [85].

New reactor technology development can be encouraged by the factors as operability with technologically feasible region, substantially safe operation, environmentally satisfactory, highest conversion of raw materials, and greatest reaction selectivity to the wanted products. To improve the existing reactor technology performance, the goals can be higher output per unit volume (higher production rate), improvement of selectivity and greater quality of product, safer operation, lower consumption of energy, and more environmentally friendly operation (less negative impacts on the environment) [85].

Reactor design envisions the development of operating protocols and reactor hardware to suit various process needs and economic concerns that are limited by the transport resistances and reaction kinetics without undermining process safety and with minor environmental footprints. Scale up refers to the transformation of information from one scale of reactor to another scale. This can be from laboratory/pilot-scale to industrial-scale reactor or from industrial-scale to laboratory/pilot-scale reactor. Scale up is required to transform newly developed technology at the laboratory/pilot-scale to the commercial-scale reactor or to interpret/extrapolate the laboratory results to the industrial-scale reactor [82]. Table 2-3 provides the information on the common values of operating parameters and scales of TBRs.

Table 2-3: Typical range of key operating parameters and scale up of TBTs [13].

Parameters	**Scale**			
	Industrial	Pilot	Bench	Micro
Liquid flowrate (kg/m^2.s)	2.5–25	0.8–6	0.08–0.25	0.03–0.09
Gas flowrate (kg/m^2.s)	0.4–4	0.01–1	0.01–0.08	0.0001–0.05
Wetting efficiency	0.6–1	0.4–0.9	0.1–0.7	0.8–1
Liquid holdup	0.16–0.25	0.1–0.2	0.05–0.14	0.15–0.25
Gas-liquid mass transfer rate (s^{-1})	0.08–0.14		0.02–0.08	3–7
Liquid-solid mass transfer rate (s^{-1})	0.1–0.3		0.9–1.4	
Bed length (m)	16	1–4	0.3–1	0.008–0.5

One of the most crucial tasks in the chemical industries is to properly control the plant and efficiently maintain the product production. The important goal of an industrial process is to produce the high-quality product while sustaining the minimum cost of operation. In the operation of a process, there are numerous operating parameters that affect the process performance. They have different degrees of effect on the process. In order to find out the influential parameters and their importance in terms of process control, the relationship among the parameters needs to be determined.

Chemical reactor is the heart of a chemical process, and its operation and control determine the whole process efficiency. Some chemical reactors are packed/equipped with a type of catalyst to fulfill the process reaction. Catalytic reactors are the main units of many chemical, petrochemical, and refinery processes.

A model is a mathematical abstraction of a real process. The mathematical model, which consists of a set of equation, cannot represent all aspects of an actual process. To avoid the computational burden, sometimes a simplified model is preferred. However, too simplified model might lead to the chance of missing related process variables/information so that the model does not support the proper understanding of the system. The incorporation of too many details in the model might result in the excessively complex model and difficult to comprehend. The goals of the modeling of a process can be the improvement of the process understanding, the plant operating personnel's training, the process controller design, and the process conditions optimization [83]. As mentioned earlier, a chemical reactor is the major process of a chemical plant. The following section gives a structured information/knowledge on the modeling endeavor steps of a catalytic reactor.

2.4.1 Problem Statement and Process Description

In a catalytic process, the most common problem is the catalyst deactivation phenomenon. When the catalyst activity drops below a threshold level, which is usually determined from the product quality, there are four choices to deal with the deactivated catalyst: to regenerate it, to reuse it for another application, to extract the expensive components, and to dispose it. Deactivation by the formation of coke and carbon can be reversed by the gasification with H_2, H_2O, or O_2 (such as in catalytic reforming of naphtha). Deactivation by sintering is usually irreversible (such a sin crude terephthalic acid hydropurification) [86]. Some operating parameters including the impurities in the reactor feed, temperature, and residence time have substantial influences on the catalyst deactivation. Therefore, to rectify the process problem, the targeted parameters need to be evaluated. This is the most important part of the modeling of a chemical reactor because it will provide knowledge that is required for the model development.

The knowledge on the process is required to properly develop the model and analyze the results. It helps find the key parameters influencing the process. The other required process information is the process data. The required data might be the impurities concentration, operation parameters values (e.g., temperature and pressure), catalyst specification (e.g., particle porosity and diameter), catalyst bed specification (e.g., bed void and bulk density), and reactor dimensions (diameter and height). The parameters in the proposed process can be evaluated in terms of the degrees of effect on the process performance. The significance of heat and mass transfer phenomena can be assessed based on some rule-of-thumb criteria. To make such a simplification, the operating data is required. Table 2-4 includes some of the rules that are applied to the catalytic reactors.

Table 2-4: Assessment of mass and heat transfer in a fixed-bed catalytic reactor.

Impacts	Criterion	Remarks	Ref
Liquid maldistribution	$\frac{d_R}{d_P} > 25$	wall flow < 10%	[87]; [88]
	$\frac{d_R}{d_P} > 18$	minimum amount for a uniform flow	[89]
	$\frac{d_R}{d_P} > 20$	min maldistribution even at high P	[90]
	$\frac{d_R}{d_P} > 4$	proper liquid distribution with no channeling (and no adverse heat transfer)	[91]
Axial mass dispersion	$\frac{L}{d_{PE}} > 20\frac{k_r\tau}{Bo} = \frac{20}{Bo} ln\frac{C_{in}}{C_{out}}$	min axial dispersion impact	[92]
	$\frac{L}{d_P} > 350$	negligible back-mixing	[93]
	$\frac{L}{d_P} > 50$	minor axial dispersion	[94]
Radial mass dispersion	$\frac{L}{d_R} > 0.04\frac{ud_R}{\varepsilon_l D_{dr}}$	min radial dispersion, persistent radial mass dispersion for $\frac{d_R}{d_p} > 25$	[95]
Axial heat dispersion	$\frac{L}{d_P} > 30$	min axial heat conduction	[92]; [96]
	$\frac{L}{d_P} > 30$	min axial heat dispersion for industrial process	[97]
Radial heat dispersion	$\frac{L}{d_P} > 4$	min radial heat dispersion	[91]
	$\frac{L}{d_P} > 10 - 20$	no significant radial heat dispersion	[98]

2.4.2 Model Development

In engineering field, process models are used to understand the proposed system. A model can be a physical model, mathematical, or statistical that mimics the behavior of a real system. The extent of model complexity is determined by the decisions made in the steps of modeling. It is suggested to begin the process of modeling with a fundamental model. The development of modeling equations is started from the conservation equations of mass and energy balances (chemical and physical laws). They might be supplemented by one or more constitutive equations, which define the terms in the balance equations.

2.4.2.1 Model selection

The main categories for the reactor models are pseudo-homogeneous model and heterogeneous model. When the intra-particle mass and heat transfer constraints are minor, a pseudo-homogeneous model is sufficient to analyze the reaction system function. When the reaction system involves considerable differences in concentration and temperature among phases, a heterogeneous model is chosen [97].

The criteria for selecting the pseudo-homogeneous model and heterogeneous model for a catalytic reactor are extensively studied. The most significant part of resistance to heat transfer for the vapor-phase systems is usually in the film (boundary layer) around the particles instead of the resistance inside the particles. This is justified by higher effective thermal conductivity for the solid compared to that in the gas phase. The film resistance to heat transfer is assumed to be dominated by that at the surface. The following criterion is to be satisfied if less than 5% deviation of the observed rate is required when neglecting the inner heat transfer resistance [99]:

$$\left|\frac{-\Delta H_j r_P d_P}{2T_b h}\right| < 0.15\,\frac{RT_b}{E} \tag{2-2}$$

where T_b is the bulk fluid temperature in K; h signifies heat transfer coefficient in cal/cm^2.s.^{o}C; ΔH represents heat of reaction in cal/mol; r_P indicates the observed reaction rate in mol/cm^3.s; d_P is the particle diameter in cm; R refers to the universal gas constant in cal/mol.K; and E symbolizes the activation energy in cal/mol. The impact of bulk mass transfer through the film for isothermal reactions with first-order kinetics can be ignored when a specific criterion is met. Such a criterion considers the effects of mass transfer coefficient, particle external surface area, intrinsic reaction rate constant, and effectiveness factor. The limitations are relaxed by any reaction order, and the mentioned mass transfer resistance can be disregarded if the following criterion is satisfied, permitting maximum 5% deviation from the observed reaction rate [99]:

$$\left|\frac{r_P d_P}{2C_b k_c}\right| < \frac{0.15}{n} \tag{2-3}$$

where C_b indicates the concentration of bulk fluid in mol/cm^3; k_c introduces the gas-particle mass transfer coefficient in cm/s; and n represents the reaction kinetics order. Intraparticle transport is a complicated topic since it involves extensive diversity of the reaction kinetics, geometries of the catalyst particles, and the system and particle thermal behaviors. The ultimate objective is to calculate the effectiveness factor. There are some criteria that can evaluate the importance of heat and mass transfer inside the particle/catalyst. For instance, for a first-order reaction and an isothermal catalyst particle, the following criterion needs to be met to ensure that the effectiveness factor is more than 0.95 [99]:

$$\frac{r_P {d_P}^2}{4C_s D_e} < 1 \tag{2-4}$$

where C_s represents the concentration of the reactant at the outer surface of the particle, and D_e stands for the effective diffusivity in a porous particle in cm^2/s. In another study, the effectiveness factor is found to be greater than 0.95 under the fluctuation of mass and heat transfer, when the following criterion should be satisfied. In such a case, the intraparticle mass and heat transfer can be neglected [99]:

$$\frac{r_P\, {d_p}^2}{4C_S D_e} < \frac{1}{|n-\gamma\beta|};\ \gamma = \frac{E}{RT_S};\ \beta = \frac{(-\Delta H_j)D_e C_S}{\lambda\, T_S} \tag{2-5}$$

in which, γ and β are the dimensionless activation energy and dimensionless axial dispersion number, respectively. In Equation (2-5), T_s is the temperature of the catalyst surface in K, and λ denotes the catalyst thermal activity in cal/cm.s.^{o}C. Selection of the flow model is another important matter in the modeling of a catalytic reactor. Dispersion model is considered for non-ideal flow, and plug flow model (PFM) is taken into account for ideal flow behavior [100].

2.4.2.2 Conservation balances

Conservation balances of mass, energy, and momentum are considered for the model development of a catalytic reaction system. In a reaction system, mass balance needs to be written for each component. In the energy balance, the terms of kinetic energy, potential energy, and work might be negligible compared to the reaction heat [97]. Another critical parameter in the modeling of a catalytic reactor is pressure drop since it contributes to the system energy loss. In a catalyst bed, smaller catalyst particles build larger pressure drop unless the bed porosity is increased. Structured beds of catalysts produce less pressure drop, providing the chance of higher operation capacity of reactor [101]. Pressure drop and friction force are usually the main parameters considered in a catalytic reactor modeling. Ergun’s equation is usually used to predict the pressure drop in a catalytic system [97].

2.4.2.3 Constitutive equations

Most chemical conservation equations contain a set of constitutive equations that define fluid properties, thermodynamics, transport, and the reaction kinetic aspects of the system. In the catalytic reactor modeling, there are two constitutive equations related to the reaction kinetics that appear in the mass and energy balance equations. The TBR reaction kinetics can be expressed by the reaction rate and catalyst deactivation rate.

Reaction Rate: Reaction rate expression is one of the most important factors in the reaction system modeling, affecting the model accuracy. This parameter is incorporated into the component mass balance to determine the conversion of individual components (concentration profile). It is also included in the energy balance to consider the heat of reaction and its effect on the reaction system temperature. The reaction rate expression is expressed in the form of empirical models that are obtained utilizing the experimental observations. It is important to provide the operating conditions in the lab so that the reaction rate expression (s) could be used for the practical system whose operating conditions are close to those of the experimental conditions. However, to tackle such an issue, it is suggested deriving the reaction rate expressions using the operating data of the proposed industrial system.

Compared to the gas-solid catalytic reactors, the existence of liquid phase (e.g., in TBRs) imposes more complexity in the mass and energy transfer among the interphases and in the hydrodynamic flow regimes, based on the operating velocities of gas and liquid phases. TBRs hydrodynamic characteristics affect the system variables and parameters such as the heat and mass transfer coefficients, axial and radial dispersion coefficients, flow distribution, and the bed/catalyst external wetting efficiency. To analyze a TBR performance, it is crucial to understand the rate analysis at catalyst particle and reactor scales. The reactor scale rate analysis needs knowledge of mass transfer properties and hydrodynamics of the gas and liquid phases. Operating parameters affecting the process performance can influence the rate processes and TBR's performance. These operating factors are the liquid distribution, bed homogeneity, geometric factors, operating modes (e.g., cocurrent or countercurrent of phases), mass transfer (e.g., gas-liquid, liquid-solid, and intraparticle diffusion), reaction kinetics (e.g., rate equations, catalyst deactivation), and non-isothermal effects (e.g., exothermic or endothermic reactions, and solvent vaporization). The rate analysis at a particle level is controlled by the wetting state (complete or partial) of the catalyst particles. These conditions depend on the phases' velocities, particle size and shape, liquid distribution, and reactant/solvent vaporization. For complete catalyst wetting, the rate at the particle level is described by equations similar to those for the three-phase catalytic reactions, excluding the mass transfer coefficients; the rate depends on the TBR hydrodynamics and operating conditions. The overall rate of reactions with various types of kinetics/mechanisms and the impact of external and intra-particle diffusion can be analyzed by overall effectiveness factor and catalytic effectiveness factor. The overall effectiveness factor includes the impacts from both the intraparticle and the external mass transfer, which is suitable in the performance analysis of TBR [13].

The intrinsic reactions kinetics is usually described by more complicated rate equations (compared to other auxiliary model equations), featuring Langmuir-Hinshelwood (LH) type models; they include additional parameters such as adsorption equilibrium constants. The analytical rate forms for the reaction effectiveness factor using these nonlinear kinetics can be developed by employing generalized Thiele modulus [13].

Numerous industrial TBRs run at low liquid flowrates (<0.5 cm/s), leading to the partial wetting of catalyst particles. At this condition, there are considerable stagnant liquid pockets. Therefore, it is crucial to assess the impact of wetting and stagnant pockets on the reaction rate and reactor performance. There are a few models suggested for the effectiveness factor that consider the effect of partial wetting. Theses models estimate that the overall reaction rate improves under the catalyst particles partial wetting for gas-limited reactions because the liquid-solid mass transfer resistance is eliminated for the dry portion of the particles. Formulating the effectiveness factor for this condition is very challenging and complicated. One suggestion is to consider the factor as the weighted summation of the effectiveness factors for completely dry and completely wetted particles. The proposed equation is different for the cases of the existence of limiting reactant resides in the gas phase compared to that in the liquid phase [85].

Another factor that considerably affects the overall reaction rate in a TBR is the exothermic reactions that impose operation under appreciable temperature gradients in most industrial TBRs. The analysis of non-isothermal impacts is very difficult since the heat liberated from the exothermic reactions can cause incomplete wetting of the catalyst, solvent/reactant vaporization, and gas solubility alteration. The impacts of exothermic reactions in a TBR can be summarized as follows:

- Large/substantial temperature gradients within a catalyst particle, which can result in hotspot formation, hysteresis phenomena, temperature runaway, alteration in reaction rates, catalyst deactivation, and change in the adsorption equilibrium parameters.
- Vaporization of reactants/solvents that can cause incomplete wetting of the bed, distorted patterns of liquid distribution, hotspot formation, and a decrease or increase in the reaction rates.

Therefore, the exothermic reactions influence numerous parameters, which impact conversion, reaction rate, and selectivity in a TBR [13].

Deactivation Rate: Due to complicated mechanisms of catalyst deactivation, estimating the deactivation rate is very intricate. Each catalyst might deactivate at a different rate, based on the undergoing process, operating conditions, and presence of chemicals that poison the catalysts. Determining the deactivation rate requires the provision of expensive experimental setup and chemicals. Moreover, to obtain deactivation rate expressions that are applicable in the industrial process, the experimental operating conditions need to be set up very closely to the industrial conditions.

The catalytic activity can be presented by the number of active sites in the simplest form through the following equation:

$$k_{obs} = N_T k_{intr} \eta \tag{2-6}$$

where k_{obs} stands for the observed rate constant in m/s; k_{intr} refers to the intrinsic rate constant in m/s; N_T is the number of active sites; and η represents the effectiveness factor. Deactivation of catalyst can occur by reduction of the active sites number (N_T reduction), reduction of active sites quality (k_{intr} reduction), and inaccessibility of the pore space (reduction). k_{intr} might change due to the catalyst poisoning. When the impurity in the feed contacts the catalyst, the catalyst chemical structure changes; therefore, the rate constant changes. Generally, sintering and fouling do not influence k_{intr}. Fouling leads to the physical blockage of the catalyst pores and active sites, influencing the catalyst effectiveness and active sites numbers. Figure 2-8 includes a summary of the conditions affecting the catalyst deactivation and k_{obs} [102].

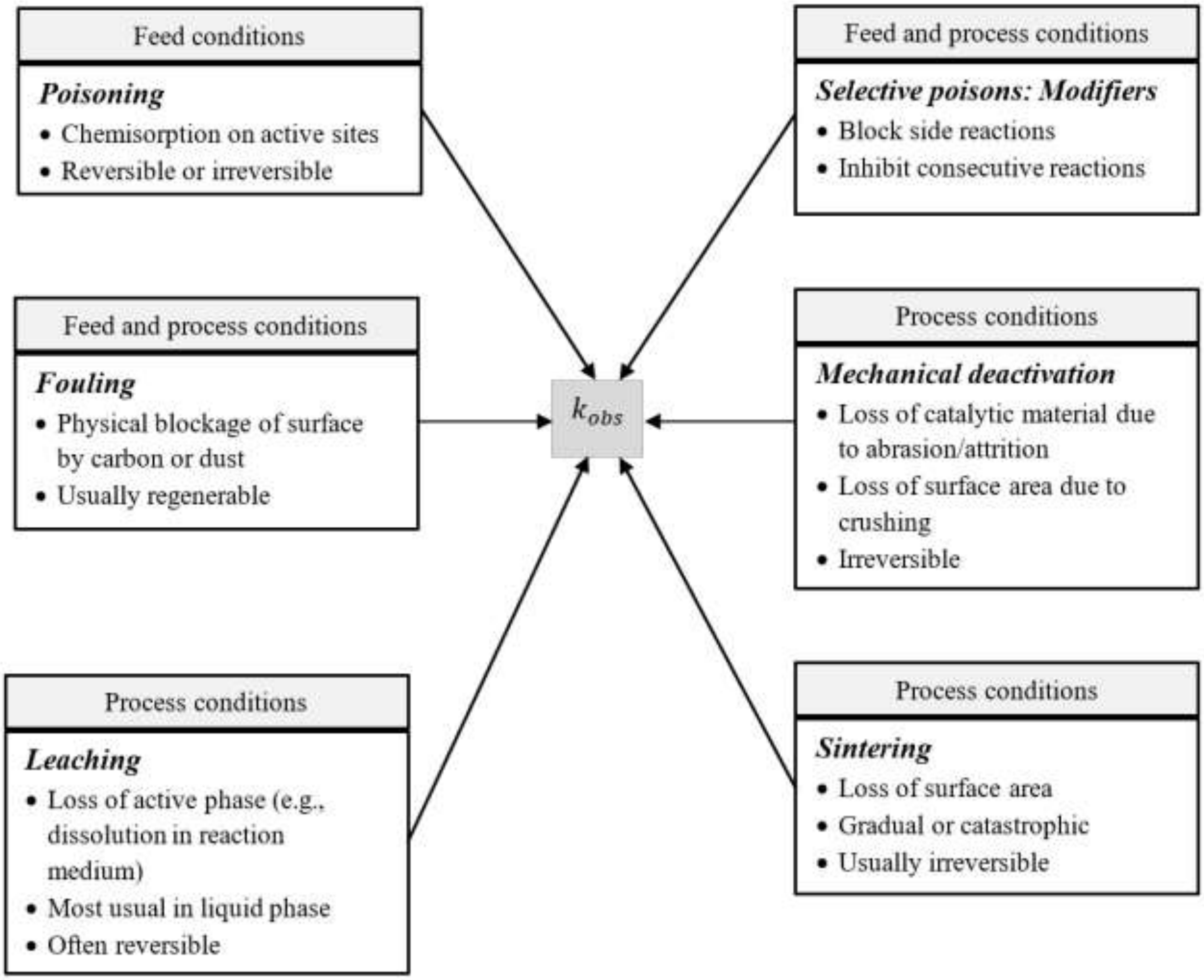

Figure 2-8: Causes and effects of deactivation phenomenon [102].

Deactivation, which is the result of active sites removal from the catalytic surface, can occur by various physical and chemical mechanisms. The three main classifications of deactivation mechanisms are poisoning, coking (or fouling), and sintering [103].

Poisoning is the strong chemisorption of impurities, reactants or products on the catalyst active sites [104]. The description/characterization of a poison, selective or nonselective, is related to the surface nature and the interaction degree of the poison with the surface. The regeneration of the poisoned catalysts depends on the degree of reversibility of the poisoning process. For example, basic organic compounds poison the SiO_2/Al_2O_3 catalyst, which can be used in the isomerization or cracking of hydrocarbons (HCs). The simplest equation representing the poisoning phenomenon of deactivation is a linear relationship between the amount of poison on the catalyst and activity. For instance, poisoning can be described by the following equation for the metal-catalyzed hydrogenation reactions:

$$a = 1 - k_p(1 - f) \tag{2-7}$$

$$f = \frac{Q_{po} - Q_p}{Q_{po}} \tag{2-8}$$

where a is the catalyst activity; Q_p stands for the poison/foulant concentration on the catalyst surface in mol/m^2; Q_{po} refers to the final capacity of the catalyst for the poison/foulant in mol/m^2; and k_p indicates a proportionality constant [103]. Numerous studies have focused on the poisoning mechanisms of catalyst deactivation [105-109].

For reactions consisting of HC molecules, carbonaceous residues can form on the catalyst surface because of the side reactions. In such a case, the catalyst deactivation is originated from the active sites covered by the carbonaceous residues that hinder the reactants access to the active sites. As the amount of coke deposited might be significant, the deactivation can become worse due to the blockage of pores. For example, in Fischer-Tropsch (FT) process using Fe catalysts, carbon is formed on the catalytic surface, which eventually leads to different types of the iron carbides. The coking/fouling kinetics is usually presented by the following equation:

$$C_c = At^{nf} \tag{2-9}$$

where C_c introduces the amount of carbon deposited on the catalyst in kg/kg$_s$; t denotes the time; A is a constant relying on the feedstock, reactor type, and reaction conditions; and nf is a value close to 0.5. There are numerous studies that considered the poisoning mechanisms of catalyst deactivation in the developed models [110-118].

Sintering is normally attributed to the loss of active surface due to the catalyst structural alteration. It is usually a thermally activated process; the thermal sintering is a physical process. Sintering can occur in both unsupported materials (e.g., zeolites or amorphous silica-alumina) and supported metal catalysts. Sintering in the supported metal catalysts takes place due to the agglomeration of the small metal crystallites into the larger ones, leading to lower surface-to-volume ratio. Sintering in unsupported materials might occur due to the failure of the internal pore structure [103]. Sintering is a function of temperature and time. Catalyst activity is a function of both in the proposed empirical relationships, as expressed below:

$$\frac{da}{dt} = k_d a^m \tag{2-10}$$

$$k_d = k_{do} \exp\left(\frac{-E_a}{RT}\right) \tag{2-11}$$

where a is the catalyst activity; k_d is the constant of deactivation rate in 1/s; E_a refers to the activation energy in J/mol; t is the time in s; m denotes the sintering order; R is the universal gas constant in J/mol.K; and T stands for the temperature in K. The catalyst deactivation is considered in the reactor modeling in numerous research studies [119-128].

The ancient proverb that states “an ounce of prevention is worth a pound of cure” applies properly to the catalyst deactivation in numerous industrial processes. A large process plant might need the investment of millions of dollars for the catalyst supply. The economic return on the mentioned investment might rely on the catalyst staying efficient over a duration up to three to five years. This is specifically true for the plants dealing with irreversible or partly reversible deactivation. Table 2-5 gives a summary for various industrial processes that use catalysts, along with their approximate lifetime and parameters influencing their lifetime. The catalyst deactivation can be caused/triggered by more than one mechanism. The catalyst lifetime ranges from a couple of seconds to 15 years. In order to improve the lifetime of the catalyst, the parameters affecting the catalyst deactivation need to be incorporated into the model for the analysis of the deactivation causes. This helps suggest the effective remedies, leading to more efficient process operation [86].

Table 2-5: Common lifetime and parameters influencing the lifetime of some catalysts in important industrial processes [86].

Process Synthesis	Operating conditions		Catalyst		Catalyst lifetime impact	
	T (˚C)	P (atm)	Type	Lifetime (y)	Process	Catalyst parameter impacted
Ammonia	450–470	200–300	Fe/Al_2O_3 with K_2O promoter	10–15	Slow sintering	Activity
Methanation	250–350	30	Ni	5–10	Slow poisoning by S, As, K_2CO_3	Pore blockage and activity
Hydrogenation of acetylene	30–150	20–30	Pd	5–10	Slow sintering	Activity/selectivity and T
Sulfuric acid	420–600	1	(V-K)sulfate/SiO_2,	5–10	Inactive compound formation, pellet fracture, plugging	Activity, mass transfer, and ΔP
Methanol	200–300	50–100	$Cu/ZnO\text{-}Al_2O_3$	2–5	Slow sintering; poisoning by S, Cl, and carbonyls	Activity
Water-gas shift (Low T)	200–250	10–30	$Cu/ZnO\text{-}Al_2O_3$	2–4	Slow sintering and accelerated sintering by poisons	Activity
Water-gas shift (High T)	350-500	20–30	$Fe_3O_4\text{-}Cr_2O_3$	1–4	Slow sintering, pellet breakage due to steam	Activity and ΔP
HDS of hydrocarbons	300–400	30	$CoMO/Al_2O_3$	1–10	Slow coking, poisoning by metal oxides in residuum	Activity, ΔP, and mass transfer
Steam reforming of natural gas	500–850	30	Ni/Al_2CaO_4, $Ni/\alpha\text{-}Al_2O_3$	1–3	Carbon formation, poisoning, and pellet blockage	Activity and ΔP
Partial oxidation of ethylene	200–270	10–20	$Ag/\alpha\text{-}Al_2O_3$ with alkali metal promoter	1–3	Slow sintering, poisoning by Cl, S	Activity and selectivity
Oxidation of butane →maleic anhydride	400–520	1–3	(V-P) oxide with transition metals	1–2	Loss of P; pellet blockage; S, Cl poisoning	Activity and selectivity
Reduction of aldehydes →alcohols	220–270	100–300	Cu/ZnO	0.5–1	Slow sintering, pellet breakage	Activity or ΔP
Oxidation of ammonia	800–900	1–10	Pt-Rh alloy	0.1–0.5	Surface roughness, loss of platinum	Selectivity, fouling by Fe
Oxychlorination of ethylene	230–270	1–10	$CuCl_2/Al_2O_3$	0.2–0.5	Loss by attrition and process disturbances	Activity and fluidized state
Catalytic HC reforming	460–525	8–50	Pt alloys/Al_2O_3	0.01–0.5	Coking, frequent regeneration	Activity and mass transfer
Catalytic cracking of oils	500–560	2–3	Synthetic zeolites	0.000002	Rapid coking, continuous regeneration	Activity and mass transfer

Even though it is impossible to eliminate the catalyst deactivation completely, the damage rate can be considerably reduced in many cases by understanding the underlying mechanisms. The catalyst deactivation process can be mitigated by controlling/modifying the catalyst properties (e.g., porosity and particle size), process operating conditions, feed impurities, contacting methods, and process design. Figure 2-9 lists common methods to eliminate or to mitigate the deactivation phenomenon via the modification in process and/or catalyst [86].

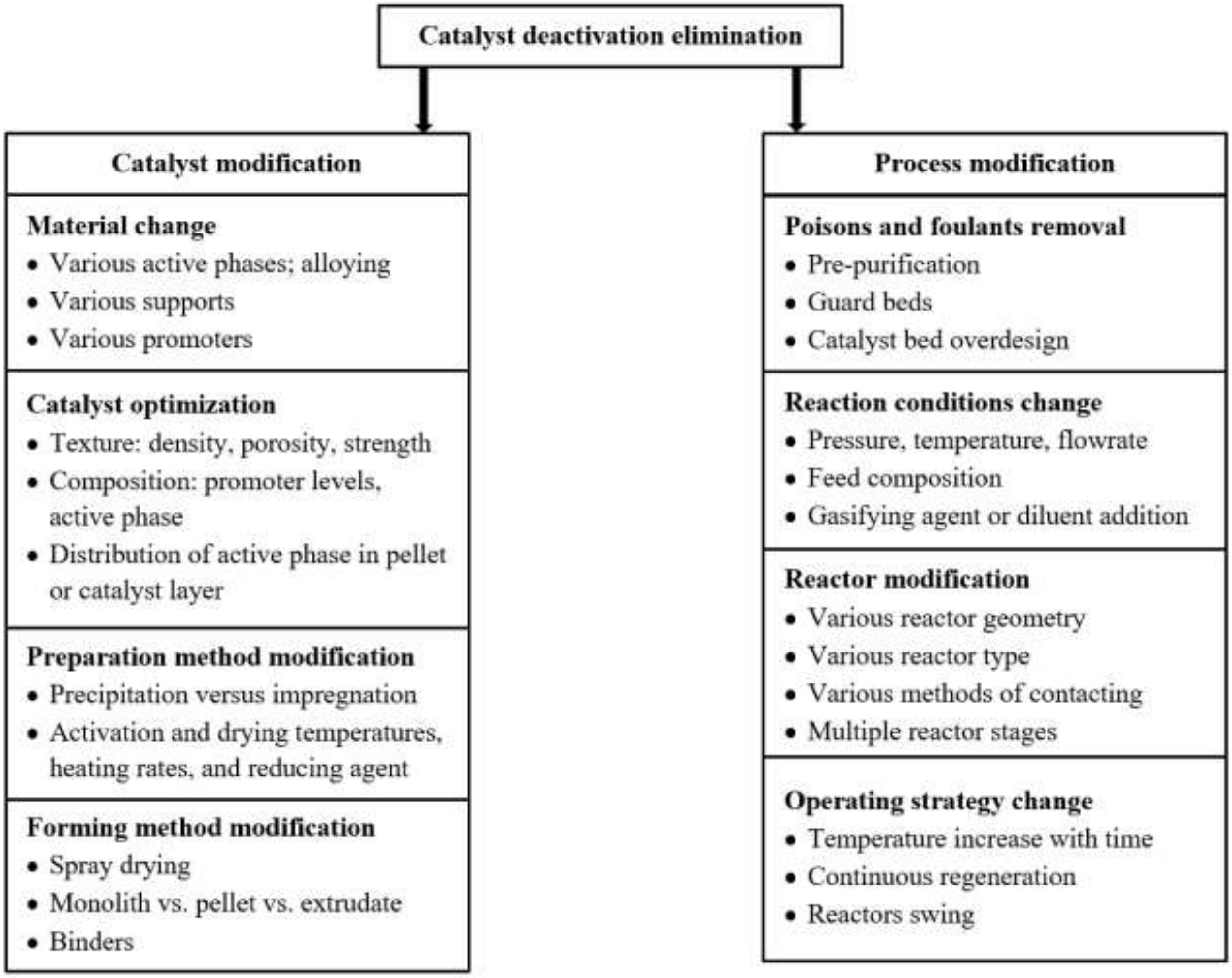

Catalyst deactivation elimination

Catalyst modification

Material change
- Various active phases; alloying
- Various supports
- Various promoters

Catalyst optimization
- Texture: density, porosity, strength
- Composition: promoter levels, active phase
- Distribution of active phase in pellet or catalyst layer

Preparation method modification
- Precipitation versus impregnation
- Activation and drying temperatures, heating rates, and reducing agent

Forming method modification
- Spray drying
- Monolith vs. pellet vs. extrudate
- Binders

Process modification

Poisons and foulants removal
- Pre-purification
- Guard beds
- Catalyst bed overdesign

Reaction conditions change
- Pressure, temperature, flowrate
- Feed composition
- Gasifying agent or diluent addition

Reactor modification
- Various reactor geometry
- Various reactor type
- Various methods of contacting
- Multiple reactor stages

Operating strategy change
- Temperature increase with time
- Continuous regeneration
- Reactors swing

Figure 2-9: Techniques to eliminate/decelerate catalyst deactivation [86].

2.4.3 Model Parameters Calculation

In this phase, the parameters of the model developed should be calculated by empirical correlations. These parameters can be mass and heat transfer coefficients, and gas and liquid holdup. The TBRs are usually operated under high pressure and temperature conditions. It is very important to calculate the parameters considering the real operating conditions. Most correlations have been obtained under atmospheric conditions. Therefore, using these correlations to calculate the model parameters (in TBR modeling) can lead to unrealistic values.

The key aspects in the design, selection, and operation of the pilot plant reactors are transport phenomena including mass and heat transfer [20]. One of the major parameters affecting the TBRs' hydrodynamics is the liquid dispersion resulted from velocity profile variation, capillary pressure gradient, and the interaction forces between phases [129]. Rastegar and Gu [130] developed an empirical correlation to relate the axial dispersion coefficient and Peclet number in fixed-bed reactors (FBRs) as follows:

$$\frac{1}{Pe_P} = \frac{d_P v}{D_{da}} = \frac{0.7D_m}{2R_P v} + \frac{\varepsilon_B}{0.18 + 0.008Re^{0.59}} \tag{2-12}$$

where Pe_P is the Peclet number based on the particle diameter ($\frac{v\, d_P}{D_{da}}$); d_P represents the particle diameter in m; v indicates the interstitial velocity in m/s; D_{da} signifies the axial dispersion coefficient in m^2/s; D_m denotes the molecular diffusion coefficient in m^2/s; R_P resembles the particle radius in m; ε_B is the bed voidage; and Re introduces the Reynolds number ($\frac{2R_P v \varepsilon_B \rho}{\mu}$).

The axial dispersion coefficient in a TBR can also be calculated by the following equation [131]:

$$\frac{u_l d_P}{D_{da,l}} = 13Re_l^{0.4} Ga_l^{-0.333} \tag{2-13}$$

In Equation (2-13), u_l stands for the liquid phase superficial velocity in m/s; Re_l represents the liquid phase Reynolds number ($\frac{\rho_l u_l d_P}{\mu_l}$); and Ga_l symbolizes the Galileo number of the liquid phase ($\frac{\rho_l g d_P}{\mu_l^2}$).

The radial dispersion coefficient can be estimated by the following equation:

$$D_{dr,l} = \frac{d_{PE} u_l}{\varepsilon_l Pe} \tag{2-14}$$

where $D_{dr,l}$ refers to the radial dispersion coefficient in m^2/s; d_{PE} is the equivalent diameter of the catalyst particle in m; ε_l denotes the liquid phase holdup; and Pe stands for the Peclet number, which has been suggested by Mederos and Ancheyta [11] as follows:

$$Pe = 7.58 \times 10^{-3} Re_l^{0.703} \tag{2-15}$$

The following correlation can also be used to predict the radial dispersion coefficient [129]:

$$D_{dr,l} = 0.015\, d_P^{0.5} \varphi^{-0.333} \tag{2-16}$$

where φ denotes the sphericity of the packing.

There are different methods to measure the gas-liquid mass transfer (e.g., dynamic absorption or adsorption, steady-state physical absorption or desorption, absorption with chemical reaction in the liquid, and use of three-phase reactor data). Adequate knowledge on the effective interfacial area (a) and mass transfer coefficient (k) is required to properly understand the mass transfer phenomenon and obtain more accurate correlations. The design of three-phase reactors involves more complexities. The common techniques for the effective interfacial area measurement are photographic method, light-scattering method, and chemical method [31]. There are a number of correlations to predict a and k. The following correlation can be used to determine the effective interfacial area in high pressure TBRs:

$$a = 375\,\left(\frac{g\mu_l^4}{\rho_l\sigma^3}\right)^{0.05}\,\varepsilon_B^{1.4}\left(\frac{\Delta P}{L}\frac{u_l}{\varepsilon_B}\right)^{0.4} \qquad (2\text{-}17)$$

where a is the effective interfacial area in m^2/m^3; g represents the gravitational acceleration in m^2/s; μ_l denotes the liquid viscosity in kg/m.s; ρ_l signifies the liquid density in kg/m^3; σ indicates the surface tension in N/m; ε_B is the bed voidage; and $\frac{\Delta P}{L}$ represents the pressure drop per unit bed height in N/m^3.

Larachi et al. [74] measured $k_{gl}\,a$ in a TBR over a broad range of pressure (3-32 bar), and introduced the following correlation:

$$k_{gl}a = a^o\frac{f'}{f'^o}\left\{k_{gl}^o + \frac{\kappa^2 D_l}{3\varepsilon_B^3}\left(\frac{\mu_g}{\mu_l}\right)^{1/3}\left(a^o\frac{f'}{f'^o}\right)\frac{Ca^2}{\varepsilon_l\varepsilon_l^o}\left(\frac{1}{\varepsilon_l}-\frac{1}{\varepsilon_l^o}\right)\left(1+2.5\left(1-\frac{\varepsilon_l}{\varepsilon_l^o}\right)\right)^2\right\} \qquad (2\text{-}18)$$

in which, superscript *o* denotes the atmospheric condition; f' represents the wetting efficiency; κ is a numerical constant; D_l indicates the diffusion coefficient in the liquid phase; and *Ca* signifies the capillary dimensionless ratio ($\frac{u_l\mu_l}{\sigma_l}$).

Bartelmus [132] introduced the following correlation for the estimation of liquid-solid mass transfer in TBRs (trickling flow):

$$\frac{Sh}{Sc^{1/3}} = \left(1.19 + 0.0072Re_g^*\right)^{1.1}(Re_l^*)^{0.494}Ga^{-0.22} \qquad (2\text{-}19)$$

where *Sh* is the Sherwood number; *Sc* represents the Schmidt number; Re_g^* signifies the interstitial gas Reynolds number ($\left(\frac{G_g d_{PE}}{(1-\varepsilon_B)\mu_g}\right)\left(\frac{\varepsilon_B}{\varepsilon_{ld}}\right)$); Re_l^* stands for the interstitial gas Reynolds number ($\left(\frac{G_l d_{PE}}{(1-\varepsilon_B)\mu_l}\right)\left(\frac{\varepsilon_B}{\varepsilon_{ld}}\right)$); and *Ga* symbolizes the Galileo number. This correlation was originated from a electrochemical technique with spherical packing (3.86 mm) [71]. This correlation has less than 10% error for both free liquid flowrate and the gas continuous flow regime [22].

Satterfield et al. [80] estimated k_{ls} over a wide range of gas and liquid flowrates. For the trickling flow regime (incomplete wetting), the correlation is given below:

$$\frac{k_{ls}d_P}{D}\frac{a_w}{a_P} = 0.815Re_l^{0.822}\left(\frac{\mu_l}{\rho_l D}\right)^{0.333} \tag{2-20}$$

In Equation (2-20), a_w stands for the wetted external area of particles per unit volume of reactor in m^2/m^3; and a_P denotes the external area of particles per unit volume of reactor in m^2/m^3.

Empirical and phenomenological models are developed to predict holdup and pressure drop in TBRs. Empirical models offer acceptable predictions for a specified range of operating conditions. A phenomenological model could be employed to extrapolate outside the range of experimental conditions that are utilized to validate them even if the uncertainties on the conditions cannot be evaluated theoretically and could be constrained by the assumptions made in the model derivation. There is no model or theory that can fully explain the TBRs hydrodynamic behaviors in a simple form. Qi et al. [42] developed a hybrid model to simultaneously predict liquid holdup and pressure drop. The liquid holdup model was developed as follows:

$$\varepsilon_l = \frac{\frac{\Delta\langle P\rangle}{\rho_l g L} - \varepsilon_B\left[\frac{\mu_g\left(J_{gl}-1\right)}{I_g\rho_l g}\langle u_g\rangle_0 + \frac{\rho_g}{\rho_l}\right]}{1 + \frac{\mu_l\left(J_{lg}-1\right)}{I_l\rho_l g}\langle u_l\rangle_0 - \frac{\mu_g\left(J_{gl}-1\right)}{I_g\rho_l g}\langle u_g\rangle_0 - \frac{\rho_g}{\rho_l}} \tag{2-21}$$

The new hybrid model to simultaneously calculate the liquid holdup and pressure in a TBR is listed below [42]:

$$\frac{\Delta\langle P\rangle}{\rho_l g L} + 1 = \left(\frac{\varepsilon_B}{\varepsilon_l}\right)^3\left(\frac{ER_1 Re_l}{Ga_l} + \frac{ER_2 {Re_l}^2}{Ga_l}\right) + f_S\frac{\varepsilon_g}{\varepsilon_l}\left(-\frac{\rho_g}{\rho_l} - \frac{\Delta\langle P\rangle}{\rho_l g L}\right) \tag{2-22}$$

where ER_1 and ER_2 are the first and second Ergun constants; and f_s refers to a shear slip factor, which can be satisfactorily estimated by the following empirical equation for any liquid velocity and geometry:

$$f_S = 7.9422\langle u_g\rangle_0 - 4.0505 \tag{2-23}$$

In a bed of porous particles, the total liquid holdup (ε_l) is the sum of the internal holdup (liquid hold inside the catalyst pore) and external holdup, which is divided into a static (or residual) holdup (ε_{ls}) and a dynamic (or free draining) holdup (ε_{ld}). Generally, ε_{ls} is affected by the physical properties of the liquid, particle size and shape, and the contacting efficiency (wettability). Correlations considering ε_{ls} and ε_{ld} have more robust theoretical basis as ε_{ld} is impacted by the operating conditions [31]. van Swaaij [133] claimed that ε_{ls} can be calculated by the following equation:

$$\varepsilon_{ls} = \left(\frac{\rho_l g d_P^2}{\sigma}\right)^{cn} \tag{2-24}$$

The term in the parentheses is the Eötvös number, and *cn* changes, depending on the experimental condition. The static liquid holdup can also be estimated by the following correlation as a function of Bond number ($B_n = \frac{\rho_l g}{\sigma a_P^2}$), as shown below [31]:

$$\frac{\varepsilon_{ls}}{\varepsilon_B} = 3.7 \times 10^{-2}\left(\frac{\rho_l g}{\sigma a_P^2}\right)^{cm} \tag{2-25}$$

For B_n<1, cm is -0.07, and for B_n>1, cm is -0.65.

220 holdup experiments were conducted in a trickle flow regime and ε_{ld} was calculated. The following correlation was developed [75]:

$$\varepsilon_{ld} = 3.8\left(\frac{\rho_l u_l d_P}{\mu_l}\right)^{0.55}\left(\frac{d_P^3 \rho_l^2 g}{\mu_l^2}\left(1+\frac{\Delta P}{\rho_l g L}\right)\right)^{-0.42}\left(\frac{a_P d_P}{\varepsilon_B}\right)^{0.65} \tag{2-26}$$

Effective thermal conductivity indicates the bed average thermal conductivity in the presence of liquid and gas phases in the radial as well as axial directions. The majority of the previous investigations have performed on the effective radial thermal conductivity due to the greater temperature gradients in the radial direction compared to the axial direction [13]. The catalyst bed thermal conductivity is always improved upon an increase in the liquid flowrate. The gas flowrate is dependent on the flow regime. However, gas flowrate has a minor effect on the bed conductivity. An increase in the gas flowrate decreases the bed thermal conductivity in pulse flow regime, and increases it in bubble flow regime. Moreover, the bed thermal conductivity increases with increasing the particle diameter. In LIR, liquid viscosity has a minor impact on the bed thermal conductivity. The wall heat transfer coefficient enhances with increasing the liquid flowrate. This coefficient is almost independent of gas flowrate, but it significantly declines in pulse flow regime at high gas flowrates [134]. To investigate the transport phenomena, especially heat transfer in FBRs, two aspects are important: particle scale and bed scale. To analyze the bed scale, the adiabatic or heating/cooling operations are considered. To evaluate the particle scale, the utilization of a solid-fluid heat transfer coefficient can properly describe the heat transfer. In a TBR, it is usually assumed that a liquid film surrounds the particles; however, this assumption needs to be revised for low liquid flowrates because of non-uniform wetting of the particles surface [135]. Knowledge on the bed inside heat transfer capacity, which is usually quantified through an effective thermal conductivity, is of high importance. Thermal conductivity is generally dependent on the particle size and the bed/tube diameter. The impact of the bed diameter is demonstrated in terms of the aspect ratio (*ar* =bed diameter/particle diameter). The wall effects are almost vanished at large values of aspect ratio. The radial thermal conductivity increases with an increase in the liquid flowrate [135]. Mariani et al. [136] suggested the following correlation for the calculation of the effective radial thermal conductivity:

$$\lambda_{er} = \lambda_{eo} + 0.281\lambda_l\left(1 + 0.00531Re_g\right)Re_l^{0.81}Pr_l\,;(ar > 8) \tag{2-27}$$

in which, λ_{er} is the effective radial conductivity in W/m.K; λ_{eo} symbolizes the stagnant effective radial thermal conductivity (stagnant contribution); λ_l represents the fluid thermal conductivity in W/m.K; and Pr indicates the Prandtl number.

The wall heat transfer (h_w) can be estimated by the following equation [136]:

$$Nu_w = Nu_{wo} + 0.471\,Pr_l^{0.33}Re_l^{0.65}\,;(ar > 15;\ Re_l < 40) \tag{2-28}$$

Nu_{wo} (Nusselt number without fluid flow) can be estimated by the equation proposed by [137].

The overall heat transfer coefficient (h_t) can be estimated by the following correlation [136]:

$$Nu = \frac{h_t d_P}{k_l} = \left[3.87 - 3.77exp\left(\frac{-1.37}{ar}\right)\right]Re_l^{0.643}Pr_l^{0.333}\,;(ar > 4.7; 5.4 < Re_l < 119.6) \tag{2-29}$$

2.4.4 Model Solution and Validation

Differential equations (DEs) have a significant role in the mathematical modeling. In the engineering applications, only a limited number of DEs can be solved analytically. DEs are divided into ordinary differential equations (ODEs) and partial differential equations (PDEs). ODEs are categorized as initial value problems (IVPs) and boundary value problems (BVPs). This categorization relies on the specification of the location of extra conditions [138]. Selection of a proper set of boundary conditions and/or initial conditions is a very important step in the formulation of the DEs while developing a mathematical model. BVPs can be solved utilizing shooting method, finite difference method, collocation method, and finite element method. The IVPs can be solved employing the explicit Euler method, the midpoint method, and Runge-Kutta method [138]. Development of the models for the majority of the physical/process systems leads to the PDEs [139]. Several phenomena in process engineering rely on space and time, and a mathematical model usually needs more than one independent variable to define the state of a system (i.e., PDEs). The processes involving chemical reaction, fluid flow, heat transfer, and population dynamics are usually described by PDEs. Numerical methods are required for the solution of the models developed for the practical engineering systems [138]. PDEs classification is crucial since methods of solution are mostly employed based on the specific class of PDEs. PDEs classification can be done by the number of variables. Moreover, a difference between linear and non-linear methods is of importance for the selection of model solution technique. Some solution techniques for PDEs are method of lines, finite element method, finite difference method, weighted residual method, finite volume method, and adaptive grid method [139]. Solution of PDEs problems by the numerical approximation is one of the difficult fields in the numerical analysis. There is some software that can be used to solve set of PDEs, such as Mathematica, Maple, and MATLAB®. After developing the models for the TBRs, the popular mathematical techniques to solve the set of equations are finite difference method (FDM), finite element method (FEM), Runge-Kutta method (RK method), and orthogonal collocation method (OCM) (Table 2-6).

The model validation is to determine whether the results of the model accurately represent the real process with the satisfactory exactness for the definite extent of conditions. Verification is to assure that the model solution is performed correctly [138]. The validation is conducted by comparing the model results with the experimental/real data [140]. Validation study is usually carried out considering the effect of the most effective parameter (s) on the process performance. For example, in a catalytic system, the validation study parameter is the concentration of determining components (e.g., impurity concentration). Poor model results can be due to the errors in the problem formulation, the development of inaccurate model, incorrect data on physical properties, the errors caused by the selection of the numerical technique, and lack of convergence in the simulations [138].

2.4.5 Results Analysis

Sensitivity analysis determines the degree of effect of variables on the results. For example, disturbing a specific parameter can show its influence on a model parameter or variable such as the estimated reactor volume [138]. In addition to the sensitivity analysis, the accuracy of the model can be examined by the incorporation or elimination of some terms involved in the developed model (e.g., the axial dispersion term or the accumulation term) [138]. The sensitivity analysis results depend on the input variables, formulation, parameters, and the modeling endeavor goals. The problems of the process, which are emerged into the objectives of investigation, are usually addressed/analyzed by the sensitivity analysis. Then, the obtained results need to be carefully discussed/scrutinized through the evaluation of the values fluctuation with focusing on the vital operating parameters influencing the process performance.

2.5 Modeling and Simulation of TBRs

The meticulous modeling of a catalytic reactor is highly challenging since numerous transport and reaction phenomena occur simultaneously in the reactor. Uncertainties in catalysis heterogeneity, catalysts random packing, fluid flow, and transport parameters elevate the complexity of the model. Moreover, the improvement of numerical techniques efficiency is another challenging issue. Therefore, approximation and trade-offs are very crucial in the development of a reactor model [141].

The reaction(s) rate analysis needs to be integrated with that of the proposed reactor model to estimate a TBR performance. A considerable number of TBR modeling studies have assumed isothermal condition with the plug flow pseudo-homogeneous model, or with the plug flow heterogeneous model. Some investigations included the liquid maldistribution and nonideality by employing an axial dispersion model. The PFM is the most employed model for the modeling of a TBR while the axial dispersion model is the most fundamental one, reflecting the differential mixing in TBRs by inclusion of axial dispersion in the

PFM. Axial dispersion model entails only one parameter (axial dispersion coefficient), which is usually described as the Peclet number. Mixing cell model is also used to analyze the TBR performance. It considers flow through a series of mixing cells in the bed. The flow is described by the number of cells (in series) and the liquid holdup. This model can be useful in complicated multistep reactions. The system encountering significant liquid stagnancy might be modeled by a cross flow model. The model assumes that liquid holdup can be divided into stagnant pockets and dynamic flowing in plug flow with exchange between them. This model needs the parameters of fraction of plug flow, the external liquid holdup, and the exchange coefficient. The accuracy of the cell model can be improved by incorporating radial porosity distribution [13].

A few empirical models were formulated at early phases of development to assess the conversion in a TBR where the reaction rate was considered to be proportional to the wetted portion of the catalyst particles and the gas phase concentration (in most HDT processes). These models were mainly developed to evaluate the effects of operating parameters on conversion [13]. The empirical proposed models are PFM [142], axial dispersion model [143], external holdup model [144], and effective wetting model [144]. Although these models are helpful as a primary estimation, they do not give detailed/accurate knowledge on the reaction kinetics, heat and mass transfer, and mixing influences. They are not suitable choices/models for convoluted multistep reactions. TBR performance depends on the numerous phenomena, taking place in sequential or parallel. Therefore, these phenomena should be considered to understand their impacts on TBR overall performance in terms of selectivity, conversion, and temperature profile. For instance, intraparticle mass and heat transfer steps are to be considered. TBRs usually operate under adiabatic condition [145]. In case of exothermic reaction in a TBR, it was verified that feeding a reactant in a periodic fashion (e.g., employing pulsing and stop flow procedure) has the advantages of overall reaction rate enhancement, better control of temperature, and greater productivity [13].

Plug flow is a simple and ideal assumption of a fluid flow, where the elements of fluid move with a uniform velocity together in parallel streamlines. It is a sole transport mechanism considered in a plug flow reactor (PFR) model. The validity of plug flow assumption can be approximated by the comparison (ratio) of catalyst particle diameter and the reactor diameter (Table 2-4). Due to the radial alteration in flow velocity and mixing impacts resulted from the existence of packing, flow in a packed bed deviates from the ideal flow mechanism. In this case, a 1D model with axial mixing consideration is a more suitable choice. Moreover, it is an oversimplification to assume that there is a uniform temperature in the catalyst bed cross section. The mixing in axial direction is tallied by superimposing an effective transport mechanism (effective diffusivities and conductivities) on the overall transport by plug flow. In 1D model, resistances to mass and heat transfer in the radial direction are neglected, and uniform conversion and temperature in the cross section are predicted. This is an oversimplification when there is a significant heat effect imposed by the reactions. Then, a 2D pseudo-homogeneous model is more justifiable [97].

The disparity between the conditions on the catalyst particle and those on the fluid results in the significant differences while employing the basic 1D pseudo-homogeneous model. It means that the system might experience multiple steady states (stability problem: changes in the temperature and concentration profiles in the particle and in the film); the transient calculations should be performed to develop a reliable model. In this case, a 1D heterogeneous model is more suitable. When the resistance to heat and mass transfer inside the particle is significant, the reaction rate is not consistent across the particle. In this case, a 1D heterogeneous model with intraparticle consideration/gradients needs to be chosen. Analytical solutions are available for isothermal particles and first order reversible reactions. The assumption of isothermal particles is valid when there is a significantly exothermic reaction. In this case, the major resistance in the film around the particle is for heat transfer, and the major resistance inside the particles is for mass transfer. Effectiveness factor is usually used in case of gradients existence inside the particles. The effectiveness factor depends on the local condition, which is introduced by Thiele modulus. The solid and stagnant films contribute to a minimum 25% in the radial heat flux even for common industrial flowrates. Thus, 2D heterogeneous model is preferred. To estimate heat transfer more accurately across the catalyst bed, the equations representing the solid phase should be developed for the total cross section of the bed instead of being limited to just one single particle, that is generally used in the literature [97].

Pseudo-homogeneous models contain one set of governing equations for the pseudo-single reactor phase. Mass/component balance equation for a dynamic (unsteady state) fixed-bed model is given below [141, 146, 147]:

$$\varepsilon_B \frac{dC_i}{dt} = D_{da}\frac{d^2C_i}{dz^2} + D_{dr}\left(\frac{\partial^2 C_i}{\partial r^2} + \frac{1}{r}\frac{\partial C_i}{\partial r}\right) - \frac{(udC_i)}{dz} + \sum_{j=1}^{k}\rho_B\,\eta_j\,r_j\,a(t) \tag{2-30}$$

where *i* and *j* are the index of components and reaction index, respectively; ε_B stands for the void fraction of the bed; D_{da} and D_{dr} introduce the axial and radial mass dispersion coefficients in m^2/s, respectively; *z* and *r* symbolize the axial and radial coordinates in m, respectively; *C* represents the concentration in $kmol/m^3$; *t* denotes the time in s; *u* indicates the superficial velocity in m/s; ρ_B resembles the bulk density of bed in kg/m^3; r_j indicates the rate of reaction in $kmol/kg_s.s$; η_j signifies the catalyst effectiveness factor; and *a* (*t*) reveals the catalyst activity.

Energy balance equation for a dynamic pseudo-homogeneous model of a fixed-bed reactor is provided below:

$$\begin{aligned}\left(\varepsilon_B(\rho_g C_{p,g} + \rho_l C_{p,l}) + (1-\varepsilon_B)\rho_B C_{p,s}\right)\frac{\partial T}{\partial t} &\\ = \lambda_a\frac{\partial^2 T}{\partial z^2} + \lambda_r\left(\frac{\partial^2 T}{\partial r^2} + \frac{1}{r}\frac{\partial T}{\partial r}\right) - \varepsilon_B(\rho_g C_{p,g} + \rho_l C_{p,l})\frac{\partial (uT)}{\partial z} &\\ + \sum_{j=1}^{k}\rho_B\,(-\Delta H_j)\eta_j r_j a(t) + \frac{4U}{d_R}(T_w - T) &\end{aligned} \tag{2-31}$$

where the subscripts g, l, and s denote the gas phase, liquid phase, and solid/catalyst phase, respectively; ρ is the density of the phase in kg/m^3; C_p represents the specific heat capacity of the phase in J/kg.K; T indicates the temperature in K; λ_a and λ_r signify the axial and radial thermal conductivity in W/m.K, respectively; U symbolizes the overall heat transfer coefficient at wall in W/m^2.K; d_R is the radius of reactor in m; ΔH indicates the heat of reaction in J/mol; and T_w stands for the reactor wall temperature in K.

To solve the above equations (Equation (2-30) and Equation ((2-31)), one initial condition (IC) and four boundary conditions (BCs) for each equation are required. The mentioned boundaries are summarized below:

$$\text{IC: } t=0;\ C_i = C_i^{ss};\ T = T^{ss};\ a = 1; \tag{2-32}$$

$$\text{BC.1: } z=0;\ u(C_i^0 - C_i) = -D_{da}\frac{\partial C_i}{\partial z};\ \varepsilon_B(\rho_g C_{p,g} + \rho_l C_{p,l})u(T^0 - T) = -\lambda_a \frac{\partial T}{\partial z} \tag{2-33}$$

$$\text{BC.2: } z=L;\ \frac{\partial C_i}{\partial z} = 0;\ \frac{\partial T}{\partial z} = 0 \tag{2-34}$$

$$\text{BC.3: } r=0;\ \frac{\partial C_i}{\partial r} = 0;\ \frac{\partial T}{\partial r} = 0 \tag{2-35}$$

$$\text{BC.4: } r = d_R;\ \frac{\partial C_i}{\partial r} = 0;\ -\lambda_r \frac{\partial T}{\partial r} = h_w(T - T_w) \tag{2-36}$$

In the boundary conditions stated above, the superscripts SS and 0 denote the steady state and the inlet conditions of the reactor, respectively; L is the reactor bed length in m; and h_w signifies the heat transfer coefficient at wall in W/m^2.K.

A dynamic 2D heterogeneous TBR model is developed considering mass balance for each component at each phase as follows:

Gas Phase:

$$\varepsilon_g \frac{\partial C_{i,g}}{\partial t} = D_{da,i,g}\frac{\partial^2 C_{i,g}}{\partial z^2} + D_{da,i,g}\left(\frac{\partial^2 C_{i,g}}{\partial r^2} + \frac{1}{r}\frac{\partial C_{i,g}}{\partial r}\right) - \frac{(u\partial C_{i,g})}{\partial z} + K_{gl,i}\xi_{gl}\left(\frac{C_{i,g}}{H_i} - C_{i,l}\right) \tag{2-37}$$

Liquid Phase (Gas component):

$$\varepsilon_l \frac{dC_{i,l}}{dt} = D_{da,i,l}\frac{\partial^2 C_{i,l}}{\partial z^2} + D_{da,i,l}\left(\frac{\partial^2 C_{i,l}}{\partial r^2} + \frac{1}{r}\frac{\partial C_{i,l}}{\partial r}\right) - \frac{\left(u\partial C_{i,l}\right)}{\partial z} + K_{gl,i}\xi_{gl}\left(\frac{C_{i,g}}{H_i} - C_{i,l}\right) - k_{i,ls}\xi_{ls}\left(C_{i,l} - C_{i,s}^{S}\right) \tag{2-38}$$

Liquid Phase (Non-gas component):

$$\varepsilon_l \frac{dC_{i,l}}{dt} = D_{da,i,l}\frac{\partial^2 C_{i,l}}{\partial z^2} + D_{da,i,l}\left(\frac{\partial^2 C_{i,l}}{\partial r^2} + \frac{1}{r}\frac{\partial C_{i,l}}{\partial r}\right) - \frac{\left(u\partial C_{i,l}\right)}{\partial z} - k_{i,ls}\xi_{ls}\left(C_{i,l} - C_{i,s}^{S}\right) \tag{2-39}$$

Solid Phase:

$$\varepsilon_P(1 - \varepsilon_B)\frac{\partial C_{i,s}^{S}}{\partial t} = k_{i,ls}\xi_{ls}\left(C_{i,l} - C_{i,s}^{S}\right) \pm \sum_{k=1}^{3} r_k\,\eta_k\rho_B a(t) \tag{2-40}$$

In the mass balance equations above, K is the overall mass transfer coefficient in 1/s; ξ represents the specific surface area of the phase interface in m^2/m^3; the subscripts *gl* and *ls* symbolize the gas phase to liquid phase and the liquid phase to solid phase, respectively; the superscript S indicates the catalyst surface; ε_P signifies the catalyst particle porosity; H is the Henry's constant in bar.m^3/kmol; and k is the mass transfer coefficient in m/s.

The energy balance should be written for each phase in a three-phase TBR reactor as follows:

Gas Phase:

$$\varepsilon_g C_{p,g}\rho_g \frac{dT_g}{dt} = \lambda_g \frac{d^2 T_g}{dz^2} + \lambda_g\left(\frac{\partial^2 T_g}{\partial r^2} + \frac{1}{r}\frac{\partial T_g}{\partial r}\right) - \rho_g C_{p,g}\frac{\partial\left(uT_g\right)}{\partial z} - h_{gl}\xi_{gl}(T_g - T_l) \tag{2-41}$$

Liquid Phase:

$$\varepsilon_l C_{p,l} \rho_l \frac{\partial T_l}{\partial t} = \lambda_l \frac{\partial^2 T_l}{\partial z^2} + \lambda_l \left(\frac{\partial^2 T_l}{\partial r^2} + \frac{1}{r} \frac{\partial T_l}{\partial r} \right) - \rho_l C_{p,l} \frac{\partial (u T_l)}{\partial z} + h_{gl} \xi_{gl} \big(T_g - T_l \big) - h_{ls} \xi_{ls} (T_l - T_s) \tag{2-42}$$

Solid Phase:

$$\varepsilon_p (1 - \varepsilon_B) \rho_B C_{p,s} \frac{\partial T_s}{\partial t} = h_{ls} \xi_{ls} (T_l - T_s) + \rho_B \sum_{j=1}^{j=k} r_j \, \eta_j a(t) \, (-\Delta H_j) - \frac{4U}{d_R} (T_s - T_w) \tag{2-43}$$

where h is the heat transfer coefficient in W/m^2.k.

To solve the energy balance equations, one IC and four BCs are required which are listed below:

IC: $t=0$; $C_i = C_i^{ss}$; $T = T^{ss}$; $a = 1$; (2-44)

BC.1: $z=0$; $u\big(C_{i,f}^0 - C_{i,f}\big) = -D_{da} \frac{\partial C_{i,f}}{\partial z}$; $\rho_f C_{p,f} u \, (T - T^0) = -\lambda_a \frac{\partial T_f}{\partial z}$ (2-45)

BC.2: $z=L$; $\frac{\partial C_{i,f}}{\partial z} = 0$; $\frac{\partial T_f}{\partial z} = 0$ (2-46)

BC.3: $r=0$; $\frac{\partial C_{i,f}}{\partial r} = 0$; $\frac{\partial T_f}{\partial r} = 0$ (2-47)

BC.4: $r = d_R$; $\frac{\partial C_{i,f}}{\partial r} = 0$; $-\lambda_f \frac{\partial T}{\partial r} = h_w (T_f - T_w)$ (2-48)

where the subscript *f* denotes the fluid phase.

2.5.1 Incorporation of VLE Calculations in TBRs Modeling

Advanced knowledge on vapor-liquid equilibrium (VLE) impacts on the TBR performance can provide a better understanding and control of hydrotreating processes. This knowledge could be used to predict deviations from the optimal operating conditions. It is a well-established knowledge that a perfect operating condition for a TBR encompasses plug flow establishment, minimum wall effects, and fully wetted catalyst to improve the contact among the reactants [148]. To fulfil a realistic process simulation, reliable VLE models in the hydrotreating reactors are required as it will predict the distribution of components in different phases. The VLE has a significant impact on the heat balance since the HC components absorb the heat generated by the chemical reactions. Therefore, VLE cannot be ignored in the modeling, simulation, and design of processes. However, the assumption of negligible vaporization is made in the modeling of hydrotreating reactors for simplicity [149]. Since the hydrogenation reactions are usually exothermic, temperature control is a serious concern. To address such an issue, more than one catalyst bed is employed with inter-bed quenching along with the recycled hydrogen addition. Since aromatics saturation is governed by the equilibrium state, the balance between the aromatic saturation and desulfurization reactions is required via detailed design of catalyst bed and proper establishment of TBR operating conditions [150]. Since there are significant amounts of HCs in the vapor phase, particularly at lower pressures, the VLE calculations at higher temperatures and greater ratios of gas to oil are to be considered for more reliable modeling and simulation of hydrotreating processes. This consideration is intensified taking into account that TBRs usually run under adiabatic mode of operation which results in the temperature increase, leading to more complicated VLE conditions and more dramatic changes in compositions, vapor and liquid flowrates, and thermophysical properties [151]. High pressure and temperature together with high flow ratio of hydrogen to HC can cause a change in the VLE and dry out portions in the catalyst bed [152]. Vaporization with exothermic reaction was reported to be much faster than that without any exothermic reactions (almost 500% higher) at the same temperature, pressure, and composition [153].

A comprehensive literature review was conducted on the VLE of H_2-HC system by Chávez et al. [154], with focus on reactor modeling. Consideration of a reliable VLE model in reactor modeling is important since it influences the conversion magnitude, relying on the operating conditions and feed properties. Design and simulation calculations of hydrotreating processes require hydrogen solubility. The solubility is commonly obtained by equations of state (EOSs); such calculation requires binary interaction parameters for different component pairs. The VLE investigations for systems involving heavy crudes are limited since their experimental endeavors are more difficult for the oil sample characterization and reliable mass balances data obtainment [154]. The studies revealed that the consideration of VLE in reactor model results in the higher hydroprocessing reaction conversions compared to not including it into the model [154]. For instance, considering VLE in the waxes hydrocracking model enhanced the model prediction while changing pressure, temperature, and weight hourly space velocity (WHSV) [155]. Some studies concluded that hydrogen solubility improves when the temperature and pressure increase. The operating conditions, such as temperature and residence time, should be carefully selected to measure the accurate VLE data since the feed thermal cracking might result in the unreliable findings. Moreover, it was found that more details on pseudo-components could lead to better and more reliable VLE predictions. Grason-Streed model is commonly used for the simulation of H_2-HC equilibrium, which has poor performance for the hydrocarbon mixtures consisting of heavy components, and at the pressures greater than 200 bar. The solubility of hydrogen depends on the type of HC. Also, it was reported in hydrotreating that by increasing the hydrogen flowrate and temperature, and by decreasing pressure, vaporization from the oil phase is increased. To decrease the error between the experimental data and VLE predictions, optimal estimation of the interaction coefficients for H_2-pseudo-components is required [154]. Alvarez-Majmutov and Chen [149] studied the effect of VLE calculations on the TBR, for the HDS and HDA reactions, using 1D PFM and adiabatic reactor assumption. Peng–Robinson (PR) EOS was considered as the phase equilibrium thermodynamic model. Densities and MWs were estimated with the correlation based on the boiling points. The binary interaction coefficients between HC pseudo-components and hydrogen were determined by using experimental data. The operating conditions were 330–340 ^{o}C, 5–9 MPa, H_2/oil ratio of 5000 scf/bbl, and liquid hourly space velocity (LHSV) of 1.5 h^{-1} in a reactor with 3.5 m diameter and 12 m length. The model without VLE consideration predicted a greater temperature rise compared to the model with VLE consideration. The model with VLE consideration predicted a constant decrease in liquid flowrate through the bed while the model with the assumption of non-vaporization forecasted a constant liquid flowrate along the bed. Furthermore, the model without VLE predicted a slightly higher HDS conversion and a lower HDA conversion compared to those calculated by the model with VLE. In general, ignoring VLE in the reactor model leads to unrealistic representation of the hydroprocessing [149]. Mijatović et al. [152] conducted a modeling and simulation study on a TBR for hydrotreatment of straight run gas oil (SRGO) mixed with fluid catalytic cracking of naphtha and light crude oil (FCC N-LCO). They developed a 1D pseudo-homogeneous model employing phase distributions resulted from the VLE calculations for the system of H_2, CH_4, and SRGO mixed with FCC N-LCO. The catalyst bed was considered as sections of wet and dry out. Kinetic equations of Hougen-Watson were utilized for different groups of sulfur compounds. To develop the model, industrial test runs were performed in an industrial adiabatic reactor with 2.135 m diameter and 5.31 m long packing with commercial trilobe shape Co-Mo/γ-Al_2O_3 catalysts (1.5 mm). The reactor pressure was 40 bar, and the feed inlet temperature was increased from 327 to 334 ^oC. The catalyst deactivation was not considered. Components (H_2, CH_4, n-$C_{12}H_{26}$, n-$C_{18}H_{38}$, tetraline, and phenanthrene) distribution and thermodynamic properties were calculated from PR EOS. ChemSep Modeling Separation Processes software was used to obtain the PR binary interaction parameters from DECHEMA, PR Parameters, and interaction parameter data (IPD). The results implied that the wetting efficiency increases with increasing the LHSV. When the inlet temperature increased, sulfur conversion remained nearly constant and the outlet temperature and aromatics conversion were increased. Model simulations could predict the significant impact of pressure and hydrogen impurity on the sulfur conversion. Moreover, a temperature increase (up to 353 ^oC) from low to average pressure (40–60 bar) together with using pure hydrogen did not decrease the sulfur content ultra-low sulfur diesel (ULSD) levels while processing light cycle oil mixtures. To attain a very low concentration of sulfur, pressure of about 100 bar and nearly pure H_2 were required [152]. Munteanu and Chen [148] included the VLE calculations in the HDT process modeling of heavy distillate. They discussed on the conditions required for the ideal operating conditions settlement. 29 HC pseudo-components extracted from the simulation distillation data were used for the flash calculation. Empirical correlations were employed to estimate MW distributions, density, and interaction coefficients between HC pseudo-components and hydrogen. The used pilot reactor had 2.54 cm diameter, catalyst particles size of 1.5 mm×5 mm, pressure of 50–90 bar, temperature of 350–420 ^{o}C, LHSV of 1.5 h^{-1}, and gas/oil ratio of 500, 800, and 1000 NL/kg. They concluded that heavy gas oil (HGO) thermal cracking at temperatures higher than 390 ^{o}C, and the light HCs (C_1–C_6) in the exit gases increase with an increase in the temperature. Pressure increase was required to maintain liquid phase plug flow when the temperature increased. In cases of increased pressure or decreased temperature, an enhanced gas-to-oil ratio was required to maintain the liquid phase plug flow. An increase in temperature needed longer catalyst bed to hold liquid phase plug flow. Either lower temperature or higher pressure (or both) were required for obtaining higher conversion and ensuring liquid phase plug flow. At low pressures, a greater LHSV was needed to maintain the plug flow [148]. Chen et al. [151] developed a 1D steady state PFM at included VLE calculation to predict the industrial HDT TBR performance. VLE calculations were performed using PR EOS at all nodes inside the TBR bed. The reactor was 9 m long and 3.5 m wide. The operating conditions were LHSV of 1.5 h^{-1}, gas/oil ratios of 600–900 NL/kg, temperature of 340–380 ^{o}C, and pressure of 40–70 bar. The reactor feed was light gas oil (LGO). VLE data were obtained by the flash experiments with various types of middle distillates at different pressures and temperatures. The data were used to calculate the interaction coefficients between HC pseudo-components and hydrogen. The temperatures predicted by the model without VLE were about 1 ^{o}C less than those predicted by the model with the VLE, and the HDA conversion without VLE was slightly lower than that with VLE. Furthermore, the HDS conversion without VLE was much lower than that with VLE. It was also found that the temperature gradient is the highest at the minimum temperature of 340 ^{o}C, and it increases only around 6 ^{o}C at the maximum temperature of 380 ^{o}C. When the gas-to-oil ratio increased, it slightly increased the HDA conversion without any significant effect on the HDS conversion. Pressure increase led to the temperature increase, significant improvement in the HDA conversion, and considerable enhancement in the HDS conversion only in the first half of the reactor bed. Finally, consideration of VLE in the TBR modeling can improve the accuracy of the model prediction [151]. Chen et al. [156] studied the hydrotreater performance considering VLE for the different middle distillate feeds. The TBR was 2.54 cm wide and 100 cm long, filled with commercial NiMo/Al_2O_3 catalysts (extrudates with 1.6 mm diameter and 5 mm length). The pressure and temperature of the hydrotreater were controlled at the range of 50–100 atm and 250–400 ^oC, respectively. The ratio of gas to oil was set at 1000 NL/kg. The middle distillates included LCO from FCC process, white oil, and a blend of white oil and LCO. They concluded that oil mole fraction in the vapor phase significantly increases with decreasing pressure and increasing temperature. The feedstock volatility was influenced by MW, boiling point, and oil aromatics content. It also revealed that to maintain the plug flow of the liquid LCO, less gas/oil ratio, greater pressure, smaller diluent particles, or longer bed of catalyst are required in comparison with the LGO feed [156]. de Jong [157] studied vacuum gas oil (VGO) hydrocracking possibility at high temperature (e.g., 450 ^oC) and at average pressure of hydrogen (e.g., 30 bar) employing catalysts having little or no activity. They evaluated the VLE effect on coke deposition in TBR. The Kuwait VGO utilized in this study contained 2.95 wt.% of sulfur, 0.068 wt.% of nitrogen, and 14.2 wt.% of aromatics. Several catalysts with different compositions (e.g., Mo) were used in the experimental efforts. The experiments were carried out in an isothermal microflow equipment having 5–15 ml of catalysts. The involved operating parameters were total pressure, temperature, ratio of H_2/oil, WHSV, and run time. The coke content (C and H) of the catalyst was measured by combustion mass spectrometric element analysis. It was concluded that a minimum amount of Mo is needed to activate molecular hydrogen. Greater amounts of Mo on the catalyst did not restrain the formation of coke. Increasing the Mo loading resulted in increased coke formation. Since the gas phase residence time was much lower than that of the liquid, evaporation of feedstock reduced the conversion of cracking. An increased degree of evaporation in the TBR resulted in the high concentration of coke precursors in the liquid phase. An increased evaporation increased the liquid phase residence time, leading to more coke formation [157]. de Jong [158] used the data obtained in their experimental attempt [157] to develop a model to describe coke formation on the catalyst for the hydroprocessing of heavy VGO under high temperatures and low hydrogen pressures. They included the reaction mixture VLE calculations in the model. The results showed that the ratio of H_2/oil has a significant effect on the cracking conversion. Moreover, reactor operation with a "drying point" (where a very small amount of oil having a large concentration of coke precursors is still in the liquid phase) led to the fast reactor blockage by coke [158]. LaVopa and Satterfield [159] studied the impacts of various operating conditions employing two different model reactions (hydrodeoxygenation (HDO) of dibenzofuran (DBF) and hydrogenation of *n*-butylbenzene (*n*-BB)) in a laboratory TBR. For the analysis, an ideal TBR model was used: liquid plug flow, catalyst particles complete wetting, and without mass and heat transfer limitations. VLE calculations were incorporated into the system analysis. Partial pressures of the components were used to estimate fugacity values that were used for VLE calculations along the catalyst bed. The TBR had a diameter of 0.5 cm packed with NiMo/Alumina catalysts with the size of 0.15–0.2 mm. The operating pressure was 7 MPa, and the temperature ranged from 350 ^{o}C to 390 ^{o}C. When the flowrate ratio of gas/liquid increased, the conversion increased. The results revealed that the gas/liquid flowrate ratio change leads to the varied performance, depending on the relative volatility of the reactants compared to the relative volatility of the feed. The conversion was mostly affected when the difference in the volatilities of the unreacting liquid and the reactant was significant. Eventually, TBR model incorporated with the VLE calculations could properly predict the reaction system performance when the operating conditions were varied [159]. Pellegrini et al. [155] developed a hydrocracking reactor model considering the VLE calculations with the effect of H_2/wax ratio. Soave-Redlich-Kwong (SRK) EOS was used for the equilibrium condition calculations at each reaction step. The TBR had a diameter of 0.53 mm and a length of 15 m packed with Pt/Si-Al catalysts, having an average particle size of 0.625 mm. The ranges of temperature, pressure, H_2/wax ratio, and WHSV were 343–375 ° C, 35–60 bar, 0.06–0.15 kg/kg, and 1–3 kg/kg$_s$.h, respectively. Molar vapor fraction of feed stream was reported as a function of pressure, temperature, and H_2/wax ratio. The model set of equations was solved with the 4th order RK method and a forward Euler method. At low temperatures, long-chain HCs went through cracking while the reaction selectivity changed for light paraffins at high temperatures. The global reaction rate increased at low pressures while conversion enhanced at high ratio of H_2/wax. Hydrogen amount had a considerable impact on the HC distribution between liquid and vapor phases, playing as a stripping agent role. Higher amounts of hydrogen led to higher molar fractions of the heavy HCs in the liquid phase [155]. Murali et al. [150] developed a diesel HDS model considering HDS, HDA, and olefins saturation reactions. Industrial diesel HDS reactor performance was simulated by utilizing the kinetic parameters predicted from the bench scale data to achieve very low sulfur contents. The bench scale isothermal tubular reactor had an internal diameter of 1.9 cm and length of 53 cm packed with CoMo catalysts. The diesel feed contained 10552 ppm of sulfur. The applied operating conditions were temperature of 340–365 °C, space velocity of 0.8–2.6 h^{-1}, pressure of 4–6 MPa, and H_2/oil ratio of 200–600 Nm^3/m^3. To simulate the bench scale reactor, a two-phase steady state model was chosen. Due to the insufficient VLE data for sulfur compounds, only H_2S and H_2 mass transfer limitations were included into the model. LH rate equation was employed to represent the HDS reaction. The kinetic parameters were estimated in MATLAB by employing unconstrained nonlinear optimization function. These parameters were used to simulate the commercial process. The experimental data implied that the sulfur content of product reduces with an increase in temperature and a decrease in WHSV. Sulfur conversion decreased with the reduction of gas/oil ratio due to the H_2S inhibition effect. The industrial diesel HDS TBR had a diameter of 3.5 m and a length of 17 m, packed with 139.4 tons of catalysts. Based on simulation results, considerable vaporization (20%) was anticipated at normal operating conditions. Diesel vaporization caused the change in enthalpy (estimated by Aspen employing Soave-Redlich-Kwong SRK EOS), and it was considered in the model by a specific heat, which was dependent on gas/oil ratio and temperature. Variable specific heat (C_P) described the effect of feed vaporization. The simulation values were in better agreement with the plant data when temperature and component dependent C_P was used. Even though the model with constant C_P predicted the temperature profile less accurately compared to the model with variable C_P, it predicted the product sulfur contents accurately. This revealed the need for employing more comprehensive feed characterization for various types of sulfur to explain the desulfurization rates [150]. Hoekstra [160] conducted an interesting study on the feed rate ratio of gas/oil that influences the optimized conditions of the operation of ULSD hydrotreaters, considering the VLE in the reaction mixture. The rate of gas/oil is usually set around 3 or 4 times more than the required H_2. Feed partial vaporization usually occurs in the diesel hydrotreaters. The sulfur-containing reactant volatilities determine their distribution in the liquid and vapor phases. Partial pressures, sulfur components reaction rates, and the reaction potentials alter due to any parameter change in the process affecting the VLE in the reactor. The change in the reactions gas/oil from 150 to 1000 nm^3/m^3 revealed that an increase in this ratio dramatically decreases the product sulfur content (P=56 barg; T=343 ^oC; LHSV=2 h^{-1}; sulfur=8000 ppm; catalyst=NiMo/Alumina). In addition, increased gas/oil ratio influenced the phase equilibrium as well as the high-boiling sulfur components reaction rates. This is important in terms of design and operation to obtain ULSD specifications [160]. Bellos and Papayannakos [161] presented a model for the investigation of hydrogen consumption and sulfur removal kinetic for the gas oil hydrotreatment, considering the feed vaporization and VLE in microreactor. The used commercial NiMo/Al_2O_3 catalysts were in the form of extrudate with a diameter of 1.2 mm. The ranges of temperature and WHSV were 320–350 ^oC and 1–4.5 kg_l/kg_s.h, respectively, applied in a microreactor of 8 mm diameter. When the WHSV increased, gas/oil ratio decreased and H_2S partial pressure increased, leading to a lower conversion. Using a higher temperature enhanced the gas oil evaporation, leading to higher concentration of organic components in the vapor phase and lower partial pressures of H_2 and H_2S; therefore, the concentrations of H_2S and H_2 in the liquid phase were increased. H_2 consumption increased when the gas/oil ratio and temperature increased.

With increasing the WHSV, hydrogen consumption decreased. The authors found that the HDS conversion achieves 99.6% at a temperature of 340 ^{o}C and WHSV of 2 kg_{l}/kg_{s}.h [161]. Avraam and Vasalos [162] developed a PFM with axial dispersion for a TBR, processing light oil consisting of volatile compounds at steady state. VLE calculations were included, and SRK EOS was used to calculate VLE at the interface and the enthalpies of liquid and gas phases. The operating conditions were temperature of 340 ^{o}C, pressure of 30 bar, WHSV of 2 h^{-1}, and H_2/oil of 1000 scf/bbl. The oil feedstock had 3.67 wt.% of sulfur compounds, and the catalysts were extrudate type CoMo with the size 1.2 mm packed in a TBR of 3 cm diameter and 17.5 cm length. It was concluded that the light oil volatility should be considered since gas and liquid holdups change along the reactor bed. Temperature increase and WHSV decrease resulted in the removal of higher sulfur compounds from the light oil [162]. The influence of the coupled liquid phase evaporation and reaction on single catalyst pellet catalytic hydrogenation of α-methylstyrene to cumene was analyzed in the study carried out by Kulikov et al. [153]. Steady state and dynamic experiments were conducted in a single catalytic pellet reactor utilizing fine catalytic pellets with various porous structures. The reactor was made of Pyrex® glass of 1.5 cm diameter. The used catalysts were 15% Pt/γ-Al_2O_3, 3.5% Pd/Ti-Al, and 0.5% Pd/Sibunit. The impact of VLE was incorporated into the analysis. The range of temperature was 80–136 ^{o}C, and the applied pressure was atmospheric with H_2 flowrate of 18.5 cm^3/s and liquid flowrate of 0–0.0025 g/s. It was observed that two stable steady states for the catalytic pellet could be obtained because of the liquid vaporization. The temperature of the pellets, their internal and external wetting, and the liquid flowrates significantly depended on the fraction of α-methylstyrene (AMS) vapor, properties of the pellets, and the gas temperature [153]. Khadilkar et al. [163] developed a detailed model for TBR at the pellet- and reactor-scales. They considered the components volatilization and the VLE calculations. The TBR was 3 cm wide and 18 cm long, housing the hydrogenation of cyclohexene to cyclohexane. The operating conditions were temperature of 300–460 K and pressure of 1 bar. For the pellet scale model, intraparticle diffusion utilizing power-law kinetics was used, and pseudo-homogeneous model was chosen for the reactor. The steady state models were solved employing orthogonal collocation on finite elements method and gPROMS software. It was found that the ratio of H_2/feed is very important. For the reactor and pellet-scale multicomponent model, when this ratio was low, the catalyst was completely wetted internally but when it was high, the catalyst was at dry condition, leading to a greater reaction rate and larger temperature increase [163]. Akgerman et al. [164] developed a model to estimate TBRs performance when the liquid feed was volatile. The developed model was compared with a non-volatile liquid phase model utilizing the same kinetics. The model took into account a plug flow condition for the reaction with no considerable wall effects and fully wetted catalyst. To estimate molar concentration and phase equilibrium, SRK EOS was selected to calculate the mixture fugacity coefficients. The isothermal reactor model was solved employing the Euler predictor-corrector method. The pressure was constant at 68 atm. The simulation results revealed that there is a significant difference in conversions by considering the volatility of the liquid phase. However, at high conversions, the difference between the models was lowered because of the limiting reactant consumption [164].

The literature review on the TBRs models development and the relevant results of the VLE calculations reveals the significant importance of VLE incorporation in the TBRs process analysis for more accurate findings and more reliable models.

2.5.2 A Literature Review on Modeling of TBRs

There have been extensive studies on the TBRs modeling and the relevant system/process analysis. Most of the investigated systems are related to the hydrotreating processes, addressing the operating issues, such as temperature control, bed pressure drop, and catalyst utilization. Hydrotreating processes have extensive applications in chemical and energy industries. In a comprehensive review, Tirado et al. [165] investigated the hydrotreatment of the vegetable oils for better understanding of the process, with focus on the kinetic models and reactor modeling. They analyzed the kinetic models and oil feedstocks utilized to produce biofuels. They concluded that the involvement of catalyst deactivation and the development of a comprehensive reactor model are the key factors for the process accurate analysis. One of the notable results reported from their exhaustive review is illustrated in Figure 2-10, which is the hydrotreatment of a refined, bleached, and deodorized palm oil (RBDPO). There were two cases: (1) Simultaneous injection of feedstock and hydrogen from the top of the reactor; and (2) Inclusion of a H_2-quenching stream adjacent to the inlet of the reactor.

Figure 2-10 (a) illustrates a peak in temperature due to the energy liberated from the exothermic reactions, while Figure 2-10 (b) depicts a high pressure drop in case b. Figure 2-10 (c) reveals that case b is a better choice since the utilized catalyst weight is lower due to the slight increase of only 9 ^{o}C in the liquid temperature.

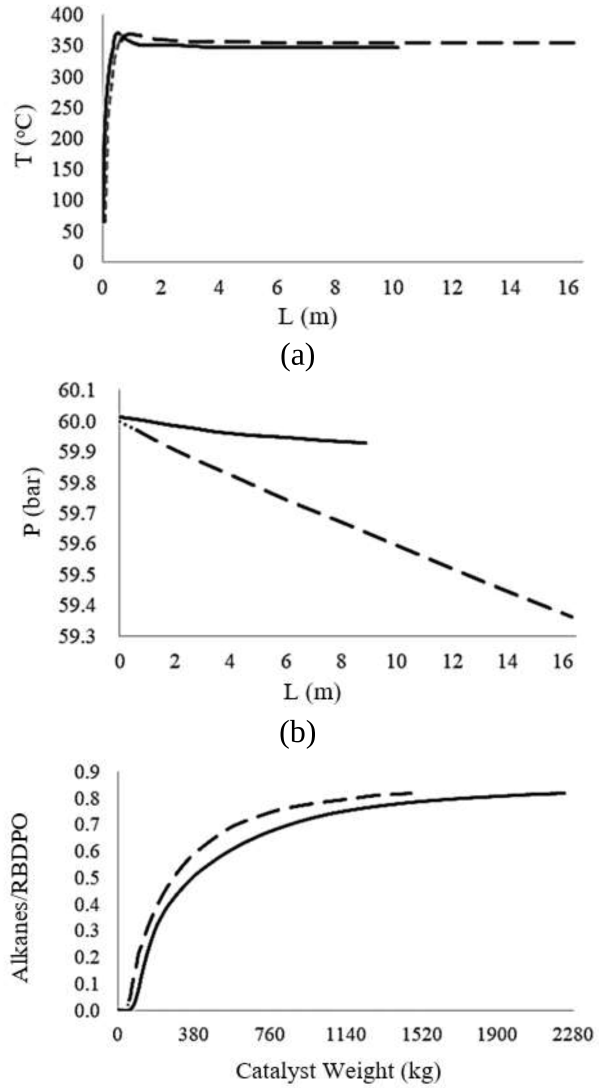

(a)

(b)

(c)

Figure 2-10: (a) Temperature, (b) pressure drop, and (c) concentration profiles of a palm oil hydrotreating reactor (Solid line for case 1, and dashed line for case 2) [165].

In a TBR process, efficient utilization of the catalyst and its lifetime improvement are the two main concerns. In a research work, the mathematical and experimental investigations were performed for the glucose selective hydrogenation to sorbitol process in a TBR, packed with commercial Ru/C catalyst. The developed mathematical model incorporated the catalyst deactivation, which was formulated by the final activity concept, was solved by the finite difference approximation technique. One of the significant results from the research by [166] is shown in Figure 2-11, revealing that catalyst with smaller particle size performs better in terms of glucose conversion. This proves the resistance to the internal diffusion [166].

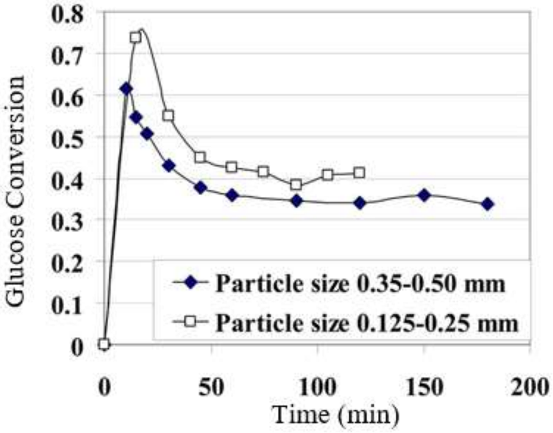

Figure 2-11: Glucose conversion for various sizes of Ru/C catalyst particles [166].

Proper control of a process (e.g., hydrotreating process) requires detailed knowledge on the process and the extent of impacts of vital operating parameters. This highlights the importance of parametric sensitivity analysis and process optimization. Another significant aspect of a TBR operation is to reduce the emission of SO_x as the environmental legislations are becoming stricter. Thus, a TBR process optimization can lead to higher chemical/product quality and lower environmental impacts. In an interesting study, the performance analysis of industrial sulfuric acid process was accomplished by the development of a dynamic model in gPROMS environment. The process consisted of the lead chamber and the current contact process. The second process included sulfur (S) burning to synthesize SO_2, SO_2 conversion to SO_3 utilizing air, and the absorption of SO_3 in water to produce concentrated H_2SO_4 (greater than 96%). The proposed reactor (multi-bed catalytic reactor) model was a pseudo-homogeneous model, considering axial dispersion and adiabatic model of operation. Figure 2-12 (a) shows the SO_2 to SO_3 conversion under the fluctuation of air flowrate fed to the process, indicating the significance of this operating parameter. Figure 2-12 (b) depicts the emission of SO_x under optimized operation and standard operation, emphasizing the importance of the optimized operation, and promising the run of the process at larger production rate while meeting the ecological restrictions [167].

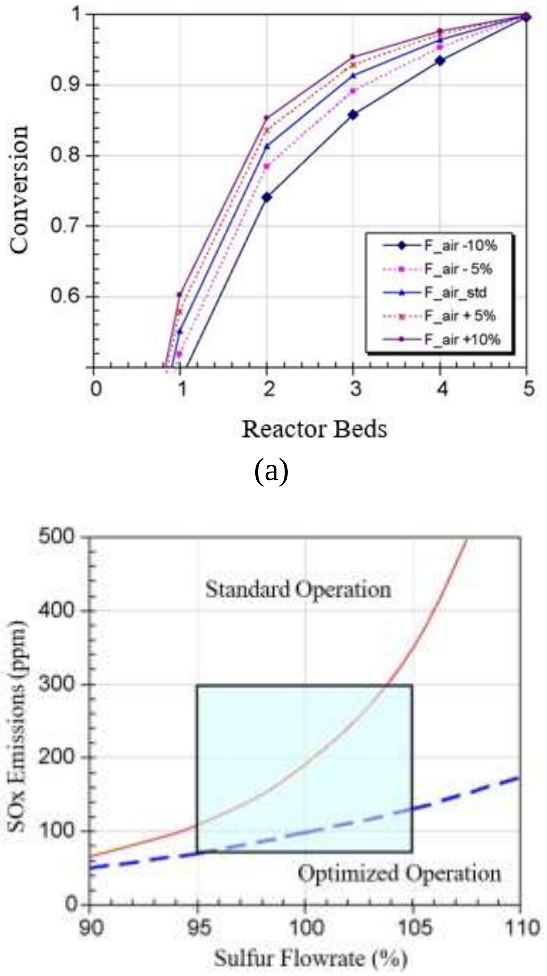

(a)

(b)

Figure 2-12: (a) Conversion profiles in the reactor under the fluctuation of the air feed flowrate; (b) SO_x emissions influenced by different reactor feed flowrates under two recognized operating conditions (e.g., optimized and standard) [167].

One of the concerning issues in the mathematical modeling of a catalytic reactor is the deactivation rate calculation and its prediction reliability. Catalyst may encounter different mechanisms for deactivation; and it is not possible to use a deactivation rate for all types of catalysts. Moreover, the derivation of any catalyst deactivation rate through the experiments is a costly and time consuming task. Azarpour et al. [146]

proposed a methodology, which can be generalized for the calculation of catalyst deactivation regardless of the catalyst type. They used a hybrid model combining a first principle model (FPM) and artificial neural network (ANN). Figure 2-13 (a) illustrates the deactivation trends of the Pd/C catalyst used in the industrial hydropurification unit of PTA plant. The percent relative error is about 1.67. Figure 2-13 (b) shows the deactivation trend of the industrial CuO-ZnO-Al_2O_3 utilized in the industrial methanol synthesis reactor. The percent relative error is around 8.8.

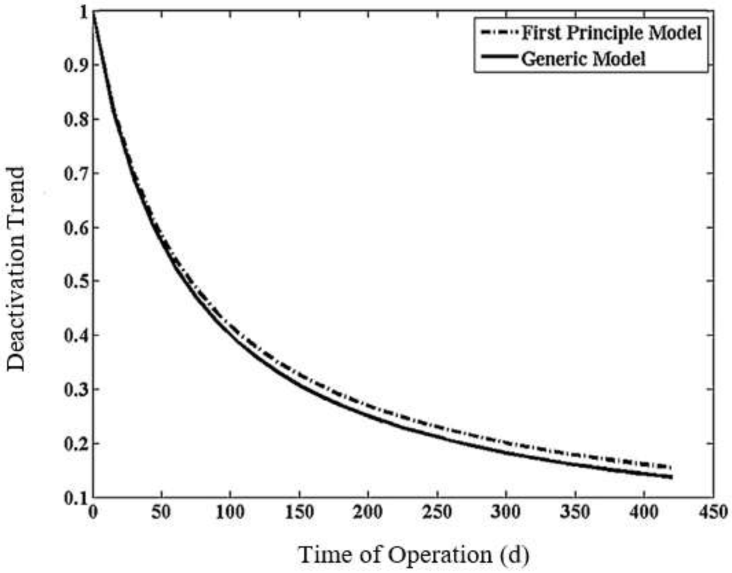

(a)

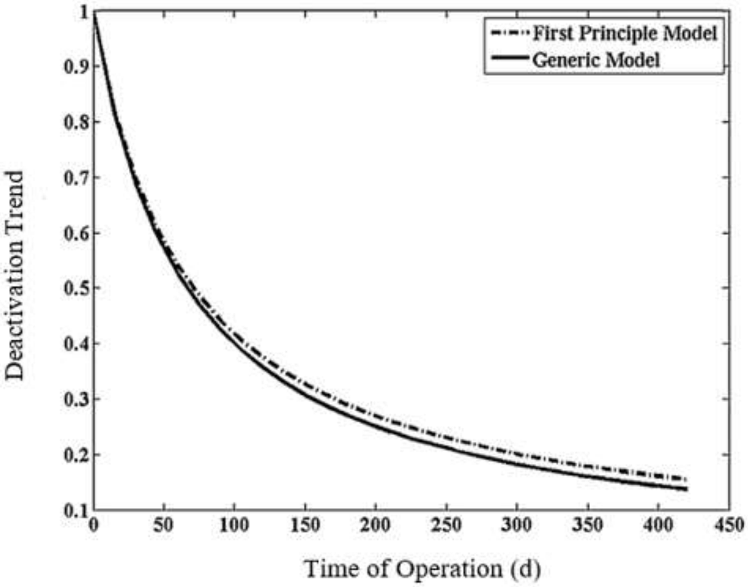

(b)

Figure 2-13: Pd/C catalyst deactivation trend (a) and CuO-ZnO-Al_2O_3 catalyst deactivation trend (b) calculated by FPM and hybrid/generic model [146].

A majority of the industrial plants (e.g., chemical, petrochemical, and pharmaceutical) produce wastewater streams containing toxic organic pollutants. The process costs are considerably high due to the requirement of high temperature (200-300 ^{o}C) and high pressure (70-130 bar) conditions for the fulfillment of the oxidation reactions. Therefore, utilizing oxygen in a dilute organic pollutant solution over a solid catalyst can be a substitute process to the uncatalyzed wet air oxidation to treat the wastewater [168]. To emphasize the importance of the environmental concern and the TBRs utilization in the wastewater treatment process, Pintar et al. [168] investigated the catalytic wet air oxidation (CWAO) of the phenol solution in an experimental TBR packed with Cu, Zn, and Co oxides. It was concluded that the conversion of phenol is controlled by the oxygen mass transfer from the gas phase to the liquid phase. Moreover, $k_{gl}.a$ has a significant impact on the phenol conversion, and the role of $k_{ls}.a$ is negligible in the phenol conversion. Figure 2-14 illustrates the concentration profiles of oxygen and phenol through the catalyst bed.

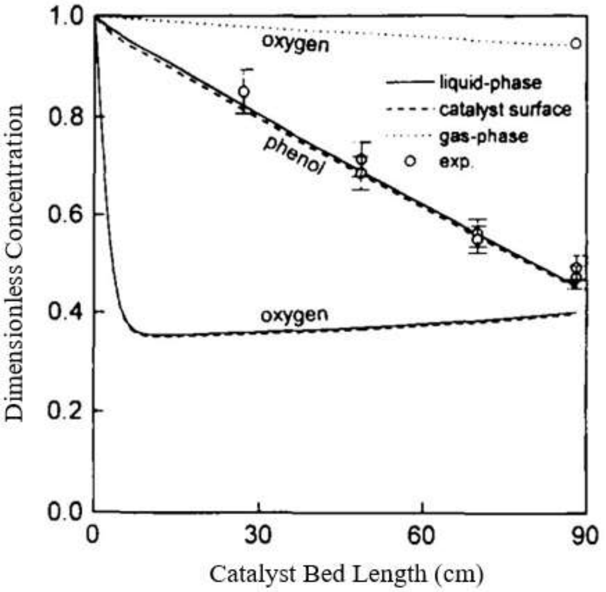

Figure 2-14: Predicted concentration profiles of oxygen and phenol along the catalyst bed (T=150 °C; P_{O2}=7 bar; P_t=11.7 bar; m_s=769 g; d_p=0.6 mm; C_{Phenol}=0.032 mol/l; liquid flowrate =1.5 l/h; gas flowrate= 1 l_n/h) [168].

Focusing on the environmental concerns and on the utilization of the green energy, several studies have been accomplished so far. The recent investigation on the biomass as a source for the sustainable energy was conducted by Kostyniuk et al. [169]. Gas phase hydrocracking process of tetralin (biomass tar model chemical compound) into benzene, toluene, and xylene (BTX) was performed over a few catalysts (e.g., H-

ZSM-5 zeolite) in a packed bed reactor under atmospheric conditions. It was found that the exceptional performance of H-ZSM-5 catalyst is due to the significant mesopore volume and mesopore surface area, the largest Bronsted to Lewis acid sites ratio, and the mild acidity compared to the other examined zeolite catalysts. Figure 2-15 describes the impact of total gas hourly space velocity ($GHSV_t$) on the product distribution. It can be noticed that the tetralin conversion is not considerably influenced by the GHSV; however, higher BTX selectivity is achieved at lower GHSV.

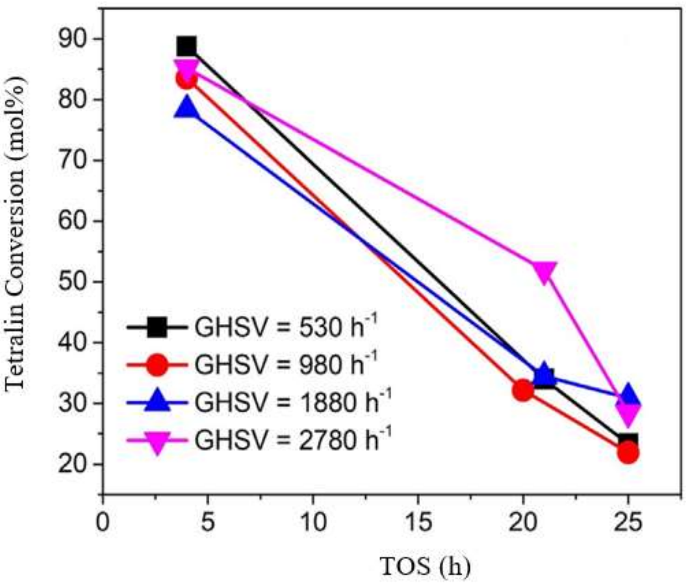

(a)

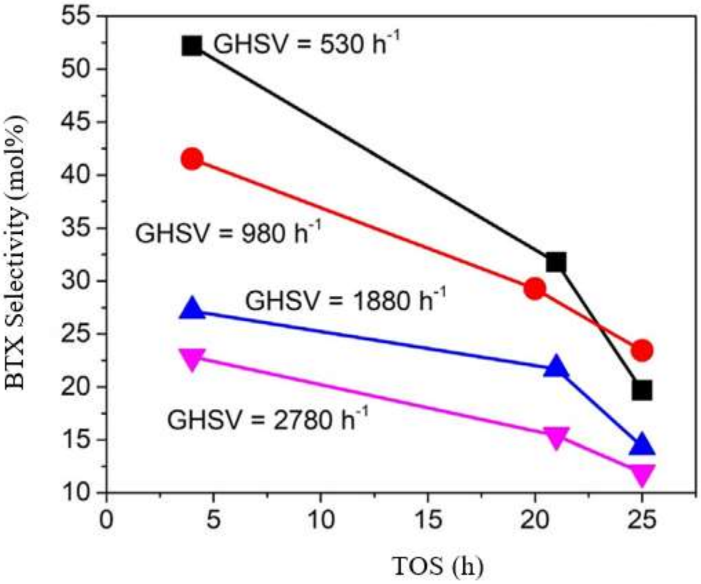

(b)

Figure 2-15: (a) Tetralin conversion and (b) BTX selectivity over H-ZSM-5(30) catalyst at various GHSV during time-on-stream (TOS) (m_s=0.5 g; T=370 °C; H_2 is carrier gas; H_2/Tetralin=1800 (volume ratio); P=1 bar).

TBRs housing continuous hydrogenation reactions are a distinguished specification which can be even applied to the pharmaceutical industry. This industry employs the TBRs to carry out continuous hydrogenation reactions for the more efficient delivery of active pharmaceutical ingredients. This enables the pharmaceutical process to shift from conventional batch process operated under low pressure conditions (less than 10 bar) to both laboratory and pilot plant TBRs operation under high pressures (more than 100 bar). This leads to the process intensification (improved quality and productivity). Moreover, using TBRs results in the advanced process control, smaller reactor size, lower reactor cleaning time, and enhanced process safety (i.e., greener process) [170]. They focused on the development of a new generation of catalysts for the continuous hydrogenation reactions in pharmaceutical-scale TBRs. They used four catalysts of palladium supported on polymer-based spherical activated carbon (see Figure 16). According to Figure 2-16, catalysts with higher particle size show narrow particle size distribution, revealing uniform particles; this leads to the uniform packing of the catalyst bed along with its homogeneity maximization.

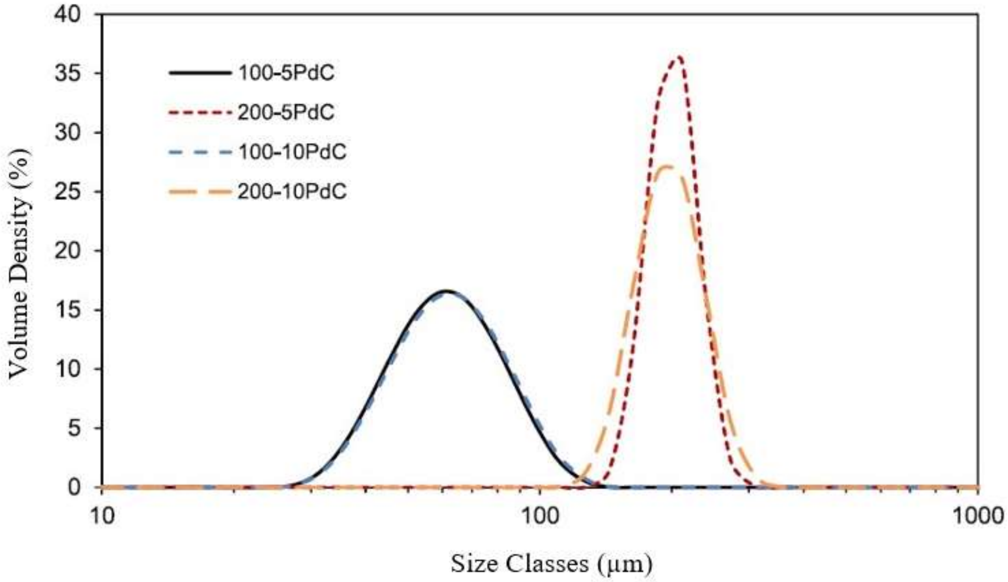

Figure 2-16: Particle size distribution for 100-5PdC, 100-10PdC, 200-5PdC, and 200-10PdC (100 and 200 are the particle size in μm, and 5 and 10 are the Pd percentage weight).

In another study, the gas phase conversion of a mixture of biomass tar into 2-methylnaphthalene, ethylene, and propane was modeled. The reaction conditions were analyzed utilizing different zeolites and metal promoted zeolites catalysts in a packed-bed reactor. The assessment of Ni metal addition and the catalyst characterization revealed that the best performance is attributed to the 5 wt.% Ni/H-ZSM-5 (SiO_2/Al_2O_3=30) with a selectivity of 96.2 mol% to 2-methylnaphthalene in the liquid phase. Figure 2-17 presents the thermogravimetric analysis (TGA) of the used catalyst (5%Ni-ZSM-5 (30)) over the temperature increment at atmospheric conditions for the estimation of the amount of coke deposited on the catalyst. Figure 17 also exhibits the initial 4.1 wt.% weight loss due to the loss of water and volatile components and the secondary 2.3 wt.% weight loss owing to the organic components (coke) removal, confirming the coke existence on the catalyst surface [171].

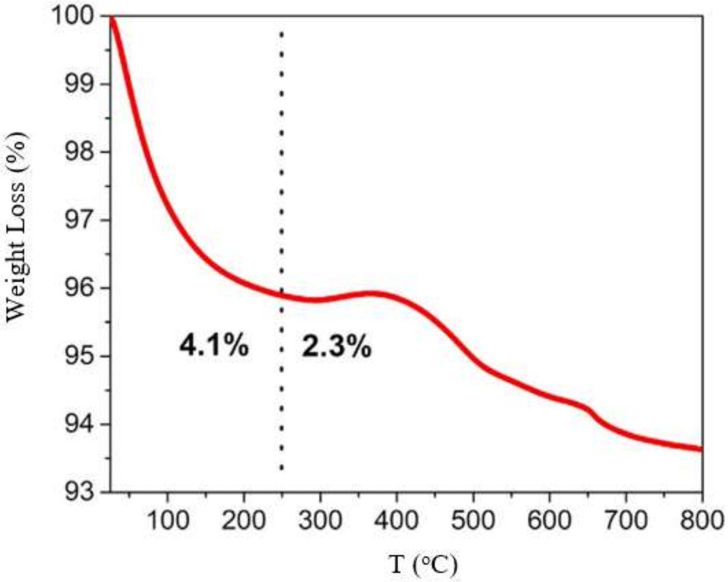

Figure 2-17: TGA profile of the 5%Ni-ZSM-5(30) catalyst.

In another experimental research, Kostyniuk et al. [172] compared the performance of different NiMo-promoted catalysts with the fresh zeolites placed in a packed-bed reactor for the hydrogenation, hydrocracking, and isomerization of biomass tar at a temperature of 370 ^oC and a pressure of 1 atm. They concluded that the most efficient performance is achieved by the 2.5 wt.%Ni-2.5 wt.%Mo/ZSM-5. It highlights that the factors of particle size dimension, diameter, and acidity facilitate the removal of poly-aromatic hydrocarbon.

There are mathematical techniques used in the solution of the catalytic process models. Finite difference method (FDM) is one of the most established methods to solve differential equations. This technique deals with the replacement of continuous variables with discrete variables. FDM yields values at discrete points chosen by the analyst. Newton-Raphson method is an efficient method to solve nonlinear algebraic equations. Laplace transformation can be effectively utilized to solve ODEs and PDEs. It is suitable for IVPs, and it is specifically helpful for the solution of simultaneous equations. Orthogonal collocation can be utilized to solve PDEs. It is applied on both spatial domains of elliptic PDEs, leading to a set of algebraic equations. Orthogonal collocation is also applied on the spatial domain of parabolic PDEs, leading to a set of ODEs of initial value problems. Runge-Kutta method is one of the most popular methods for differential equations integration [173]. One of the most difficult tasks in modeling complex catalytic TBR processes is to obtain the mathematical solution to the model. Selection of a suitable mathematical technique is of great importance, which is also a computationally demanding step. The level of complicatedness is determined by the developed model features, such as the time-dependency of the model (dynamic nature), number of the variable parameters, and the non-linearity of the terms involved into the model (e.g., reaction rate expressions). Table 2-6 includes the modeling studies fulfilled on TBRs, presenting the models, solution techniques, and utilized software packages.

The reactant component flowing in the liquid phase through the fixed bed experiences molecular diffusion, turbulent diffusion, and convective diffusion stemmed from the non-uniform distribution of the velocity vector. Axial dispersion is not significant under normal operating conditions. Therefore, FBRs are normally modelled employing ideal flow considerations, such as PFR and/or CSTR. A FBR/TBR cannot be always analyzed employing ideal models, such as plug flow since significant back-mixing might take place in the liquid phase [174]. Hydrodynamics in TBRs is described by the critical operating parameters of pressure drop, liquid holdup, fluid phases' dispersion, catalyst wetting efficiency, and flow regime. Thus, a primary understanding and analysis of flow hydrodynamics and reaction conversions is crucial for the scale up and design of TBRs [175].

Numerous investigations have been conducted on the modeling and simulation of TBRs. Table 2-7 summarizes the most significant works on the mentioned area of study.

Table 2-6: Models, solution techniques, and software utilized in the modeling studies of TBRs.

Process	Reactor		Modeling/Simulation			Ref
	D_R (cm)	L_R (cm)	Model features	Solution	Software	
CTA HDP	2800	7400	3-phase 1D dynamic heterogeneous	FDM, method of lines	MATLAB	[176]
HDS		27.8	Catalyst particle scale (Dynamic and SS)	FEM		[177]
CWAO of phenol	1.9	77	1D heterogeneous; LH formulation	SQP	g-PROMS	[178]
Hydrogenation of MAPD			3-phase homogeneous (SS)	Gauss-Newton	MATLAB	[179]
FT synthesis	5	800	2-phase 3D downflow dynamic isothermal (Eulerian)	OCM, gear integration	Aspen	[180]
HDS, HDN, HDA, HDC, olefin saturation			1D heterogeneous adiabatic (SS)	FDM	MATLAB	[181]
4-CBA hydrogenation	280	740	3-phase dynamic heterogeneous	FDM	MATLAB	[182]
Hydrogenation of acetophenone	0.71	25	1D heterogeneous isothermal (PFM)	RK method	MATLAB	[183]
HDT and HDC of gas oil	16	122	2D 4-lump kinetic network (SS)	FDM, NL2SOL algorithm	Aspen	[184]
Hydrogenation of MAPD			1D heterogeneous	Powell, FDM, Jacobian	FORTRAN	[185]
CWAO of phenol		77×30×1.9	1D heterogeneous two film theory (PFM)		gPROMS	[186]
Hydrogenation of DBT	5.7	200	Two-phase 3D dynamic adiabatic	OCM, gear integration	Aspen	[187]
ODS of DBT	1.6	77	Pseudo-homogeneous isothermal (PFM) (SS)	SQP	gPROMS	[188]
Hydrogenation of BD	270	350	1D heterogeneous adiabatic (SS)	FDM, differential evolution		[189]
	14	100	Effective diffusion model; stochastic model	Analytical	Tomoflow, Flowan	[129]
Hydrogenation L-arabinose	0.1	0.2	Axial dispersion heterogeneous	FDM	MATLAB, Python	[190]
HDC of paraffinic FT wax	1	3.66	PFM (SS)	Levenberg-Marquardt	MATLAB	[191]
FT synthesis	2.54	610, 850	1D homogeneous (SS)	FDM		[192]
Hydrogenation of α-methylstyrene	3	21	CSTR; PFR; dispersed PFR; CSTR with exchange volume (dynamic)	FVM		[193]
Detoxification (CWAO)	5	100	CFD with VOF	FVM	Fluent	[194]
Detoxification (CWAO)	5	100	CFD (dynamic)	FVM	Fluent	[195]
Detoxification (CWAO)	5	100	Eulerian CFD model (volume averaged)	FVM	Fluent	[196]
Hydrogenation of α-methylstyrene			1D and 2D effectiveness factor; classic diffusion model for inside the pores	FEM	COMSOL	[197]
Hydrogenolysis of LA	1.3	45	1D PFM (liquid phase) (SS)	Euler's method	Excel	[198]
HDV, HDN, and HDNi of crude oil	2	65	3-phase 1D heterogeneous isothermal (SS)	Non-linear regression	gPROMS	[199]
CWAO of phenol	5	100	Euler-Euler gas-liquid-solid drag; turbulence	FVM	Fluent	[200]
CWAO phenolic wastewater	5	100	VOF (Naiver-Stokes, free surface model, 2-phase *k*-*ε* turbulence)	FVM	Fluent	[201]
GO hydrogenolysis	1.25	61	1D PFM (SS)	FDM, Euler's method	MATLAB	[202]

Process	Reactor		Modeling/Simulation			Ref
	D_R (cm)	L_R (cm)	Model features	Solution	Software	
CWAO of phenol			Axial dispersion isothermal PFM (SS) (dimensionless form)		gPROMS	[203]
HDS of gasoil	3	125	3-phase 1D dynamic heterogeneous isothermal	FDM	MATLAB	[204]
Hydrogenation of DCPD	2.4	82	1D dynamic heterogeneous (PFM)	FDM		[205]
CWAO of vanillic acid	5	100	Multifluid 2D dynamic (Eulerian-Eulerian)	SIMPLE, upwind and PRESTO schemes	Fluent	[206]
Hydrogenation of DCPD	2.4	85	Heterogeneous PFM (SS)	FDM		[207]
CWAO of phenol	2.5	60	1D heterogeneous; Cell stack model (SS)	FDM, OCM	FORTRAN	[208]
Hydrogenation of AMS	2.2	59	Bulk species transfer, bulk energy transfer, continuity equations, interphase mass and heat transfer (dynamic)	Semi-implicit (predictor-corrector, marker-and-cell)		[209]
HDS, HDN, HDA, and HDC of diesel fraction	2.54, 380	80, 800	3-phase heterogeneous two-film theory (SS)	FDM, shooting technique		[210]
CWAO of phenol	2.54	135	1D axial dispersion	FDM		[211]
CWAO of phenol	26	150	Pellet-scale (diffusion-reaction); reactor scale (PFM) (SS)	OCM, FEM		[212]
HDS, HDN, HTO, and HTA of light oil	3	17.5	Homogeneous axial dispersion (PFM) (SS)	OCM, FEM		[162]
HDS and HDA of diesel oil	1.9	50	Isothermal/isobaric (PFM) (SS)	FDM	FORTRAN	[213]
HDS of gas oil	2.3	80	3-phase heterogeneous isothermal/isobaric (SS)	FDM	FORTRAN	[214]
Hydrogenation of cyclohexene	3	18	Pellet-scale (intraparticle diffusion), reactor scale (pseudo-homogeneous), SS	OCM, FEM	gPROMS	[163]
Hydrogenation of DNT	1.5	30	Partial wetting, stagnant liquid, intraparticle mass transfer resistance (PFM) (SS)	FDM		[215]
Hydrogenation of ketone	5.08	200	2D pseudo-homogeneous	OCM	FORTRAN, Aspen Plus	[216]
Hydrogenation of acetophenone	1.5	30	PFM (SS)	OCM, FDM		[217]
Hydrogenation of HPA	7.63	146	PFM (liquid), diffusivity (solid phase) (SS)	Newton-Kantorovich		[218]
Hydrogenation of toluene	150	500	PFM; Maxwell-Stefan; effective diffusivity (SS)	FDM	FORTRAN	[219]
Hydrogenation of cyclohexene	3.5	200	Pseudo-isothermal/isobaric; simultaneous diffusion and exothermic reaction (SS)	FDM		[220]

Table 2-7: A summary of the modeling details of the literature on TBRs.

Process /Reaction	Results	Remarks	Reference
CTA HDP	• Reactor feed impurities can be efficiently controlled by a sophisticated control strategy. • Hydrogen solubility has a significant effect on the product quality.	• The dynamic model can be further completed by considering the radial coordinate.	[176]
HDS of Heavy oil	• No much change in sulfur mass fraction with a fresh catalyst particle • Catalyst deactivation caused by demetallization and coking during HDS	• Separate consideration of reactor model and catalyst deactivation • Steady state model for reactor even though catalyst deactivation occurs;	[177]
MAPD hydrogenation for PR production	• Increase in diluent flowrate increased PR concentration • Increase in temperature reduced PR production rate	• No deactivation rate included into the model • 3 phase heterogeneous model could be considered	[179]
FT synthesis	• The performance of FT synthesis increased slowly with inclination of packed bed • Asymmetric oscillating TBR has better performance compared to vertical TBR	• No catalyst deactivation considered	[180]
hydrogenation of 1-octene	• k_{ls} increased with increasing Re_L for a given 1-octene/H_2 ratio • The local intra-pellet compositions revealed the evidence of mass transfer limitation	• No catalyst deactivation considered in the model	[221]
VGO HDT	• The conventional TBR series and parallel configurations were better than POLF configurations • Minimal difference in the performance between conventional TBR configurations	• No catalyst deactivation considered in the model • The product quality change has not been evaluated	[181]
CTA HDP	• Increase in gas holdup improved the HDP process performance • Increase in liquid holdup negatively impacted the HDP process performance	• No consideration of some important hydrodynamic parameters (e.g., catalyst particle dimeter)	[182]
Acetophenone hydrogenation on Rh/Al_2O_3 catalyst	• Bubbly flow enhanced the reaction rate for acetophenone hydrogenation over TFC • The reaction rate decreased with increased gas flowrate, which can be explained by partial wetting	• No discussion on the possibility of catalyst deactivation	[183]
MAPD hydrogenation into propylene	• The model predicted a higher outlet temperature due to the adiabatic reactor assumption • The model predicted MAPD concentration values well	• No consideration of the catalyst deactivation as the main reason on the product quality change	[185]
Co-oligomerization of linoleic methyl ester and hydrogenation of the co-oligomers	• Higher iodine values led to significantly higher Rh loads • A comparison of different carrier materials (AC, silica, and alumina oxide) indicated that the choice of fixed-bed catalyst did not influence the absorbed amount of Rh	• The extensive study lacks the parametric sensitivity analysis to prioritize the effects of the parameters on the newly developed process	[222]
CWAO of phenol	• Increasing temperature, oxygen partial pressure, initial phenol concentration, and gas flowrate resulted in higher conversion of phenol • An increase in LHSV decreased the phenol conversion	• No catalyst deactivation considered	[186]
Hydrogenation and hydrogenolysis of DBT	• The significant reduction of HDS performance at higher packed bed inclinations	• No catalyst deactivation considered	[187]

Process /Reaction	Results	Remarks	Reference
	• The significant reduction of symmetric oscillating HDS TBR performance due to the substantial decline of the effectiveness factor;		
Hydrogenation of AMS to cumene	• The flow around the spheres depended on the local packing • Large reaction rates were achieved if the two-phase velocity and the gas holdup were high	• The experimental effort should be done under real operating conditions of a TBR	[223]
A nitrogen-water flow	• The profiles at different gas flowrates were essentially parallel to each other for each packing type suggesting consistency in bed structure • At low liquid flowrates axial dispersion increased with increasing liquid velocity	• The study could be done considering the operating conditions of a real hydrotreating process with the chemicals involved	[224]
Detoxification reaction of phenol-like pollutants (CWAO)	• PFC was a promising flow regime to improve the environmental performance of TBRs, especially when the mass transfer of a key reactant was rate limiting • The frequency of travelling liquid pulsations was responsible by the shape of the axial concentration profile	• It would be interesting to show that how this periodic operation could impact the catalyst performance (e.g., catalyst lifetime)	[194]
Detoxification reaction of phenol-like pollutants (CWAO)	• Increase of temperature promoted the pulsation intensity • The most intense pulse intensities were found under gas/liquid alternating mode	• The process could be considered the quality/conversion of the main pollutant considering the change in the catalyst activity	[195]
Transesterification of SFO with methanol	• The FAME yield increased linearly with bed height • The FAME yield increased with the reaction temperature	• The catalyst activity could be discussed more closely, and its effect on the product quality could be examined	[225]
Hydrogenation of AMS in a structured TBR and monolithic reactor	• The presence of particles caused a greater gas-liquid interfacial area and micro turbulences in the liquid slugs, enhancing mass transfer • The monolithic catalyst provided the lowest pressure drop	• The process could be analyzed under higher operating pressure considering the catalyst deactivation affecting the hydrogenation conversion;	[226]
Detoxification reaction by CWAO	• PFC was responsible to move the maximum bulk temperature increase towards the reactor outlet in comparison to TFC • The frequency of the traveling liquid pulsations was responsible by the shape of the axial concentration profile	• It would be interesting to show that how this periodic operation could impact the catalyst performance (e.g., catalyst lifetime)	[196]
Hydrogenation of AMS to cumene	• The spreading of the wetted surface was positive on the effectiveness factor for a slab geometry • Evaporation amplified discrepancies between 1D and 2D models due to non-symmetrical heat transfer boundary conditions	• The more reliable results could be achieved applying higher pressure and temperature reflecting the real operations of TBR	[197]
An air-kerosene flow	• The duration of decaying period was longer in cases of fast mode operation • In case of slow mode operation, the shock wave plateau retained its identity • The decay time got shortened with the incorporation of turbulence	• The study could be done considering the chemicals involved in a real TBR operation considering higher pressure and temperature	[227]
CWAO of phenol in wastewater	• Liquid flowrate had more prominent effect on radial pressure drop at higher values • The gas flowrate had a pronounced influence at lower interaction regimes	• It could be interesting to involve the catalyst deactivation into the model	[200]
A nitrogen/helium-water/hexane flow	• Increasing gas velocities resulted in higher pressure drop and lower liquid holdup • The body force depended on liquid density which was not substantially affected by pressure in the usual operating range of TBRs (less than 30 MPa)	• Since the temperature has considerable effect on the TBR system and physical properties, temperature fluctuation could be studied in-detail	[228]

Process /Reaction	Results	Remarks	Reference
Hydrogenation of AMS to cumene	• The conversion nonlinear decrease implied that incomplete wetting determined the overall reaction rate • Huge discrepancies between the model results and the experimental data revealed that local phenomenon of incomplete wetting could not be justified by a global wetting parameter	• The study could be fulfilled applying higher pressure and temperature for the better analysis of the TBR performance	[193]
Hydrogenolysis of LA to PG	• Partially wetted model always produced a higher conversion compared to the fully wetted reactor model • At large liquid flowrates, fines had a minor impact on the LA conversion	• Operation on higher temperature and the involvement of catalyst deactivation could be considered to improve the outcomes	[198]
CWAO of phenolic wastewater	• The model could predict the system performance at low temperatures more precisely implying that a separate enthalpy equation was more effective on the temperature prediction • Higher liquid flowrate decreased the rate of decontamination	• The catalyst deactivation could be included in the model developed;	[201]
A nitrogen-liquid flow	• The particles shape did not change the wetting efficiency considerably • At very low liquid flowrates, the internal liquid-solid wettability determined the wetting efficiency	• Since the wetting efficiency is dependent on the physical properties which are affected by temperature, higher temperature condition can result in more reliable findings;	[66]
CWAO of vanillic acid	• The hydrodynamic parameters could be well predicted by the Eulerian model • Temperature had a significant effect on the oxidation process	• The incorporation of catalyst deactivation could present the system performance more realistically	[206]
An air-water flow	• The values of holdup for the beds of spherical particles were much smaller than those of the beds of cylindrical extrudates • The largest pulse intensities took place at the smallest frequencies	• Higher temperature and pressure implementation could result in the more reliable results in terms of actual application of TBRs	[229]
AMS hydrogenation	• The reactor performance enhanced at larger space-time • The reactor performance decreased at very low cycle times since there was a huge supply of liquid reactant and insufficient time for gas component supply	• Applying higher pressure and temperature along with the catalyst activity involvement could strengthen the findings in terms of TBRs applications	[209]
HDS and HDM of the petroleum residue	• Incorporation of hydrodynamic parameters improved the system modeling • Low TBR efficiency at low mass flowrate could be due to the axial dispersion (non-ideal flow)	• Considering the catalyst deactivation could result into more applicable findings	[230]
Catalytic wet oxidation of phenol	• Extrudates had lower dynamic liquid holdup and higher pressure gradient compared to CDS pellets • Larger conversion was accomplished with CDS trilobes in comparison with extrudates	• Catalyst activation could be involved into the model to more properly reflect the TBR performance	[211]
An air-kerosene flow	• The transition between trickling flow and pulsing flow took place faster when using large fines • When liquid holdup increased, the transition took place at smaller quantities of fines	• Using the data of the studies carried out on the actual TBR hydrotreating process could result into more reliable findings	[231]; [232]
CWAO of phenol	• The activated carbon catalyst activity was greater than the commercial catalyst • To estimate the accurate values of process parameters, employment of porosity profiles in the TBR modeling was essential	• The involvement of higher pressure and temperature with the catalyst deactivation could give better representation of a TBR performance	[233]

Process /Reaction	Results	Remarks	Reference
HDT and HDC of gas oil	• The radial liquid velocities increased at higher temperatures due to the lower viscosity and density • Pressure drop at axial direction decreased by increasing temperature	• The incorporation of catalyst deactivation can present more realistic model	[184]
ODS of DBT in LGO	• The conversion rate increased with the increase in initial concentration • Increase in LHSV and temperature decreased the effectiveness factor	• The catalyst deactivation could be incorporated into the model to represent the actual process of the relevant systems	[188]
Hydrogenation of BD	• BD flowrate determined the reduction of reacting column length • Reactor's length could be reduced at higher temperature operation	• A more sophisticated model incorporating the catalyst deactivation could lead to more realistic results	[189]
Hydrogenation of L-arabinose to arabitol	• Large particles of catalyst and concentrated solution made a strong resistance of gas-liquid mass transfer • Gas-liquid mass transfer resistance had more considerable effect than liquid-solid mass transfer resistance	• The analysis of temperature fluctuation could determine the performance of TBR in terms of conversion and catalyst deactivation	[190]
HDC of paraffinic FT wax	• With increasing temperature, the conversion of wax increased • The conversion decreased with increasing the wax flowrate	• The incorporation of the catalyst deactivation and the development of more sophisticated model could lead to more acceptable results	[191]
CWAO of BPA by utilizing newly TNCs	• TNCs had much more specific surface area in comparison with the reference TiO_2 powder • No considerable catalyst deactivation was achieved even for long operation time of TNCs	• This catalyst could be tested for a hydrotreating process to assess its generic application	[234]
A flow of Ar-water	• The model was able to predict the hydrodynamic parameters of heat and mass transfer coefficients, gas holdup, and liquid holdup satisfactorily;	• Implication of higher temperature and pressure operating conditions with a typical chemical reaction could result in a more reliable finding	[235]
FT Synthesis	• The bed temperature and reaction rate increased with increasing effective diffusivity • Gas recycle enhanced the heat transfer by rising the flowrate and reducing partial pressures of the reactants	• Incorporation of catalyst deactivation into the model and the development of a more sophisticated one could lead to the more applicable results;	[192]
HDV, HDN, and HDNi of crude oil	• Hydrogen pressure increase improved the removal of vanadium, nitrogen, and nickel • The conversion of HDV was less than HDNi • The best reaction orders of hydrogen were 0.63, 0.35, and 0.56;	• Incorporation of catalyst deactivation and temperature fluctuation in the developed model could result in the more practical findings	[199]
GO hydrogenolysis	• The partial wetting had a more significant effect on the GO conversion at the lower conversion values • The overall reaction rate was limited by the gas-liquid mass transfer resistance	• The incorporation of the catalyst deactivation into the developed model could lead to the more reliable results	[202]
CWAO of phenol	• Axial dispersion did not have a significant effect on the phenol conversion • Gas-liquid mass transfer impeded the CWAO of phenol, and had more significant role compared to liquid-solid mass transfer	• The incorporation of catalyst deactivation into the developed model could result in more accurate predictions	[203]
Hydrogenation of DCPD to endo-THDCPD	• At greater LHSV values, steady state model does not result in acceptable outcomes for the prediction of temperature profiles • When the inlet temperature enhanced, THDCPD yield, DCPD conversion, and global rate of hydrogenation increased;	• The incorporation of catalyst deactivation could lead to more reliable results reflecting the actual phenomenon taking place in the TBR;	[207]

Process /Reaction	Results	Remarks	Reference
CWAO of phenol in catalytic TBR and upflow FBR	• The dry pellet surface improved the contact between oxygen and phenol, leading to higher phenol conversion when the reaction was liquid phase reactant limited • The effect of gas flowrate was significant for downflow reactor and insignificant for upflow reactor	• Applying higher pressure and temperature along with the catalyst deactivation incorporating into the developed model could lead to the more reliable findings	[208]
HDS, HDN, HAD, and HDC of diesel fraction	• The H_2S concentration in the feed gas had a dramatic effect on the sulfur content of the product • The sulfur content of the product decreased with the increase in pressure	• The developed model could be more in detail with the more accurate by considering the product quality fluctuation with the catalyst deactivation phenomenon	[210]
CWAO of phenol	• **Isothermal operation**: Incomplete wetting had a positive effect on the phenol conversion • **Non-isothermal operation**: Water evaporation had a significant effect on TBR performance	• Since catalyst deactivation plays a significant role in the CWAO process, the model is to be developed considering this adverse phenomenon	[212]
Styrene hydrogenation in a TBR and monolithic reactor;	• The catalyst activity of the smaller catalyst particles was nearly 25% larger than that of the larger catalyst particles • It was demonstrated that a structured catalyst was beneficial for a reaction system dealing with a considerable mass transfer limited condition	• The model development could be improved by considering the catalyst deactivation;	[236]
HDS, HDN, HTO, and HTA	• The lighter oil fractions volatilization limited the phase temperature increase • The lighter oil fractions excessive volatilization decreased the liquid holdup and increased the gas holdup	• For more reliable results, the model should be incorporated the catalyst deactivation;	[162]
HDN of non-basic and basic nitrogen compounds in HGO	• Increase in LHSV decreased the carbazole HDN conversion • Basic nitrogen compounds needed lower reaction time compared to the non-basic nitrogen compounds	• The numerical assessment of the process via the development of a reactor model could optimize the operating parameters' values	[237]
HDS and HAD of diesel oil	• The sulfur content of product decreased with increasing temperature and decreasing LHSV • The H_2S present in the feed gas stream inhibited the HDS of diesel oil	• A more sophisticated model capturing temperature fluctuation and catalyst deactivation could lead to more reliable results;	[213]
HDS of gas oil (LH kinetic model)	• The pressure impact on the conversion of sulfur was not significant at high operating pressure • The sulfur conversion increased with increasing temperature	• Considering catalyst deactivation and temperature fluctuation in the model could present a more sophisticated model	[214]
Hydrogenation of DNT	• The conversion dramatically decreased with increasing liquid flowrate for the stagnancy model as well as the partial wetting model • The reaction was strongly diffusion controlled;	• Consideration of axial dispersion effect and catalyst deactivation into the developed model could lead to more realistic results;	[215]
Hydrogenation of ketone in the presence of CO_2 solvent	• VLE calculations must be considered for the TBR modeling when supercritical solvents are involved into the process • The model accuracy could be improved by applying more reliable experimental endeavors/data	• Incorporating the catalyst deactivation and flow non-ideality into the model could result more accurate findings	[216]
Hydrogenation of acetophenone utilizing cyclohexane as solvent	• **SAR**: Deactivation of catalyst affected each reaction; It had the higher productivity per unit mass of catalyst • **TBR**: Moderate catalyst deactivation took place; Low yield of intermediate products was obtained due to the significant internal and external mass-transfer limitations;	• To consider the catalyst deactivation could obtain more accurate results	[217]
Hydrogenation of HPA to PDO	• The catalyst activity parameter was a considerable factor in the TBR model	• The interrelation of catalyst deactivation and time affecting the catalyst efficiency and the	[218]

Process /Reaction	Results	Remarks	Reference
	• Hydrogen was the only limiting reactant when the liquid flowrate was the highest • Incomplete wetting on the reactor scale resulted in a lower catalyst effectiveness;	reactor performance could be discussed and analyzed through a more sophisticated mathematical model	
Hydrogenation of toluene	• High mass transfer resistance resulted from the huge difference over the liquid film • The mass transfer coefficients at the liquid side of the gas-liquid interface are about two times less than those of the other films	• Including some parameter, such as axial dispersion and catalyst deactivation, could lead to more advanced model	[219]
Hydrogenation of AMS to cumene in a hexane solvent;	• At high AMS concentration and low pressure, the reaction was gas limited, and TBR performed better than upflow reactor • At low liquid flowrates, TBR achieved higher conversion than upflow reactor	• The experiments could be carried out for high exothermic reaction, especially for incompletely wetted conditions;	[238]
Hydrogenation of cyclohexene	• The kinetic constant determined by the model was lower than that of experimentally measured • Dramatic increase in the reaction heat parameter and diffusion coefficient indicated the reaction transition to the gas phase	• The model could improve by incorporating more hydrodynamic parameter, which significant affect the wetting efficiency	[220]
Hydrocracking of VGO	• Complete evaporation of oil took place at high ratio of hydrogen to oil, therefore limiting the coke formation and diluting the coke precursors in the vapor phase • Average ratio of hydrogen to oil led to the significant evaporation of oil, resulting in the large amount of coke deposition	• Mode sophisticated model of the reactor could more properly interrelated the operating parameter to the catalyst deactivation (coke deposition/formation)	[158]
CWAO of phenol in a hybrid process of TBR and RO	• **TBR**: Increase in temperature and phenol inlet concentration led to the high phenol removal • **RO**: Increase in inlet feed flowrate or inlet phenol concentration improved phenol removal • **Hybrid** arrangement: It was more effective in terms of the treatment efficiency; It could remove higher phenol concentration	• The model could improve by incorporating the catalyst deactivation and providing the typical industrial operating conditions	[178]
HDS of gasoil in an experimental TBR	• The shape of H_2S molar concentration profile was determined by the balance between the mass transfer and the reaction rate • The optimized condition led to the lower H_2S concentration because of the enhanced gas-liquid mass transfer	• The incorporation of temperature fluctuation and catalyst deactivation into the model could result into more reliable findings	[204]
Hydrogenation of DCPD to DHDCPD and then to THDCPD	• The performance of TBR decreased with the increase in the cycle period • Periodic modulation of flowrate seemed to be a strategy of operating a TBR in the region of hotspot development	• The analysis of the performance including the continuous operation and catalyst deactivation could lead to more sophisticated model	[205]

2.5.3 Hysteresis in TBRs

The concept of hysteresis is usually speculated as the various degrees of packing wetting between decreasing and increasing modes of operation [239]. In another definition, hysteresis is the dependency of the hydrodynamic parameters, such as pressure drop, on the flow history of particles bed [240]. At the macroscopic level, the presence of gas or liquid phase dictates different flow regimes (trickling, pulsing, spray, and bubble). From microscopic viewpoint, several liquid flow textures (film, rivulet, pendulum structure, liquid-filled pocket, and liquid-filled channel) are identified in a TBR. Some factors, such as inlet gas and liquid distribution, particles size and shape, wetting properties, the existence of inert fines, packing methods, start up procedures, gas and liquid flowrates, and the fluid physical properties considerably affect the transport phenomena and hysteresis in TBRs [239]. The procedures of TBRs design are inevitably dependent on the liquid holdup, which represents the reactants residence time in the liquid phase. Moreover, the value of pressure drop might change from one hydrodynamic state to another by even 100%, significantly influencing the operating costs. Therefore, the existence of hysteresis complicates the scale-up from the pilot plant reactor to the commercial reactor scale. Maiti et al. [239] found that addition of wetting agent (reduction in the liquid surface tension) decreases hysteresis even though there is a small increase in the pressure drop. Investigating the impact of particle porosity, it was found that nonporous particles (e.g., glass) have higher hysteresis in comparison with the porous particles (e.g., alumina). In addition, more hysteresis is observed at high gas flowrates. There is a reduction in the hysteresis of the pressure drop as well as the liquid holdup when the reactor diameter increases. This impact decreases upon an increase in the particle size. Both pressure drop hysteresis and liquid holdup hysteresis are influenced by the liquid initial distribution. The observed hysteresis with spray distributor is lower than that with the perforated distributor since the spray model has better liquid distribution. Also, lower hysteresis is caused by the larger particle sizes. An increase in the liquid operating range throughout the trickling flow regime leads to more hysteresis due to more dry regions [239]. The prewetting method has a significant impact on the wetting distribution and its efficiency [241]. Saroha and Nandi [242] investigated the pressure drop hysteresis using two different operation modes (Kan prewetting and Levec prewetting). It was found that hysteresis phenomenon takes place due to the start-up and operational conditions/modes. It was confirmed that the pressure drop hysteresis is significantly influenced by the prewetting method [242]. It was also concluded that the utilization of smaller diameter particles leads to more striking in Levec prewetting while the hysteresis is not affected by the particle size in Kan prewetting. It was found that the key factor in the pressure drop hysteresis in the trickling flow regime is the variation of flow structure throughout the packed bed [242]. In an experimental work, Kuzeljevic et al. [240] investigated the hysteresis in a high pressure TBR, and introduced a factor to quantify the magnitude of hysteresis. They reported that the hysteresis is strongly dependent on the operating gas and liquid flowrate and pressure. At lower liquid flowrates, the hysteresis is present; however, the degree of hysteresis decreases upon an increase in gas flowrate and pressure. They concluded that the difference in the predicted pressure drop can reach 300-400% in a high pressure TBR [240]. Maiti et al. [243] studied the impact of particle porosity on the hysteresis, examining particles with various pore densities (porous, semiporous, and nonporous), which have identical sizes and shapes, and made from the same material. It was explored that there is a difference in pressure drop up to 90% between decreasing and increasing modes of operation [243]. Figure 2-18 demonstrates the effect of the liquid viscosity on the pressure drop hysteresis loop in Levec's mode of operation in a TBR. The experiments were conducted with air+water and air+water+CMC (carboxymethyl cellulose) systems. As it is clear that an increase in the two-phase pressure drop occurs with increasing the liquid viscosity. Generally, liquid holdup increases with an increase in the liquid viscosity, leading to increased two-phase pressure drop. As it can be seen, change in the liquid viscosity does not result in a significant fluctuation in the hysteresis loop area [242].

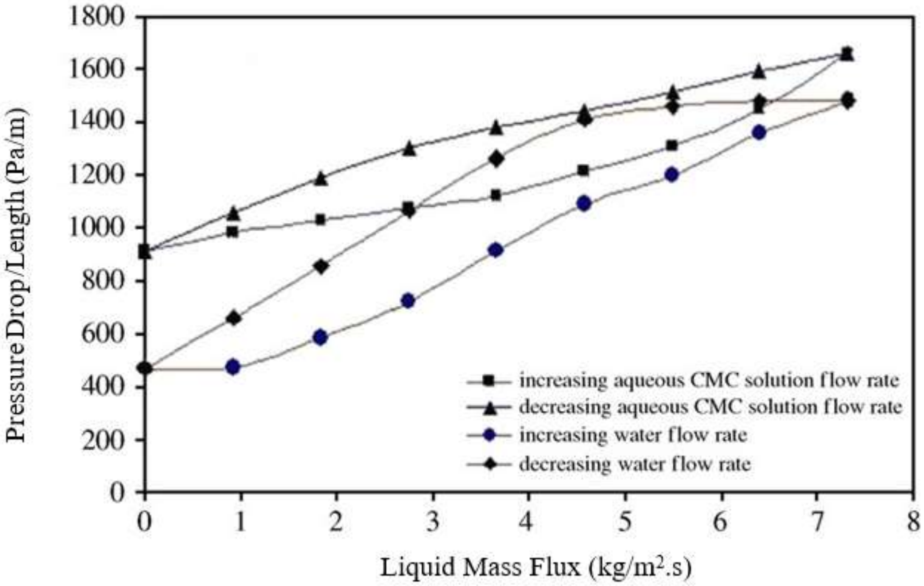

Figure 2-18: Influence of liquid viscosity on the two-phase pressure drop hysteresis loop in Levec's mode of operation in a TBR (Gas mass flux=0.0915 kg/m^2.s; CMC stands for carboxymethyl cellulose).

2.5.4 Technical Issues in Design and Operation of TBRs

TBRs operation can be problematic depending on the operating conditions and the reactor specific characteristics. Pressure drop could be a concern for lower catalyst particle sizes; however, the rates of reactions might be limited due to the intraparticle and interphase heat and mass transfer. Another more significant concern could be the considerable radial temperature gradients for highly exothermic reactions, which makes it challenging to control the reactor temperature in industrial-scale operation. Lower liquid flowrate results in incomplete wetting of catalyst particle and liquid maldistribution, which might lead to inefficient performance of a TBR. Incomplete wetting could promote gas phase reactions, hotspot creation, or even reactor runaway. Highly exothermic reactions in a TBR could cause considerable temperature gradients within catalyst particles, vaporization of the reactant or solvent, and reduction of reaction rate/conversion. These issues can be tackled by the utilization of excess solvent, intermediate cooling, and liquid redistributors [13]. Multiphase reactors' analysis and design is likely the extensively studied/investigated subject in the field of chemical reaction engineering [81]. Design and modeling of a three-phase reactor necessitate the knowledge on hydrodynamic (e.g., pressure drop, flow regime, and phases' holdups) and transport (e.g., back-mixing degree in each phase, gas-liquid mass transfer, liquid-solid mass transfer, and fluid-wall heat transfer) parameters [81].

The following items are among the most concerning issues of TBRs design:

- Determination of flow regime for a specified set of operating conditions of a TBR, which is mainly dependent on the gas and liquid flowrates, flows applicable orientation (cocurrent downward, cocurrent upward, and/or countercurrent), packing materials size and status, fluids properties, and phases’ distributors [81]. The effects of wetting efficiency on operating conditions are required to relate laboratory/pilot-scale reactor data for reliable scale up and design of industrial TBRs [82].

- Transition of flow regimes that occurs due to the fluctuations of operating conditions [12].
- Accurate estimation of gas-liquid and liquid–solid mass transfer parameters [12].
- Determination of catalyst wetting efficiency/catalyst utilization [12].
- Flow maldistribution affects the RTD, leading to bypassing, channeling, and dead zones. Channeling and bypassing in TBRs result in ineffective utilization of catalyst [81]. Liquid distributor design plays a key role in such a malfunction [81]. Conventional distributor designs, such as chimney tray, sieve tray, and bubble cap tray have poor performance; however, advanced distributors, such as Exxon’s Spider Vortex technologies, Topsoe Vapor-Lift tray, Shell’s HD tray, Fluor’s Swirl Cap tray, and Akzo Nobel’s Duplex tray promote complete sprinkling of the catalyst bed [82]. The most significant mechanical design aspect of tray is the liquid discharge pattern since it identifies the percentage of wetted catalyst at the top of the catalyst bed [82]. Even though the uniform liquid distribution forms in the top part of the reactor, uneven wetting condition might occur as the liquid flows along the reactor length [13].
- Catalyst porosity has a considerable effect on the RTD. The porous catalyst traps some liquid, which is known as a portion of the system static liquid holdup [81]. Local particle configuration and, therefore, local porosity variation depend on the packing type, particle size, particle shape, and the ratio of particle diameter to reactor diameter. This variation in

porosity affects the capillary forces, influencing the catalyst particles wetting efficiency [13].

- Various packing arrangements are proposed for randomly packed-bed reactors. The voids formed among the particles impact the flow distribution in the bed, controlling the mixing and transport rates of mass and heat. Moreover, it affects the catalyst bed stagnant and dynamic liquid holdup [13].
- Novel catalyst designs, and modification of existing catalyst in terms of higher stability and selectivity (e.g., monolithic or foam substrates and surface coating) are other key design issues of the catalytic TBRs [82]. In catalyst design and development for the industrial applications, the porosity is usually given in the subsequent order: selectivity>stability>activity [82]. Other than the catalyst selection, design of catalyst particle size and shape appropriate for TBR operation is critical for successful and efficient operation. The main target of catalyst particle size and shape is to accommodate maximum load of catalyst per reactor unit volume without dramatically influencing other operating parameters such as liquid holdup, pressure drop, wetting, interfacial area, catalyst effectiveness factor, and mechanical and thermal characteristics of catalysts [13].
- Catalyst deactivation is another critical issue in the design of TBRs. In this condition, macrokinetic analysis needs to be considered for the determination of reaction rate parameters. Successful reactor design needs the kinetic models that are based on the steady state chemical activity. Therefore, the intrinsic reaction rates of catalyzed reactions in TBR are to be modified [82].

- To control the TBRs temperature, managing the heat generated/consumed in the reactor is a key factor in the design of TBRs [13, 82]. One of the heat management strategies in the control of the TBRs temperature is to use different configurations of reactor vessel including single bed, adiabatic reactor with inter-stage gas injection, and multiple adiabatic beds with inter-stage heat exchange [82].

2.5.5 Chemical Engineering Software

The scope of scientific computation includes the development of techniques to deal with various mathematical models, corresponding mathematical analysis, and computer codes to obtain satisfactory results [244]. Application programs obeying definite algorithms for the solution of mathematically formulated problems are written by users in some programming languages. These programs are called source code. FORTRAN (FORmula TRANslation) was designed by IBM Corporation in 1957. It was created for the scientific computing purpose. Other important programing languages are C developed by Bell Laboratories, and JAVA developed by Sun Microsystems. C and JAVA are not designed solely for the scientific computations. MATLAB (evolved by Math Works Inc.) and PYTHON (designed by Centrum Wiskunde and Informatica) are other popular programming languages in the field of scientific computations [244].

Chemical engineering field lacked the tools to design an entire process till the 1960s. Moreover, process control was growing as a critical discipline in chemical engineering. Roger Sargent, the father of process system engineering, introduced SPEEDUP (Simulation Program for the Economic Evaluation and Design of Unsteady state Processes) in 1964. In 1981, various specialized packages were available, such as ASPEN, HYSYS, DESIGN II, PRO II, and

CHEMCAD. Better understanding and analysis of the process was pursued with the development of computers. Table 2-8 summarizes some of the chemical engineering software packages. It should be highlighted that a majority of software/tools are able to solve most of the engineering problems in some way or other [245].

Table 2-8: A summary to the chemical engineering software [245].

Subject	Software	Example
Fluid mechanics	MATLAB®, CHEMCAD, Excel, COMSOL Multiphysics ®	Fluid flow, Piping
Heat transfer	MATLAB®, COMSOL Multiphysics®	2D conduction
Mass transfer	MATLAB®, COMSOL Multiphysics®, gPROMS®	Mass and momentum transfer, 2D diffusion
Mass and energy balances	gPROMS®, Excel, Mathcad	NH_3 oxidation, Ammonia production, Synthesis gas, $CaCO_3$ furnace
Unit operation	gPROMS, CHEMCAD, Excel, MATLAB®	CO_2 capture Cooling tower, Distillation column
Unit operation (particles)	EDEM®	Rotary drum
Reactor engineering	GAMS®, MATLAB, gPROMS, Mathcad	Multibed reactor for SO_3 Polymer reactor (semibatch), Simultaneous reactions, Bioethanol second generation (batch), SO_2 to SO_3 (pressure drop)
Control and dynamics	MATLAB/Simulink®	Control loop, System response to perturbation
Equipment design	gPROMS, CHEMCAD, MATLAB®, Excel/Mathcad	Heat exchangers Distillation columns, Evaporators
Process analysis and design	gPROMS, GAMS, CHEMCAD ASPEN-HYSYS®, Excel	Utility plant, Ammonia synthesis, Methanol production, HNO_3
Plant allocation	GAMS	Supply chain design
Plant operation	AIMMS®	Scheduling

For many years, trial and error was the only approach for the development and improvement in the chemical industries. Costly experimental runs at pilot and industrial scales in the matter of money and time put a huge pressure on modeling and simulation of processes as a tool for systemized process design, optimization, and analysis. The modeling endeavor is dependent on determining chemical, biological, and physical laws that govern any operation, such as heat and mass transfer, momentum, mass and energy balances, and kinetics and chemical equilibria to develop a reliable mathematical image of the process so as its performance to be evaluated in a more efficient way. With increase in the computers power, their abilities along with the development of software, such as CHEMCAD®, ASPEN®, gPROMS®, ANSYS®, COMSOL®, and EDEM®, provide sophisticated tools for the solution of complicated phenomena more practically [245].

Microsoft Excel® is a perfect interface or tool to carry out calculations, and also to connect various software. Therefore, the results of the modeling/simulation run from software such as MATLAB®, CHEMCAD®, GAMS®, and Mathcad could be delivered/stored in Excel [245]. MATLAB® (Matrix Laboratory) is one of the most extensively utilized software in chemical engineering. MATLAB is a programming language in addition to being performing operations. Its performance is relied upon the utilization of *m* files, which are classified into scripts and functions. Mathcad® is a symbolic software in engineering. The strengths of Mathcad are built-in unit functionality, readable format for showing equations, and the capability to cope with symbolic calculations [245]. CFD is a numerical technique/method to solve conservative equations of momentum, mass, energy, and species and relevant phenomena by utilizing programming languages [245, 246]. As the mentioned conservation equations are solved by computers, knowledge on programming languages, such as C++, FORTRAN, MATLAB or Java is equally crucial. The idea of describing flow with mathematical equations came from Claude-Louis Navier (French engineer) and George Gabriel Stokes (British mathematician and physicist) in the nineteenth century, explained the fluids' motion by Newton's second law. The commercial CFD-based software modeling tools are ANSYS®, Fluent®, ANSYS®CFX®, ANSYS® Multiphysics™, Flow-3D®, COMSOL

Multiphysics®, STAR-CD®, STAR-CD®, STAR-CCM+®, OpenFOAM®, AVL FIRE®, and ANSYS® Polyflow® [245].

The most suitable approach for particulate solids process analysis is the utilization of computer simulation by the distinct element method (DEM). It is applied for the understanding of particles' bulk behavior in the processes of granulation, mixing, size reduction, compaction, fluidization, powder dosing in capsules and dispersion, flow out of storage vessels, and particles' sedimentation in fluids [245]. The idea of DEM was introduced by Cundall and Strack [247]. In this approach, Newton's law of motion is utilized to explain particles motion, and contact mechanics is used to describe the interaction among the particles [245].

A process simulator (process flowsheeting package) performs equipment sizing, mass and energy balancing, and cost calculation. A process simulator can solve the challenges of simulation, design, and optimization. The most powerful process simulators are Aspen Plus, CHEMCAD, Aspen HYSYS®, PRO II, SuperPro Designer, gPROMS, and ProSimPlus. Most of the current process simulators are established considering an object-oriented approach by utilizing programming languages, such as Java or C++. Any process model is grouped into three main classifications of continuous or discrete, steady state or dynamic, and stochastic or deterministic. One of the classification methods of process simulator is based on the process description and solution methods of the developed equations. Therefore, the resulting types of process simulators are sequential modular, equation oriented (or simultaneous nonmodular), and simultaneous modular. Figure 2-19 illustrates the interrelations among the major components of a simulation package [245].

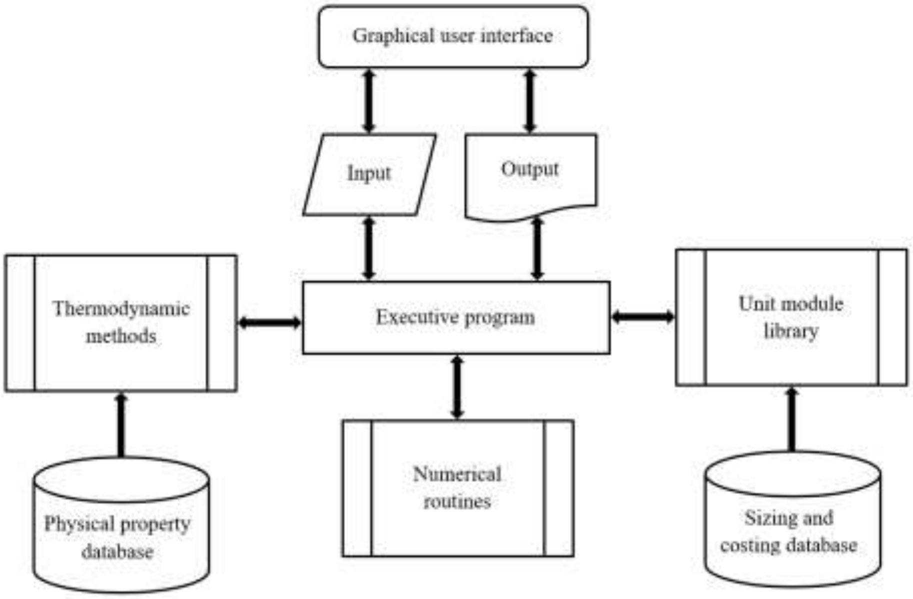

Figure 2-19: Elements of a process simulator software.

gPROMS (General Process Modeling System) is an efficient software for the process modeling and optimization and the equipment design [245]. gPROMS ProcessBuilder is the next generation of Advanced Process Modeling environment to optimize the process plants' design and operation. It unites the industry-lead steady state and dynamic models with the gPROMS equation-focused modeling, optimization, and analysis platform [248].

GAMS (General Algebraic Modeling System) is a top-level algebraic modeling technology developed by GAMS Development Corporation. It can solve nonlinear and linear mathematical models. In GAMS environment, optimization models can be evaluated/incorporated in similar fashion to how they are introduced/written in a research paper or a book. It is able to solve extensive linear programming problems and integer linear programming problems, and to determine global or local optima of mixed integer problems and nonlinear problems, having different levels of convolution [249, 250].

Athena Visual Studio provides an integrated environment for modeling, optimal experimental design, and graphical interpretation of chemically reactive and nonreactive systems. It allows user to develop his own models. Athena Visual Studio can solve the developed model equations, and estimate the parameters for many applications. The model might include ODEs, PDEs, differential algebraic equations, implicit differential equations, or solely algebraic equations [251].

Design of experiment (DOE) software is more complete, efficient, insightful, and less prone to error than the same design by hand with tables. Also, it is able to produce algorithmic designs, which are usually needed to adapt constraints that are commonly experienced in practice [252].

Evolutionary computation is a powerful technique to develop sophisticated algorithms for the solution of convoluted optimization problems. The best-known evolutionary computation algorithms are genetic algorithms (GAs), evolution strategies, evolutionary programming, and genetic programming. Among them, GAs are the powerful and extensively applied stochastic search and optimization techniques. GAs and ANNs are evolved by computation in biological systems. The proposed/developed biological neural architecture can be structured/determined genetically [253].

However, there are still pitfalls in the presented engineering software packages, which are used to properly represent the phenomena taking place in the complicated reaction systems, such as TBRs. In order to accurately analyze the performance of TBRs, the variable operating parameters need to be simultaneously incorporated into the mathematical models. For example, the nonlinear equations of chemical reactions rate, nonlinear expression of the deactivation rate, the structure/form of the catalyst particles in the bed, changes in the wetting efficiency of the catalyst particles, changes in the patters of fluid distribution along the bed, changes in the profiles of operating parameters in all spatial coordinates along with their dependency on time, position of fluid nozzles, and transition in the flow regimes in the TBRs should be considered all together since they affect the reaction system performance. In other words, they are interrelated. This becomes more critical in the TBRs performance analysis over the difficult operation of the catalyst processes. In general, the industrial processes/plants experience numerous fluctuations over the operation, such as product quality alteration, catalyst activity variation, fluctuation in the operating conditions, startup and shutdown of the process, and change in the production rate. It appears to be important to use the results of the reactor modeling for modeling/analyzing the other operation units, especially separation systems (e.g., distillation columns). Although it is not practical to simulate all these complicated phenomena/conditions in most real cases, the development of a particular software to reliably model chemical reaction systems (e.g., TBRs) seems vital.

2.6 Challenges in TBRs Modeling and Design

One of the important factors influencing the development of societies is the countless products produced in the chemical industries; this clearly reflects the importance of reaction engineering. Multiphase reactors (e.g., TBRs) are extensively used in industries, having numerous applications (e.g., chemicals, pharmaceuticals, polymer, biomass, and petroleum refining). This highlights the significance of multiphase reactors design, modeling, and operation. There has been considerable progress in the field of modeling and simulation of TBRs due to the advancement in the engineering software and the technological enhancement in the experimental devices. However, there are many challenges that need to be addressed to increase the reliability of the developed model and the accuracy of the results obtained from the proposed model. In addition to the theoretical aspects of the TBRs performance evaluation, their operation requires improvement, leading to more efficient process. This can be accomplished by better design of the TBRs and more active catalyst utilization and synthesis in terms of lifetime, which provide proper environment for the reaction fulfillment. Proper design of TBRs and its continuous improvement lead to a more efficient process, and consequently a higher quality product production and more environmentally friendly process. The following are the concerning issues related to the modeling and operation of the TBRs:

- Design of the novel solid catalysts with higher selectivity and stability
- Novel reactor configuration
- Development of new catalyst supports and coating surfaces to lengthen catalyst lifetime even in the cyclic/periodic operation
- Kinetic data acquisition for model development in the absence of physical transport effects
- Accurate estimation of phase holdup interfacial areas and mass transfer coefficients
- Loading method of the catalyst in the bed
- Catalyst bed design
- Reactor pressure fluctuations, catalyst abrasion, and product quality
- Increasing the production capacity to meet the increasing demand for fuels
- Higher quality of the final product
- Much lower quality of the feedstock (to process a greater amount of heavier feedstock)
- Controlling highly exothermic reactions
- Operating TBRs under adiabatic condition

- Combination of flow patterns and their quantification
- Maintaining product quality to achieve stringent product quality
- Catalyst deactivation
- Wetting efficiency measurement
- Liquid flow maldistribution
- Unsuitability of atmospheric data and models or correlations to extrapolate to operation at elevated pressures
- Lack of an accurate and phase/liquid distribution model
- Development of dispersion model in the transition state
- Nonlinear response of the process to the change in the production rate
- Lack of reliable correlations for the calculation of gas (e.g., hydrogen) solubility
- Incorporation of VLE calculations in the model development

Other challenges in TBRs modeling can be the selection of suitable numerical techniques to tackle the non-linearity of the equations of the developed model. Uncertainties in the process parameters values and the utilized catalyst characteristics calculated either by the correlations and analytical techniques or by the collected field data might lead to an unreliable developed model. One of the most recent challenges is the utilization of the data and understanding on a molecular level for the chemical reactor modeling. Quantum mechanical methods, molecular simulation (molecular dynamics and Monte Carlo), and continuum equations can be utilized for multi-scale models development, describing reactions kinetics features, multicomponent diffusion and adsorption inside the pores structure, and the entire reactor. There is an increasing interest in the application of the mentioned approaches in the heterogeneous catalysis, such as pore geometry impacts on the reactions, metal-support interactions, and multi-scale modeling. To conclude, an efficient process requires an appropriate catalyst, a suitable reactor, a desirable chemical conversion, and ability to apply these conditions to the commercial process.

A mathematical model cannot be employed without being validated where the proper correlations for the accurate estimation of the transport phenomena parameters are required. In this regard, a pilot test/experimental phase plays a significant role. A pilot plant as an experimental rig demonstrates part of the operation corresponding to an industrial plant, providing the simultaneous analysis of chemical and physical mechanisms. Pilot plant experiments provide a necessary step in the process investigation of a commercial plant. A pilot plant is able to use the microkinetic data resulted from the laboratory tests, providing knowledge on the process macrokinetics (e.g., macroscopic fluid elements, impacts of the macroscopic streams of mass and energy on the process, and true residence time of a full-scale plant). Even though advanced software packages make the data analysis for the process optimization and statistical evaluation purposes an easy task, more experimental data with high accuracy are required for assessment of the complicated reaction systems to obtain optimized yield and high product quality. Therefore, more efforts are required to improve the pilot plant performance and utilization. For instance, they usually have low flowrates, leading to significant heat and mass gradients that can be rectified by the specific arrangements of catalysts and inert components. Another concern is the data collection from a system which is highly sensitive to temperature. For example, only 5% error in the deactivation energy can result in 75% error in the calculated reaction rate. Therefore, a fail-safe approach based on the suitable selection of experimental procedure is required to deal with the possible uncertainties (i.e., using proper pilot reactors). Another example that highlights the importance of the pilot plant experiments is the lifetime of the new catalysts, which provide reliable information for the catalytic process efficiency and the catalyst manufacturer (e.g., installing a pilot reactor next to the actual reactor). Also, pilot plant experiments are required for validation of the developed model and even hazard identification. Thus, construction of a more sophisticated pilot plant with the most advanced control system and design can provide more reliable results on the flow patterns (e.g., complete mixing, plug flow, and a selection between dispersion, cascade, and combined models), estimation of thermal parameters (i.e., more realistic correlations), impacts of accurate prediction of the various parameters, investigation of the dynamic state with disturbances, and development of more accurate mathematical models toward better validation and model optimization.

2.7 Conclusions

This review paper provides detailed information on the current understanding of the TBRs modeling and simulation. The paper summarizes the current challenges and concerns in TBRs modeling and operation. It seems that the cost of operation and production can be reduced if the addressed challenges could be rectified. One of the most serious issues presented is catalyst deactivation. The catalyst characteristics, such as shape, size, porosity, support, and active sites, can be modified in such a way that it could lead to a more stable and active catalyst with a more stabilized/stable structure. Researchers and manufacturers play critical roles in the accomplishment of such a demanding goal. Regarding the development of a more reliable model, collection of the required data at the real operation time is crucial. The data need to be collected when normal operation is established. The data collection during the plant start up and shut down is not advised. However, the sensitivity analysis of the vital variables of the developed model for the proposed operation needs the data of the variables' fluctuation for the validation investigation. Data collection for the key operating variables involved in an industrial process is not possible since proper operation and efficient product quality control require fixed set-points for some of the critical operating parameters (e.g., reactor pressure, reactor feed flowrate, and reactor feed concentration), depending on the type and conditions of the process. Another concern is the model parameters estimation of a process, which is operated at high pressure and temperature. Most of the existed correlations have been obtained at low pressure. An example is calculation of the catalyst wetting efficiency. Structured loading of a catalyst can enhance its effective utilization. Moreover, optimal control of high pressure TBRs can result in longer catalyst lifetime, particularly for a fragile catalyst, and for sustaining an acceptable product quality. This adverse phenomenon is more noticeable at the condition of high gas flowrate and high gas molecular weight. Hence, numerous investigations need to focus on the pressure impacts on the TBR operation, design, and scaling. Another critical matter is related to the temperature control of the highly exothermic process and the importance of the periodic operation and its quantification.

In addition to the conclusion remarks mentioned above, the following subjects can be considered as the future research works related to modeling of TBRs:

- Involvement of the catalyst deactivation into the model
- Development of the catalyst deactivation rate using industrial data
- Incorporation of catalyst wetting efficiency into the model
- Development of a vigorous model, considering the fluid flow non-ideality
- Considering the change of the vital operating parameters in the model
- Incorporation of the possibility of the flow regime transition into the model

- Considering the catalyst characteristics (e.g., shape and pore structure) in the model
- Modification/changes in the design of the TBRs
- CFD modeling on the optimal position of the feed nozzles (e.g., feed nozzle and gas nozzle)
- CFD modeling on the optimal structure/load of the catalyst particles in the bed of a TBR
- Energy/exergy model development for a high pressure and temperature TBR process

Efficient transformation of the knowledge and information from the small-scale reaction systems to the industrial scales with the least deviation is an exceptional achievement that can be obtained through implementing the key and fundamental reaction engineering aspects; this can lead to a considerable progress in the performance of multiphase reactors (e.g., TBRs). To sum up, more advanced models of a TBR considering the vital operating parameters affecting the process efficiency can contribute to the less costs of operation, higher product quality, safer operation, and cleaner process/environment. Development of more efficient technologies can help make more improvements in the design, operation, and optimization of TBRs.

NOMENCLATURES

Acronyms

4-CBA - 4-carboxybenzaldehyde

AC - active carbon

AMS - α-methylstyrene

ANN - artificial neural network

BBM - black-box model

BC - boundary condition

BD - 1,3-butadiene

BTX benzene, toluene, and xylene

BVP - boundary value problem

CDS - computer designed shape

CFD - computational fluid dynamics

CMC - carboxymethyl cellulose

CSTR - continuous stirred tank reactor

CTA - crude terephthalic acid

CWAO - catalytic wet air oxidation

DBF - dibenzofuran

DBT - dibenzothiophene

DCPD - dicyclopentadiene

DE - differential equation

DEM - distinct element method

DHDCPD - dihydrodi-cyclopentadiene

DOE - design of experiments

DNT - 2,4 dinitrotoluene

EOS - equation of state

FAME - fatty acid methyl ester

FBR - fixed-bed reactor

FCC N-LCO - fluid catalytic cracking naphtha and light crude oil

FDM - finite difference method

FEM - finite element method

FL - fuzzy logic

FT - Fischer-Tropsch

FPM - first principle model

FVM - finite volume method

GA - genetic algorithm

GAMS - general algebraic modeling system

GO - glycerol

HC - hydrocarbon

HDA - hydrodearomatization

HDC - hydrocracking

HDM - hydrodemetalation

HDN - hydrodenitrogenation

HDNi - hydrodenickelation

HDO - hydrodeoxygenation

HDP - hydropurification

HDS - hydrodesulfurization

HDT - hydrotreating

HDV - hydrodevanadization

HGO - heavy gas oil

HIR - high interaction regime

HPA - hydroxypropana

HTA - hydrogenation of mono-, di-, and tri-aromatics

HTO - saturation of olefins

IC - initial condition

IPD - interaction parameter data

IVP - initial value problem

LA - lactic acid

LCO - light crude oil

LGO - light gas oil

LH - Langmuir-Hinshelwood

LHSV - liquid hourly space velocity

LIR - low interaction regime

MAPD - methylacetylene and propadiene

MD - molecular dynamic

MRI - magnetic resonance imaging

n-BB - *n*-butylbenzene

OCM - orthogonal collocation method

ODE - ordinary differential equation

ODS - oxidative desulfurization

PDE - partial differential equation

PDO - propanediol

PFC - pulsing flow condition

PFM - plug flow model

PG - propylene glycol

PFR - plug flow reactor

POLF - pre-saturated one liquid flow

PR - Peng-Robinson

RBDPO - refined, bleached, and deodorized palm oil

RK - Runge-Kutta

RKS - Redlich-Kwong-Soave

RO - reverse osmosis

RTD - residence time distribution

SAR - slurry airlift reactor

SFO - sunflower oil

SPEEDUP - simulation program for the economic evaluation and design of unsteady state processes

SQP - successive quadratic programming

SRGO - straight run gas oil

SRK - Soave-Redlich-Kwong

SS - steady state

TBR - trickle-bed reactor

TFC - trickling flow condition

TGA - thermogravimetric analysis

THDCPD - tetrahydrodicyclopentadiene

TNC - titanate nanotubes catalyst

TOS - time-on-stream

ULSD - ultra low sulfur diesel

VGO - vacuum gas oil

VLE - vapor-liquid equilibrium

VOF - volume of fluid

WBM - white-box model

WHSV - weight hourly space velocity

List of Variables/Symbols

A	constant depending on the feedstock reactor type, and reaction conditions	
a	catalyst activity	
a	effective interfacial area	$m^2\ m^{-3}$
a_P	external area of particles per unit volume of reactor	$m^2\ m^{-3}$
a_w	wetted external area of particles per unit volume of reactor	$m^2\ m^{-3}$
ar	aspect ratio	
Bo	Bodenstein number	
C	concentration	$kmol\ m^{-3}$
C_c	amount carbon deposited on the catalyst	$\mathrm{kg\ kg_s^{-1}}$
C_p	heat capacity	$J\ kg^{-1}\ K^{-1}$
Ca	capillary dimensionless ratio	
cm	parameter in Equation (2-25)	
cn	parameter in Equation (2-24)	
d	diameter	m
d_{PE}	equivalent diameter of catalyst particle	m
D	diffusion coefficient	$m^2 s^{-1}$
D_{da}	axial mass dispersion coefficient	$m^2 s^{-1}$
D_{dr}	radial mass dispersion coefficient	$m^2 s^{-1}$
D_e	effective diffusivity	$m^2 s^{-1}$
E	intrinsic activation energy for chemical reaction	$J\ mol^{-1}$
E_a	catalyst activation energy	$J\ mol^{-1}$
ER	Ergun constant (Equation (2-22))	
f	parameter defined in Equation (2-7)	

f'	wetting efficiency	
f_s	shear slip factor	
g	gravitational acceleration constant	$m\ s^{-2}$
G	superficial mass velocity	$kg\ m^{-2}\ s^{-1}$
Ga	Galileo number	
h	heat transfer coefficient	$W\ m^{-2}\ K$
H	Henry’s constant	$barg\ m^3\ kmol^{-1}$
ΔH_j	heat of reaction	$J\ mol^{-1}$
I	permeability tensor for gas or liquid phase	m^2
J_{gl}	viscous drag tensor for gas phase over liquid phase	-
k	mass transfer coefficient	$m\ s^{-1}$
k_c	gas-particle mass transfer coefficient	$m\ s^{-1}$
k_r	rate constant per unit particle volume of catalyst	s^{-1}
k_{intr}	intrinsic rate constant	$m\ s^{-1}$
k_{obs}	observed rate constant	$m\ s^{-1}$
k_P	proportionality constant	
k_d	deactivation rate constant	s^{-1}
k_{do}	pre-exponential factor	s^{-1}
$k.a$	volumetric mass transfer coefficient	s^{-1}
K	overall mass transfer coefficient	s^{-1}
L	reactor length	m
m	sintering order	
n	order of reaction	
nf	a value in the coking/fouling kinetics (Equation (2-9))	
N_T	number of active sites	

Nu	Nusselt number	
P	pressure	Pa
$\Delta\langle P\rangle$	average pressure drop	Pa
$\frac{\Delta P}{L}$	pressure drop per unit bed height	$N\ m^{-3}$
Pe_P	Peclet number based on particle diameter	
Pr	Prandtl number	
Q_P	poison/foulant concentration	$mol\ m^{-2}$
Q_{Po}	final capacity of the catalyst for poison/foulant	$mol\ m^{-2}$
r	radial coordinate	m
r_j	rate of reaction	$kmol\ kg_s\ s^{-1}$
r_P	rate of reaction per unit volume of particle	$kmol\ m^{-3}\ s^{-1}$
R	universal gas constant	$J\ mol^{-1}\ K^{-1}$
R_P	particle radius	m
Re	Reynolds number	
Sc	Schmidt number	
Sh	Sherwood number	
t	time	s
T	temperature	K
u	superficial velocity	$m\ s^{-1}$
$\langle u\rangle$	superficial average velocity vector of gas phase or liquid phase	$m\ s^{-1}$
U	overall heat transfer coefficient	$W\ m^{-2}\ K^{-1}$
v	interstitial velocity	$m\ s^{-1}$
z	axial coordinate	m

Greek letters

β	dimensionless axial dispersion number

γ	dimensionless activation energy	
ε_B	void fraction	
ε	phase holdup	
ε_{ld}	dynamic liquid holdup	
ε_{ls}	static liquid holdup	
ε_P	particle porosity	
η	catalyst effectiveness factor	
κ	numerical constant	
λ	thermal conductivity	$W\ m^{-1}\ K^{-1}$
λ_e	effective thermal conductivity	$W\ m^{-1}\ K^{-1}$
ξ	specific surface area of the phase interface	$m^2\ m^{-3}$
ρ	density	$kg\ m^{-3}$
ρ_B	bed bulk density	$kg\ m^{-3}$
τ	space time	s
σ	surface tension	$N\ m^{-1}$
φ	sphericity	

Subscripts

a	axial
b	bulk
f	fluid (gas or liquid) phase
g	gas phase
gl	gas phase to liquid phase
i	index of components
in	inlet to the reactor
j	reaction index

k	number of reactions
l	liquid phase
ls	liquid phase to solid/catalyst phase
m	molecular
n	normal
out	outlet from the reactor
P	particle
r	radial
R	reactor
s	solid/catalyst
t	total
w	wall

Superscripts

0	reactor inlet condition
o	atmospheric condition and stagnant condition
S	catalyst surface
ss	steady state

3 CHAPTER THREE: A Dynamic Heterogeneous Dispersion Model Evaluates Performance of Industrial Catalytic Hydrotreating Systems

Preface

A version of this chapter was published in the Journal of Industrial and Engineering Chemistry Research 57, 8267-8282 (2018). I am the primary author of this paper. With the advice and help of the co-author, Sohrab Zendehboudi, I developed the mathematical model and designed the manuscript's structure. The majority of the literature review, data collection, and the analysis of the results were done by me as the first author. I prepared the first version of the manuscript, and revised the manuscript based on the co-author's suggestions, and comments received from the journal reviewers. Sohrab Zendehboudi also helped me to develop the methodology and analyze the results. The co-author was of a great help to me in preparation process of the manuscript so that several comments in terms of technical and editorial prospects were received from him.

Abstract

Catalyst deactivation is one of the most problematic matters in industrial operations. Therefore, any improvement in the operation of costly catalytic processes can be considered as a valuable contribution to the corresponding industrial sectors. In this chapter, a dynamic heterogeneous model is developed for the crude terephthalic acid hydropurification process. The model incorporates the effects of the axial mixing and deactivation of the commercial catalyst of palladium supported on carbon (0.5 wt.% Pd/C) on the efficiency of the hydropurification operation. Moreover, the developed model is utilized to analyze the impacts of catalyst particle size and its porosity on the performance of the catalytic purification process. The transport phenomena governing equations lead to a series of partial differential equations which are simultaneously solved through employing a suitable numerical method. The mathematical modeling and parametric sensitivity analysis are conducted through computer programming via MATLAB 2016a©. The model validation is accomplished using the industrial data. The results reveal that the proposed model satisfactorily simulates the real process, and it is more accurate than the plug flow model to forecast the process behaviors of hydropurification operation. It is found that a decline in the catalyst particle size improves the performance of Pd/C catalyst by about 16% while maintaining an acceptable pressure drop along the length of the catalyst bed. In addition, an increase in the catalyst porosity prolongs the catalyst lifetime up to 8%; increasing 4-CBA concentration in the reactor feed results in a 45.3%-reduction in the catalyst lifetime. Based on the study outcome, 3.5% increase in the reactor inlet temperature enhances the catalyst lifetime by about 12%. In addition, the catalyst lifetime is extended by about 20% if the hydrogen partial pressure increases by 13%. The results imply that the traditional commercial catalyst of the process

can be synthesized to result in the longer utilization of the catalyst and higher efficiency of the process. It is also concluded that effective and accurate control of para-xylene oxidation reactor and temperature rise of the hydropurification reactor lead to more efficient purification process. The modeling approach proposed in this study can be applied to the relevant industrial processes for the purposes of optimal operation and process modification.

3.1 Introduction

Proper design and optimization of industrial operations require strong modeling and optimization tools to accurately represent the process units. This is feasible through considering all transport phenomena mechanisms, physical phenomena (e.g., deactivation of catalyst), and the process chemistry to predict the important process parameters including efficiency and distribution of temperature, pressure, and concentration with high reliability and precision [254, 255].

Hydrotreating (HDT) is a catalytic process, which is widely employed in the petrochemical and refinery industries. This process is designed to yield products with high quality through elimination of impurities including sulfur, oxygen, nitrogen, and the saturated aromatic rings and olefins from the main products. HDT is commonly accomplished in trickle bed reactors (TBRs) which are a sub-category of fixed-bed reactors (FBRs). In the process, both gas and liquid phases flow concurrently downward through a catalytic fixed bed [256, 257].

Catalyst deactivation, which is defined as the reduction of catalytic activity and selectivity over time, is a major problem to efficiently operate the industrial units. Deactivation of catalyst is a serious concern in the HDT processes, leading to the loss of production time and investment waste [256, 257]. The deactivation rate is strongly dependent on several parameters such as the concentration of feed impurities, fluctuation of operating conditions, frequency of plant emergency and shut-down situations, equipment efficiency, and product quality.

There are a number of theoretical investigations on the FBR modeling in the literature. For instance, a steady-state model of a TBR was proposed by Dietz et al. [70] for 1,5,9-cyclododecatriene hydrogenation on a Pd/Al_2O_3 catalyst. The developed model takes into account the catalyst partial wetting and the resistances to heat and mass transfer. They concluded that the developed model is able to precisely forecast the outlet concentration of the hydrogenation products. Guo and Al-Dahhan [258] also suggested a model to analyze the catalytic hydrogenation of alpha-methylstyrene and wet oxidation of phenol. The modeling study was carried out through combination of a reactor dispersion model with a pellet -scale model. However, they did not incorporate the pellets liquid wetting contact efficiency and non-linear reaction kinetic expression. The proposed approach was employed to study the behaviors of the pellets and reactor during an aqueous phenol catalytic wet oxidation on a fast-deactivated catalyst (MnO_2/CeO_2). It was found that bubble columns can attain greater phenol conversion at the expense of faster catalyst deactivation. In another research study, Shahrokhi and Baghmisheh [259] investigated the dynamic behavior of the methanol synthesis FBR from control point of view. A one-dimensional heterogeneous model was developed where the model took advantages of proportional-integral-derivative (PID) controller tuning system. The model was planned to compare the performance of adaptive and fixed PID controllers for set point and load rejection. The suggested model was linked with a controller to online optimize the reactor performance and to avoid hot spot formation. Sandelin et al. [260] developed a generic dynamic model for liquid-phase FBRs, while considering catalyst deactivation and complex reaction kinetics. The model was utilized to simulate a catalytic liquid-phase reaction. The model was able to accurately predict the reactor performance. It was concluded that the optimization of the production life cycles of FBRs experiencing deactivation phenomenon is possible through applying the developed model. Mederos and Ancheyta [11] introduced a model to predict the performance of TBRs which are employed for oil fractions catalytic HDT. A one-dimensional heterogeneous model was developed where the model simulated the hydrotreating process through involving three main reactions including hydrodesulphurization (HDS), hydrodearomatization, and hydrodenitrogenation (HDN) [11]. According to their results, the countercurrent operation mode has a considerable potential for efficient HDS of oil fractions. A three-phase plug-flow model (PFM) was suggested by Alvarez and Ancheyta [255] to describe the behavior of residue HDT in a multi-FBR system. The model took into account the liquid/solid and gas/liquid mass-transfer phenomena where important reactions including HDN, HDS, hydrodemetallization (HDM), hydrodeasphaltenization, and hydrocracking were incorporated in the model. The developed model was applied for simulation of an industrial-scale residue HDT unit. Furthermore, Zahedi et al. [261] modeled a heterogeneous industrial FBR used for the dehydrogenation of heavy paraffin with Pt-Sn-Al_2O_3 catalyst. The modeling strategy involved the mass balance (using a reliable reaction rate), momentum balance, and deactivation equations. The results showed that there is no appreciable conversion of paraffin since the surface reaction is the controlling/limiting rate. Moreover, the production of hydrogen was considerable at the entry of the catalyst bed. Toukoniitty et al. [262] performed the transient kinetic experiments concerning hydrogenation of ethyl benzoylformate in a FBR where a supported platinum catalyst was utilized. They investigated the stability of the catalyst and provided adequate info/date on the adsorption-desorption behavior of the reaction participants. Adsorbed surface and liquid-phase components were included in the developed model. It was found from the study results that the model is able to precisely predict the behavior of the organic system. Pellegrini et al. [1] conducted an investigation on the deactivation of 0.5 wt.% palladium supported on carbon (Pd/C) catalysts taken from different crude terephthalic acid (CTA) hydropurification TBRs. The catalysts were classified in terms of lifetimes, location in the bed of catalyst, degree of sintering, and type of contaminants. It was concluded that the process of Pd sintering happens in all catalyst samples. Moreover, the amount and nature of contaminants had no impact on the rate of sintering, except sulphur poisoning. They also claimed that the formation of agglomerates is the major reason for the Pd surface area loss and the catalyst activity reduction. In a modeling investigation, a dynamic model for an industrial TBR of CTA hydropurification was proposed by Azarpour and Zahedi [263]. In their study, a heterogeneous PFM was developed to simulate the dynamic behavior of the catalytic reactor. Their results revealed that the model can forecast the performance of the hydropurification unit and formulate the model for appropriate control strategies. A dynamic model was derived by Alvarez and Ancheyta [264] to investigate the kinetic and thermodynamic behaviors of the FBR system in a HDM process. The developed mathematical approach considered the main hydroprocessing reactions, catalyst deactivation, and mass transfer aspects. The model was utilized to examine the performance of an industrial reactor. It was noticed that the best strategy to start up the reaction system is to stabilize the catalyst at low temperature. Aksikas et al. [265] studied a control problem for a time-changing partial differential equation (PDE) model introduced for a FBR. The dynamic behavior of the model was evaluated through employing the conception of evolution systems. Simulation results revealed that the suggested controller exhibits a better performance regardless of the catalyst deactivation when the deactivation time is almost the same as the resident time of the reactor. Farsi and Jahanmiri [266] conducted a research study concerning the dual-membrane reactor of methanol production where the catalyst deactivation was considered. They developed a dynamic one-dimensional heterogeneous model. They concluded that the proposed reactor leads to a longer lifetime of the catalyst and higher reaction conversion. Tohidian et al. [189] performed a research on an industrial

TBR employed for 1,3-butadiene hydrogenation to produce n-butane. Through considering a suitable series of reactions, they discussed about the effect of various parameters such as flowrate and temperature on the TBR performance. Li et al. [267] studied the CTA hydropurification section in terms of operational control system to obtain an appropriate control configuration where the results obtained by Azarpour and Zahedi [263] were used in their study. Results showed that the proposed control system leads to a greater process performance. A generic hybrid model combining first principle model (FPM) and artificial neural network was developed by Azarpour et al. [146] to investigate the performance of industrial FBRs that experiences catalyst deactivation. The generic model was validated through utilizing the real data of two industrial cases, implying that the proposed model is able to generate satisfactory results. The developed generic idea can be employed for the behavior analysis of FBRs regardless of the type of the catalyst. Izadi et al. [268] carried out a research work on 0.5 wt.% Pd/C catalyst with macro-structured carbon nano-fibers aggregates and micro-nano-porous activated carbons as an alternative for hydropurification of CTA. It was confirmed that 0.5% Pd/microporous catalyst is able to significantly catalyze the hydrogenation of 4-CBA (4-carboxybenzaldehyde) to pta. The catalyst with more micro surface area results in a maximum yield to produce the intermediate product of 4-hydroxymethylbenzoic acid (4-HMBA). Furthermore, it was concluded that the desired selectivity to pta (para-toluic acid) is highly dependent on the micro-porous structure.

The literature review shows that there are many research and engineering activities on the FBR modeling; especially on the hydrotreating processes. To the best of our knowledge, no studies have been conducted to investigate the effect of axial dispersion on the hydrotreating catalytic process. Moreover, there is no theoretical study about the catalyst particle diameter and porosity impacts on the performance of the hydrotreating process. Lack of research works on these important aspects motivates us to develop a new model for the CTA hydropurification FBR where the axial dispersion, catalyst deactivation, and variation of the catalyst specifications in terms of size and porosity are taken into account. We also incorporate the effect of temperature on the reactor performance. The derived PDEs to describe the developed model are solved through employing an apt numerical method in the Matlab 2016a© environment. The validation of the proposed model is conducted using the real data of the production plant.

3.2 Theoretical and Practical Aspects

In the production of purified terephthalic acid (PTA), Amoco-MC process technology is extensively being utilized. PTA is used to synthesize polyethylene terephthalate (PET) [269]. Ethylene glycol (EG) and PTA are raw materials to commercially produce PET. This polymer is broadly used to manufacture beverage bottles, fibers, cosmetics, pharmaceutical products, household stuff, and food packaging films. PTA production has considerably grown due to the significant increase in the production of polyesters. Figure 3-1 illustrates the block diagram of production processes of PTA and PET. PTA is processed in two separate sections. In the first stage, oxidation of para-xylene (PX) is performed using a homogeneous catalyst; including, manganese acetate, cobalt acetate, and hydrogen bromide in a continuous stirred tank reactor where acetic acid (AA) as a solvent is used. Air is usually injected into the reactor through four nozzles which are fixed symmetrically. The operational conditions reported for the real reactor are a temperature of about 200 °C and a pressure of 20 atm. CTA as the final product of this process stage consists of impurities; mainly including, 4-CBA and pta. The ranges of pta and 4-CBA concentrations are generally 300-1000 ppm and 2000-3000 ppm, respectively [3]. Since the impurity concentration of CTA is high for the polymerization process, a purification process is carried out separately. In the second step, CTA is hydrotreated through the catalytic hydrogenation of 4-CBA to pta in a TBR packed with 0.5 wt.% Pd/C catalyst [2].

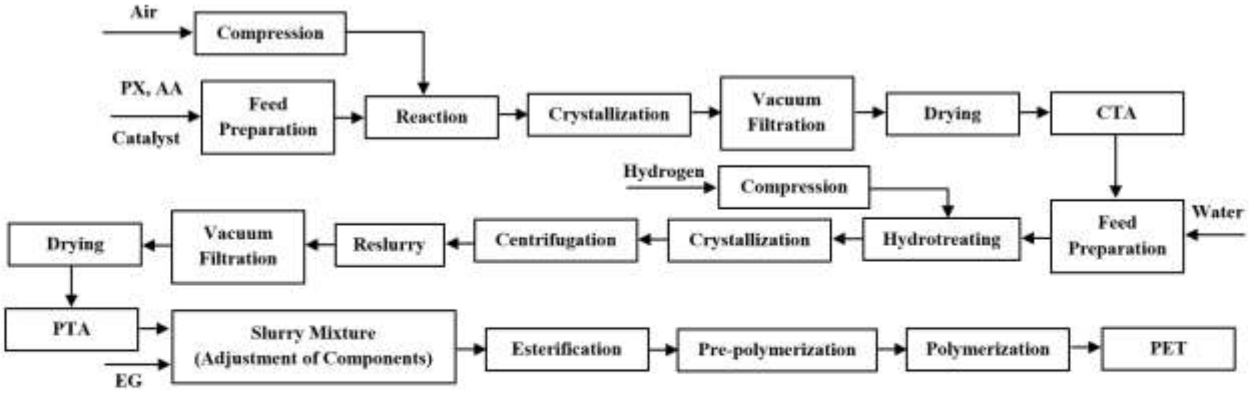

Figure 3-1: Block flow diagram of production processes of PTA and PET. Adapted with permission from ref [146]. Copyright 2017 Elsevier B.V.

The annual world usage of granular 0.5 wt.% Pd/C catalyst for CTA purification exceeds 1000 tons. It contains nano-dispersed 4×8 mesh size particles of palladium supported on coconut activated carbon [2]. Palladium particles are precipitated by gradually building up the solution of acidic precursor into carbon alkaline slurry which results in impregnated samples. Thereafter, the chemical reduction is implemented by utilizing Na-formate which leads to the reduction of chemical samples. Na-formate decreases the palladium particles. Then, the synthesized catalyst is needed to be reduced in the hydrogen stream for the completion of the reaction process [270].

3.2.1 Process Description

Figure 3-2 illustrates the hydropurification unit of PTA production process. Mixing of CTA powder with water is conducted in a slurry feed drum (SFD). The water is mostly the filtrate coming from the rotary vacuum filter (RVF). The temperature and pressure of the reactor feed are increased via the heat exchangers and centrifugal pumps. To attain complete dissolution of CTA powder into water, hot oil system is provided. Hot oil supply (HOS) exchanges the heat with the reactor feed and the hot oil returns (HOR) to the furnace. In the TBR containing Pd/C catalyst, the hydrogenation of 4-CBA, which is the main impurity of CTA powder, takes place, and it is converted to pta. The outlet product of the reactor is transferred to the crystallizers. Separation of terephthalic acid (TA), which is the main product, from the liquid phase consisting of the impurities is carried out in the crystallizers. The pressure of the crystallizers is reduced gradually. The pressure of the last crystallizer is controlled so that pta remains in the liquid phase. The solid TA is extracted from the liquid phase through the centrifugation and filtration (RVF) processes. The wet cake of the product is dried in the dryer heated by a low-pressure steam. The dried product is moved to the checking silos. If the product specifications meet the standard quality criteria, the powder as PTA is conveyed to the final silos. Otherwise, the off-spec product is recycled back to CTA silo via a powder conveying system (PCS). Table 3-1 provides information/data on the hydropurification process and Pd/C catalyst specifications.

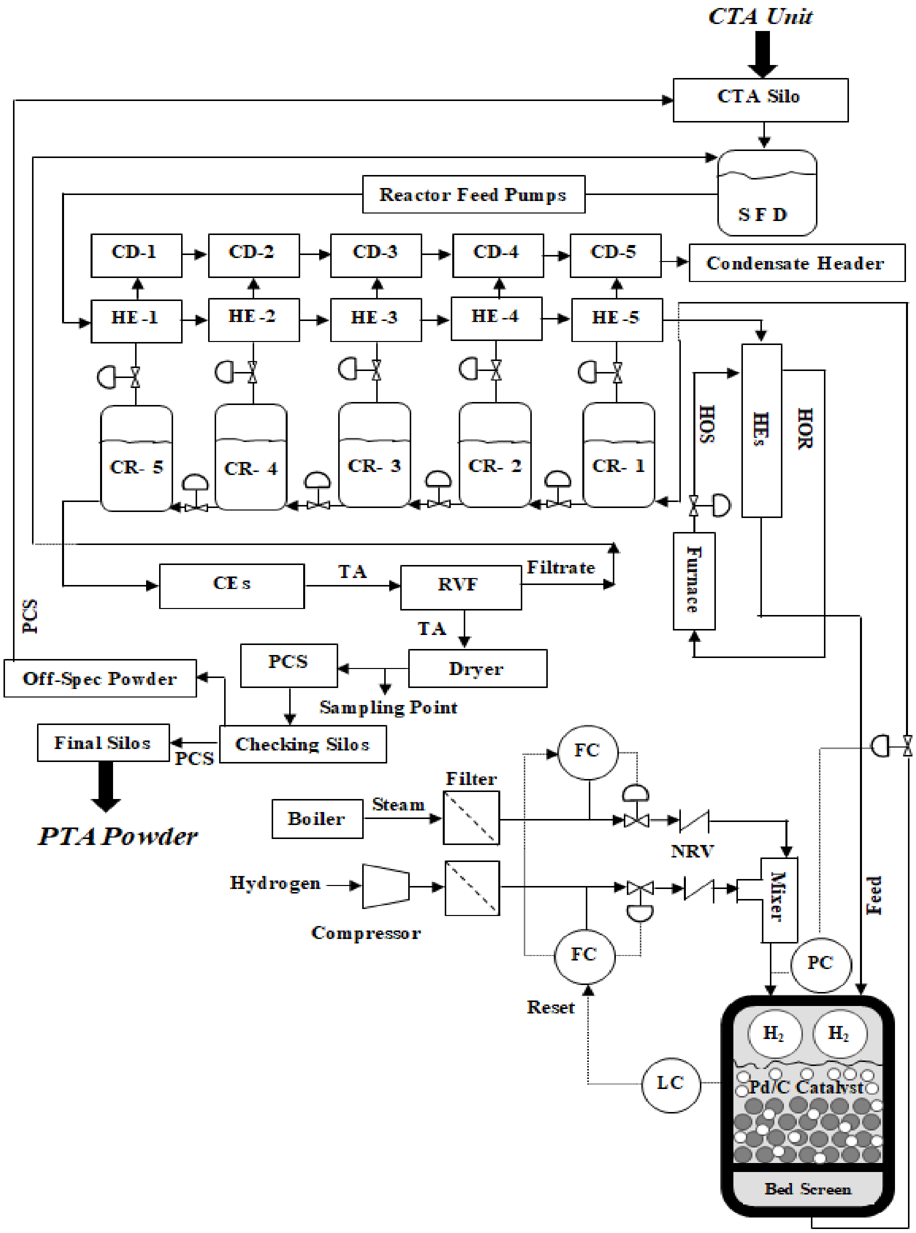

Figure 3-2: Hydropurification process of PTA production plant [CD: Condensate Drum; CE: Centrifuge; CR: Crystallizer; FC: Flow Controller; HE: Heat Exchanger; LC: Level Controller; NRV: Non-Return Valve; PC: Pressure Controller]. Adapted from ref [271].

Table 3-1: Hydropurification process data and Pd/C catalyst specifications. Adapted from ref [271].

Parameter	**Amount**
Pressure, P (barg)	73.5
Temperature, T (°C)	285
Reactor feed flowrate, FF (t h^{-1})	196
Flowrate of hydrogen, FH (kg h^{-1})	13.2
Concentration of TA, C_{TA} (wt.%)	23
Length of reactor bed, L (m)	7.4
Diameter of reactor bed, d_B (m)	2.8
Diameter of catalyst particle, d_P (mm)	3.53
Catalyst particle surface area, a_P (m^2 g^{-1})	900-1100
Bulk density of reactor bed, ρ_B (kg m^{-3})	475
Void fraction of reactor bed, ε_B (-)	0.44
Catalyst particle porosity, ε_P (-)	0.61
Content of Pd (wt. %)	0.5
Activated carbon (wt. %)	99.5
Water content in wet catalyst (wt. %)	38
Distribution of catalyst partcile size (%)	4 - 8 (mesh) = 97 4.75 – 2.36 (mm) less than 4 (mesh) = 2 over 8 (mesh) = 1

3.2.2 Practical Challenges/Problems

One of the most important specifications of PTA product quality is 4-CBA content. The allowed maximum concentration of 4-CBA is 25 ppm. PTA powder having a high amount of 4-CBA should not be used for the polymerization process since it increases PET polymerization side reactions and reduces the molecular weight [6]. Moreover, the polyester manufactured by

PTA powder containing high 4-CBA does not have an acceptable color appearance [272]. In fact, high concentration of 4-CBA considerably affects the performance of PTA process. For instance, it disturbs the optimal conditions of RVF due to its sticky nature. It also negatively influences the efficiency of the centrifuges. If the process produces off-spec products, they need to be reprocessed. This unfavorable occurrence increases the cost of operation. Besides controlling 4-CBA concentration in the product, deactivation of Pd/C catalyst, which is expensive, needs to be carefully investigated in research and engineering activities to achieve optimal conditions for minimization of this incident. There have been many efforts to improve the catalyst activity and to extend the lifetime of the catalyst. The catalyst is usually deactivated after one year of operation. Thus, any improvement in the catalyst efficiency can significantly enhance the industrial production of PTA in terms of the reaction conversion, production rate, and economic prospect. The current study systematically addresses the problems mentioned above and proposes the effective remedies to improve the performance of hydropurification operations.

3.3 Data Collection and Analysis

Analysis of CTA and PTA powder samples is conducted in the industrial plant laboratory. The real data are used to validate the proposed mathematical model.

The samples are collected at the dryer outlet of each unit. The sample is usually taken after four hours of operation. This duration might change, depending on the operating conditions. For example, if the process encounters abnormal conditions so that it produces off-spec products, the sample might be taken after each two or three hours of the operation. The sample is examined/analyzed through employing high-performance liquid chromatography (HPLC) machine with an auto-sampler, a class A 100 volumetric flask, a STRODS column with 4 mm thickness and 150 mm length, an analytical scale with an accuracy of 0.1 mg, an ultrasonic bath, a 2-N ammonia solution, standard samples with certain amounts of 4-CBA, and a mobile phase including acetonitrile (21 vol %), trifluoro AA (0.1 vol %), and HPLC grade water (78.9 vol %). The HPLC machine is operated at a temperature of 50 °C, 260 nm wavelength, and flowrate of 0.5 mL min^{-1}. A solution of 20 ml aliquot with 0.5 N ammonia is introduced into the HPLC by an auto-sampler. Then, 10 mL of 2 N ammonia and deionized water are blended with 0.5 g of standard samples to produce a 100-mL solution. About 5 mL of the solution is filtered by a 0.45-mm syringe. Thereafter, it is moved to an auto-sampler machine vial. A 10 μL aliquot of standard samples is introduced into the instrument. The calibration of the amount of 4-CBA is carried out by the produced peaks. Then, the solution filtration is transferred to the machine and the injection of 10 μL of standard samples is reiterated to measure the required amounts from the chromatography [4]. Table 3-2 includes the data based on the samples analysis. The samples are collected under the normal operations, and the amounts are the average values of the powders analysis at different hours of the daily operation. Figure 3-3 depicts the data points (4-CBA concentration) recorded in different days of the operation. In the case, the data seem wrong; they are removed and not considered in the analysis. The errors might be due to the contamination of the taken samples and malfunction of the instruments and machines utilized for the analysis of the samples. It should be noted that each sampling and test analysis are repeated two times at the same conditions to examine the reproducibility of the tests and results. The average absolute difference (or error) between the replicates was lower than 2% in this study, implying the reliability of the data.

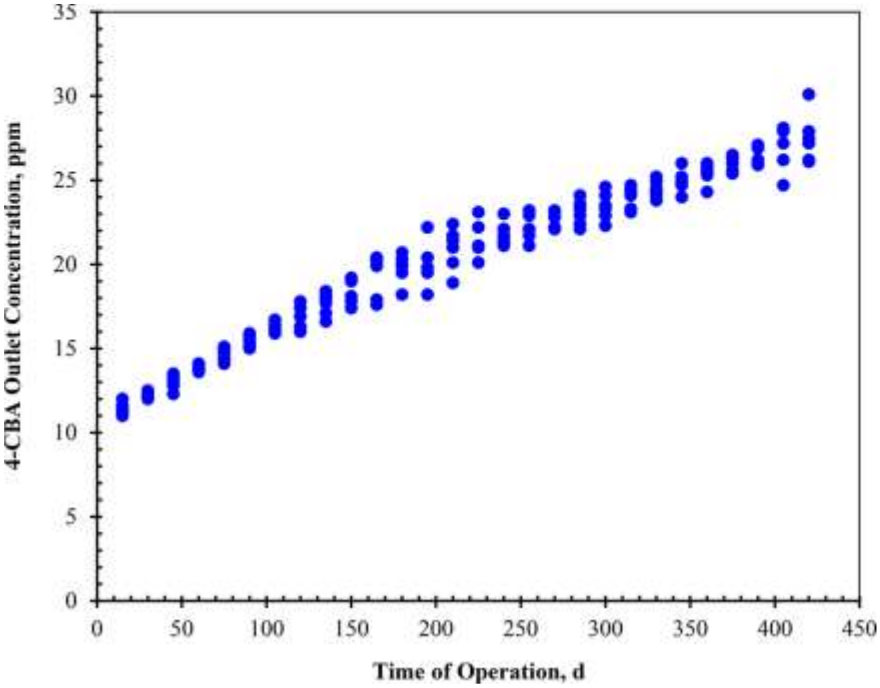

Figure 3-3: 4-CBA concentration in various days of operation.

Table 3-2: Data resulted from the CTA and PTA powders analysis. Adapted from ref [271].

Time, d*	**4-CBA (CTA Powder), ppm**	**4-CBA (Product), ppm**	**Time, d**	**4-CBA (CTA Powder), ppm**	**4-CBA (Product), ppm**
15	1100	11.4	225	2000	21.4
30	1200	12.2	240	2200	21.8
45	1500	13	255	2000	22.2
60	1400	13.8	270	3000	22.6
75	1700	14.6	285	2000	23.1
90	1000	15.4	300	2000	23.5
105	1700	16.2	315	2500	24
120	2000	16.9	330	1900	24.5
135	2000	17.7	345	2000	25
150	2000	18.4	360	1500	25.5
165	1750	19.4	375	2000	26
180	1700	19.8	390	2000	26.5
195	2000	20.4	405	2000	27
210	2500	20.9	420	2000	27.5

*d stands for the day. The samples were collected under normal operation conditions, and the data represent the average values of concentrations (obtained at different hours during the corresponding daily operation) based on the powder analysis.

3.4 Methodology

To develop a mathematical model for a certain system/process, it is assumed that the input and output parameters are closely related to each other. Since there are complicated phenomena/mechanisms involved in chemical reaction systems, it is almost unfeasible to construct a model that incorporates all parameters/aspects of the process. However, it is clear that the rigorous models can be developed to produce acceptable results through considering logical/appropriate assumptions. The modeling strategy needs to be accurate enough to acceptably forecast the process behaviors and to offer useful guidelines for possible changes and optimization in process conditions and stages.

Figure 3-4 depicts the methodology used in this research study. Based on the operating conditions and the relevant data, the most vital variables are determined to be incorporated in the model. The proposed strategy involves a dynamic heterogeneous model that considers the mass and energy balances for each phase. The FPM with focus on axial dispersion is developed where 4-CBA hydrogenation reactions and Pd/C catalyst deactivation are the main elements in the modeling strategy. After applying the mass balance for each component and energy balance for each phase, the model parameters such as mass and heat transfer coefficients are determined. The obtained PDEs are then transformed into ordinary differential equations (ODEs) using a proper numerical technique. We obtain the aid from the MATLAB© software to calculate the parameters and to solve the governing equations. The developed model is then validated through comparing the model outcomes with the plant data. After model validation, a comprehensive parametric sensitivity analysis is performed so that the influences of the main factors such as the operating parameters and catalyst specifications (e.g., particle size and porosity) on the target variable/process performance are studied. The results are discussed to evaluate the level of the model reliability and relative importance of the input variables. Finally, we are able to make a decision on appropriate process conditions/procedures to attain greater efficiency in terms of technical, economic, and environmental aspects.

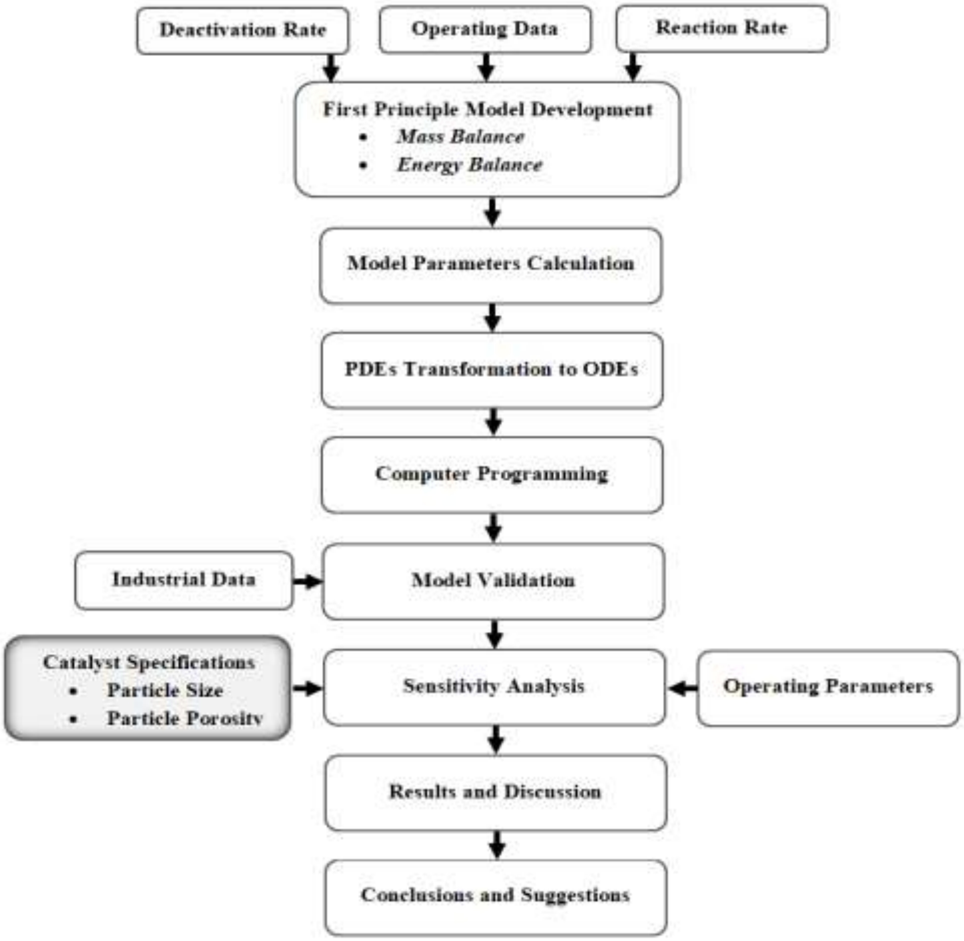

Figure 3-4: Methodology employed in this modeling strategy.

3.4.1 Model Development

A heterogeneous model is considered for the hydropurification three-phase TBR of the PTA production plant. To properly represent the reaction system performance, axial mixing and bulk diffusion of the reaction mixture components are considered. Moreover, we incorporate the dynamic behavior of the system/process affected by the catalyst deactivation in the model.

Reaction rate. 4-CBA experiences complicated reactions in the purification process. In addition, the decarbonylation reaction occurs in the reaction mixture. Although benzoic acid (BA) is easily separated, the synthesized carbon monoxide (CO) is considered as a poison to Pd/C catalyst. The decarbonylation reaction is greatly influenced by the oxygen content in the reaction solution such that the dissolved oxygen improves the decarbonylation phenomenon. In the hydrogenation of 4-CBA, the concentration of the intermediate component of 4-HMBA first reaches a maximum value to ensure a steady reduction. This confirms the mechanisms of 4-CBA hydrogenation reactions suggested by Zhou et al. [269]. Figure 3-5 depicts the CTA hydropurification reactions.

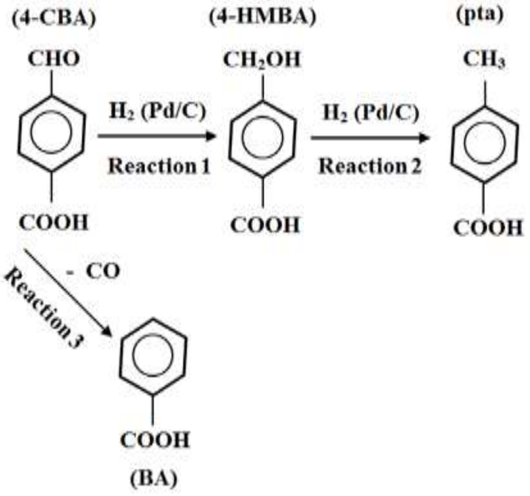

Figure 3-5: Hydropurification reactions of 4-CBA. Adapted with permission from ref [269]. Copyright 2006 Elsevier B.V.

The corresponding rates of 4-CBA hydrogenation reactions are as follows [273]:

$$r_1 = 0.047\, exp\left(-\frac{16.97}{RT}\right) C_{4-CBA}^{0.96}\, C_{H2}^{0.24} \qquad ; \Delta H_1 = -83.82\ kJ\ mol^{-1} \tag{3-1}$$

$$r_2 = 0.153\, exp\left(-\frac{23.44}{RT}\right) C_{4-HMBA}^{0.61}\, C_{H2}^{0.75} \quad ; \Delta H_2 = -121.88\; kJ\; mol^{-1} \tag{3-2}$$

$$r_3 = 3406.6\, exp\left(-\frac{88.87}{RT}\right) C_{4-CBA}^{0.54} \quad ; \Delta H_3 = 18.73\; kJ\; mol^{-1} \tag{3-3}$$

in which, r stands for the rate of reaction in kmol kg_s^{-1} s^{-1}, R represents the universal gas constant in J mol^{-1} K^{-1}, T is the temperature of reaction mixture in K, C denotes the concentration in kmol m^{-3}, and ΔH refers to the heat of reaction in kJ mol^{-1}.

Catalyst deactivation rate. The most significant reason for the deactivation of the industrial Pd/C catalyst is sintering. It was found that the surface area of Pd significantly reduces when the treatment temperature increases. It implies that palladium easily experiences the sintering phenomenon. The research studies show that the smaller particles of palladium become bigger, and the sintering causes the gradual enhancement of palladium agglomerates [1, 2].

To develop a suitable model, Pd/C catalyst deactivation rate is required. This rate was determined based on the experimental data obtained at various conditions by Azarpour et al. [271]. In the current study, the same deactivation rate is employed as given below:

$$-r_d = -\frac{da}{dt} = 0.00092\; exp\; (\frac{-5279}{R}(\frac{1}{T} - \frac{1}{T_R}))\; a^{2.1} \tag{3-4}$$

where r_d represents the rate of deactivation in h^{-1}, t denotes the time, T stands for the temperature, and a is the dispersion parameter of metallic sintering. The value of reference temperature (T_R) is 558 K.

First principle model. Indisputably, in terms of physicochemical modeling of catalytic reactors, the more fundamental and realistic the model the fewer limiting assumptions there will be. However, there is no need to involve all minor factors in the mathematical modeling which do not prevent achieving the main goals of design, operation, and optimization of the catalytic system if they are ignored [274].

FPM of the three-phase reactor is obtained through considering the mass balance for each component of the reaction mixture and energy balance for each phase. The axial dispersion or axially-dispersed PFM is included to describe the non-ideal flow in the reactor [275]. There are some assumptions with mass and energy conservation laws in this study: There is no wall effect [276]; there are no radial gradients of mass and energy [20, 277]; the pressure drop is negligible [278]; the particle wetting efficiency is complete [67]; and the reactor is operated under adiabatic conditions.

The equation of the hydrogen mass balance in the gas phase is given below:

$$\varepsilon_g \frac{\partial C_{H_2,g}}{\partial t} = D_{ax,H_2,g} \frac{\partial^2 C_{H_2,g}}{\partial z^2} - u_g \frac{\partial C_{H_2,g}}{\partial z} - k_{H_2,gl} \xi_{gl} \left(\frac{C_{H_2,g}}{H_{H_2}} - C_{H_2,l}\right) \tag{3-5}$$

The following equation expresses the hydrogen mass balance in the liquid phase:

$$\varepsilon_l \frac{\partial C_{H2,l}}{\partial t} = D_{ax,H_2,l} \frac{\partial^2 C_{H_2,l}}{\partial z^2} - u_l \frac{\partial C_{H2,l}}{\partial z} + k_{H_2,gl} \xi_{gl} \left(\frac{C_{H2,g}}{H_{H2}} - C_{H2,l}\right) - k_{H_2,ls} \xi_{ls} (C_{H2,l} - C_{H_2,s}^{S}) \tag{3-6}$$

The mass balance of other components (e.g., 4-CBA, 4-HMBA, pta, and BA) in the liquid phase is represented as follows:

$$\varepsilon_l \frac{\partial C_{i,l}}{\partial t} = D_{ax,i,l} \frac{\partial^2 C_{i,l}}{\partial z^2} - u_l \frac{\partial C_{i,l}}{\partial z} - k_{i,ls} \xi_{ls} (C_{i,l} - C_{i,s}^S) \tag{3-7}$$

The overall mass balance expression for the solid phase is written as follows:

$$\varepsilon_P (1 - \varepsilon_B) \frac{\partial C_{i,s}}{\partial t} = k_{i,ls} \xi_{ls} \left(C_{i,l} - C_{i,s}^S\right) \pm \sum_{k=1}^{k} r_k \, \eta_k \rho_B a(t) \tag{3-8}$$

in which, ε denotes the phase holdup, *C* represents the concentration in kmol m^{-3}, *t* is the time in s, *D* stands for the dispersion coefficient in m^2 s^{-1}, *z* refers to the axial coordinate in m, u is the symbol for the superficial velocity in m s^{-1}, *k* is the mass transfer coefficient in m s^{-1}, ξ symbolizes the interface specific surface area in m^2 m^{-3}, *H* is the Henry's constant, *r* represents the rate of reaction in kmol kg$_s^{-1}$ s^{-1}, η is the effectiveness factor, ρ_B is the bulk density in kg m^{-3}, *a* is the metallic sintering parameter, and ε_p stands for the particle porosity.

The gas phase energy balance is represented by the following expression:

$$\varepsilon_g \rho_g C_{p,g} \frac{\partial T_g}{\partial t} = \lambda_g \frac{\partial^2 T_g}{\partial z^2} - u_g \rho_g C_{p,g} \frac{\partial T_g}{\partial z} - h_{gl} \xi_{gl} (T_g - T_l) \tag{3-9}$$

Equation (3-10) describes the energy balance of the liquid phase:

$$\varepsilon_l \rho_l C_{p,l} \frac{\partial T_l}{\partial t} = \lambda_l \frac{\partial^2 T_l}{\partial z^2} - u_l \rho_l C_{p,l} \frac{\partial T_l}{\partial z} + h_{gl} \xi_{gl} \left(T_g - T_l\right) - h_{ls} \xi_{ls} (T_l - T_s) \quad (3\text{-}10)$$

The solid phase energy balance is given below:

$$(1 - \varepsilon_B) \rho_s C_{p,s} \frac{\partial T_s}{\partial t} = h_{ls} \xi_{ls} (T_l - T_s) + \sum_{k=1}^{k} r_k \eta_k \rho_B a(t) \, (-\Delta H_k) \quad (3\text{-}11)$$

where ρ is the phase density in kg m^{-3}, C_p refers to the heat capacity in J kg^{-1} K^{-1}, T denotes the temperature in K, λ is the conductivity in W m^{-1} K^{-1}, ΔH is the heat of reaction in kJ mol^{-1}, and h stands for the heat transfer coefficient in W m^{-2} K^{-1}.

To solve the PDEs obtained above, two boundary conditions (BCs) and one initial condition (IC) are required. The conditions are summarized below:

BC 1 : at $z=0$ $C_i=C_{i,in}$; $T_g=T_l=T_s=T_{in}$

BC 2 : at $z=L$ $\frac{\partial C_i}{\partial z} = 0; \frac{\partial T}{\partial z} = 0$

IC : at $t=0$ $C_i=C_i^{ss}$; $T_g=T_g^{ss}$; $T_l=T_l^{ss}$; $T_s=T_s^{ss}$; $a=1$

3.4.2 Determination of Parameters in Mass and Energy Balances

The vital parameters in the governing equations such as mass and heat transfer coefficients, heat capacities, and Henry's constants are calculated via utilizing proper correlations. The chosen correlations have been obtained under the operating and thermodynamic conditions which are close to the conditions of the real case (s). Indeed, the real conditions should be within the intervals/ranges at which the correlations are valid and trustable. Henry's constant, which is a very important parameter in the developed model, is calculated using the following equation, which was derived for the proposed system:

$$H_{H_2} = 0.0127 \exp(-\frac{2023}{RT}) \tag{3-12}$$

where H_{H_2} is the Henry’s constant in bar m^3 kmol^{-1}; R represents the universal gas constant in J mol^{-1} K^{-1}; and T denotes the temperature of the solution in K.

The correlations and values of the parameters used in this study are provided in Azarpour et al. [146] and Azarpour et al. [271]. Since the axial dispersion process occurs by the molecular diffusion during laminar flow regime, the dispersion coefficient is the molecular diffusion coefficient [275]. The Reynolds number is 208, which is calculated using the normal operating conditions, implying the flow regime is laminar.

3.4.3 Model Mathematical Solution

The main equations developed in this study are in the category of coupled nonlinear PDEs. These initial-boundary problems are solved numerically by discretization on the computational domain. The available techniques to solve these non-linear equations include finite element methods (FEMs), finite difference methods (FDMs), spectral methods, and collocation approach. The FDM is the most popular numerical technique in engineering applications due to its flexibility, efficiency, and simplicity. Two critical points, which are to be considered in the solution of transient PDEs, are: simultaneous space-time discretization versus space discretization, and stability of the numerical solution to manage stiffness of ODEs obtained from only space discretization. Separation of space and time discretization is called method of lines (MOL). It converts PDEs to ODEs or differential algebraic equations (DAEs). In other words, the spatial dimensions are discretized explicitly. The stiffness problem is efficiently managed by an ODE/DAE solver. Moreover, this separation simplifies the error analysis of the employed numerical technique [173, 279].

If each axial increment through the reactor is considered q, using MOL and backward FDM, the PDEs of mass and energy balances (Equations (3-5) to (3-11)) are transformed into the following ODEs at each time step:

$$\varepsilon_g \frac{dC_{H_2,g}^{q}}{dt} = D_{ax,H_2,g} \frac{C_{H_2,g}^{q} - 2C_{H_2,g}^{q-1} + C_{H_2,g}^{q-2}}{\Delta z^2} - u_g \frac{C_{H_2,g}^{q} - C_{H_2,g}^{q-1}}{\Delta z} - k_{H_2,gl}\xi_{gl} \left(\frac{C_{H_2,g}^{q}}{H_{H_2}} - C_{H_2,l}^{q}\right) \tag{3-13}$$

$$\varepsilon_g \frac{dC_{H_2,l}^{q}}{dt} = D_{ax,H_2,l} \frac{C_{H_2,l}^{q} - 2C_{H_2,l}^{q-1} + C_{H_2,l}^{q-2}}{\Delta z^2} - u_l \frac{C_{H_2,l}^{q} - C_{H_2,l}^{q-1}}{\Delta z} + k_{H_2,gl}\xi_{gl} \left(\frac{C_{H_2,g}^{q}}{H_{H_2}} - C_{H_2,l}^{q}\right) - k_{H_2,ls}\xi_{ls}\left(C_{H_2,l}^{q} - C_{H_2}^{s\,q}\right) \tag{3-14}$$

$$\varepsilon_l \frac{dC_{i,l}^{q}}{dt} = D_{ax,i,l} \frac{C_{i,l}^{q} - 2C_{i,l}^{q-1} + C_{i,l}^{q-2}}{\Delta z^2} - u_l \frac{C_{i,l}^{q} - C_{i,l}^{q-1}}{\Delta z} - k_{i,ls}\xi_{ls}\left(C_{i,l}^{q} - C_{i,s}^{s\,q}\right) \tag{3-15}$$

$$\varepsilon_P (1 - \varepsilon_B) \frac{dC_{i,s}^{q}}{dt} = k_{i,ls}\xi_{ls}\left(C_{i,l}^{q} - C_{i,s}^{q\,S}\right) \pm \sum_{k=1}^{k} r_k^{q}\, \eta_k \rho_B a(t) \tag{3-16}$$

$$\varepsilon_g \rho_g C_{p,g} \frac{dT_g^q}{dt} = \lambda_g \frac{T_{i,g}^q - 2T_{i,g}^{q-1} + T_{i,g}^{q-2}}{\Delta z^2} - u_g \rho_g C_{p,g} \frac{T_g^q - T_g^{q-1}}{\Delta z} - h_{gl} \xi_{gl} (T_g^q - T_l^q) \tag{3-17}$$

$$\varepsilon_l \rho_l C_{p,l} \frac{dT_l^q}{dt} = \lambda_l \frac{T_{i,l}^q - 2T_{i,l}^{q-1} + T_{i,l}^{q-2}}{\Delta z^2} - u_l \rho_l C_{p,l} \frac{T_l^q - T_l^{q-1}}{\Delta z} + h_{gl} \xi_{gl} (T_g^q - T_l^q) - h_{ls} \xi_{ls} (T_l^q - T_s^q) \tag{3-18}$$

$$(1 - \varepsilon_B) \rho_s C_{p,s} \frac{dT_s^q}{dt} = h_{ls} \xi_{ls} \left(T_l^q - T_s^q\right) + \sum_{k=1}^{k} r_k^q \, \eta_k \rho_B a(t) \, (-\Delta H_k) \tag{3-19}$$

To establish the initial conditions for the solution of the PDEs, Equations (3-13)-(3-19) are set to zero, implying the steady state (SS) conditions. In other words, the time terms of the equations are set to zero, and the generated algebraic equations are solved simultaneously. The results of the steady state solution of the model are ICs for the solution of the model under dynamic or unsteady state conditions.

To attain the dynamic solution of the set of Equations (3-13)-(3-19), they need to be solved simultaneously from the entrance of the reactor to the outlet of the reactor (the axial increment at *z* coordinate) at each time step (*m*). This procedure is repeated for the entire time steps.

The determination of physical and model parameters and the solution strategy of the model equations are performed through computer programming in MATLAB 2016a© environment. Figure 3-6 illustrates the computer algorithm to achieve the objectives of this study.

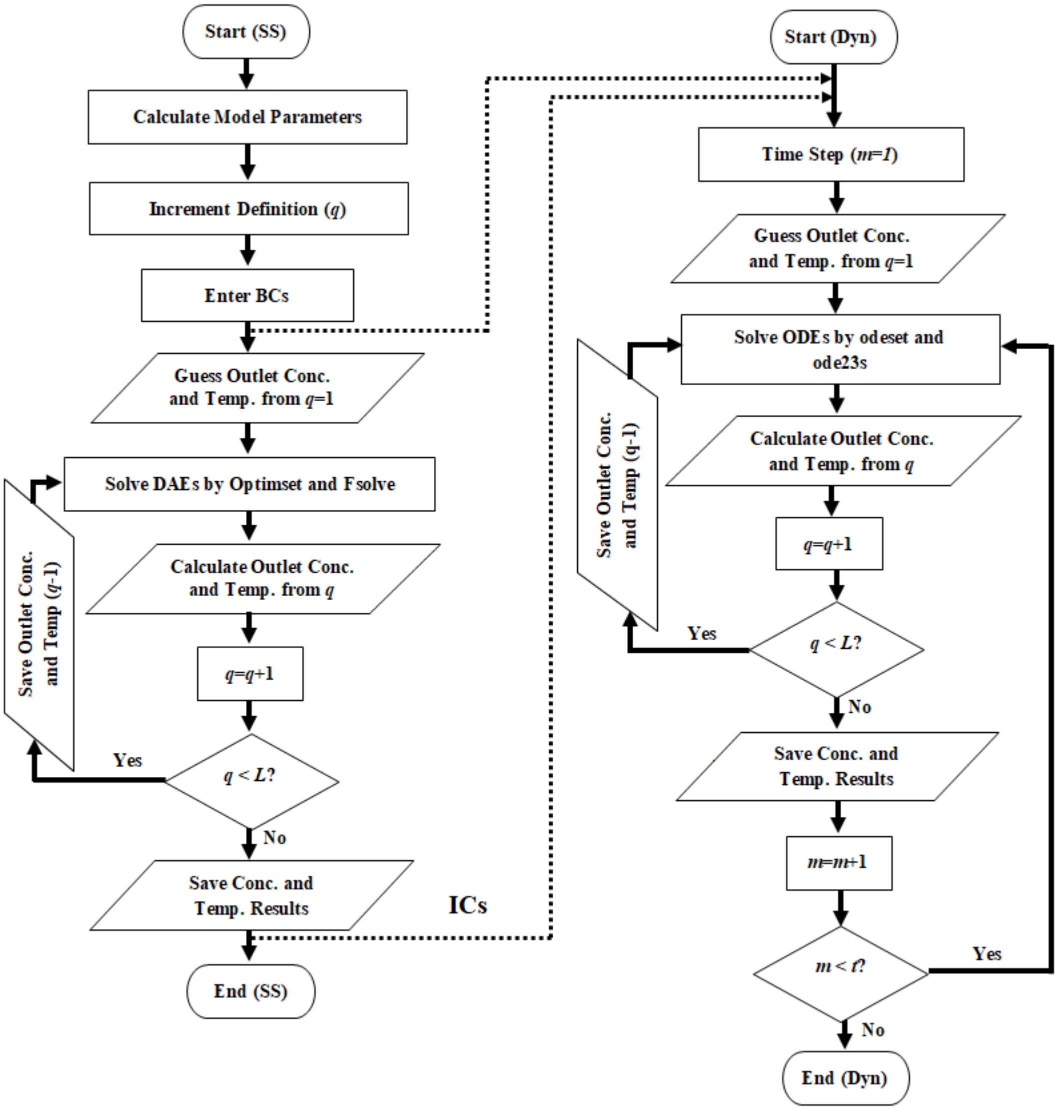

Figure 3-6: Computer algorithm employed to solve governing equations.

3.5 Results and Discussion

The process of hydropurification is essential to remove 4-CBA that negatively influences the progress of the oxidation reaction. In this study, the effect of axial dispersion on the performance of the hydropurification process is investigated. The mathematical model developed in this study takes into account the catalyst deactivation where the impacts of important process and operating parameters such as temperature, hydrogen partial pressure, concentration, particle porosity, and particle diameter on the performance of the purification process are discussed. The obtained differential equations are solved using an appropriate numerical technique, called MOL and backward FDM.

Figure 3-7 illustrates a comparison of the simulation results and the real data, implying a very good closeness between them. According to the results shown in Figure 3-7, it can be concluded that the catalyst is deactivated after 375 days of the operation since the product 4-CBA content exceeds 25 ppm. This corresponds to the time that the catalyst needs to be replaced with a new catalyst.

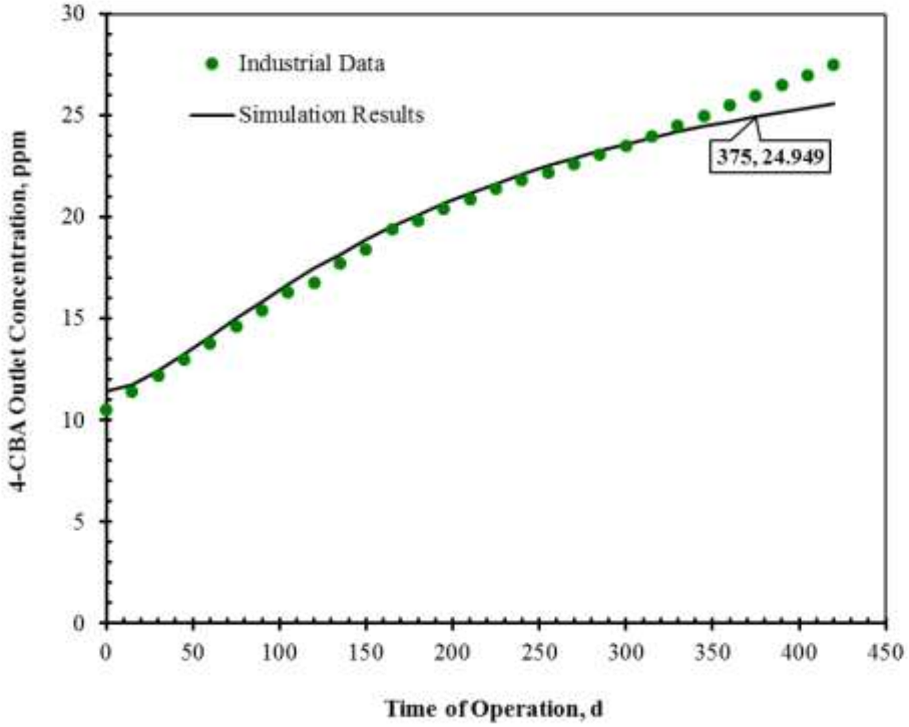

Figure 3-7: Outlet concentration of 4-CBA against the operation time using both modeling predictions and industrial data (T=285 °C; $\varepsilon_p = 0.61$; $d_p = 3.53\ mm$; $\varepsilon_B = 0.44$; FF=196 t/h; P=73.5 barg).

To provide more accurate information based on the error analysis, the relative error percentage, showing the difference between the modeling results and industrial plant data, is determined over the entire operation time. Since the most important quality criterion of PTA product is 4-CBA concentration, the data (which are presented in Table 3-2 and Figure 3-7) are employed for the validation purpose. Figure 3-8 demonstrates the relative error percentage values based on the model outputs and real data. The error calculation reveals that the maximum and average error percentages of the dispersion model are about 4.5% and 2.2%, respectively, while these values are around 7.5% and 2.6%, respectively, for the heterogeneous PFM prior to the catalyst deactivation [271]. This implies that the axial dispersion model is more accurate than the heterogeneous PFM approach. Although the accuracy of the reactor simulation/modeling using the method developed in this study is not improved considerably, the proposed model leads to much more reliable results particularly if the degree of reactor non-ideality increases through variations in concentration, temperature, and flow rates of the streams over the reactor operation.

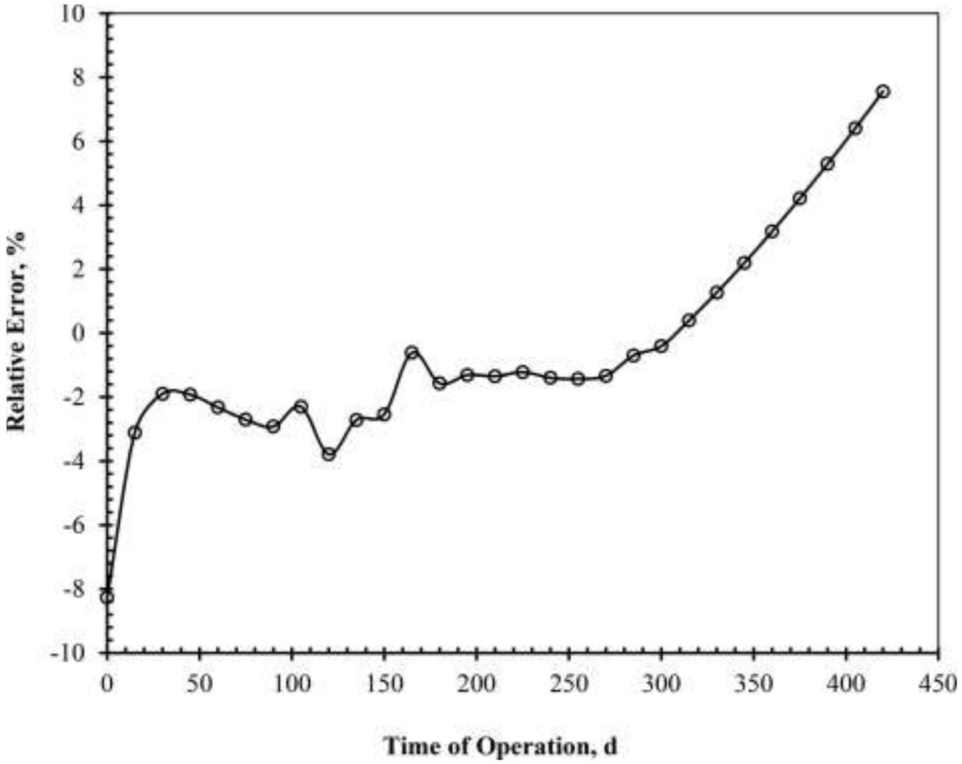

Figure 3-8: Relative error percentage of the model implying the model accuracy.

Figure 3-7 and Figure 3-8 clearly convey the message that the developed model is able to successfully simulate the behavior of hydropurification process in terms of mixture composition and catalyst activity.

Figure 3-9 compares the results of the PFM with those of the dispersion model proposed in this study. It reveals that there is a good agreement between the two modeling approaches in terms of reactor simulation. As discussed earlier, the dispersion model is more reliable that can be used for the purposes of parametric sensitivity analysis to obtain optimal conditions for better performance of the reaction system.

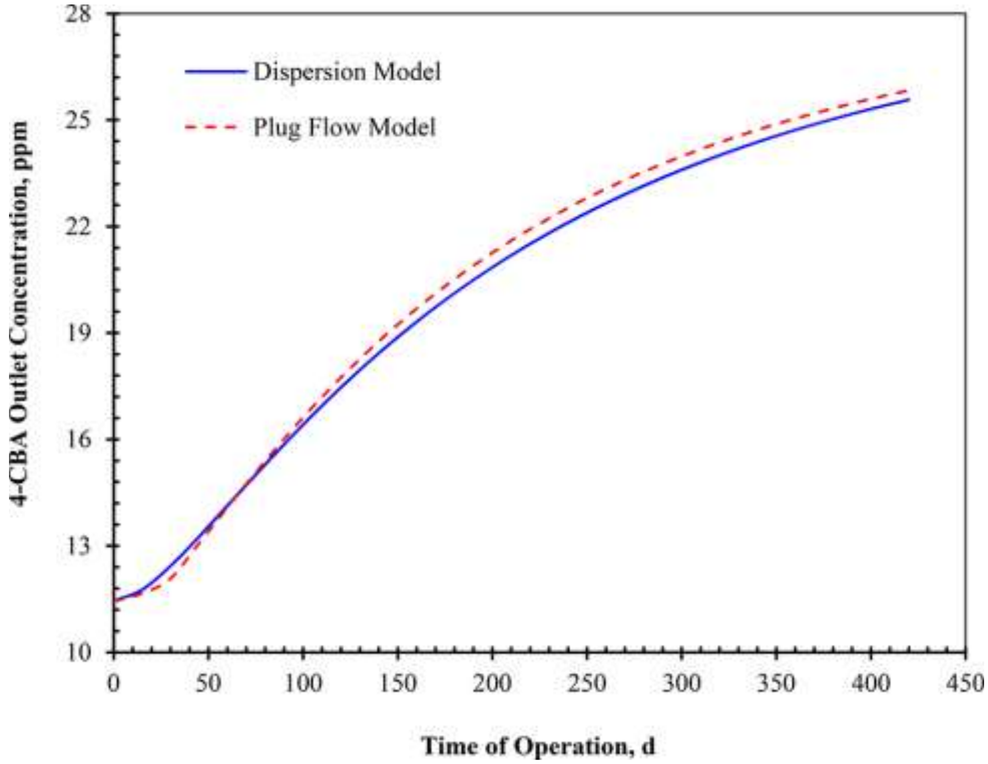

Figure 3-9: Comparison of PFM with dispersion model in terms of prediction of 4-CBA outlet concentration (T=285 °C; $\varepsilon_p = 0.61$; $d_p = 3.53\ mm$; $\varepsilon_B = 0.44$; FF=196 t/h; P=73.5 barg).

To examine further capability of the axial dispersion model, the effects of the particle size, catalyst porosity, 4-CBA inlet concentration, reactor inlet temperature, and hydrogen partial pressure on the system performance are investigated in this section.

Particle size of the catalyst is an important factor that affects the reaction rate and pressure in the reactor. Although the catalyst effectiveness normally improves with decreasing the size of the catalyst particles, it is often at the expense of higher pressure drop along the reactor length. Therefore, a design compromise seems necessary [274]. Small catalyst particles are free of pore diffusion resistance; but they are difficult to be utilized. On the other hand, a bed with large catalyst particles exhibits a low pressure drop; however, the particles likely experience the strong pore diffusion regime where a majority of particles internal surface are unused or not actively participating in the reaction [280]. The actual reaction rate can be increased by employing smaller particles when the effectiveness factor is low [281]. Moreover, small particle size improves the wetting efficiency of the bed [13]. The rate of reaction over externally partially wetted catalyst can be smaller or larger than the rate of reaction occurred over completely wetted catalyst. This relies on whether the limiting reactant is only in the liquid phase or in both gas and liquid phases. For example, if the reaction is liquid-limited, and the liquid reactant is nonvolatile, which usually takes place in many hydrotreating processes, a reduction in the catalyst-liquid contact surface lowers the mass transfer between the liquid and catalyst, leading to a reduction in the reaction rate [67]. Figure 3-10 represents the effect of the particle size reduction on the product quality and catalyst deactivation. To understand this impact, the normal size of catalyst particle is reduced from 3.53 mm to 3 mm, 2.65 mm, 2.30 mm, and 2.12 mm. Based on the results demonstrated in Figure 3-10, the lower particle size results in the improvement of the product quality and an increase in the catalyst lifetime. It is concluded that the product quality for the catalyst particle sizes of 3 mm, 2.65 mm, 2.30 mm, and 2.12 mm improves by around 2.4%, 3.3 %, 3.8%, and 4.04%, respectively. At the same conditions, the catalyst lifetime also increases up to 8%, 12%, 14.7%, and 16%, respectively (e.g., the lifetime of the catalyst is changed from 375 days to 435 days). As it can be seen in the figure, reduction in the particle size from 2.12 mm to 1.94 mm leads to no changes in the product quality and the catalyst lifetime. Hence, the best particle diameter for the system is 2.12 mm. This small improvement can be still considered a valuable achievement for an industrial production. It is clear that the practical implementation of the theoretical results to the real cases is not always an easy (and feasible) task. For instance, it might not be possible to synthesize the catalyst with a certain size while maintaining other important specifications. The other concern is normally attributed to the pressure drop along the length of the catalyst bed, though for the particular case in this study, the pressure drop calculation based on the correlations available in the literature [278, 282] shows that the magnitudes of the pressure loss for the catalyst bed containing particles with the size of 3.53 mm, 3 mm, 2.65 mm, 2.30, and 2.12 mm are 5.7 kPa, 7.1 kPa, 8.3 kPa, 10.8 kPa, and 11.9 kPa, respectively. This increase in the pressure drop is due to the particle size reduction, which is acceptable in a catalyst bed having 7.4 m high and 2.8 m diameter. Highlighting the drawbacks of theoretical research outcome, it should be noted that theory development always helps to further understand the physics and mechanisms behind various processes such as hydropurification and to provide appropriate guidelines and recommendations for performance enhancement.

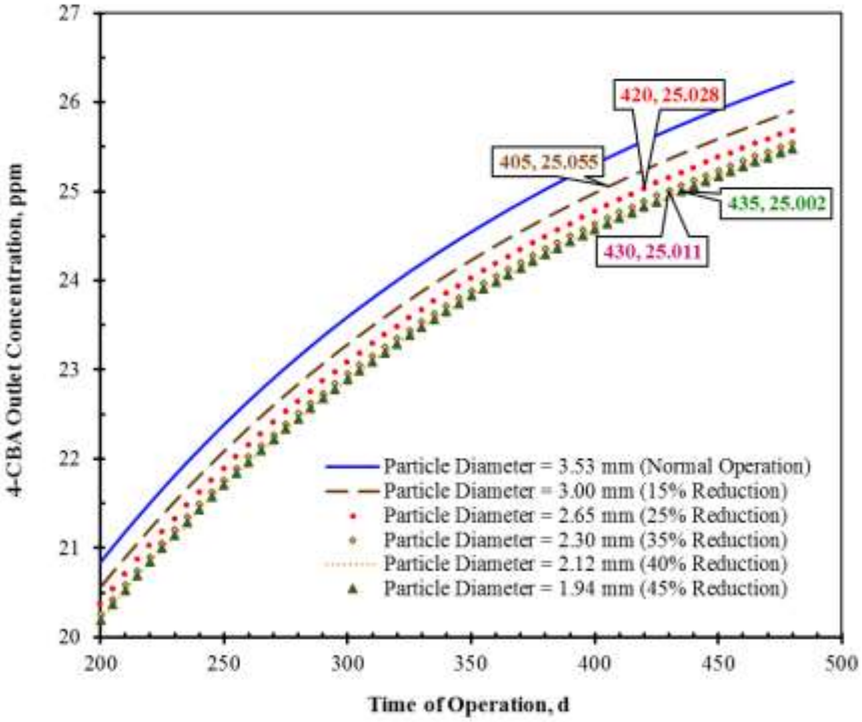

Figure 3-10: Catalyst particle size influence on the product quality and catalyst lifetime (T=285 ºC; $\varepsilon_p = 0.61$; $\varepsilon_B = 0.44$; FF=196 t/h; P=73.5 barg).

Change of concentration of 4-CBA outlet (as an indicator of hydropurification performance) with the catalyst porosity is reflected in Figure 3-11. An increase in the Pd/C catalyst porosity from 0.61 to 0.7, 0.76, 0.79, and 0.82 improves the product quality by about 1.8%, 2.1%, 2.3%, and 2.5%, respectively. It also lengthens the catalyst lifetime by 4%, 5.3%, 6.7%, and 8%, respectively. Providing further details, the lifetime of the catalyst increases from about 375 days to nearly 390 days, 395 days, 400 days, and 405 days, respectively. Evaluating the results obtained, more increment in the catalyst particle porosity from 0.82 to 0.85 has no impact on the quality of PTA product and Pd/C catalyst lifetime. From quantitative viewpoint and regardless of the elaborate endeavor of the catalyst synthesis, the optimal porosity is 0.82. Certainly, this even small variation/improvement in the normal or conventional specifications of the catalyst has a considerable impact on the production process in terms of production rate and economical prospective. The manufacturer (or supplier) of the catalyst might not be able to produce or provide this product with higher porosity, while it maintains the same characteristics which are required for the targeted reaction process.

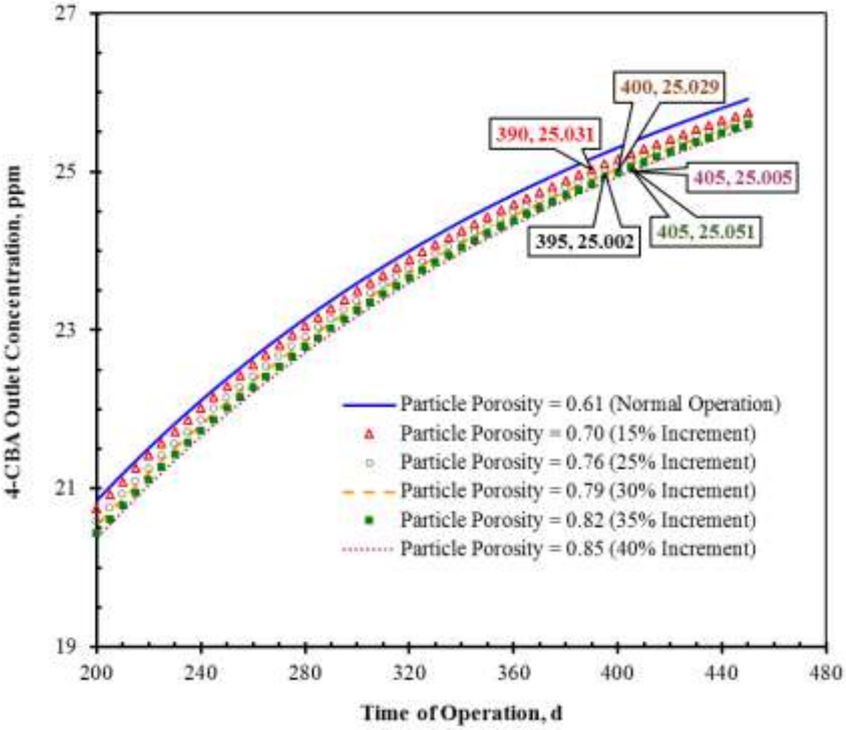

Figure 3-11: 4-CBA outlet concentration versus operation time for various particle porosities to analyze the product quality and catalyst lifetime (T=285 °C; $d_p = 3.53\ mm$; $\varepsilon_B = 0.44$; FF=196 t/h; P=73.5 barg).

Figure 3-12 represents the influence of 4-CBA concentration in the feed stream on the outlet composition of the catalytic process. Under the normal condition at which 4-CBA concentration is 579 ppm, the catalyst is deactivated after 375 days of the operation. However, when the inlet concentration of 4-CBA in the reactor feed increases by 10% and 15%, the catalyst deactivation occurs after 255 and 205 days of the operation, respectively. In other words, the catalyst lifetime drops by 32% and 45.3%, respectively. This implies that the concentration of 4-CBA in the feed stream has a substantial influence on the reactor efficiency and catalyst deactivation. The high concentration of 4-CBA not only negatively affects the Pd/C catalyst activity/lifetime but also adversely influences the downstream separation processes, equipment function, and polymerization process efficiency. Final product of PTA consisting of a high content of 4-CBA is not proper to be used in the PET polymerization process [283]. In fact, a high amount of 4-CBA gives an unfavorable color to the PET product [272]. In addition, elevated concentrations of 4-CBA in the PTA product promote the side reactions of PET polymerization process and decrease the molecular weight [6]. In consequence, the high concentration of 4-CBA reduces the efficiency of the centrifugation and filtration processes. The off-spec production also increases the operating cost of the process.

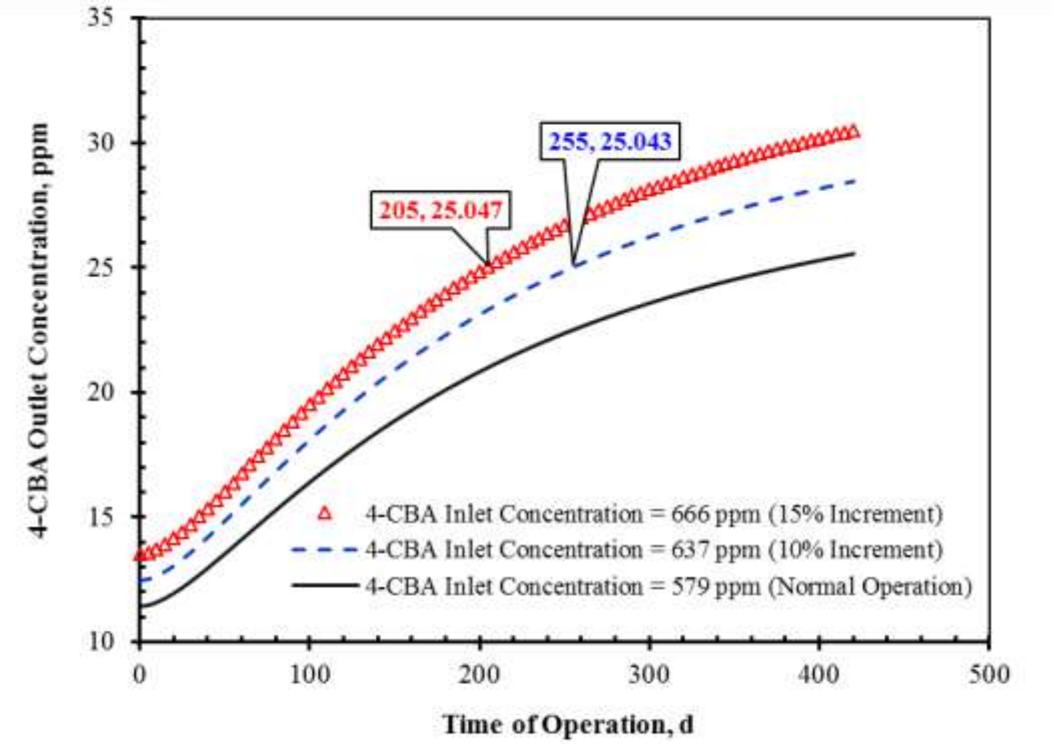

Figure 3-12: Impact of 4-CBA inlet concentration on the hydropurification process (T=285 ºC; $\varepsilon_p = 0.61$; $d_p = 3.53\ mm$; $\varepsilon_B = 0.44$; FF=196 t/h; P=73.5 barg).

Figure 3-13 depicts the temperature profile along the length of the catalytic reactor. Increase in the temperature is expected as the overall hydropurification reaction is exothermic. Indeed, it shows that the temperature slightly increases from the inlet to the outlet of the reactor since the amount of 4-CBA involved in the hydrotreating process is not significant in the feed stream. Moreover, it is noticed that the temperature rise at the beginning of the reactor is significant as the temperature change mostly occurs within the first 3 m length of the reactor. The main reason for this behavior is that the conversion of 4-CBA to pta is higher at the beginning of the catalyst bed, compared to the rest of the catalyst bed. As it is clear from Figure 3-13, there is a good agreement between the predicted outlet temperature and real exit temperature.

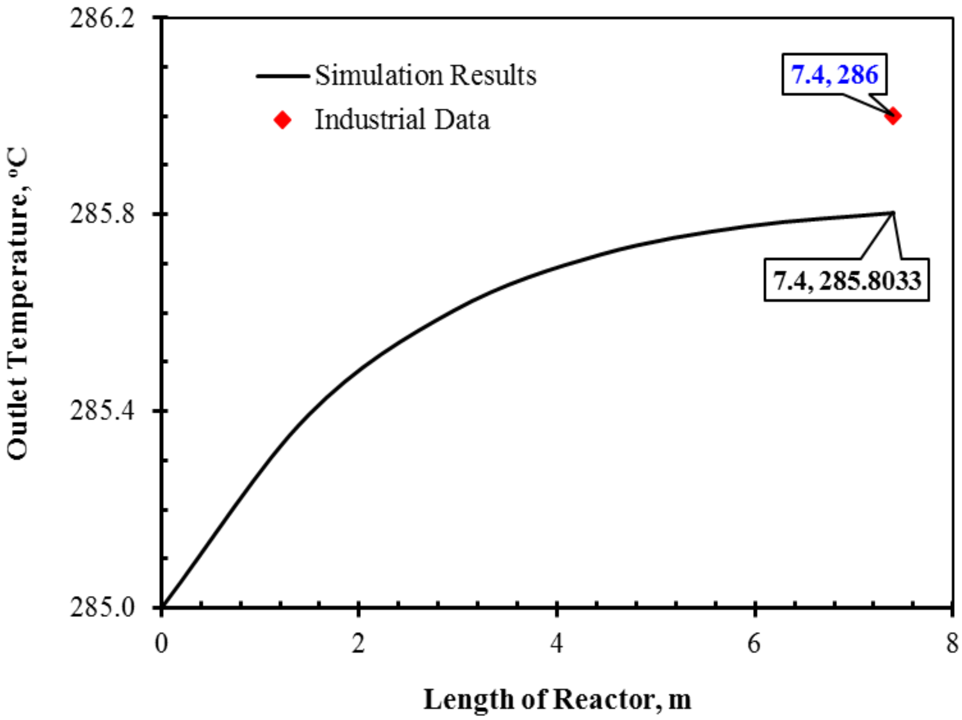

Figure 3-13: Temperature profile in the reactor catalyst bed.

The effect of reactor inlet temperature on the hydropurification reactor performance is demonstrated in Figure 3-14. According to the modeling results, it is found that increasing the inlet temperature lowers the outlet concentration of 4-CBA, which is considered as an improvement in the reactor performance. Thus, an increase in the lifetime of the catalyst is expected (e.g., from 375 days to 420 days), implying an increase of 12% in the catalyst lifetime. This analysis has been made based on 4-CBA concentration in the final product. It is clear that the temperature plays an important role in the reaction system of the hydrogenation process. It is also concluded that among 4-CBA hydropurification reactions, the conversion of 4-HMBA to pta is more sensitive to the temperature than that of 4-CBA to 4-HMBA. This provides proper conditions for the reaction of 4-CBA to 4-HMBA, and consequently pta synthesis [284]. The other important aspect on the temperature effect is that increasing temperature enhances the endothermic reaction of 4-CBA decarbonylation which leads to greater conversion of 4-CBA to BA in the reaction mixture [285]. BA concentration in the final product is one of the criteria of PTA powder quality. The maximum allowed concentration of BA in PTA product is 30 ppm [4]. The rate of endothermic decarbonylation reactions improves with the temperature increase [285]. Figure 3-15 illustrates the trend of BA concentration rise in the final product versus reactor inlet temperature. The maximum reactor inlet temperature increase considering BA concentration in the final product is 289 ^{o}C. The detailed analysis of the temperature effect on the hydrotreating reactor has been reported in Azarpour et al. [271], and calculated that the rate of PTA production cannot be improved through the enhancement of temperature beyond the mentioned temperature. It is to be noted that for the implement of the results into the actual operation, some modifications are required. One of the most important changes is the improvement of the pressure control valve of the reactor, which is a very sophisticated type of valve installed at the exit of the reactor.

Another adverse effect of the temperature increase is a decrease in the active surface area of the catalyst. Increasing temperature leads to the progress of sintering rate of Pd [2]. However, the overall impact of the reaction mixture temperature increase is the improvement of the rector performance. From a practical point of view, the temperature change cannot be implemented in the production plant easily as even a moderate change in the reaction temperature results in a considerable increase in the reactor operating pressure. In this case, the control of pressure and reactor liquid level (which is a key factor to control the product quality) would be difficult, leading to high fluctuations in the product quality and unacceptable appearance and transparency of the produced powders.

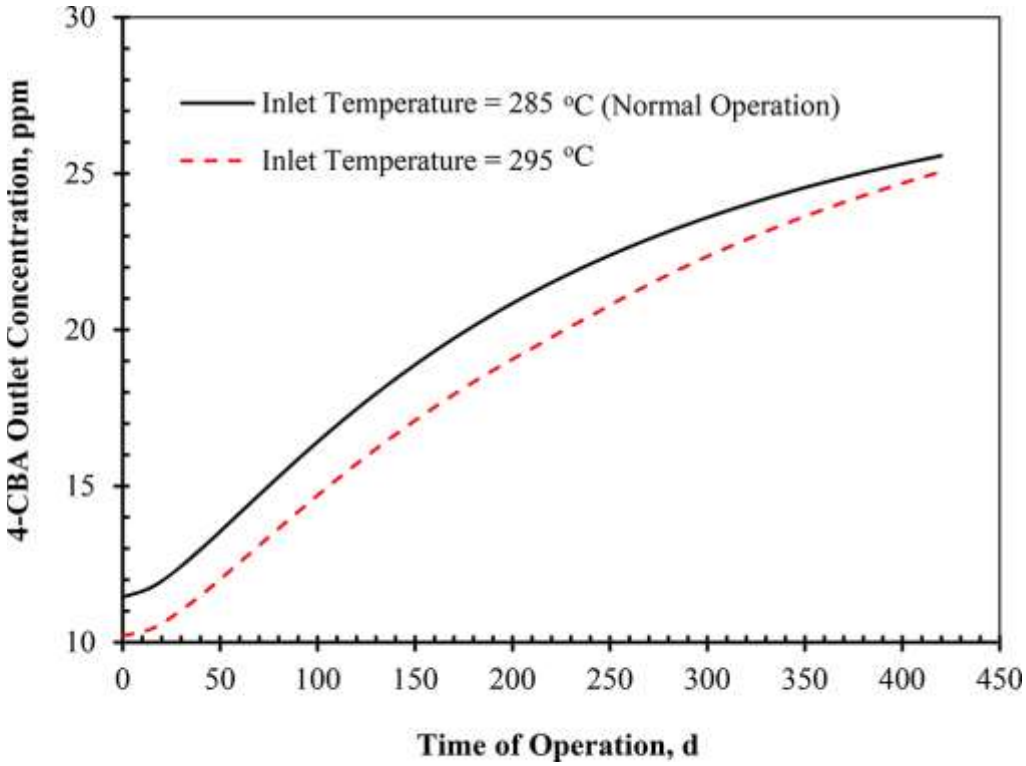

Figure 3-14: Inlet temperature effect on the operation performance ($\varepsilon_p = 0.61$; $d_p = 3.53\ mm$; $\varepsilon_B = 0.44$; *FF*=196 t/h; *P*=73.5 barg).

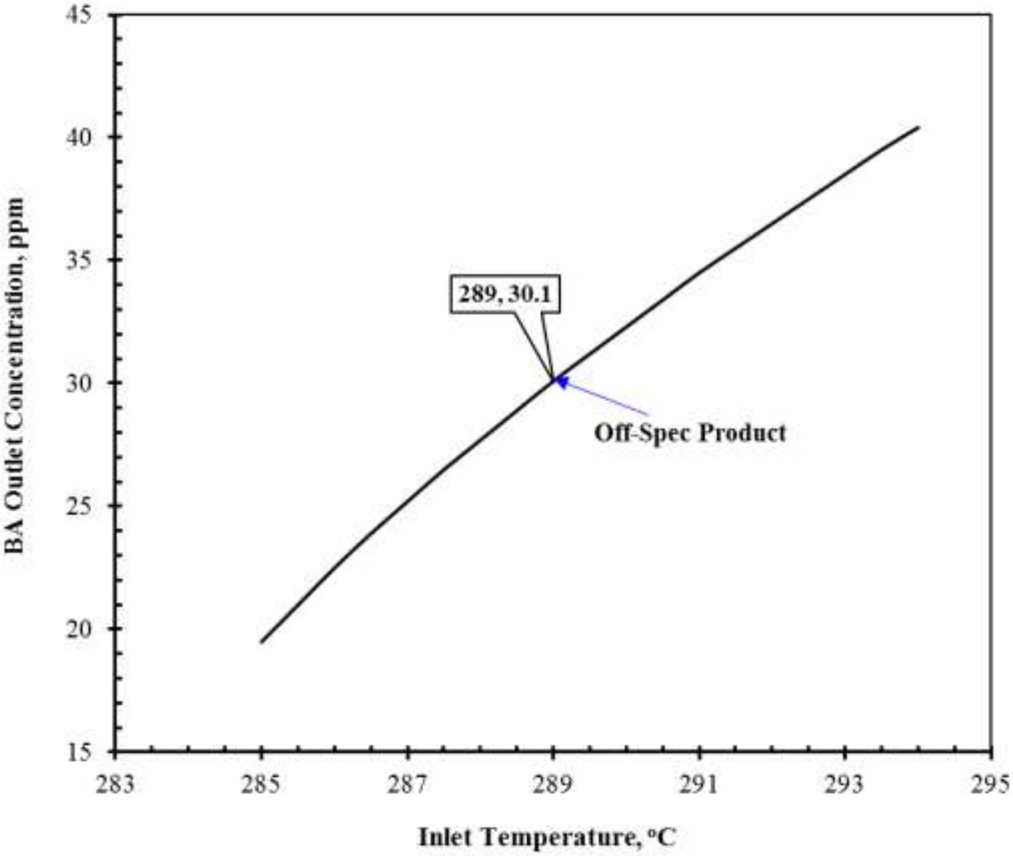

Figure 3-15: BA concentration in PTA product versus reactor feed temperature ($\varepsilon_p = 0.61$; $d_p = 3.53\ mm$; $\varepsilon_B = 0.44$; *FF*=196 t/h; *P*=73.5 barg).

In the hydrotreating process, hydrogen plays an important role in the conversion of the main impurity. Therefore, it is expected that a change in the concentration of hydrogen in the reaction mixture appreciably alters the product quality. Figure 3-16 illustrates the impact of the hydrogen partial pressure on the conversion of 4-CBA in the final product and the overall performance of the catalytic process. It is found that a slight increase in the partial pressure of hydrogen has a considerable influence on the powder quality and process efficiency. It can be explained that a low concentration of the main impurity in the reaction mixture leads to a significant reduction in the

4-CBA in the product since the availability of the hydrogen in the reaction system is more than the amount of hydrogen needed for the normal operation condition. For instance, a 13% increase in the hydrogen partial pressure (from 7.5 barg under normal operation to 8.5 barg) leads to an increase of 3.6% improvement in the product quality and 20% increase in the lifetime of the catalyst. It should be noted that greater increase in the hydrogen partial pressure might cause considerable variations (or/and increase) in the reactor pressure which results in the unfavorable appearance for the powder product, owing to breakage of the fragile structure of the catalyst carbon support.

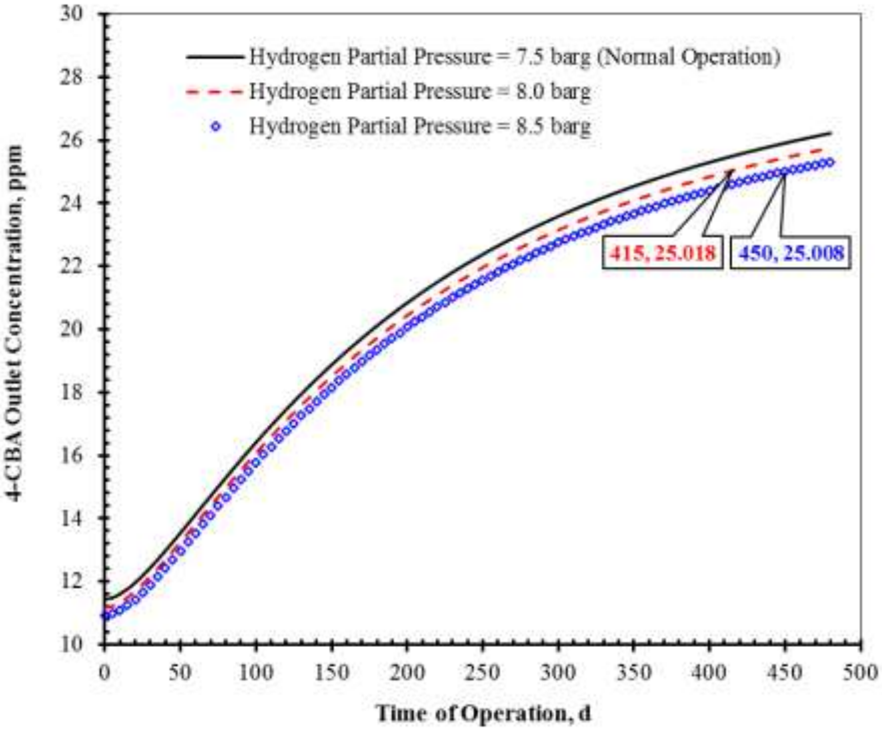

Figure 3-16: Hydrogen partial pressure impact on the hydropurification process ($\varepsilon_p = 0.61$; $d_p = 3.53\ mm$; $\varepsilon_B = 0.44$; *FF*=196 t/h; *P*=73.5 barg).

The results obtained in this study reveal that the dispersion model is more reliable and accurate approach to simulate the reaction system in the hydropurification process. Employing this appropriate modeling strategy, parametric sensitivity analysis can be conducted for possible modifications for the purposes of process improvement. The catalyst characteristics such as catalyst particle size and porosity can be modified to increase the efficiency of the hydropurification section. It should be noted that the values of particle size and porosity of the catalyst obtained in this study are based on the theoretical analysis. To put it more simply, the tough operation of hydrotreating process of PTA production which deals with the critical risk of terephthalic acid crystallization in the reaction system due to the fluctuation of process temperature and the vital operating parameters such as pressure, the best particle size and porosity might be 2.30 mm and 0.7 considering the degree of improvement in the product quality and catalyst lifetime. Through proper control of PX oxidation reactors as well as accurate control of 4-CBA content in the hydropurification reactor feed, the process can be optimized in the way to lower the amount of byproducts in the reactor outlet and to extend the effective lifetime of Pd/C catalyst. Furthermore, increasing the reaction temperature can lead to a better operation of the reactor. To achieve this goal, more efficient hot oil system and better control on the reactor pressure might be required. In addition, an increase in the partial pressure of hydrogen improves the performance of the hydrotreating process. This strategy might be practically effective if the reactor operating pressure and the reactor liquid level are accurately controlled using a proper/effective process control system.

3.6 Conclusions

A dynamic heterogeneous dispersion model is developed in this research work to simulate the transport phenomena behaviors in the hydropurification TBR of PTA production plant. The derived PDEs are solved by MOL employing FDM where the programing is performed using the software of MATLAB 2016a©. The industrial plant data are used to validate the developed model. The validation phase shows that the dispersion model results in more accurate outcomes, compared to the PFM. The results obtained from this theoretical study indicate that the reduction of catalyst particle size and an increase in the catalyst porosity can improve the PTA product quality and the performance of Pd/C catalyst. Moreover, decreasing 4-CBA concentration in the reactor feed and increasing the reactor inlet temperature lead to a more efficient hydropurification process. Higher hydrogen partial pressure causes better product quality and longer catalyst lifetime. The process improvement in this study corresponds to increasing the lifetime of Pd/C catalyst and lowering the operational cost, as well.

It is expected that the proposed model can be modified to attain better outcome if possible limitations and difficulties of the catalyst synthesis and characterization are considered.

We believe that such a modeling approach can be utilized to simulate the behavior/performance of similar polymerization production systems in petrochemical companies if the model input variables/parameters are accurately determined and the reaction mechanisms are well explored.

SUPPORTING INFORMATION

The Supporting Information is available free of charge on the ACS Publications website. The physical properties of the chemicals involved in the hydrotreating process of PTA production plant and the magnitudes of the physical properties and important parameters incorporated into the developed model.

NOMENCLATURES

Acronyms

4-CBA	-	4-carboxybenzaldehyde
4-HMBA	-	4-hydroxymethylbenzoic acid
AA	-	acetic acid
BA	-	benzoic acid
BC	-	boundary condition
CD	-	condensate drum
CE	-	centrifuge
CR	-	crystallizer
CTA	-	crude terephthalic acid
DAE	-	differential algebraic equation
Dyn	-	dynamic
EG	-	ethylene glycol
FBR	-	fixe-bed reactor
FC	-	flowrate controller
FDM	-	finite difference method
FEM	-	finite element method
FPM	-	first principle model
HDM	-	hydrodemetallization
HDN	-	hydrodenitrogenation
HDS	-	hydrodesulphurization
HDT	-	hydrotreating
HE	-	heat exchanger
HOS	-	hot oil supply

HOR - hot oil return

HPLC - high-performance liquid chromatography

IC - initial condition

LC - level controller

MOL - method of lines

NRV - non-return valve

ODE - ordinary differential equation

PC - pressure controller

PCS - powder conveying system

Pd/C - palladium supported on carbon

PDE - Partial differential equation

PET - polyethylene terephthalate

PFM - plug flow model

PID - proportional-integral-derivative

PTA - purified terephthalic acid

pta - para-toluic acid

PX - para-xylene

RVF - rotary vacuum filter

SFD - slurry feed drum

SS - steady state

STPC - Shahid Tondgooyan petrochemical company

TA - terephthalic acid

TBR - trickle-bed reactor

Variables/Symbols

a - metallic sintering dispersion parameter (-)

a_P - catalyst surface area (m^2 g^{-1})

C - concentration (kmol m^{-3})

C_P - heat capacity (J kg^{-1} K^{-1})

C_{TA} - feed concentration of terephthalic acid (wt. %)

d_B - diameter of catalyst bed (m)

d_P - catalyst particle diameter (mm)

D - diffusivity (m^2 s^{-1})

D_{ax} - axial dispersion (m^2 s^{-1})

FF - feed flowrate (t h^{-1})

FH - hydrogen flowrate (kg h^{-1})

h - heat transfer coefficient (W m^{-2} K^{-1})

H - Henry's constant (m^3 MPa mol^{-1})

H_k - heat of reaction (kJ mol^{-1})

k - mass transfer coefficient (m s^{-1})

L - length of reactor bed (m)

m - time step (-)

P - pressure barg

q - z direction increment (-)

r - rate of reaction (kmol kg$_s^{-1}$ s^{-1})

r_d - rate of deactivation (h^{-1})

R - universal gas constant (J mol^{-1} K^{-1})

t - time (s)

T - temperature (K)

T_R - reference temperature (K)

u - superficial velocity (m s^{-1})

z - axial coordinate (m)

Greek Letters

ε_B	-	bed void fraction	(-)
ε	-	holdup	(-)
ε_P	-	particle porosity	(-)
η	-	effectiveness factor	(-)
λ	-	conductivity	(W m^{-1} K^{-1})
μ	-	viscosity	(Pa.s)
ν	-	molar volume	(cm^3 mol^{-1})
ξ	-	specific surface area of the phase interface	(m^2 m^{-3})
ρ	-	density	(kg m^{-3})
ρ_B	-	bulk density	(kg m^{-3})

Subscripts

g - gas phase

gl - gas to liquid

i - index of components

in - inlet to reactor

k - index of reaction

l - liquid phase

ls - liquid to solid

s - solid (catalyst) phase

Superscripts

S - surface of the catalyst

ss - steady state

3.7 Supporting Information

Table S3-1: Physical properties of the chemicals involved in the hydrotreating process [286].

Chemical	**Formula**	**Molecular weight (g mol^{-1})**	**Density (g cm^{-3})**	**Solubility in Water (g L^{-1} at 20 °C)**	**Melting Point (°C)**	**Vapor Pressure (mmHg)**
TA	$C_8H_6O_4$	166.13	1.52	1.492	402	1.69×10^{-6}
4-CBA	$C_8H_6O_3$	150.13	1.32	1.862	245	1.76×10^{-4}
pta	$C_8H_8O_2$	136.15	1.06	2.22	130	9.03×10^{-4}
4-HMBA	$C_8H_8O_3$	152.15	1.3	14.13	128	9.73×10^{-7}
BA	$C_7H_6O_2$	122.12	1.26	9.02	123	7×10^{-4}
PET	$(C_{10}H_8O_4)_n$	$(192)_n$	1.38	Insoluble	260	-

Table S3-2: Values of variables involved in the developed model.

Parameter	**Value**	**Unit**
Density (ρ)		
Gas (ρ_g)	6.86	kg m^{-3}
Liquid (ρ_l)	839	
Solid (ρ_s)	2100	
Viscosity (μ)		
Gas (μ_g)	0.0095×10^{-3}	Pa.s
Liquid (μ_l)	0.15×10^{-3}	
Henry's constant (H)	0.0082	m^3.MPa mol^{-1}
Hydrogen solubility	0.0215	kmol m^{-3}
Molar volume (v)		
$v_{4\text{-}CBA}$	416.5	cm^3 mol^{-1}
$v_{4\text{-}HMBA}$	366.5	

v_{pta}	399.5	
v_{BA}	344.5	
v_{TA}	423.5	
***Diffusivity* (*D*)**		
D_{H2}	60.62×10^{-5}	$cm^2\ s^{-1}$
$D_{4\text{-}CBA}$	9.01×10^{-5}	
$D_{4\text{-}HMBA}$	9.77×10^{-5}	
D_{pta}	9.25×10^{-5}	
D_{BA}	10.16×10^{-5}	
***Mass transfer coefficient* (*k*)**		
$k_g\xi_{gl\text{-}H2}$	0.058	s^{-1}
$k_l\xi_{\mathrm{ls\text{-}H2}}$	1.37	
$k_l\xi_{ls\text{-}4\text{-}CBA}$	0.38	
$k_l\xi_{ls\text{-}4\text{-}HMBA}$	0.4	
$k_l\xi_{ls\text{-}pta}$	0.39	
$k_l\xi_{ls\text{-}BA}$	0.42	
Specific surface area (ζ)	951.84	$m^2\ m^{-3}$
***Heat capacity* (C_p)**		
Gas ($C_{p,g}$)	14500	$J\ kg^{-1}\ K^{-1}$
Liquid ($C_{p,l}$)	4900	
Solid ($C_{p,s}$)	1340	
***Conductivity* (λ)**		
Gas (λ_g)	67.23×10^{-5}	$W\ m^{-1}\ K^{-1}$
Liquid (λ_l)	0.57	
***Heat transfer coeffcient* (*h*)**		
g-l (h_{gl})	65.84	$W\ m^{-2}\ K^{-1}$
l-s (h_{ls})	140.33	
Liquid holdup (ε_l)	0.385	-
Wetting efficiency	0.97	-

4 CHAPTER FOUR: Dynamic Modeling Strategy to Assess Impacts of Hydrodynamic Parameters on Industrial Hydropurification Process by Considering Catalyst Deactivation

Preface

A version of this chapter was published in the Journal of Industrial and Engineering Chemistry Research 57, 13671-13688 (2018). I am the leading author of this paper. Sohrab Zendehboudi provided me with valuable guidelines and tips to develop the model and structure the research paper. The first draft of the manuscript was prepared by me, and I revised the manuscript by applying the comments and suggestions received from the co-authors and journal reviewers. Nima Rezaei also commented on the different sections of the manuscript and helped in editing the text.

Abstract

In this study, modeling simulation of the dynamic behavior of an industrial-scale trickle-bed reactor (TBR) with application to hydropurification process for production of purified terephthalic acid (PTA) is carried out. The impact of hydrodynamic parameters such as reactor bed porosity, liquid hourly space velocity (LHSV), and liquid-solid mass transfer coefficient on the industrial hydropurification TBR performance (in particular, on the catalyst lifetime) is analyzed. As the palladium supported on carbon (Pd/C) catalysts deactivate over the course of operation time, the concentration of impurities in the product, especially 4-carboxybenzaldehyde (4-CBA) as the main impurity of PTA, increases. A three-phase dynamic mathematical model developed is validated against the plant data, and an average relative error of 2.2% is obtained for the concentration of 4-CBA. The lifetime of catalyst based on the plant data is (348.2 ± 5.0) days; this value is estimated to be 365.1 days from the simulation results, showing a 4.8 % error. The effects of LHSV and bed porosity are in the same direction and magnitude, while the effect of liquid-solid mass transfer coefficient is in the opposite direction, and its impact is also less pronounced. These parameters are disturbed in a range of up to ± 15%, compared to normal operation that results in absolute catalyst lifetime change of 2.9–14.2%. The maximum and minimum of change in the catalyst lifetime is obtained when LHSV is disturbed by ±10%, exhibiting the catalyst lifetime change by 14.2% at a -10% disturbance (416.9 days) and -6.5% at a +10% disturbance (341.3 days). A +15% disturbance in the liquid-solid mass transfer coefficient increases the catalyst lifetime by 2.9% (375.8 days) and a -15% disturbance decreases it by 3.7% (351.8 days). Eventually, the findings of this study might be applied to the relevant industrial sector providing the required close and meticulous control of the process.

4.1 Introduction

Trickle bed reactors (TBRs) are an important type of fixed-bed three-phase catalytic reactors, which are widely employed in hydrotreating processes in petrochemical, petroleum, food, and chemical industries. Their applications in the petrochemical industries are still growing. In general, the three-phase catalytic reactors are used in processes such as hydrogenation of unsaturated oils, synthesis of butynediol and propargyl alcohol, hydrodesulfurization of petroleum feedstocks, hydrodenitrogenation, hydrocracking, Fischer-Tropsch synthesis, sorbitol manufacture from glucose, cellulose hydrogenation, pollution control, polymer-bound catalysis, and hydropurification of aromatics [31].

Studies on the effects of hydrodynamic parameters on the performance of TBRs are extensive. For instance, Iliuta et al. [287] studied a 1D implicit hydrodynamic model of TBR to estimate reactor bed porosity and the two-phase flow parameters such as wetting efficiency, liquid hold up, pressure drop, and bed porosity. The model successfully predicted these variables at high pressures and high temperatures under the trickle flow regime in undiluted and diluted beds of catalysts. Xiao et al. [288] investigated the hydrodynamics of a TBR under forced pulsing flow regime. The experimental results showed that both the radial and axial liquid distributions are more uniform in the forced (as opposed to natural) pulsing flow regime. It was also found in their study that the frequency of pulsations affects the liquid hold up the most [288]. Callijas and Martínez [230] studied the effects of hydrodynamics on deviation of model from plug flow conditions in hydrodesulfurization and hydrodemetalation of petroleum residue in a TBR reactor. The reactions were conducted in a continuous small pilot-scale TBR, using NiMo/Al_2O_3 catalysts. A first-order liquid-limited nickel removal reaction was utilized to evaluate the impact of hydrodynamics on the catalyst use based on the different models. The incorporation of hydrodynamic parameters of wetting efficiency and external transport resistance in the models improves the data fit [230]. For instance, Iliuta et al. [289] developed a 1D transient hydrodynamic model, based on macroscopic multiphase transport equations; experiments were also conducted and the model was validated with the experimental results. They investigated the effects of changes in porosity, surface area, gas density, gas velocity, liquid velocity, liquid viscosity, and fine concentration (in feed) on the plugging dynamics. The experiments were conducted in the trickle flow regime for the hydrotreating reaction, occurring in a TBR with spherical catalysts. They used magnetic resonance imaging (MRI) technique to quantify the experimental observations [289]. Sales et al. [290] determined the hydrodynamic parameters of a fluidized-bed reactor and a TBR by dynamic residence time analysis for the gas and liquid phases. Experiments were conducted using a TBR at different flowrates of individual phases, having a tracer in the liquid phase. They developed transfer functions to predict the hydrodynamic parameters such as liquid hold up, the liquid phase Péclet number, and wetting efficiency [290]. Iliuta and Larachi [291] studied fines release from the catalysts bed and their aggregation due to hydrodynamics and colloidal forces in a TBR. Using Euler–Euler fluid dynamic model, volume average transport conservation rules, Brownian motion, discrete population balance for particles, and the aggregate filtration equations, they modeled the aggregation behavior. The Brownian particle aggregation was explained by the rate at which a definite aggregate size was obtained from smaller aggregates [291]. Tukač et al. [292] assessed the scale up performance of hydrodynamic parameters such as pressure drop and wetting efficiency in bench (continuous) and pilot (periodic) TBRs. The chosen typical reactions were the toluene solution of styrene and/or dicyclopentadiene hydrogenation on Pd catalyst. The results showed the profound impact of catalyst wetting efficiency on the TBR productivity; an enhancement of up to 30% (compared to steady state) was obtained in the hydrogenation of styrene [292]. In another study [293], the analysis of TBR hydrodynamics was conducted under gas- and liquid-limited reactions, for α-methyl styrene hydrogenation reaction system. The fluctuations in the liquid flowrate had a great effect on the reaction conversion. Moreover, in liquid-limited and gas-limited reactions, the liquid-solid and gas-liquid mass transfer rates were the limiting step, respectively [293]. Lopes and Quinta-Ferreira [294] modeled a TBR to study the hydrodynamics behavior in trickling flow conditions. The computational fluid dynamics (CFD) model was in agreement with experimental data of two-phase pressure drop and liquid hold up. At lower gas flowrates, a better fit to the experimental data was achieved [294]. Prokešová et al. [295] investigated liquid hold up, axial dispersion, and pressure drop of a laboratory-scale TBR in hydrodesulphurization reactions (of motor oil and petrochemical fractions) in a bed of diluted catalyst particles with inert fines. Under the trickle flow regime, the liquid hold up and axial mixing were strongly improved at lower flowrates. The gas and liquid flowrates did not significantly change the pressure drop of a TBR in the up-flow configuration. Further, the decrease in the gas flowrate significantly increased the residence time [295]. Salimi et al. [296] studied the effects of tortuosity and fluid volume fractions on the performance of TBR. The Hydrodynamics of a TBR filled with industrial trilobe catalysts was investigated for two different catalyst loadings through conducting the experiments and CFD modeling. The Eulerian-Eulerian method was used to model the three-phase reaction system, which considered the interfacial momentum transport. The velocity distributions revealed that liquid hold up and pressure drop are decreased at sharp corners due to the increased void fraction, influenced by the reactor boundaries [296]. In an experimental study [297], the hydrodynamics of a TBR filled with paper or ceramic bead catalysts was studied through residence time distribution. The paper composite showed a better wettability and internal diffusion for the liquid reactants, compared to the ceramic beads; which is in favor of heterogeneous flow. Moreover, the effective catalytic oxidation of various alcohols was achieved with the paper-structured catalysts. Uniform films of liquid on the catalyst surfaces can justify this point [297]. Su et al. simulated pyrolysis gasoline hydrogenation unit, using the TBR model. They used a semi-empirical model to calculate the residue catalyst activity for a highly exothermic hydrogenation reactor. The model was able to forecast the plant behavior such as bed temperature profile and the relationship between the flowrate and pressure drop [298]. Nawaf et al. [188] proposed a kinetics for the oxidative desulfurization of dibenzothiophene in light gas oil process, where the hydrodynamic parameters such as effectiveness factor, wetting efficiency, and internal diffusion in a TBR were taken into account. Employing the modeling approach, they were able to precisely predict the product conversion [188]. Mohammed et al. [186] modeled the catalytic wet air oxidation of phenol process, and obtained the kinetic parameters for scale up purposes by considering the hydrodynamic parameters such as the ratio of reactor length-to-diameter [186]. Rabbani et al. [299] developed a phenomenological pore-scale hydrodynamic model to estimate the liquid hold up and pressure drop in steady gas-liquid flow in a TBR. They used a 1D three-phase Eulerian model where the influence of liquid film tortuosity on liquid hold up and pressure drop was considered; the results were in agreement with the existing models [299]. In a recent study [300], the hydrodynamics and mass transfer parameters of a multiphase monolithic reactor were determined by experiments and CFD simulation. According to the research results, the gas-liquid mass transfer coefficient increased with the superficial velocities of both phases. This coefficient was mainly influenced by the liquid superficial velocity. The gas-liquid phase distributions were also governed by the liquid superficial velocity, while the gas superficial velocity had a negligible effect [300].

The majority of the previous studies on the evaluation of dynamic behaviors of TBRs are experimental works. The numerical studies also overlook the dynamic effects when assessing the hydrodynamic parameters in a TBR system. For example, the hydrodynamic performance evaluation of TBRs with catalyst deactivation is of great interest in the context of quality control in the petrochemical industry, which has been investigated to a much less extent. Hence, it seems vital to accomplish a detailed study to investigate the hydrodynamic effects on the performance of TBRs in which the product quality is affected by the catalyst deactivation.

The objective of this research work is to study the deactivation phenomenon of the catalyst, palladium supported on carbon (Pd/C), and its impact on the product quality in a TBR of an industrial-scale hydropurification plant where a dynamic mathematical model is developed based on the three-phase mass transfer and heat transfer interactions. The proposed model involves the catalyst deactivation and the hydrodynamic parameters such as the gas and liquid hold ups, bed porosity, gas and liquid superficial velocities, and pressure drop. Moreover, other important parameters including the liquid−solid and gas−liquid mass transfer coefficients and liquid hourly space velocity (LHSV) are investigated by setting a maximum tolerable concentration threshold of 25 ppm for 4-carboxybenzaldehyde (4-CBA) in the product as a measure of the product quality. Practical recommendations are made to improve the industrial hydropurification process with the aid of a systematic parametric sensitivity analysis, after the model is validated with the plant data.

The modeling strategy introduced in this study offers effective tips/guidelines to improve the product quality and to lengthen the process catalyst lifetime. To the best of our knowledge, no models exist in the literature to consider all the above important phenomena (catalyst deactivation, pressure drop, mass transfer, and heat transfer) in simulating the TBR behaviors in terms of process engineering and transport phenomena prospects under unsteady-state conditions.

4.2 Technical Aspects of Trickle Bed Reactors

In a three-phase catalytic reactor, gas and liquid phases contact each other in a bed of solid catalyst phase, and the reaction occurs between a dissolved gas and a reactant, existed in the liquid phase, in the presence of the catalyst. The three-phase catalytic reactors can be classified according to the solid phase, being fixed or suspended. The former category covers fixed-bed reactors with concurrent or countercurrent gas-liquid flow such as trickle bed reactors (TBRs) and submerged up-flow reactors. The second category covers slurry stirred reactors and slurry bubbling reactors where the catalyst is suspended in the flowing liquid. Fixed-bed reactors with concurrent downflow of gas and liquid are more common due to a lower potential of flooding and lower pressure drop. The TBR is a three-phase reactor where the gas and liquid phases move downwards, concurrently in a fixed bed of solid catalysts. In the TBRs, the liquid trickles down over the particles in the form of rivulets or film, and the gas concurrently flows in the void spaces [301]. Usually, industrial TBRs are operated at high pressures (200–300 bar) to lower the catalyst deactivation rate, to enhance the gaseous reactant solubility, to increase reaction conversion, and to improve heat transfer [67]. TBRs have the most complicated hydrodynamics among the catalytic reactors since trickling flow regime reveals the distinctive features of solid partial wetting, predominantly at a low liquid flowrate [66]. Efficient design of a catalytic reactor requires sufficient knowledge on the hydrodynamics and transport parameters [302]. The TBRs feature advantages such as plug flow condition (due to fixed catalyst bed), low energy dissipation rate, and high catalyst loading per unit processing volume of liquid. However, they have a limited performance for the reactions with rapidly deactivating catalysts (e.g., in heavy oil hydrotreating processes), and have the risk of non-uniform liquid distribution, leading to the formation of hot spots and reactor runaway condition. Due to the prevalence of TBRs, effective control and optimization of TBRs will significantly contribute to the process economy; the petroleum industry alone demands TBRs annual processing capacity of about 1.6 billion metric tons for the hydrotreating processes [12]. Commercial TBRs that are used in the hydrotreatment processes usually operate at adiabatically conditions at high pressures and high temperatures, which normally contain hydrogen and non-aqueous liquids. The reactions, occurring in the TBRs, demand high temperatures that cause gas expansion, and decrease the solubility of gaseous reactants in the liquid phase. Therefore, increasing pressure up to 300 bar is required to increase the gas solubility, to enhance the mass transfer and heat transfer rates, to provide high mass flowrate of gas at a lower capital cost, and to decelerate the catalyst deactivation (through catalyst hydrogen starvation).

Different hydrodynamic flow regimes can be established in a TBR, based on the packed bed structure, preferential wettability condition of the catalyst particles, physical properties of the fluids, and the velocities of the liquid and gas phases, flowing in the reactor [78]. Although several flow regimes can be observed in the TBRs, they are commonly classified into two different categories. These include low interaction regime (LIR) which occurs in the trickle flow regime, and high interaction regime (HIR) that cover pulse, spray, bubble, and dispersed bubble flow regimes [282, 303]. The LIR is dominant under particular operating conditions such as low gas and liquid flowrates; the extent of gas-liquid interactions is enhanced in the trickle flow regime at high gas and liquid flowrates and also at an elevated pressure. The liquid, trickling down onto the catalyst particles in the form of droplets, films, and rivulets, and the liquid phase can be either foaming or non-foaming. The continuous gas phase occupies the remaining of the bed void space and flows separately. The HIR is established under moderate to high gas-liquid shear conditions because of the flowrate of one or both fluids, being in the moderate to high range [12]. A schematic of different flow regimes in the TBRs is shown in Figure 4-1 that distinguishes the flow regime boundaries with regard to the gas and liquid flowrates [25].

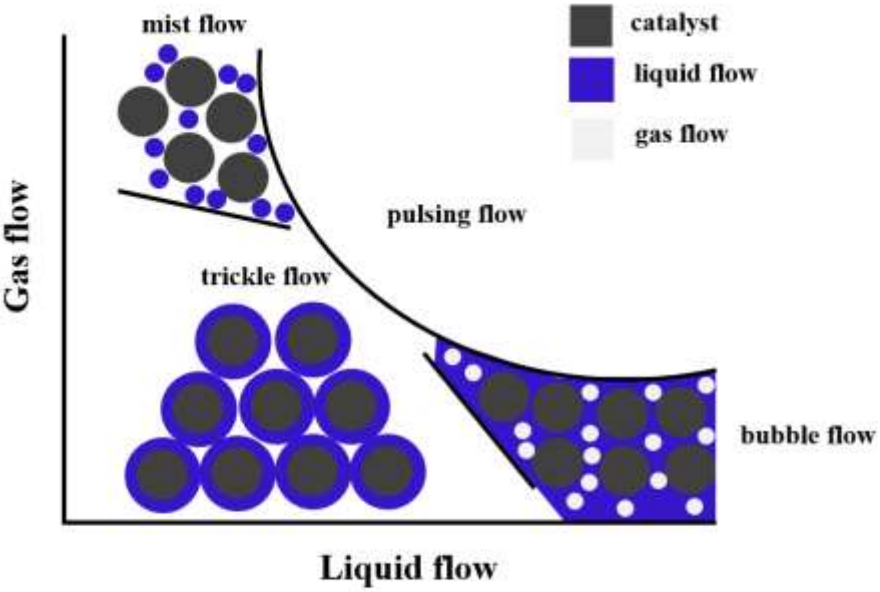

Figure 4-1: Layout of the position of the trickle, mist, bubble, and pulsing flow regimes considering gas and liquid flowrates [25]. Adapted with permission from ref [25]. Copyright 2005 Elsevier B.V.

As shown in Figure 4-1, the trickle flow regime boundaries are limited to low flowrates of both the liquid and gas phases. It is generally classified into two regions. At low flowrates of gas and liquid, the flow of liquid is laminar, and a portion of the particles remains unwetted. If the liquid flowrate is increased, the complete wetting trickling regime is established in which the particle is entirely covered by a liquid film. At low flowrates of liquid and high flowrates of gas, the mist flow regime occurs. In this regime, the liquid phase moves down through the bed in the form of droplets entrained by the continuous gas phase. The bubbly flow regime takes place at low gas flowrates and high liquid flowrates. In the bubbly flow regime, the bed is occupied by the liquid phase, and the gas phases is in the form of moderately extended bubbles. If the flowrate of the gas phase is further increased, the bubbles are shaped highly irregular. This behavior corresponds to the dispersed bubble regime. The pulse flow regime prevails when both flowrates of the liquid and gas are high. This flow regime is attained when the flow channels among particles are plugged by a liquid slug, followed by blowing off of the slug by the flow of gas. Pulses always are generated at the bottom of the bed, where the gas velocity is larger due to the lower pressure. As the gas flowrate is increased, the emerging pulses travel to the upper section of the bed [21].

Despite disadvantages of TBRs such as difficulties in temperature control, and non-uniform liquid distribution (wetting, especially at low flowrates), the three-phase catalytic reactions are mostly implemented in the TBRs [70]. In trickling flow regime, the catalyst particle external surface may be either partially or completely wetted by the liquid films as depicted in Figure 4-2. Partial catalyst wetting in the industrial TBRs is at lower liquid velocities. The internal catalyst wetting efficiency by the liquid is equal to unity because of the capillary imbibition effects. The catalyst external wetting efficiency is a significant parameter in the TBR design and scale up. It is also critical in designing catalyst loading in the TBRs. The reaction rate with partially wetted catalysts (externally) can be higher or lower than that with fully wetted catalysts, depending on whether the limiting reactant is only in the liquid phase or in both gas and liquid phases. For example, if the reaction is liquid-limited and the liquid reactant is nonvolatile, which is the case in most hydrogenation processes, a reduction in the catalyst-liquid wetting efficiency decreases the mass transfer area/surface between the liquid and the catalyst, resulting in a decrease in the reaction rate [67, 304].

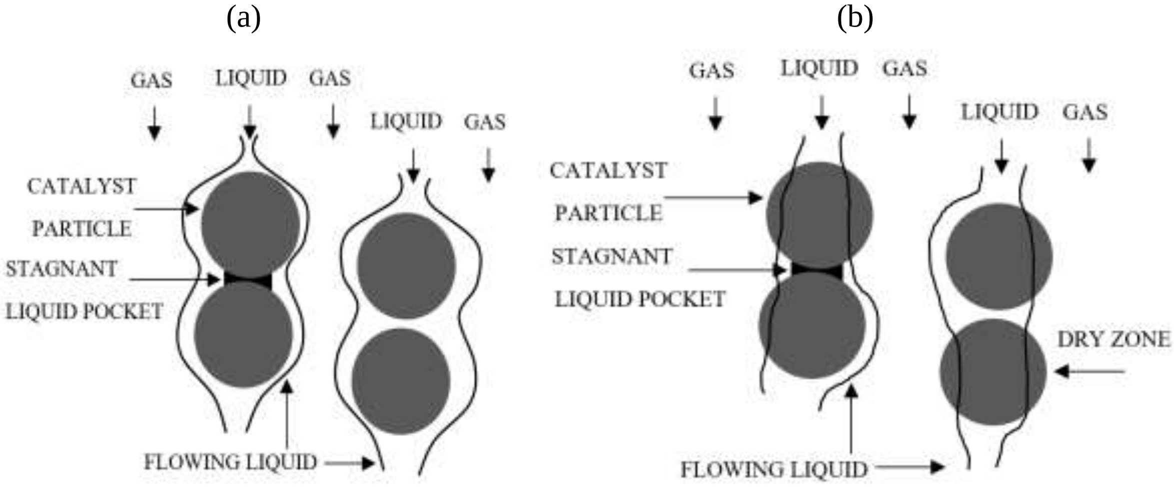

Figure 4-2: Layout of liquid-gas flow arrangements in trickling flow regime and the state of particles wetting; (a) complete external wetting; (b) partially external wetting [67]. Adapted with permission from ref [67]. Copyright 1995 Elsevier B.V.

Structured packings significantly improve the contract area per operating volume and the wetting efficiency. They are effectively applied in industrial distillation and absorption columns since the 1960s [305] and about 25% of all refinery towers have structured packings [306]. The structured packings have not yet found commercial applications in TBRs, and their applications in TBRs are only limited to lab-scale investigations. Process intensification has received an extensive interest, and the structured reactors are expected to gain significant attention in the near future [307]. A structured reactor can be regarded as an intensified configuration of packed bed reactors. For instance, a monolith is a structured reactor in which there is a low pressure drop, and high geometrical surface area can be achieved [308, 309]. The main advantage of a structured reactor is that it might be fully designed (shape and size) with a high precision [310]. In addition, the structured reactors effectively allow the disengagement of intrinsic reaction kinetics, transport phenomena, and hydrodynamics. Hence, it is possible to independently optimize the mentioned three factors, leading to the improvement of the catalytic reactor performance [311]. The independent optimization of the reaction rate and the reactor hydrodynamics aspects has applications in TBR. For example, in the conventional TBRs, smaller particles are required for a high catalyst effectiveness, while large particles are needed for a lower pressure drop (as an important hydrodynamic parameter). Structured packings can avoid these limitations [307].

4.3 Hydropurification Process Overview

One of the important applications of TBRs is in the hydropurification process of purified terephthalic acid (PTA) production plant, which is a raw material to produce polyethylene terephthalate (PET) [1, 269]. PTA and Ethylene glycol (EG) are the feedstocks for the commercial production of PET, which is extensively used to produce fibers, beverage bottles, pharmaceutical products, cosmetics, and food packaging films. Since PET market demand is increasing, the PTA production has significantly increased as well. The process of PTA production includes two main units. In the first process unit, *p*-xylene (PX) is oxidized in a catalytic continuous stirred tank reactor (CSTR). The homogeneous catalysts used is a mixture of cobalt acetate, manganese acetate, and hydrogen bromide in the solvent medium of acetic acid (AA). Compressed air is introduced into the reactor through four symmetrically installed nozzles. The reactor is controlled at a temperature and a pressure of 200 °C and 20 atm, respectively. The product from this unit is crude terephthalic acid (CTA) that contains different impurities. 4-carboxybenzaldehyde (4-CBA) and *p*-toluic acid (pta, to be distinguished from PTA for purified terephthalic acid) are the most critical impurities in the CTA powder, with concentrations of 300–1000 ppm and 2000–3000 ppm, respectively. The produced CTA (raw) has high an impurity content, which is not suitable for the polymerization process. Therefore, in the second process unit, the raw CTA is hydropurified in a TBR that is packed with palladium supported on carbon (Pd/C) catalyst [1, 2].

4.3.1 Description of Hydropurification Plant

In this study, we focus on an industrial-scale hydropurification plant for the production of PTA. The plant data are used to study the effects of hydrodynamic parameters on the process, particularly the lifetime of catalyst. The CTA powder produced through the oxidation process should be purified as they reduce the terephthalic acid (TA) sale value and prevent it to be used as a precursor in other polymerization processes. A TBR with 0.5 wt.% Pd/C catalysts is employed for the purification process. 4-CBA is the main impurity in the CTA powder. In the hydropurification process, the concentration of 4-CBA should be less than 25 ppm to meet the required product (e.g., PTA) specifications [5]. Therefore, we use the concentration threshold of 25 ppm for CTA in this research investigation. As the Pd/C catalyst is deactivated, the concentration of 4-CBA in the product (PTA) is increased. When the concentration of this impurity reaches the threshold value of 25 ppm, the catalysts have reached their lifetime, from the viewpoint of product quality control constraint.

A simplified process flow diagram for the hydropurification process in the PTA production plant is demonstrated in Figure 4-3. In this process, the CTA powder is discharged from CTA silo into a mixing drum where it is mixed with filtrate, which is the separated water from the slurry, coming from rotary vacuum filter (RVF). The CTA powder should be completely dissolved in water. This condition can be met at high temperature conditions. To increase the temperature of TBR feed, a total of seven heat exchangers (HEs) are employed in two stages. In the first stage, five HEs are used whose hot service fluid is from the steam generated in the crystallizers (CRs). In the second heating stage, two HEs are utilized with hot oil supply (HOS) as the service fluid, which is heated in a furnace. After the CTA is completely dissolved in water, it is fed to a TBR whose bed is filled with fixed Pd/C catalysts. The TBR is controlled at a temperature and a pressure of 285 ^{o}C and 73.5 bar, respectively. The liquid mixture effluent from TBR is transferred to five CRs where their pressures are controlled to avoid penetration of pta into the TA solid phase. In order to separate the TA from the liquid phase, the separation process is performed in two subsequent processes of centrifugation (CE) and filtration. The filtrate from RVF is transferred to the mixing drum, and the wet cake of TA is discharged into a rotary dryer. The wet cake is heated, using a low pressure steam (LPS) in this rotary dryer. Dried PTA is then transferred to a checking silo through a powder conveying system (PCS) for quality control. If the product meets the required specifications (on-specification), it is transferred to a final silo designated for the PTA product. Otherwise, the off-spec powder is recycled back to the CTA silo for further processing [271].

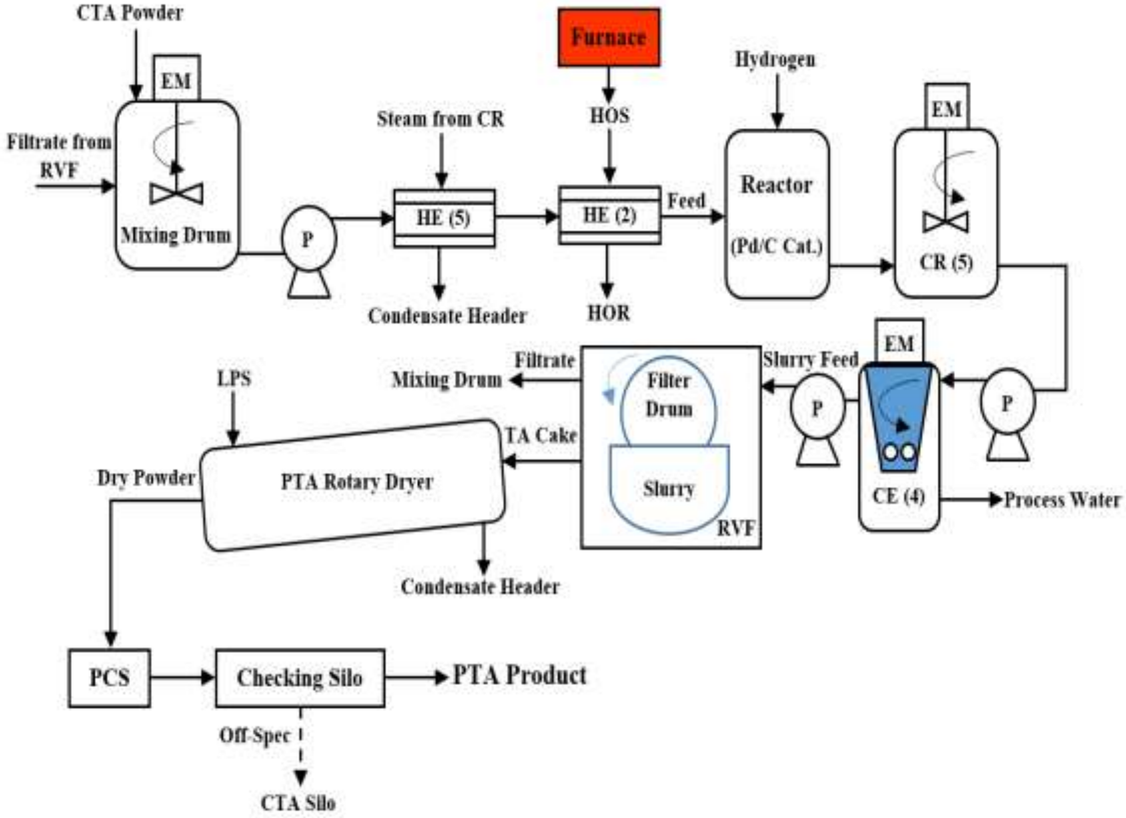

Figure 4-3: A simplified process flow diagram of hydropurification process and the PTA production plant (CE: Centrifuge; CR: Crystallizer; EM: Electromotor; HE: Heat Exchanger; HOS: Hot Oil Supply; HOR: Hot Oil Return; P: Pump; PCS: Powder Conveying System; and RVF: Rotary Vacuum Filter [271].

4.3.2 Plant Specifications

To validate the mathematical model, we need to use the industrial-scale plant data. The information on the hydropurification plant is listed in Table 4-1, including the specifications for different attributes of the process such as process operating conditions, TBR bed, and Pd/C catalysts used for hydropurification of crude terephthalic acid (CTA) to produce purified terephthalic acid (PTA).

Table 4-1: Data for industrial hydropurification of CTA to produce PTA in a TBR, using Pd/C catalyst [271].

Attributes	Variables	Values	Unit
Process	Pressure, P	73.5	bar
	Temperature, T	285	˚C
	Concentration of TA in feed, C_{TA}	23	wt %
	Flowrate		
	Feed, F_F	196	t/h
	Hydrogen, F_{H2}	13.2	kg/h
Reactor bed	Length, L	7.4	m
	Diameter, d_B	2.8	m
	Bulk density, ρ_B	475	kg/m^3
	Porosity, ε_B	0.44	m^3/m^3
Catalyst	Diameter, d_P	3.53*	mm
	Porosity, ε_P	0.61	m^3/m^3
	Surface area, a_P	900-1100	m^2/g
	Composition		
	Pd	0.5	wt %
	Activated C	99.5	wt %
	H_2O in wet catalyst	38.0	wt %

* Catalyst size distribution: d_p= 4-6 mesh (97%), d_p<4 mesh (2%), and d_p> 8 mesh (1%)

The dynamic concentration of the product impurities in the plant are another important data. The catalyst deactivation causes an increase in the impurity of the product stream with time. The PTA powder sample is taken for analysis, on a routine basis. Usually, the sample is collected from the end of the dryer after each 4-hour of operation. In abnormal conditions (off-spec production scenario), samples of PTA powder are taken more frequently. During the data collection, a great attempt is made to record the data under normal operation of the plant and under minimal deviation of the operating parameters from designed setpoints. The PTA sample is analyzed using high-performance liquid chromatography (HPLC). Moreover, a class A 100 volumetric flask, an analytical scale (accuracy of ± 0.1 mg), a STRODS column (4 mm thickness and 150 mm length), an ultrasonic bath, ammonia (2 N solution), standard samples of 4-CBA, and a mobile phase (including 21.0 vol.% of acetonitrile, 0.1 vol % trifluoro AA, and HPLC-grade water at 78.9 vol. %) were used. The HPLC machine is controlled at 260 nm wavelength, a temperature of 50 °C, and a flowrate of 0.5 mL/min. A 20 ml-aliquot solution with 0.5 N ammonia is injected into the HPLC by an auto-sampler. Thereafter, 10 mL of 2 N ammonia and deionized water are mixed with 0.5 g of standard samples to make a 100 mL solution. About 5 mL of the solution are filtered by a 0.45-mm syringe filter, and placed inside the auto-sampler machine vial. A 10 μL aliquot of standard samples is transferred into the instrument. The 4-CBA amount calibration is carried out by employing the generated peaks from the machine. Then, the filtration solution is conveyed to the machine, and the 10 μL of standard samples injection is done several time to determine the required amounts from the chromatography [312].

A summary of the concentration of 4-CBA in the plant feed and product streams are illustrated in Figure 4-4. The data shown in Figure 4 are collected from the beginning of a Pd/C fresh catalyst until its replacement time when the catalyst is practically deactivated [271].

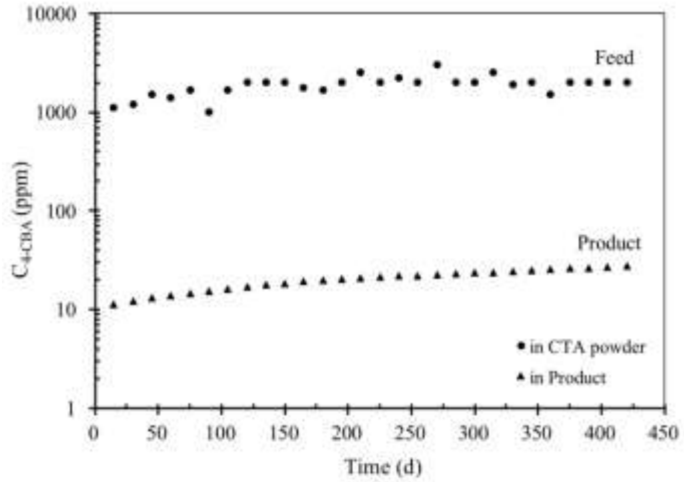

Figure 4-4: A summary of concentration of 4-CBA in the feed (CTA powder) and product streams from the plant data. These results show daily average values for the plant data, covering up to about 420 operating days [271].

4.3.3 Need and Goals of Modeling Study

This study addresses imperative aspects (e.g., kinetics and catalyst deactivation) of the PTA production process through development of a dynamic model by incorporating the vital process parameters, especially the hydrodynamic variables. The operational problems are to be effectively rectified to improve the process efficiency. The PTA production plant is considered as a difficult chemical process from operation viewpoint. The hydropurification process control is critical since the process is operated under high pressures and temperatures. There are two serious concerns with the plant operation. The first one is the efficient control of impurities concentration, especially 4-CBA in the final product, and the second issue is related to the deactivation of an expensive metal catalyst of Pd/C. Improper control of the process, which results in the high concentration of 4-CBA, can considerably affect the downstream process operation. This undesirable phenomenon not only produces off-spec products, but also negatively influences the operation of centrifugation and filtration processes. This adverse impact shows itself in the low efficient separation of TA from the liquid phase. It will then lead to more impurities remaining in the product stream. When the product is off-spec, it needs to be reprocessed. In this scenario, the plant will lose the operation and productivity time. Since the reprocessing stage is expected to alter the powder specifications (especially the particle size), it might lead to operational difficulties in the transfer lines of crystallizers and consequently lower the efficiency of the separation equipment, particularly RVF. Another critical issue in the hydropurification process is the catalyst deactivation, which needs careful considerations in terms of operating and design prospects. A reduction in the catalyst activity results in declining the product quality. It is worth noting that increasing the catalyst lifetime is a key goal in this research study as the continuous hydropurification operation needs to be at the shutdown condition for the replacement of the deactivated catalyst. Therefore, a feasible (practical) parametric sensitivity analysis should consider the dynamic behaviors of the system. This systematic approach is proposed to find the most suitable remedies/strategies for prolonging the catalyst lifetime and maintaining the PTA product quality.

4.4 Mathematical Model Development

We present a first principle model (FPM) for the reaction system of hydropurification of PTA, being conducted in a TBR. The model is constructed by a set of equations, including the mass balance for individual components and energy balance that is combined with a reaction kinetic model and a model for the catalyst deactivation. The input data to the reaction system is taken from the plant data shown in Table 4-1 and Figure 4-4. These results are the mean values for four consecutive data, using 1700 samples. Other auxiliary correlations/data are also employed for the thermodynamics and transport aspects of the system. The initial and boundary conditions are then imposed, and the model is solved numerically using MATLAB® package. Details of the simulation algorithm are not given in this section for brevity. The research conducted by Azarpour et al. [271] also provides a part of modeling methodology.

The FPM should be able to simulate realistic behaviors of the process so that the prevailing mechanisms of flow, mass, and heat transfer for an industrial-scale TBR are well recognized. The hydrodynamic aspect also adds further complications to the simulation work. The dominant flow mechanisms of plug flow or dispersion are central as they notably influence the model complexity. Moreover, the liquid distribution on the catalyst bed, interphase mass/energy transfer, and axial and radial mass/energy dispersion terms are to be analyzed prior to the model development stage. The axial dispersion model accounts for nonuniform liquid distribution, and the parameters of reaction rate (and mechanisms) depend on the reactor fluid dynamics/mechanisms. Reaction system specifications such as the operating conditions, reactor and catalyst characteristics, components concentrations, mass/heat transfer coefficients, and hydrodynamics are employed to conduct a systematic parametric sensitivity analysis. Given the plant data of the hydropurification system, the plug flow mechanism is expected to hold. We also incorporate the dispersion flow model to study the impacts of flow nonideality and back mixing at an industrial scale. Although a more precise system behavior is achieved with the dispersion flow model, it contributes to more computational burden.

4.4.1 Model Assumptions

In order to properly develop a mathematical model, which closely captures the complicated phenomena taking place into a catalytic process, various involvements of the reaction system components with the catalyst deactivation and with the operating parameters fluctuations are to be carefully considered. In the reactor modeling methodology, it is assumed that there is a close mathematical relation between the input and output operating parameters. It is nearly impossible to evolve a model which includes all the essential variables of the process. Though, the complexity might be lessened via considering some reasonable assumptions to establish an appropriate model. The modeling thoroughness and difficulty have to match with the modeling objectives. The reactor model simplification might be required to handle the modeling complexity while maintaining the actual reactor performance. To simplify a catalytic system model and propose acceptable assumptions, there are some parameters that need to be analyzed to justify the assumptions made. The parameters can be reactor dimensions, catalyst particle size, rate of reactions conditions including components concentration and reaction heat, system hydrodynamics, and heat and mass transfer rates. Through the evaluation of such parameters, the model developed can be simplified with the assumptions made. Considering the hydropurification system operating conditions reported in Table 4-1 along with the utilizations of the suitable correlations [146], the following assumptions are made:

- The effect of reactor boundaries (wall) is minimal [276].
- Radial mass [95] and energy [98] dispersions are neglected. This is a logical assumption as the mass and energy transports in the radial direction may be neglected in an industrial scale TBR [20, 277].
- The reactor operates adiabatically.
- Flow is uniform throughout the catalyst bed [89, 91].
- The liquid reactant phase does not vaporize under the TBR operating conditions.
- Temperature is uniformly distributed within the catalyst pore spaces.
- The catalyst particle is fully wetted [67].

4.4.2 Mass and Energy Balance Equations

In the heterogeneous model, the mass balances for individual components are developed for each phase in the TBR. Hence, H_2 mass balances in the gas and liquid phases are written as follows:

$$\frac{\partial(\varepsilon_g C_{H_2,g})}{\partial t} = D_{H_2,g}\frac{\partial^2 C_{H_2,g}}{\partial z^2} - \frac{\partial(u_g C_{H_2,g})}{\partial z} - k_{H_2,gl}\xi_{gl}\left(\frac{C_{H_2,g}}{H_{H_2}} - C_{H_2,l}\right) \tag{4-1}$$

In Equation (4-1), the first term on the left implies the accumulation of hydrogen in the gas phase, the first term on the right signifies the dispersion/molecular effect of mass transfer (flow nonideality), the second term illustrates the convective/bulk aspect of the mass transfer, and the last term reflects the mass transfer of hydrogen from the gas phase to the liquid phase.

$$\frac{\partial(\varepsilon_l C_{H_2,l})}{\partial t} = D_{H_2,l}\frac{\partial^2 C_{H_2,l}}{\partial z^2} - \frac{\partial(u_l C_{H_2,l})}{\partial z} + k_{H_2,gl}\xi_{gl}\left(\frac{C_{H_2,g}}{H_{H_2}} - C_{H_2,l}\right) - k_{H_2,ls}\xi_{ls}(C_{H_2,l} - C_{H_2,s}^{S}) \tag{4-2}$$

In Equation (4-2), the first term on the left shows the accumulation of hydrogen in the liquid phase, the first term on the right signifies the dispersion/molecular impact of mass transfer, the second term demonstrates the convective/bulk aspect of the mass transfer, the third term reflects the mass transfer of hydrogen from the gas phase to the liquid phase, and the last term indicates the mass transfer of hydrogen from liquid phase to the solid phase.

In Equations (4-1) and (4-2), ε_g and ε_l are the gas and liquid hold up, respectively in m^3/m^3; $C_{H_2,g}$, $C_{H_2,l}$ and $C_{H_2,s}$ stand for the concentrations of H_2 in the gas, liquid, and solid phases, respectively in kmol/m^3; t represents the time in s; u_g and u_l denote the gas and liquid phase superficial velocities, respectively in m/s; $D_{H_2,g}$ and $D_{H_2,l}$ symbolize the axial dispersion coefficient of H_2 in the gas and liquid phases, respectively in m^2/s; z is the axial length in m; $k_{H_2,gl}$ represents the mass transfer coefficient of H_2 between gas and liquid phases in m/s; ξ_{gl} and

ξ_{ls} introduce the gas-liquid and liquid-solid specific interfacial surface areas, respectively in m^2/m^3; and H_{H_2} is the dimensionless Henry's constant at the reactor temperature.

Mass balance equations for the other components in the liquid phase (i = 4-CBA, 4-HMBA, pta, and BA) are given below:

$$\frac{\partial(\varepsilon_l C_{i,l})}{\partial t} = D_{i,l}\frac{\partial^2 C_{i,l}}{\partial z^2} - \frac{\partial(u_l C_{i,l})}{\partial z} - k_{i,ls}\xi_{ls}(C_{i,l} - C_{i,s}^S) \tag{4-3}$$

In Equation (4-3), the first term on the left specifies the accumulation of the respective component in the liquid phase, the first term on the right implies the dispersion/molecular effect of mass transfer, the second term illustrates the convective/bulk influence of the mass transfer, and the last term denotes the mass transfer of the respective component from the liquid phase to the solid phase.

Mass balance for component i in the solid phase (i = H_2, 4-CBA, 4-HMBA (4-hydroxymethylbenzoic acid), pta, and BA (benzoic acid) is expressed by the following relationship:

$$\varepsilon_P(1-\varepsilon_B)\frac{\partial C_{i,s}^S}{\partial t} = k_{i,ls}\xi_{ls}\left(C_{i,l} - C_{i,s}^S\right) \pm \sum_{k=1}^{3} r_k\,\eta_k\rho_B a(t) \tag{4-4}$$

In Equation (4-4), the first term on the left reflects the accumulation of the respective component in the solid phase, the first term on the right implies the mass transfer from liquid phase to the solid phase, the second term illustrates the production (+) and consumption (-) of the respective component in the solid phase considering whole reactions and the catalyst/solid phase deactivation phenomenon.

In Equation (4-4), ε_P and ε_B stand for the catalyst particle and reactor bed porosities in m^3/m^3, respectively; $C_{i,l}$ and $C_{i,s}$ are the concentrations of component *i* in the liquid and solid phases, respectively in $kmol/m^3$; $D_{i,l}$ denotes the axial dispersion coefficient of component *i* in the liquid phase in m^2/s; r_k is the rate of k^{th} reaction in $kmol/(kg_s.s)$; η_k stands for the effectiveness factor of k^{th} reaction; ρ_B is the bulk density in kg/m^3; and a represents the catalyst sintering dispersion parameter (activity) at time *t*.

In the heterogeneous model, the energy balance is written for each phase in the TBR. Energy balance in the gas phase is given below:

$$\rho_g C_{p,g} \frac{\partial(\varepsilon_g T_g)}{\partial t} = \lambda_g \frac{\partial^2 T_g}{\partial z^2} - \rho_g C_{p,g} \frac{\partial(u_g T_g)}{\partial z} - h_{gl}\xi_{gl}(T_g - T_l) \tag{4-5}$$

In Equation (4-5), the first term on the left specifies the accumulation of the energy in the gas phase, the first term on the right denotes the conductive/diffusive impact of heat transfer, the second term illustrates the convective/bulk fluid flow influence of the heat transfer, and the last term denotes the heat transfer from the gas phase to the liquid phase (interfacial heat transfer).

Energy balance in the liquid phase is written as follows:

$$\rho_l C_{p,l} \frac{\partial(\varepsilon_l T_l)}{\partial t} = \lambda_l \frac{\partial^2 T_l}{\partial z^2} - \rho_l C_{p,l} \frac{\partial(u_l T_l)}{\partial z} + h_{gl}\xi_{gl}\left(T_g - T_l\right) - h_{ls}\xi_{ls}(T_l - T_s) \tag{4-6}$$

In Equation (4-6), the first term on the left implies the accumulation of the energy in the liquid phase, the first term on the right depicts the conductive/diffusive impact of heat transfer, the second term illustrates the convective/bulk fluid flow effect of the heat transfer, the third term denotes the interfacial heat transfer from the gas phase to the liquid phase, and the last term reflects the interfacial heat transfer from the liquid phase to the solid/catalyst phase.

The following expression represents the energy balance in the solid phase:

$$(1-\varepsilon_B)\rho_s C_{p,s}\,\frac{\partial T_s}{\partial t} = h_{ls}\xi_{ls}(T_l - T_s) + \sum_{k=1}^{3} r_k\,\eta_k \rho_B a(t)\,(-\Delta H_k) \qquad (4\text{-}7)$$

In Equation (4-7), the first term on the left indicates the accumulation of the energy in the solid/catalyst phase, the first term on the right signifies the interfacial heat transfer from the liquid phase to the solid phase, and the last term demonstrates the generation or consumption of energy due to the chemical reactions taken place in the solid/catalyst phase taking into account the deactivation phenomenon.

In Equations (4-5) – (4-7), ρ_g , ρ_l, and ρ_s are the density of gas, liquid, and solid phases, respectively in kg/m^3; $C_{p,g}$, $C_{p,l}$, and $C_{p,s}$ denote the specific heat capacity of gas, liquid and solid phases at constant pressure, respectively in J/(kg.K); T_g, T_l, and T_s represent the temperature of gas, liquid, and solid phases, respectively in K; λ_g and λ_l denote the conductivity of gas and liquid phases, respectively in W/(m.K); ΔH_k stands for the heat of k^{th} reaction in J/kmol; and h_{gl} and h_{ls} introduce the heat transfer coefficients between gas-liquid and liquid-solid phases, respectively in W/(m^2.K).

4.4.3 Chemical Reaction Kinetics

The chemical reaction kinetics can be shown with a system of three main reactions, as summarized in Table 4-2. In the first reaction (r_1), $C_8H_6O_6$ (4-carboxybenzaldehyde or 4-CBA) reacts with H_2

to produce the intermediate component $C_8H_8O_3$ (4-hydroxymethylbenzoic acid or 4-HMBA), using Pd/C catalysts. This reaction is exothermic for which the reaction kinetic model [273] is shown. Initially, the concentration of 4-HMBA reaches a maximum amount, but it is not stable. It reacts with H_2 on Pd/C catalysts (through r_2) to produce $C_8H_8O_2$ (*p*-toluic acid or pta) and H_2O. In addition to the main reaction (r_1), the decarbonylation reaction (r_3) may occur (in parallel with the first reaction) to produce $C_7H_6O_2$ (benzoic acid or BA) and carbon monoxide (CO), which the latter is a poison to the Pd/C catalyst. The decarbonylation reaction is significantly affected by the oxygen concentration in the reaction mixture. The dissolved oxygen increases the decarbonylation reaction rate [269]. The 4-CBA hydropurification reactions and the corresponding rates are given in Table 4-2 [273]:

Table 4-2: A summary of reaction system for the hydropurification plant to produce PTA in a TBR.

Stoichiometry	Kinetics	Heat of reaction
$\underset{(4\text{-CBA})}{C_8H_6O_3} + H_2 \xrightarrow[r_1]{Pd/C} \underset{(4\text{-HMBA})}{C_8H_8O_3}$	$r_1 = 0.047\exp\left(\frac{-16.97}{RT}\right)\left(C_{C_8H_6O_3}\right)^{0.96}\left(C_{H_2}\right)^{0.24}$	$\Delta H_{r_1} = -83.82\ (\mathrm{kJ/mol})$
$\underset{(4\text{-HMBA})}{C_8H_8O_3} + H_2 \xrightarrow[r_2]{Pd/C} \underset{(pta)}{C_8H_8O_2} + H_2O$	$r_2 = 0.153\exp\left(\frac{-23.44}{RT}\right)\left(C_{C_8H_8O_3}\right)^{0.61}\left(C_{H_2}\right)^{0.75}$	$\Delta H_{r_2} = -121.88\ (\mathrm{kJ/mol})$
$\underset{(4\text{-CBA})}{C_8H_6O_3} \xrightarrow[r_3]{Pd/C} \underset{(BA)}{C_7H_6O_2} + CO$	$r_3 = 3406.6\exp\left(\frac{-88.87}{RT}\right)\left(C_{C_8H_6O_3}\right)^{0.54}$	$\Delta H_{r_3} = +18.73\ (\mathrm{kJ/mol})$

in which, r_1, r_2, and r_3 are the rate of first, second, and third reactions in kmol/(kg$_s$.s); R is the universal gas constant in J/(mol.K); C_{C8H6O3}, C_{H8HO3}, and C_{H2} represent the concentrations of 4-CBA, 4-HMBA and H_2, respectively in kmol/m^3; and ΔH_1, ΔH_2, and ΔH_3 denote the heat of reaction for the first, second, and third reactions, respectively in kJ/mol.

Pd/C catalyst deactivation model: The industrial Pd/C catalysts deactivate during the hydropurification process because of thermal sintering. It is found that the available surface area of Pd considerably is declined with increasing temperature as a result of sintering phenomenon. The smaller catalyst particles are more prone to the sintering as the temperature distribution will increase in the bulk of catalyst faster. Through catalyst deactivation, smaller Pd particles agglomerate and cause a gradual increase in the catalyst size (and consequently, a decrease in available surface area) [1, 2]. The rate of Pd/C catalyst deactivation in the hydropurification process was obtained by fitting the following equations to the plant data in the range of catalyst lifetime as suggested by Azarpour et al. [271]:

$$-r_d = -\frac{da}{dt} = A\, exp\left(\frac{-E}{R}\left(\frac{1}{T} - \frac{1}{T_R}\right)\right) a^m \tag{4-8}$$

where r_d is the deactivation rate (h^{-1}); A introduces a parameter, which is equal to 0.00092 h^{-1}; E stands for the activation energy parameter which is estimated to be equal to 5,729 $J.mol^{-1}$; R is the universal gas constant which equals 8.314 $J.(mol^{-1}.K^{-1})$; a denotes the metallic sintering dispersion parameter (or catalyst activity), exponent m equals to 2.1; and T_R is the reference temperature which is equal to 558 K.

4.4.4 Initial and Boundary Conditions

The set of partial differential equations (PDEs) developed in Equations (4-1) to (4-7) requires two boundary conditions at the reactor inlet (BC-1 in Equation (4-9)) and the reactor outlet (BC-2 in Equation (4-10)) and an initial condition (IC, in Eq. (4-11)). In these equations, the subscript i resembles the components (e.g., i=H2, 4-CBA, 4-HMBA, pta, and BA). The superscript ss in the IC (Equation (4-11)) is used for the steady-state condition.

BC-1: $$\begin{cases} C_{i,\alpha}(z=0,t) = C_{i,\alpha,in}(t) \\ T_\alpha(z=0,t) = T_{in}(t) \end{cases} \qquad \alpha = g, \text{ and } l \qquad (4\text{-}9)$$

BC-2: $$\begin{cases} \dfrac{\partial C_{i,\alpha}(z=L,t)}{\partial z} = 0 \\ \dfrac{\partial T_\alpha(z=L,t)}{\partial z} = 0 \end{cases} \qquad \alpha = g, \text{ and } l \qquad (4\text{-}10)$$

IC: $$\begin{cases} C_{i,\alpha}(z,t=0) = C_{i,\alpha}^{ss}(z) \\ T_\alpha(z,t=0) = T_\alpha^{ss}(z) \\ a(t=0) = a^{ss} = 1 \end{cases} \qquad \alpha = g, l \text{ and } s \qquad (4\text{-}11)$$

4.4.5 Physical Properties and Model Parameters Calculations

The model parameters are a function of physical properties of the phases and the components involved into the system. Therefore, the physical properties (e.g., density, viscosity, surface tension, and diffusivity) need to be calculated prior to the model parameters calculation. The methods and correlations are generally able to calculate the physical properties under low temperatures and pressures. Thus, the applied methods and correlations should have been derived under very high temperatures and pressures, since the proposed process system is operated under high temperatures and pressures. The same scenario is followed for the calculation of the model parameters such as mass and heat transfer coefficients, gas and liquid hold up, interfacial area, and heat capacity through employing the correlations resulted under high temperatures and pressures. The correlations utilized in the current research work can be found in Azarpour et al. [271] and Azarpour and Zendehboudi [313].

4.4.6 Discretization and Numerical Modeling

The set of PDEs given in Equations (4-1) to (4-7) integrated with the set of non-linear equations for the kinetics of hydropurification reaction system (as tabulated in Table 4-2) define the mathematical structure of the model. Backward finite difference approximation is used to discretize the model along the spatial co-ordination (z). Initially, the set of equations are solved at steady-state condition to determine the initial conditions for the dynamic model. Then, the set of equations are solved at each grid point along the length of reactor (z-coordinate) to obtain the spatial variations of the variables at steady-state condition. For the dynamic model solution, the PDEs are converted to a set of ordinary differential equations (ODEs) using method of lines (MOL) and backward finite difference approximation. In the dynamic solution, the set of ODEs are simultaneously solved numerically [313].

4.5 Results and Discussion

Hydropurification catalytic processes are extensively used in the petrochemical industry to produce products with a high quality by removing impurities such as sulfur, oxygen, nitrogen, and saturated aromatic rings and olefins through reaction with hydrogen. The hydropurification reaction system is commonly conducted in TBRs that are required to be controlled for achieving a desired product quality. Fluctuations in the operating parameters may negatively affect the product quality. This research work is planned to forecast the dynamic behaviors of the TBR in the hydropurification in terms of operating conditions. To attain the goal, a three-phase dynamic model is developed by incorporating the hydrodynamic parameters and catalyst deactivation model to simulate the performance of reaction system with a dynamic catalyst deactivation.

After the mathematical model is developed (and the modeling simulation runs are conducted), the performance of the proposed model is validated against the plant data. The model is then used to study the effect of different factors. We analyze the wetting efficiency of the reactor bed in a broad range of operating conditions, including the plant normal operation. The hold up for the gas and liquid phases is investigated at various superficial velocity values. The pressure drop of the bed for normal operating condition is studied using available models. The catalyst lifetime (as a key objective) in this study is scrutinized through parametric sensitivity analysis where the influences of the bed porosity, liquid-solid mass transfer coefficient, and hourly liquid space velocity on the objective functions are discussed.

4.5.1 Model Validation Results

Before using the model in any investigations, its validity should be confirmed by comparing the modeling results and real data. In this section, the appropriateness of the mathematical model for a hydropurification plant is assessed. As the concentration of 4-CBA is a major constraint in the product quality control, a comparison between the model outputs and plant data is made based on the results for this impurity as illustrated in Figure 4-5. The concentration of 4-CBA from plant data and mathematical model over a period of up to 365 d is shown in Figure 5. The results show a good agreement between the model and plant data in the period of operation. The average percent relative error is around 2.2%. This model is more accurate than plug flow model (PFM) whose error is about 2.6% [313]. Given the variability in the plant data, the model performance in estimating the concentration of the main impurity is excellent.

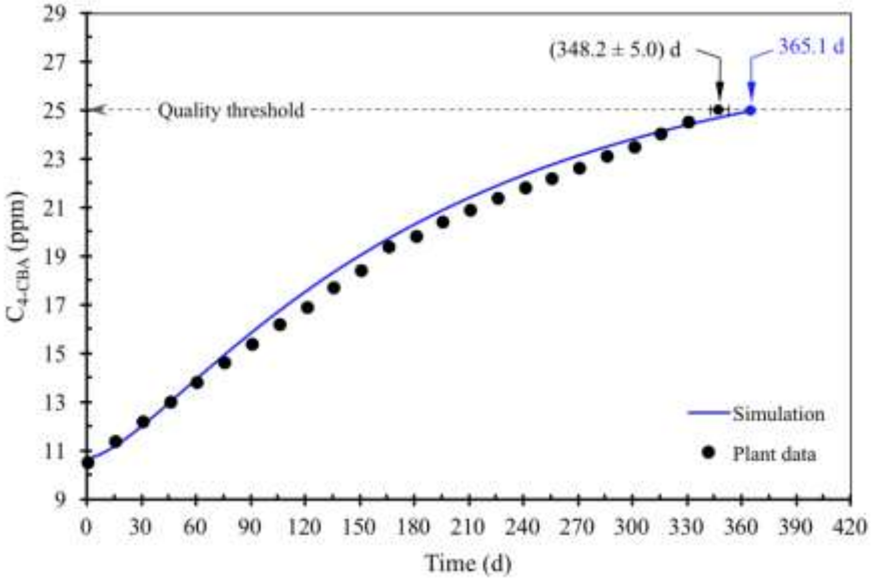

Figure 4-5: Comparison of the simulation results and plant data in terms of the concentration of 4-CBA in the product.

Based on the values of 4-CBA concentration at reactor outlet (recorded every 4 h), the catalyst lifetime to reach a concentration threshold of 25 ppm is obtained to be (348.2 ± 5.0) d. The catalyst lifetime is estimated to be 365.1 d according to the simulation results. This is about 4.8% error in estimating the catalyst lifetime from the mathematical model. Due to the fluctuations in the concentration of 4-CBA in the plant data, a liner regression was applied to the proximity of $C_{4\text{-}CBA}$=25 ppm to obtain the catalyst lifetime.

Although the plant was allowed to operate for a period of 420 d, Figure 4-5 is truncated at 365 d which is imposed by the quality control constraint. When the concentration of 4-CBA reaches the threshold value of 25 ppm, the catalysts have reached their practical lifetime. It implies that the operation beyond this particular concentration results in product that does not meet the required specifications. When the catalyst is fresh, the concentration of impurity in the product is low. For example, in the first day of operation, the concentration of 4-CBA is about 10.5 ppm. This value increases to 15.4 ppm, 19.8 ppm, 22.6 ppm and 25.0 after 3, 6, 9 and 12 months of operation, respectively. After 420 d, the concentration of 4-CBA increases beyond the threshold value and reaches 27.5 ppm. As depicted in Figure 4-5, the model tends to slightly overestimate the concentration of 4-CBA after 60 d up to about 315 d, and it starts to slightly underestimate it after 365 d. It will continuously underestimate the 4-CBA concentration in the range of 365 d to 420 d (this part is not shown because the concentration of 4-CBA exceeds the threshold concentration of 25 ppm). The reason for such a variation in the model performance is that the catalyst deactivation model (e.g., A, E, m and T_R in Eq. (4-8)) may well describe the catalyst behavior as long as 4-CBA concentration is lower than 25 ppm (threshold concentration).

Figure 4-6 illustrates the concentrations of the reaction mixtures components leaving the hydropurification TBR. Hydrogen is injected to the system in an excess amount. The concentration of the hydrogen leaving the system does not fluctuate considerably since the amount of 4-CBA leaving the reactor is not in an extensive range. The same trends are observed for the other components of the reaction system including 4-HMBA, pta, and BA.

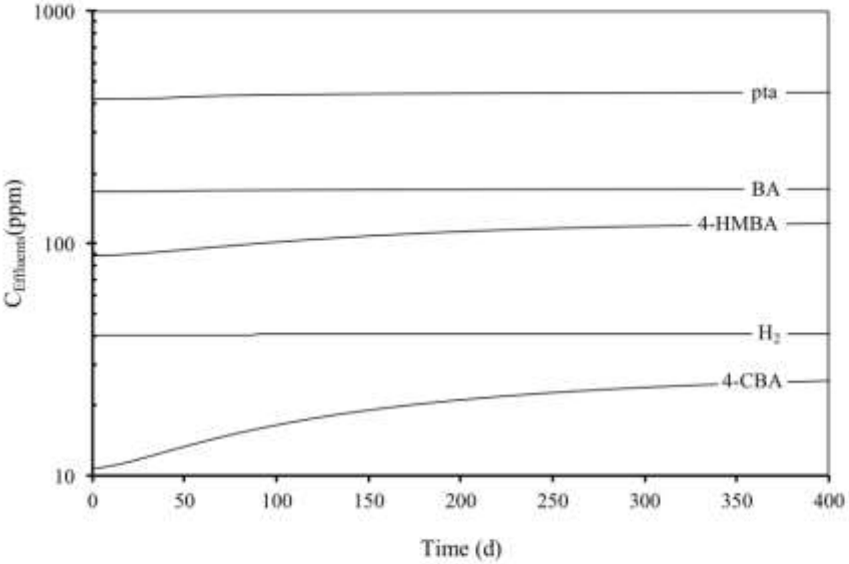

Figure 4-6: Outlet concentrations of the reaction mixture components versus time.

4.5.2 Pressure Drop Analysis

An increase in the gas and liquid superficial velocities, liquid viscosity, gas density, and the reduction in particle diameters increase the pressure drop in the reactor [314]. According to Ergun [278], the gas velocity has a higher impact on the pressure drop than the gas density (or reactor pressure). Figure 4-7 summarizes the pressure drop in the catalyst bed from four different models, with application to the TBR. The results show that that pressure of the reactor almost linearly drops along the catalyst bed of the reactor. Normal operating conditions of the hydropurification plant are used to estimate the pressure drop in the TBR. Figure 4-7 reveals that the pressure drop estimated from Turpin and Huntington [315] gives the highest pressure drop (32 kPa) compared to other three models. It is also found that the results obtained by Ergun [278], Midoux [282], and Larkin [316] are in a better agreement with each other. The pressure drop considered in this study is about 5.7 kPa based on the model proposed by Ergun [278].

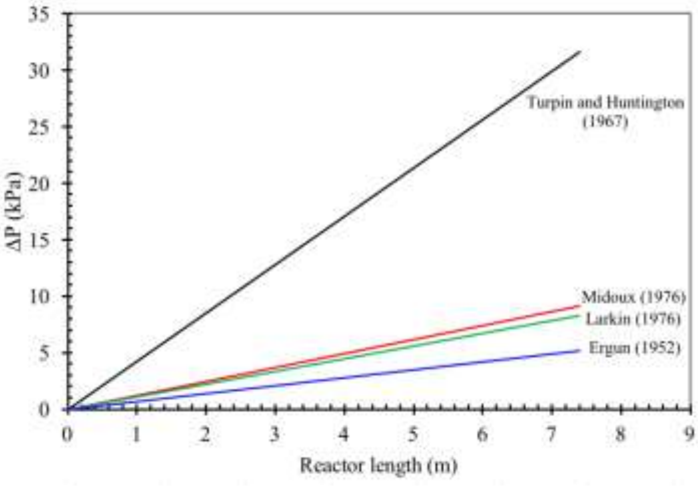

Figure 4-7: Pressure drop in the catalyst bed from different models utilizing the actual operating conditions of the hydropurification process.

4.5.3 Gas and Liquid Hold Up

The TBR performance is considerably affected by the hydrodynamics parameters such that the liquid hold up is one of the most significant parameters, which influences the TBR performance, design, and scale up [44]. The hold up of liquid phase increases with an increase in the liquid velocity and the diameter of catalyst particles, while it is reduced with an increase in the superficial velocity of the gas and the gas-liquid interfacial tension [314]. Moreover, the liquid hold up decreases with an increase in the gas density, exception for very low gas velocities, where it becomes independent of the gas density [314]. Furthermore, non-coalescing liquids have much smaller hold ups than coalescing liquids. The gas viscosity has the minimal impact on the liquid hold up and pressure drop [314]. Adding fine particles increases the liquid hold up at the cost of increased pressure drop [314]. The liquid hold up has a crucial impact on the liquid residence time distribution that affects mass and heat transfer and also the pressure drop in the TBR [44]. It is also important in safe operation to avoid hotspot creations and possible reactor runaways [76, 317-321]. On the other hand, the catalyst wetting efficiency is dependent on the liquid hold up [12, 44, 62, 67].

The variations of liquid and gas hold ups in the hydropurification TBR as a function of liquid superficial velocity are described in Figure 4-8. It is concluded from Figure 4-8 that the liquid hold up increases with increasing the liquid superficial velocity, while the gas hold up decreases. At the minimum value of 0.21 cm/s for the liquid superficial velocity, the magnitudes of hold up for the liquid and gas phases are 0.30 and 0.14, respectively. At the maximum value of 1.37 cm/s, the hold up of liquid increases to 0.39, while the hold up of gas lowers to 0.05. Under the normal operating conditions, the liquid superficial velocity is 1.05 cm/s with the liquid and gas hold ups of 0.38, and 0.06, respectively.

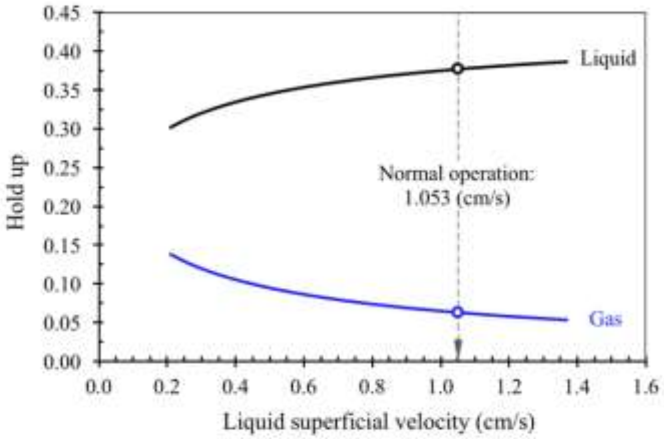

Figure 4-8: Liquid and gas phase hold up profiles in the hydropurification TBR in terms of liquid superficial velocity.

4.5.4 Wetting Efficiency

The wetting efficiency is an important parameter that can change not only the production rate of the reaction products, but also the selectivity of reaction system when multiple reactions are involved [70]. The selectivity can be influenced whether the reaction occurs only on the wetted portion of the catalyst particle area or on both portions of dry and wetted catalyst particle [12]. Therefore, an increase in the liquid superficial velocity (reactor liquid feed) can affect the reaction yield and product impurities concentrations. Therefore, there is an optimum value for the reactor feed flowrate (production rate) with constraints such as pressure drop, and production rate, and quality of the product (PTA powder).

The impact of liquid superficial velocity on the wetting efficiency of TBR filled with Pd/C catalysts is depicted in Figure 4-9. The wetting efficiency increases with an increase in the liquid superficial velocity (or liquid flowrate) in the reactor which is due to an increase in the pressure drop and liquid hold up [62, 67, 70]. At high pressures and high gas flowrates, both wetting efficiency and pressure drop increase, while the liquid hold up dramatically decreases for a constant liquid mass velocity [67]. This finding is in contradiction with the studies carried out by Baussaron et al. [66] and Dietz et al. [70]. These studies reveal that the wetting efficiency is improved when the particle size decreases [62, 322-324]; however, there are some conflicting results mentioning that the wetting efficiency increases with the enhancement of the particle size [143, 325]. In addition, an increase in the bed porosity decreases the wetting efficiency as the porosity increase lowers the number of particle-to-particle contact points. Hence, less liquid curve/surface are available to propel the liquid rivulets/streams [62, 66]. The particle shape does not have a significant impact on the wetting efficiency [62, 66]. The addition of fines (nonporous particles) boosts the wetting efficiency of the catalyst bed [326]. The presence of fines (such as silicon carbide) can decrease the porosity and increase the number of contact points between the solid particles [62]. The increase in the number of the particle's contact points is a key parameter to describe the local heterogeneities of wetting efficiency in TBRs [327].

The results for wetting efficiency with the liquid superficial velocity is shown in Figure 4-9 [67]. At the normal operating conditions of the hydropurification plant, the superficial velocity is about 1.053 cm/s where the wetting efficiency is close to 96.6%.

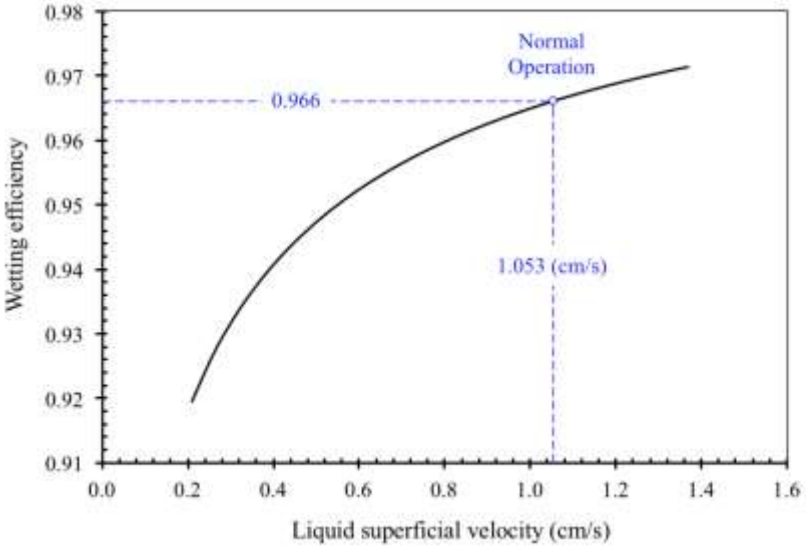

Figure 4-9: Wetting efficiency of Pd/C catalyst particle versus reactor liquid feed superficial velocity.

As the limiting reactant in the hydropurification process is carried in the liquid phase, it is important to increase the contact/wetting efficiency of the Pd/C catalyst particles. Even minor improvements in the wetting efficiency can considerably increase the reaction conversion, resulting in a lower concentration of the impurities in the product (e.g., greater product quality).

Therefore, a decrease in the bed porosity improves the reaction conversion and also enhances the wetting efficiency of the catalyst particles, leading to the more efficient control of the hydropurification process in terms of quality and catalyst lifetime. The reduction of catalyst particle size can therefore improve the performance of hydropurification process due to more effective mass transfer and improved contact efficiency. In summary, reducing the bed porosity and using smaller catalysts can significantly contribute to the efficiency of hydropurification process in term of product quality, production rate, and catalyst lifetime [313].

4.5.5 Parametric Sensitivity Analysis

In this section, the effects of reactor bed porosity (ε_B), liquid-solid mass transfer coefficient (k_{ls}), gas-liquid mass transfer coefficient (k_{gl}), and liquid hourly space velocity (*LHSV*) on the performance of hydropurification TBR are investigated. The influences of the above variables/parameters on the various objective functions such as product quality and catalyst lifetime are studied by perturbing the parameter within ± 15 % of that from normal operation.

Effect of reactor bed porosity (ε_B): The reactor bed is found to significantly influence the contact/wetting efficiency, hold up, pressure drop, and heat/mass transfer. Figure 4-10 demonstrates the impact of bed porosity perturbations on the concentration of 4-CBA (as a vital parameter) that governs the catalyst lifetime. As shown in Table 4-1, the design value for the bed porosity is 0.44 under normal operations. In the sensitivity analysis, this parameter will be perturbed in the range ± 5.0 % around the design value. The results reveal that a 5 % -increase (relative to design value) in the bed porosity leads to a reduction in the catalyst lifetime, while a 5 % - decrease (-5 % perturbation) in the porosity causes an increase in the catalyst lifetime.

Moreover, at a similar operating time (day), the product quality increases as the bed porosity decreases, and the effect of bed porosity becomes more pronounced over time as the catalyst is being deactivated. Under normal operating conditions, the catalyst lifetime is 365.1 d. Perturbing the bed porosity by +5 %, the catalyst lifetime decreases to 346.9 d, which corresponds to a 5.0 %- decrease in the catalyst lifetime. Varying the bed porosity by -5 %, the catalyst lifetime increased to 385.5 d, which corresponds to a 5.6 %- increase in the catalyst lifetime.

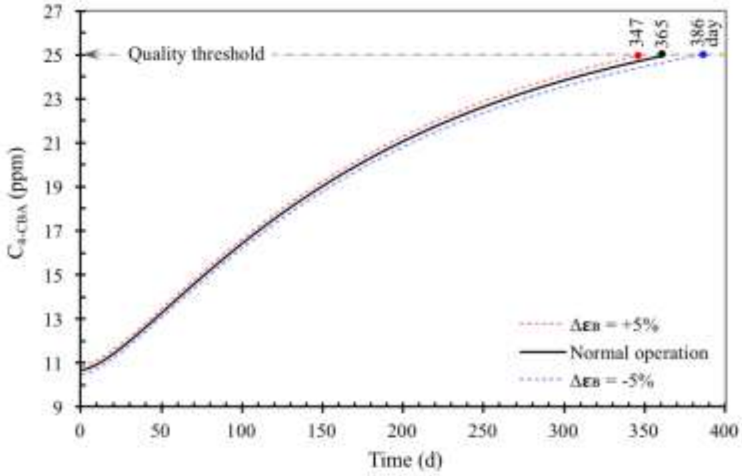

Figure 4-10: Effect of porosity of reactor bed on the product quality and Pd/C catalyst lifetime. The bed porosity is 0.44 at normal (design) operating conditions. The solid line shows the normal operation; red and blue dash lines show +5 % and -5 % perturbations, respectively.

The behavior observed in Figure 4-10 can be explained by the effect of porosity on the catalyst loading and wetting efficiency, and contact between the liquid and gaseous reactants on the surface of catalysts (which also affects the reaction rate). A reduction in the bed porosity increases the catalyst wetting efficiency, gas-liquid contact, catalyst loading capacity (weight of catalyst particles) for the same reactor dimensions, and reaction rate [62, 66]. These all contribute to a higher product quality (or, a lower concentration of 4-CBA in the product stream). Similarly, an increase in the bed porosity decreases these factors that negatively influence the catalyst lifetime in a TBR. When the porosity decreases, the catalysts can be packed into the column more efficiently, which may considerably contribute to the product quality and production rate. In other words, the available space in the reactor can accommodate more catalyst particles for each batch. This results in the longer catalyst utilization, which allows the plant to operate longer before a total shutdown becomes inevitable for the plant. This also reduces the final production cost. However, a decrease in the catalyst bed is expected to significantly increase the pressure drop in the bed, which increases the energy demand for pumping fluids. Hence, it causes higher capital costs due to the increase in the reactor pressure.

Effect of gas-liquid mass transfer coefficient (k_{gl}): In TBRs, the gas-liquid mass transfer resistance can significantly affect the reactor performance. Hence, its accurate prediction is important for accomplishing successful reactor design and scale up. The surveys reveal that gas-liquid mass transfer coefficient is influenced by pressure in TBRs, and it enhances with increasing pressures. The pressure effect is due to an increase in gas density and, therefore, can be implemented by the increase in molecular weight of the gas [12]. The reason is that when pressure or gas density escalates, gas shear over the trickling liquid film becomes more pivotal for a given superficial gas velocity. Therefore, the momentum transfer through the gas-liquid interface might be considerable enough to make gas to be entrained into the liquid [73]. To explain the phenomenon more closely, it takes place by suggesting a two-zone flow pattern: liquid-free gas continuous phase (microscopic interface) and a gas-liquid film emulsion flowing down the packing (macroscopic interface). The microscopic interface consists of tiny bubbles which are generated in the films because of the strengthening of gas-liquid interfacial stress with pressure. However, the macroscopic interface is the boundary between the liquid-free continuous gas bulk and the trickling film [74].

Figure 4-11 illustrates the effect of gas-liquid mass transfer coefficient on the hydropurification reactor performance. The simulation results suggest that the effect of k_{gl} on the reactor performance in terms of final product quality and catalyst deactivation is insignificant. The reason for such a negligible impact is the hydrogen in introduced into the catalytic hydropurification TBR is excess amount. This is done to ensure that the main impurity as 4-CBA is efficiently contacted with the hydrogen for the purpose of its conversion to pta. Moreover, to increase the reactor pressure by increasing the hydrogen introduction into the system is not a practical solution. This strategy not only makes the reactor pressure control very difficult but also fractures the fragile structure of Pd/C catalyst which leads to the increase of the powder turbidity as one of the critical criteria of the powder quality specifications.

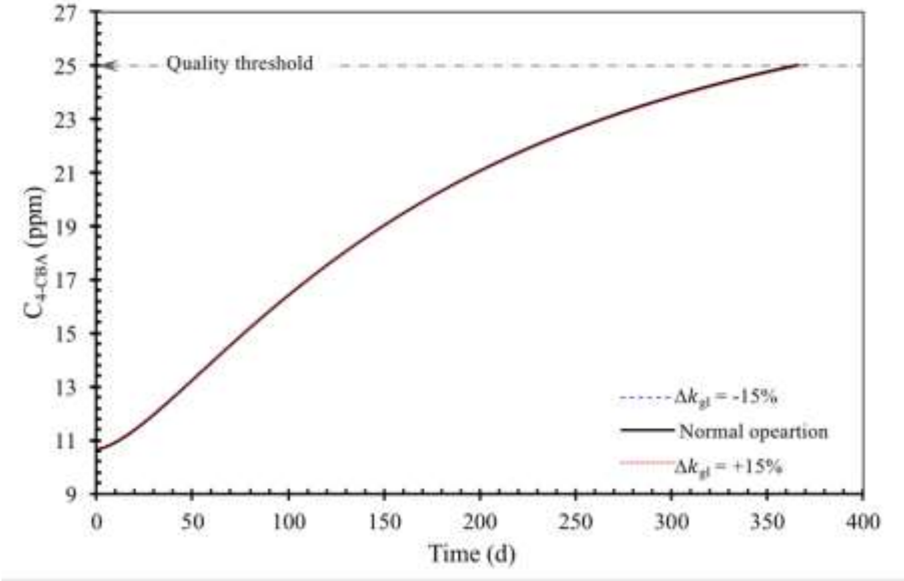

Figure 4-11. Effect of gas-liquid mass transfer effect (k_{gl}) on the product quality and Pd/C catalyst lifetime. The solid line shows normal operation; the red and blue dash lines show +15 % and -15 % perturbations.

Effect of liquid-solid mass transfer coefficient (k_{ls}): The liquid-solid mass transfer coefficient is one of the main hydrodynamic parameters in the design and scale up of TBRs [71]. The rate of reactants mass transfer from liquid to catalyst particle surface is a crucial step in the overall mechanism of hydropurification process that affects the performance of TBRs. Pressure drop and liquid hold up are influenced by the gas and liquid velocities which have a strong impact on the wetting efficiency and mass transfer coefficient [328]. The reactor pressure and gas phase velocity positively affect the catalyst wetting efficiency. At a constant liquid mass velocity, the thickness of liquid film decreases with the pressure and gas phase velocity, leading to liquid films spreading more efficiently over the external packing area [12]. The liquid-solid mass transfer predominantly relies on the catalyst wetted area and the degree of turbulence in the liquid phase. One of the conditions that adversely influences the liquid-solid mass transfer is the stagnant liquid film covering the catalyst particles, while the surfaces (which cause turbulence in the liquid phase) promote the interactions between the liquid and solid phases. There are several investigations on the mass transfer measurements between liquid and solid particles in TBRs. Experimental methods such as using packings (featuring some limited solubility in water) [80] and electrochemical technique [329] are employed for such measurements. The mass transfer rate is found to be increased with increasing the liquid flowrate. In the case of LIR, the controversial results are obtained while studying the effect of gas flowrate on the liquid-solid mass transfer coefficient. For instance, Hirose et al. [330] claimed that the gas flowrate has no effect, whereas Satterfield et al. [80] concluded that an increase of around 10 % under the trickling flow regime is observed.

Figure 4-12 depicts the effect of liquid-solid mass transfer perturbations on the product quality (concentration of 4-CBA). It is found that the quality of product and the catalyst lifetime improve with increasing the liquid-solid mass transfer coefficient. The lifetime of Pd/C catalysts under normal operating conditions is about 365.1 d, which increases to 375.7 d (2.9 % increase) upon +15 % perturbation in the liquid-solid mass transfer coefficient, and decreases to 351.8 d (3.7 % decrease) upon -15 % perturbation in the liquid-solid mass transfer coefficient. Although the extent of increase in the catalyst lifetime upon a +15% perturbation in the liquid-solid mass transfer coefficient is small; however, this catalyst lifetime increase has still a great impact on the economy of process.

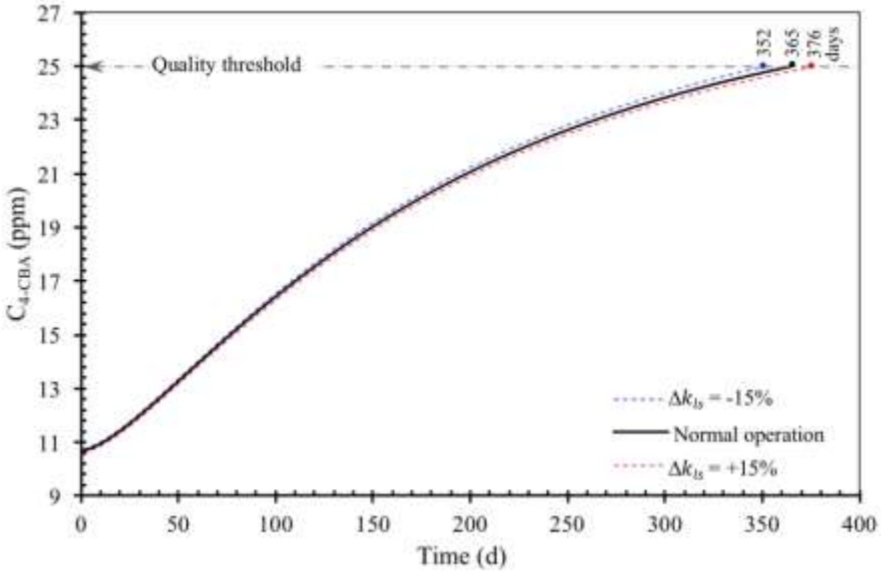

Figure 4-12: Effect of liquid-solid mass transfer effect (k_{ls}) on the product quality and Pd/C catalyst lifetime. The solid line shows normal operation; the red and blue dash lines show +15 % and -15 % perturbations.

Therefore, operating conditions that promote mass transfer coefficients should be evaluated for product quality improvement. In the TBR, pressure noticeably influences the liquid-solid mass transfer at high gas and liquid flowrates. At a constant pressure, the liquid-solid mass transfer coefficient increases with an increase in the superficial gas velocity and superficial liquid mass velocity [71]. Moreover, the liquid-solid mass transfer coefficient improves for all pressures and superficial gas velocities when the superficial liquid velocity enhances [71]. The effect of gas velocity on the liquid-solid mass transfer coefficient is more pronounced at higher operating pressures [12]. This is because of the gas phase drag effect on the liquid film, flowing over the packing external surfaces [71].

Effect of liquid hourly space velocity (LHSV): The effect of LHSV variation on the quality of product is illustrated in Figure 4-13. In this study, ± 5 % and ± 10 % perturbations around the normal operating condition are considered. At normal operating conditions, the LHSV=5.14 h^{-1} for which catalyst lifetime is 365.1 d. According to Figure 12, an increase in the LHSV consistently decreases the product quality and catalyst lifetime. With +5 % and +10 % perturbation in the LHSV, the catalyst life time is decreased to 350.1 d and 341.2 d, respectively which lead to a 4.1 % and a 6.5 % reduction in the catalyst lifetime, respectively. The catalyst life time is increased to 388.7 d and 416.9 d upon -5 % and -10 % variation in the LHSV, respectively, resulting in a 6.5 % and a 14.2 % increase in the catalyst lifetime, respectively. The improvement in the hydrotreating process with a decrease in LHSV is also reported by others [331-334]. When the LHSV decreases, the reaction mixture components stay in the catalyst bed for a longer time. This provides a chance for a higher conversion of the main impurity (e.g., 4-CBA) to produce pta and BA. Therefore, the product quality improves and the catalyst can be more efficiently utilized for a longer period.

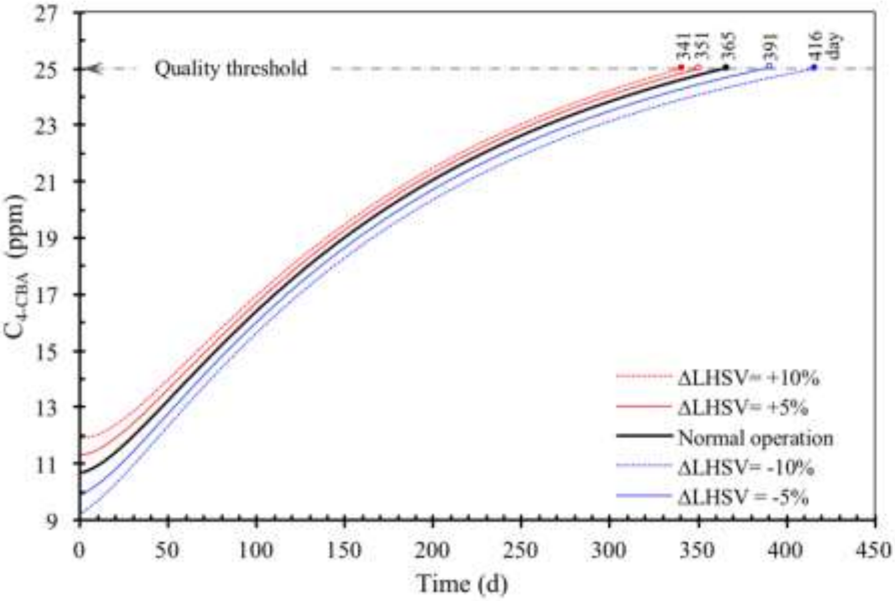

Figure 4-13: Effect of LHSV on the product quality and Pd/C catalyst lifetime. The value of LHSV at normal operation is 5.14 h^{-1}. The solid line shows the normal operation; the red (dash) lines show the positive perturbations; and the blue (dash) lines show the negative perturbations.

4.5.6 Catalyst Lifetime Analysis

The main goal for the model development is to study the catalyst lifetime, which is defined as the time at which the concentration of the main impurity (4-CBA) in the product stream reaches a value of 25 ppm. Initially, the concentration of this impurity is low; however, it increases as the catalysts become deactivated. The product quality control involves a constraint of concentration of 4-CBA<25 ppm. Table 4-3 summarizes the effects of perturbations in the hydrodynamic parameters such as bed porosity, liquid-solid mass transfer coefficient, and liquid hourly space velocity in the range up to ± 15 %. The impact of parameter perturbation on different attributes of the catalysts such as catalyst lifetime (in d) and % enhancement in the catalyst lifetime are given in Table 4-3. The catalyst lifetime under normal operating conditions of the plant is about 365.1 d. A maximum catalyst lifetime of 416.9 d is obtained at -10 % perturbation in the LHSV, which is equivalent to 14.2 % enhancement in the catalyst lifetime, compared to that for the normal operation. The catalyst lifetime declines to 341.3 d at +10 % perturbation in the LHSV, which is equivalent to a 6.5 % reduction in the catalyst lifetime.

Table 4-3: Summary of Catalyst Lifetime and Percent Catalyst Lifetime Improvement upon Variations in the Model Variables.

Attribute	Perturbed Variable	Level of perturbation						
		-15%	-10%	-5%	0	+5%	+10%	+15%
Catalyst lifetime† (d)	ε_B	-	-	385.5	365.1	346.9	-	-
	k_{ls}	351.8	-	-	365.1	-	-	375.8
	k_{gl}	362.7	-	-	365.1	-	-	368.1
	LHSV	-	416.9	388.7	365.1	350.3	341.3	-
	$C_{4\text{-}CBA,in}$	-	461.3	-	365.1	-	254.6	-
Catalyst lifetime increase‡ (%)	ε_B	-	-	+5.58	0	-5.00	-	-
	k_{ls}	-3.66	-	-	0	-	-	+2.91
	k_{gl}	-0.66	-	-	0	-	-	+0.81
	LHSV	-	+14.18	+6.46	0	-4.41	-6.54	-
	$C_{4\text{-}CBA,in}$	-	+26.34	-	0	-	-30.27	-

The simulation results on parameter sensitivity analysis are also demonstrated in Figure 4-14. As it is clear from Figure 4-14, the effects of different variables studied on the catalyst lifetime are in the following order: $C_{4\text{-}CBA,in} > LHSV \sim \varepsilon_B > k_{ls} > k_{gl}$. The inlet concentration of 4-CBA has the greatest impact, and the gas-liquid mass transfer coefficient has the lowest effect on the objective function (e.g., catalyst lifetime). The effects of $C_{4\text{-}CBA,in}$, *LHSV,* and ε_B are in the opposite direction of those of k_{ls} and k_{gl}. Perturbations in the reactor bed porosity and LHSV have the similar influence on the catalyst lifetime in the examined range so that their importance is almost at the same level. For example, upon a +5 % change in the reactor bed porosity and LHSV, the catalyst life time is decreased to 385.5 d and 388.7 d, respectively. The same negative perturbation increases the catalyst lifetime to 346.9 d and 350.3 d, respectively. The catalyst lifetime is not much sensitive to the variations in the liquid-solid and gas-liquid mass transfer coefficients as their slopes appear to be smaller, compared to other process variables.

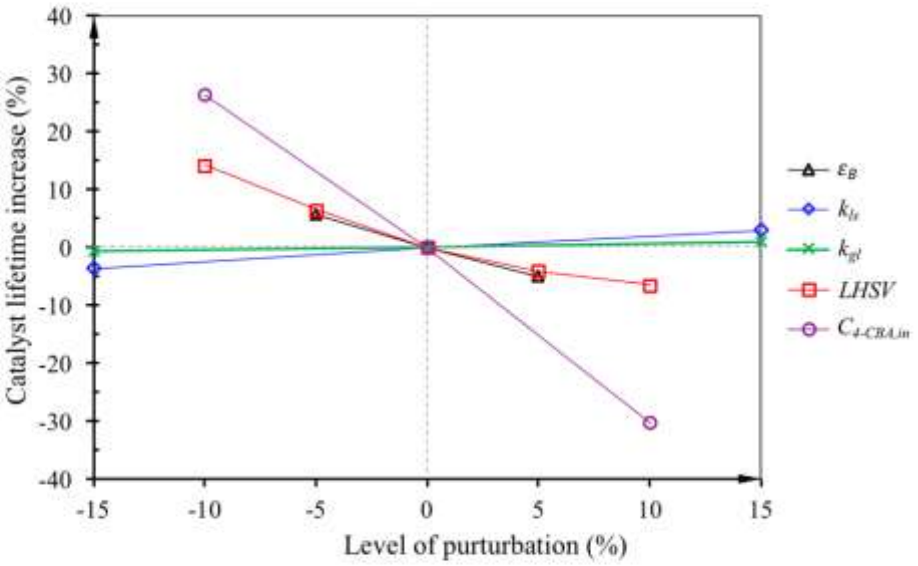

Figure 4-14: Pd/C catalyst lifetime increase (in %) at different perturbation levels of reactor bed porosity (ε_B), liquid-solid mass transfer coefficient (k_{ls}), gas-liquid mass transfer coefficient (k_{gl}), hourly liquid space velocity (*HLSV*), and inlet concentration of 4-CBA ($C_{4\text{-}CBA,in}$).

The operation of a Hydropurification plant is affected by the fluctuation of the vital parameters and the adverse phenomenon of the catalyst deactivation such that some of the operating parameters strongly influence the performance of the catalytic system. Since the minor changes in the process control can lead to the production of off-spec products, the analysis of the operating parameters can help avoid the possible problems in terms of product quality and capital and operating expenses. In this study, the results reveal that the product quality and the lifetime of the catalyst can be considerably improved through the proper control of the hydrodynamic parameters such as LHSV and bed porosity. It is worth noting that improving the process performance through the changes of the normal operation setpoints requires careful modifications and a more sophisticated control system. For instance, the LHSV fluctuation can be minimized through maintaining an accurate control on the feed composition. However, variation of concentrations of the feed components normally limits the positive impact of the LHSV changes. Moreover, the catalyst loading contributing to the desired bed porosity is not an easy procedure to be implemented. It is expected that even a slight improvement in the product quality through the mass transfer coefficient alteration can be regarded as a considerable asset in the hydropurification process. Although the influence of the mass transfer coefficient on the product characteristics and catalyst lifetime is not as significant as the other process and hydrodynamic parameters, it is still crucial to investigate this factor as even a small reduction in the concentration of 4-CBA (as the main impurity) in the hydropurification process can result in a greater cumulative production of the final product over longer production process. The mass transfer coefficient can be improved through an increase in the liquid and gas velocities and the system pressure. In summary, a minor improvement in the operation of the hydropurification process might be considered as a significant benefit to this industrial sector in terms of economic, environmental, and process performance prospective.

4.6 Conclusions

In this research study, we model the dynamic behavior of a hydropurification process for the production of purified terephthalic acid (PTA) in the face of Pd/C catalyst deactivation. The model results are compared with the real data. Based on the modeling outcome, the following conclusions are made:

- The three-phase dynamic model can successfully capture the process behaviors of the reaction system. The average error is 2.2%, while predicting the concentration of 4-carboxybenzaldehyde (4-CBA, as the main impurity) at the reactor effluent.
- The catalyst lifetime, which corresponds to a concentration of 25 ppm for 4-CBA, is 348.2 ± 5.0 d on the basis of the plant data; this value is estimated to be 365.1 d from the simulation approach, implying a 5% relative error.
- The relative significance of the variables studied on the catalyst lifetime follows this order: $C_{4\text{-}CBA,in} > LHSV \sim \varepsilon_B > k_{ls} > k_{gl}$.
- The catalyst lifetime increases by a decrease in $C_{4\text{-}CBA,in}$, $LHSV$, and ε_B; however, it lowers with decreasing k_{ls} and k_{gl}.
- Increasing LHSV by 5% and 10% reduces the catalyst lifetime to 350.3 d (4.1% decrease) and 341.3 d (6.5% decrease), respectively. Decreasing the LHSV by 5% and 10% increases the catalyst lifetime to 388.7 d (6.5% increase) and 416.9 d (14.2% increase), respectively.
- Increasing the Pd/C catalyst bed porosity (ε_B) by 5% results in a decrease in the catalyst lifetime to 346.9 d (5.0% decrease), while a 5% reduction in the bed porosity increases the catalyst lifetime to 385.5 d, corresponding to a 5.6% increase. An improvement in the

liquid−solid and gas−liquid mass transfer and the contact efficiency results in a more efficient process. For instance, increasing the liquid−solid mass transfer coefficient (k_{ls}) by 15% increases the catalyst lifetime to 375.8 d (2.9% increase), while decreasing this mass transfer coefficient by 15% lowers the catalyst lifetime to 351.8 d (3.7% decrease).

- Using structured packing (as a process intensification) may be a practical recommendation in TBRs, potentially leading to a better performance, compared to the conventional TBRs with randomly packed catalysts. The TBRs with structured packings are more flexible with respect to the process variations in the hold up, hydrodynamic regimes, pressure drop, flow rates, and heat transfer properties, which are the key parameters for process intensification.

NOMENCLATURES

Acronyms

4-CBA - 4-carboxybenzaldehyde

4-HMBA - 4-hydroxymethylbenzoic acid

AA - acetic acid

BA - benzoic acid

BC - boundary condition

CE - centrifuge

CFD - computational fluid dynamics

CO - carbon monoxide

CR - crystallizer

CSTR - continuous stirred tank reactor

CTA - crude terephthalic acid

D - dimension

EG - ethylene glycol

EM - electromotor

FPM - first principle model

HE - heat exchanger

HIR - high interaction regime

HOS - hot oil supply

HOR - hot oil return

HPLC - high-performance liquid chromatography

IC - initial condition

LHSV - liquid hour space velocity

LIR - low interaction regime

LPS	-	low pressure steam
MOL	-	method of lines
MRI	-	magnetic resonance imaging
ODE	-	ordinary differential equation
P	-	pump
PCS	-	powder conveying system
Pd/C	-	palladium supported on carbon
PDE	-	Partial differential equation
PET	-	polyethylene terephthalate
PFM	-	plug flow model
PTA	-	purified terephthalic acid
pta	-	para-toluic acid
PX	-	para-xylene
RVF	-	rotary vacuum filter
TA	-	terephthalic acid
TBR	-	trickle-bed reactor

Variables/Symbols

A	-	parameter of dynamic deactivation model	(h^{-1})
a	-	metallic sintering dispersion parameter	(-)
a_P	-	catalyst surface area	($\text{m}^{2}.\text{g}^{-1}$)
C	-	concentration	(kmol.m^{-3})
C_P	-	heat capacity	($\text{J.kg}^{-}1.\text{K}^{-1}$)
C_{TA}	-	feed concentration of terephthalic acid	(wt. %)
d_B	-	diameter of catalyst bed	(m)
d_P	-	catalyst particle diameter	(mm)
D	-	axial dispersion coefficient	($\text{m}^{2}.\text{s}^{-1}$)

E - catalyst activation energy (J.mol^{-1})

F_F - feed flowrate (t.h^{-1})

F_{H2} - hydrogen flowrate (kg.h^{-1})

h - heat transfer coefficient (W.m^{-2}.K^{-1})

H - Henry’s constant (m^{3}.MPa.mol^{-1})

ΔH - heat of reaction (kJ.mol^{-1})

k - mass transfer coefficient (m.s^{-1})

L - length of reactor bed (m)

m - exponent in catalyst deactivation model (-)

P - pressure barg

r - rate of reaction (kmol.kg$_{s}^{-1}$.s^{-1})

r_d - rate of deactivation (h^{-1})

R - universal gas constant (J.mol^{-1}.K^{-1})

t - time (s)

T - temperature (K)

T_R - reference temperature (K)

u - superficial velocity (m.s^{-1})

z - axial coordinate (m)

Greek Letters

ε_B - bed porosity (-)

ε - hold up (-)

ε_P - particle porosity (-)

η - effectiveness factor (-)

λ - conductivity (W.m^{-1}.K^{-1})

ξ - specific surface area of the phase interface (m^{2}.m^{-3})

ρ - density (kg.m^{-3})

ρ_B - bulk density (kg.m^{-3})

Subscripts

g - gas phase

gl - gas to liquid

i - index of components

in - inlet to reactor

k - index of reaction

l - liquid phase

ls - liquid to solid

out - outlet from reactor

s - solid (catalyst) phase

Superscripts

S - surface of the catalyst

ss - steady state

5 CHAPTER FIVE: Product Quality Control in Hydropurification Process by Monitoring Reactor Feed Impurities: Dynamic Mathematical Modeling

Preface

A version of this chapter was published in the Journal of Industrial and Engineering Chemistry 92, 62-76 (2020). I am the primary author of this paper. All authors were involved in defining/introducing the objectives and outlines of the paper. I wrote the original draft. I was mainly responsible for the proposed conceptualization and methodology. Nima Rezaei helped analyze the results, structure the methodology, and review the manuscript. Sohrab Zendehboudi was involved in carefully reviewing and editing the manuscript, and helped me in the development of the model, results analysis, and the conceptualization.

Abstract

Control of product quality plays a crucial role in petrochemical industries. In this chapter, we propose a new strategy to control the quality of purified terephthalic acid (PTA) product. In this approach, the PTA quality is controlled by monitoring the concentration of the main impurity in the hydropurification process, which is 4-carboxybenzaldehyde (4-CBA) in the crude terephthalic acid (CTA) powder. To attain the research objectives, a dynamic dispersion model is developed in the face of catalyst deactivation, and by considering the vital operating parameters. The CTA powder with low and high 4-CBA concentrations can be effectively used through a proper mixing procedure. This strategy can be applied by controlling the ratio of the mass flowrates of the two streams. The positive effect of H_2 partial pressure on the system performance can be implemented by a small decrease in reaction temperature. Off-spec PTA powder can be used with the CTA powder having a high 4-CBA concentration. Increasing temperature can accelerate reduction rate of the Pd/C catalyst surface area, leading to an unfavorable sintering phenomenon. The decreased activity of Pd/C catalyst is in good agreement with the normalized ratio of decrease in the surface area of pure Pd with increasing temperature.

5.1 Introduction

Hydroprocessing is an important process with near 70-year maturity to produce clean fuels. Catalyst deactivation is a key aspect in the design and operation of catalytic processes. Different methods are proposed to improve the lifetime of the catalysts. Usually, fixed-bed catalytic hydroprocessing reactors demand prolonged catalyst lifetime. It is of practical importance to study the catalyst lifetime under the industrial operating conditions. However, the slow kinetic rate of catalyst deactivation challenges mimicking the industrial operational conditions in laboratory-scale tests [335].

Trickle-bed reactors (TBRs) are extensively used in petrochemical, chemical, biochemical, pharmaceutical, wastewater treatment, and electrochemical processes [183, 336, 337]. For example, the petroleum fuel quality and the middle-distillate productivity can be improved through reducing contaminants, such as sulfur, vanadium, nitrogen, nickel, and asphaltene [338]. Hydrotreating enhances the quality of the petroleum fractions distillate through reducing the concentration of impurities, hydrogenating olefins and aromatics, and hydrocracking heavy fractions such as asphaltenes. In hydrotreating, the raw materials react with H_2 in a fixed-bed catalytic reactor [339]. The optimal design and operation of the process/plant improve the product quality and process efficiency [340]. Another strategy for production of high quality product and efficient operation of hydrotreating is to use catalysts that sustain undesirable operating conditions without considerable loss of activity [341].

Modeling approaches can be useful to study the equilibrium and non-equilibrium behaviors (thermodynamically and kinetically) of TBR systems for optimization and scale-up purposes.

Computational fluid dynamics simulation can model the effect of hydrodynamic parameters and/or flow regime on a TBR performance [200]. Mathematical models can be used to investigate hydrodesulfurization (HDS), hydrodenitrogenation (HDN), and hydrodearomatization reactions in industrial TBRs [342]. Reliable TBR models for crude oil hydrotreating require accurate estimation of reaction kinetic parameters [199]. Understanding the catalyst deactivation kinetics is also essential to develop a reliable mathematical model for a catalytic system facing catalyst deactivation. The estimated deactivation rate strongly affects the accuracy of the TBR mathematical model, experiencing catalyst deactivation. An experimental phase to collect required data is usually costly and lengthy [343].

In the oil and petrochemical industries, the main processes conducted in TBRs are hydrotreating, HDS, hydrocracking, hydrodewaxing, HDN, hydrofinishing, and hydrodemetallization [344]. Researchers have focused on the product quality control of the catalytic reactors through modeling studies. Cotta et al. [345] used a 1D pseudo-homogeneous model to investigate HDS and HDN of middle distillates in an industrial TBR, packed with Ni-Mo/γ-Al_2O_3 catalyst [345]. Harsh operating conditions (95 atm and 390°C) were required to improve the HDN conversion [345]. The influence of catalyst composition on hydroprocessing product quality was analyzed by Oyama et al. [346]; they studied the impacts of the catalyst phosphorus content on Ni_2P/SiO_2 catalyst structure and on the hydroprocessing operation. The phosphorus-content in the catalyst was found to considerably affect the catalyst stability and activity [346].

Bhaskar et al. [210] analyzed the performance of an industrial-scale TBR using a three-phase non-isothermal heterogeneous model. They considered the main hydrotreating reactions, which are HDS, HDN, hydrodearomatization, and hydrocracking; complete catalyst wetting for NiO-

MoO_3/Al_2O_3 was assumed. Their sensitivity analysis showed that the feed flowrate and reaction temperature contribute the most to the product quality [210]. Tukač et al. [292] concluded that the operation mode can appreciably affect the reaction efficiency and the product quality. The dicyclopentadiene hydrogenation reactions were conducted in a TBR, using Pd/Al_2O_3 catalysts. Periodic operation of the liquid feed led to a 30% increase (compared to the steady-state) in the reactor productivity of styrene hydrogenation, improving the product quality [292]. Wu et al. [203] studied wet-air oxidation of phenol in a TBR packed with Cu/C catalysts. They developed a steady-state model that considered axial dispersion and plug flow pattern. The liquid-to-solid mass transfer and axial dispersion terms were found insignificant, compared to the gas-to-liquid mass transfer term [203]. Lopes and Quinta-Ferreira [347] studied the transition of trickling flow regime to pulsing flow regime in a TBR. The establishment of pulsing flow regime generally improves the mass and heat transfer rates [347], and consequently reactor performance (in terms of longer contact time, more homogeneity of the fluid flow distribution [348], and heat transfer [349]).

Jarullah et al. [199] optimized the kinetic models of TBRs, employed for HDN and hydrodemetallization reactions of crude oil. They found high temperature, high H_2 partial pressure, and low liquid hourly space velocity (LHSV) to enhance the vanadium and Ni conversion [199]. Jarullah et al. [338] optimized the kinetic parameters of the hydrodeasphaltenization reactions conducted in a TBR [338]. It was found that the reaction temperature appreciably influences the component diffusivity (also, mass transfer coefficients), gas and liquid mass flowrates, H_2 solubility, density, and viscosity [338].

Nawaf et al. [350] investigated the effect of $Co_3O_4/\gamma\text{-}Al_2O_3$ and $MnO_2/\gamma\text{-}Al_2O_3$ catalysts for the production of high-quality fuels. The experiments were conducted in an isothermal TBR; it was revealed that both catalysts perform excellent. At the same process conditions, the MnO_2/γ-Al_2O_3 catalyst exhibited a higher conversion, compared to the Co_3O_4/γ-Al_2O_3 catalyst [350]. The applicability of three activated carbon-based Ni-Mo catalysts was examined for the hydroprocessing of tire oil for the conversion of heavy fractions and sulfur removal, to produce lighter naphtha and diesel [351]. The catalysts' support was synthesized through the physical activation of petcoke, which was later functionalized and treated with HNO_3. The catalyst support activated for nine hours showed an outstanding performance of 99.99% HDS conversion. In the commercial tire oil hydroprocessing, the same Ni-Mo/AC catalyst features a 96.3% sulfur removal, enhancing diesel cetane number [351].

Azarpour et al. [146] implemented a hybrid model composed of artificial neural network and first principle model to predict the deactivation rate of catalysts. The model effectiveness was examined by testing the model for two industrial catalytic reactors [146]. A 1D heterogeneous isothermal model was proposed for HDS reaction of low-temperature coal tar in a TBR packed with Ni-Mo/Al_2O_3-SiO_2 catalysts at the steady-state conditions [352]. Increasing temperature and LHSV, and decreasing pressure decreased the catalyst particle effectiveness factor [352]. In a recent study, da Silva and Secchi [353] used a model-based predictive control to monitor/control the sulfur concentration at the reactor exit in a HDS process. They effectively controlled the end-state contamination by adjusting the oil and gas flowrates, and system temperature [353].

Catalyst deactivation is overlooked in most simulation studies in the literature related to hydroprocessing unit. Some studies have only reported the experimental catalyst deactivation data without proposing a mathematical model that explains the deactivation kinetics. Therefore, integrating catalyst deactivation in the structure of a dynamic mathematical model is essential to identify critical system parameters and their impacts on the product quality in a hydrotreating process. This research aims to propose an effective strategy to control the quality of purified terephthalic acid (PTA) powder. We control the product quality by regulating the hydropurification reactor feed (and H_2) flowrate and monitoring the concentration of contamination in the crude terephthalic acid (CTA) charged to an industrial-scale hydropurification system. The reactions are conducted in a TBR, using Pd/C catalysts.

The hydropurification process suffers from catalyst deactivation, adversely affecting the product quality. High concentration of impurities in the feed of hydrotreating reactor accelerates the catalyst deactivation. To compensate for deactivation, the rate of production should be reduced. The other problems created by the high concentration of the impurities are failure of the separation units due to the low efficient equipment and an increase in utilities and process solvent consumption.

The proposed operating strategy postpones the catalyst bed replacement by controlling the raw material mass flowrates and the H_2 partial pressure. The introduced approach extends the production period, before catalyst deactivation significantly reduces the product quality to a degree demanding catalyst bed replacement. Therefore, the developed strategy has potential to lower costs of maintenance over the unit lifetime, cause more efficient operation of the equipment, and improve the control flexibility of the product quality. The concentration of the main impurity (4-carboxybenzaldehyde (4-CBA)) in the final product (PTA) is obtained from the plant data. The developed model simulates the dynamic behavior of the system due to the deactivation phenomenon, mass transfer rates for all components, heat transfer between three phases, and the process and thermodynamic conditions.

5.2 Theory and Background

In a TBR, liquid hydrocarbons flow downward in rivulets over the solid catalyst particles while H_2 travels down through the remaining void space [183, 344, 354-356]. The TBR operation is usually adiabatic and involves processing of the organic liquids with H_2 [336]. A high pressure up to 30 MPa is required to guarantee the gas solubility in the liquid mixture for improvement of mass transfer rate; high temperature (e.g., 300–380˚C) leads to proper operating conditions because of the kinetics characteristics [336].

Terephthalic acid (TA) is an aromatic carboxylic acid [7]. PTA is one of the essential products in the petrochemical industry [267] so that it is recognized as the ninth largest industrial chemical [357]. The major commercial producers of PTA are British Petroleum, British Petroleum Zhuhai Chemical Company, and JBF Petrochemicals Ltd. [358]. PTA's global demand has increased at an annual growth rate of 5.3% since 2011 and has reached 60 MT in 2020 [359, 360]. The PTA production has significantly increased in the last ten years [361-364]. *p*-xylene (PX) is the raw material for PTA production, which is synthesized from catalytic reforming of naphtha [267]. PTA is utilized to produce polyethylene terephthalate (PET) [1, 269], which is mainly used in the textile and polyester industries [267]. Indeed, the widespread use of PET has motivated further developments of the TA industrial processes [7]. The history of TA is strongly tied to that of polyester [7]. About 70% of TA that is used in PET production comes from the oxidation process of PX [358]. PTA and ethylene glycol are the raw materials for industrial production of PET [1, 2]. About 90% of the worldwide PTA production is used in the polyester manufacturing industry [362]. Figure 5-1 illustrates the uses of TA in the polyester industry [358]. The PTA production has a yearly growth rate of 7% since 2008, which is related to the global growth rate of textile and polyester industries [267].

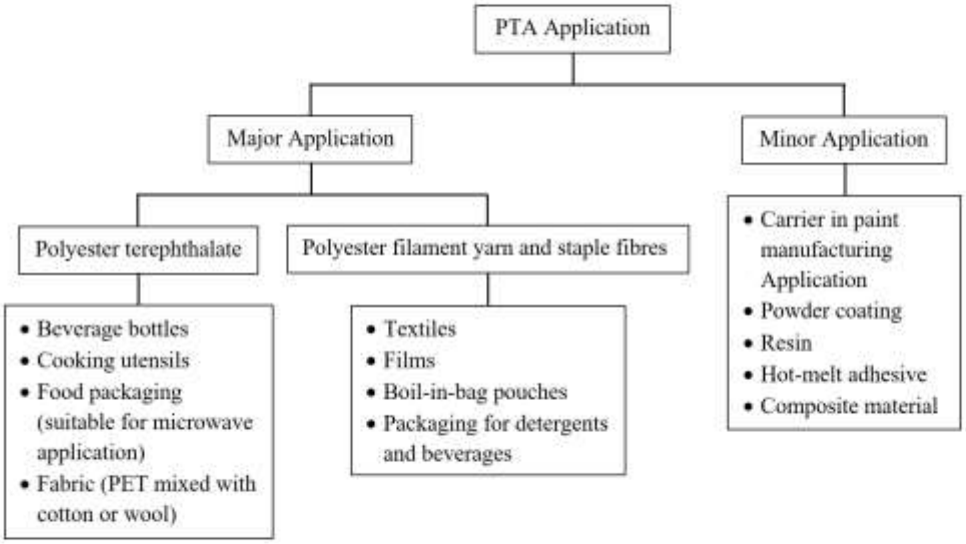

Figure 5-1: TA applications in polyester industry [358].

The PTA production plant consists of two main units: PX oxidation unit and hydropurification unit. In the first unit, PX is oxidized to TA in the temperature range of 150–210˚C [365] and the pressure range of 15–30 bar [358]. The oxidation of PX is exothermic and liberates 200 MJ/kg heat [7]. In the oxidation reactor, acetic acid is used as a solvent; air is utilized as the O_2 source; manganese acetate and cobalt acetate are used as catalysts; and bromide is utilized as the promoter (Co-Mn-Br catalyst system) [358]. The heat of reaction is removed by the evaporation of acetic acid and water, which is the byproduct of PX oxidation reaction [7]. Since the TA solubility in acetic acid is low, most of the TA is precipitated [7]. The typical sources for bromide ion are HBr, NaBr [358], and tetrabromoethane [7]. The Mn catalyst provides a better oxidation to aldehyde, while the Co catalyst does not improve the oxidation. Hence, the symbiotic effect of both Mn and

Co catalysts is crucial to efficiently oxidize PX to TA [358]. It is necessary to create an active catalyst [7]. Bromide acts as a promoter to produce radical compound species [358]. The mechanism of PX oxidation reaction is a common catalyst-modified free radical chain [365]. The most accepted kinetic model of PX oxidation is the lumped kinetic model [7, 365]. Figure 5-2 illustrates the lumped kinetic model of the PX oxidation to TA [7, 365]. In the proposed model, the reaction series include conversions of PX to *p*-tolualdehyde (PTLD), to *p*-toluic acid (pta), to 4-CBA, and finally to TA. The reactions of PTLD to pta and 4-CBA to TA require 0.5 moles of O_2, and the reactions of PX to PTLD and pta to 4-CBA require one mole of O_2 [365, 366]. The reaction step of pta to 4-CBA has the slowest reaction rate and controls the oxidation process [367]. More than 98% of PX is reacted, and the overall yield to form TA is higher than 95 mol% [7]. Even though more than 96% selectivity is obtained, there are always some partial oxidation byproducts [3]. A portion of the hydrocarbons, solvent, and intermediates are wasted by the side reactions of decarbonylation and decarboxylation during the PX oxidation process. They over-oxidize to form CO, CO_2, H_2O, benzoic acid (BA), methyl acetate, and methyl bromide [368]. Methyl acetate is one of the main byproducts of the PX oxidation that can be efficiently controlled by using an optimized ratio of PX to acetic acid [7]. There are extensive studies, aiming to improve the Co-Mn-Br catalyst system by the addition of a fourth catalytic component, such as alkali, lanthanide, and transition metals; the results show significant improvement in the catalytic activity, and in some cases, enhanced selectivity [365]. The final product from the PX oxidation unit as crude terephthalic acid (CTA) contains 4-carboxybenzaldehyde (4-CBA, as main impurity), with a concentration of around 3000 ppm [267]. The CTA powder has a light-yellow color [7].

4-CBA is similar to TA in terms of physical and chemical characteristics. Hence, separating 4-CBA from TA is challenging [366]. Since 4-CBA is less soluble in acetic acid than pta [7], 4-CBA is crystallized with TA [7, 358]. 4-CBA impurity reduces the average molecular weight of the polymer and lowers the polymerization rate in the production of polyester [363]. Therefore, in the second unit, hydropurification process is used to reduce the 4-CBA concentration of the CTA [1, 2]. This impurity (4-CBA) reacts with H_2 in the presence of water in a temperature range of 270–290˚C and pressure of 79 bar in a TBR packed with 0.5 wt.% palladium supported on carbon (Pd/C) catalyst. In the TBR, 4-CBA is converted to pta, which usually separated from TA through crystallization and centrifugation processes. PTA (as the final product) should contain <25 ppm 4-CBA and <150 ppm pta [267]. These levels of PTA contaminations have negligible effects on polyester production process [363].

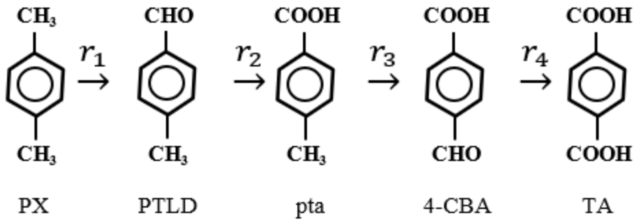

Figure 5-2: Lumped kinetic model of PX conversion to TA [7, 365].

5.2.1 Description of Hydropurification Unit

In this section, we explain the hydropurification unit in the PTA production. AMOCO is the most widely used technology to produce PTA [7, 357]. Figure 5-3 illustrates a simple schematic of the hydropurification unit for the production of PTA [32]. The CTA powder is charged into a drum and mixed with the filtrate coming from the rotary vacuum filter. The slurry prepared in this drum is the feed to hydropurification reactor. One of the initial stages in the production process startup is to completely dissolve the CTA powder in water (as a solvent) [32]. The TA solubility in water increases almost linearly with temperature [4]. Therefore, the feed is heated in two sets of heat exchangers. The first set uses the steam leaving the crystallizers as the service fluid. The steam energy is not sufficient to increase the reactor feed temperature to the desired level. The second set of heat exchangers uses a special oil (e.g., Therminol 66 and Jarytherm) that is heated in a furnace to provide the additional heat duty. The outlet process stream leaving the second set of heat exchangers has a temperature of about 285˚C, that is sufficient to completely dissolve the CTA powder into water. The hydrogenation reactions of 4-CBA occur in the hydropurification TBR packed with Pd/C catalyst, having a pressure of 73.5 barg. The pressurized H_2 is fed into the reactor, and the outlet stream from the reactor goes through a series of five crystallizers, where the synthesized pta remains in the liquid phase and becomes separated from the crystallized TA. Then, the slurry is pumped into four centrifuges to separate the solid TA from the liquid phase. For improved separation efficiency, the solid leaving the centrifuges is mixed with water, and the slurry mixture is pumped into the rotary vacuum filter to separate the TA. The wet TA is charged into a rotary dryer, where water is removed from the powder using a low-pressure steam. Samples are taken at the dryer discharge and is sent to the laboratory for quality analysis. The powder is first sent to the checking silos by a powder conveying system. If the laboratory results show that the product is on-spec, the powder is directed to the product (final) silos by a powder conveying system; otherwise, the off-spec product is recycled to the beginning of the process [32].

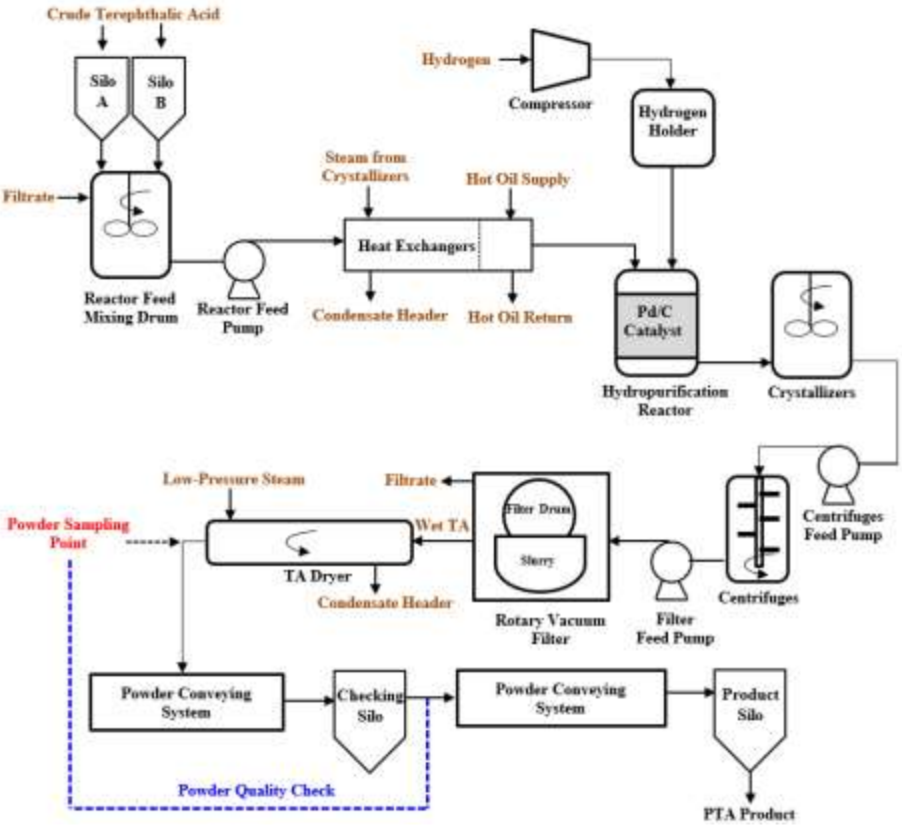

Figure 5-3: A simplified diagram of the hydropurification process of PTA production plant.

5.2.2 Operating Conditions of Hydropurification Unit

Table 5-1 includes the operating conditions of the hydropurification unit, Pd/C catalyst specifications, TBR characteristics, and the process parameters designed set-points [271].

Table 5-1: Operating conditions and catalyst specifications of hydropurification unit [271].

Attribute	**Parameters**	**Values**	**Unit**
Operating conditions	Pressure	73.5	barg
	Temperature	285	˚C
	TA concentration in feed	23	wt %
	Feed flowrate	196	t/h
	H_2 flowrate	13.2	kg/h
Catalyst bed (Reactor)	Length	7.4	m
	Diameter	2.8	m
	Porosity	0.44	m^3/m^3
Catalyst	Bulk density	475	kg/m^3
	Particle diameter	3.53*	mm
	Particle porosity	0.61	m^3/m^3
	Total surface area	900-1100	m^2/g
	Pd content	0.5±0.02	wt.%
	Activated carbon	99.5	wt.%
	Water in wet catalyst	38±2	wt.%

* Catalyst size distribution: d_p= 4-6 mesh (97%), d_p<4 mesh (2%), and d_p> 8 mesh (1%).

Product quality control of the hydropurification unit is critical, which considerably affects the operating costs. A decrease in the product quality is caused by the catalyst deactivation and has to be accounted. The PTA powder sample is taken every 4 hours (under normal process conditions); more frequent sampling is required at abnormal operating conditions. The PTA samples are analyzed by high-performance liquid chromatography (HPLC). Analytical scale (±0.1 mg resolution), volumetric flask (class A), ultrasonic bath, STRODS column (150 mm length and 4 mm thickness), 4-CBA standard samples, ammonia solution (2 N), and a mobile phase consisting of 0.1 vol. % trifluoro acetic acid, 21 vol. % acetonitrile, and 78.9 vol. % water are used in the analysis. The operating conditions of the HPLC machine are 50 ^oC, 0.5 mL/min, and 260 nm wavelength. An autosampler is employed to inject a 20 mL aliquot solution with 0.5 N ammonia into the HPLC machine. Then, a 100 mL solution is made by the mixture of 0.5 g of standard samples with deionized water and 10 mL of 2 N ammonia. 5 mL of the solution is placed into the autosampler machine vial after being filtered by a 0.45 mm syringe. Then, a 10 µL aliquot of the standard samples is transferred to the instrument. The filtration solution is transferred to the machine, and the injection of 10 µL of standard samples is conducted a couple of times to obtain the corresponding data from the chromatography [312].

5.2.3 Operational Challenges in Hydropurification Unit

The deactivation of Pd/C catalyst in the hydropurification process decreases the product quality over time. There are some parameters that are considered as the quality specifications of PTA powder, as listed in Table 5-2 [4, 271].

Table 5-2: PTA powder quality specifications [4, 271].

Specification		Value	Unit
Δy (turbidity indicator)		1 - 10	NA
b-value (yellowish appearance)		<2	NA
C_{pta}		<150	ppm
$C_{\text{4-CBA}}$		<25	ppm
C_{BA}		<30	ppm
Volatility		0.1 - 0.2	%
Tr (340 nm)		>85	%
Acidity		673 - 677	mgKOH/g
Moisture		<0.2	%
Total metal		<8	ppm
Crystal size	>250 µm	Maximum of 3.0	%
	40 - 250 µm	Balance	
	<40 µm	Maximum of 20.0	

Carbon support of the catalyst might be responsible for an increase in the turbidity (Δy). *b*-value reflects the 4-CBA concentration and Fe contamination. The concentrations of 4-CBA, pta, and

BA are maintained below the limit values, set by the licensor and industry. The transparency level of the product is determined by Tr (340 nm). The powder acidic activity and humidity are measured by acidity and moisture specifications, respectively. Total metal concentration in the powder is obtained by Fe, Mn, Ni, Cr, and Ti. The crystal size distribution is an important quality parameter since it determines the dissolution of PTA (as raw material) in the polymerization process.

To attain the on-spec product, the concentration of 4-CBA should be less than 25 ppm. The product quality is not only affected by the catalyst deactivation but also by improper control of parameters such as feed flowrate and impurities concentration. One solution is to transfer the off-spec product to the beginning of the process for reprocessing. Another option is to sell the product at a cheaper price. The PTA production plant and polymer/polyester plants are usually built in a petrochemical complex.

The PTA containing high content of 4-CBA negatively affects the polymerization process. It promotes the polymerization side reactions, decreases the polymer molecular weight due to the presence of the acidic group, and hinders the polymer chain [6]. The optimal properties of PET should be based on customer requirement and aesthetic reasons [283]. PTA powder with a high amount of 4-CBA adversely influences the PET whiteness and its branched structure because of the aldehyde group reactions [272]. Recycling the off-spec product leads to a reduction in the production rate, adding further expenses to the PTA plant operation. Another issue in reprocessing the off-spec PTA is operational problems, including equipment malfunction and product quality reduction. A PTA stream with a high 4-CBA content reduces the efficiency of centrifugation and rotary vacuum filter due to the 4-CBA stickiness. Furthermore, the reprocessing step can create very small TA crystals; this negatively influences the crystal size distribution of PTA powder, reducing the powder quality since the crystal size distribution is one of the PTA powder quality specifications. When the product becomes off-spec, it takes at least a few hours to bring the plant to design conditions, due to the residence time of the substances in the process system. Thus, it is necessary to maintain the product quality and return the plant from abnormal condition (off-spec production) to normal condition (on-spec production) through a timely, practical, and economical strategy.

5.3 Methodology

The most important parameter affecting the PTA product quality is the 4-CBA concentration in the reactor feed [263]. The CTA powder produced in the oxidation unit has varying concentration of 4-CBA, and there are two silos for CTA powder in the plant. Therefore, we propose a procedure to mix the CTA powder with low and high 4-CBA concentrations to control the PTA powder quality. One operating parameter that can also decrease the 4-CBA content in the final product is the amount of H_2 fed to the TBR. The partial pressure of H_2 in the reactor depends on the reaction temperature. By controlling the reaction temperature and increasing the partial pressure of H_2, the PTA powder quality can be improved [313]. Another parameter that influences the hydrogenation reactions is temperature. It can dictate the H_2 solubility in the reaction mixture [369] and CTA dissolution into water [370]; it also has a considerable effect on the catalyst deactivation since the main reason for Pd/C catalyst deactivation is thermal sintering [1, 2, 371]. Therefore, a practical strategy should consider the product quality, catalyst lifetime, and equipment performance.

Figure 5-4 demonstrates the methodology used in this study for optimal operation of the hydropurification process.

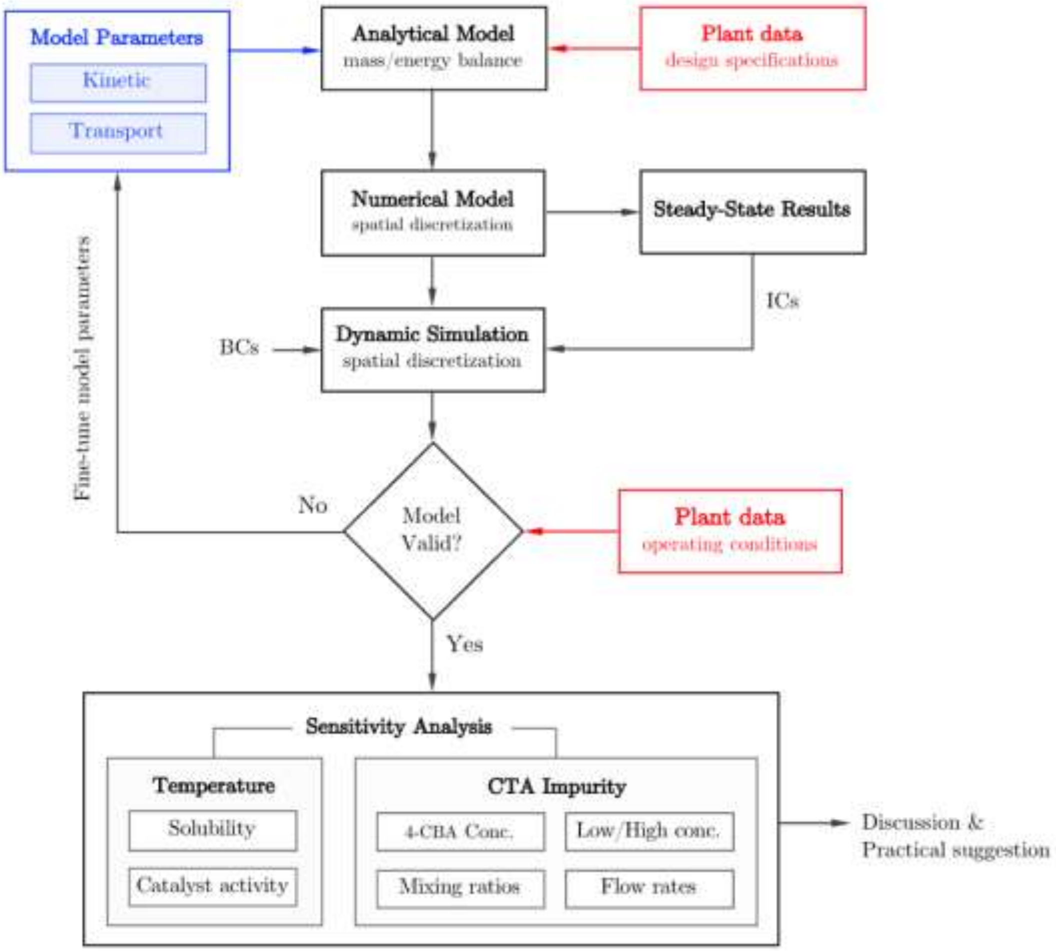

Figure 5-4: Methodology implemented in this study (BCs: boundary conditions; ICs: initial conditions).

The plant data are collected for an industrial hydropurification process, which is used to analyze the process performance. The development of a first principle model needs the operating data, hydropurification reaction rates, and catalyst deactivation rate. The first principle model is developed using the mass balance for all components and energy balance in each phase. Auxiliary model parameters (kinetics, and transport) are obtained from empirical correlations. The set of partial differential-algebraic equations are solved with a numerical method after applying the boundary conditions (BCs) and initial conditions (ICs). The simulation is coded into MATLAB software environment. The dynamic model is first solved at steady-state (SS) condition, and the SS results are used as ICs. Then, the dynamic model is run to simulate the plant results for up to the lifetime of the catalyst. The model is validated by comparing the model results with the plant data. The influence of each parameter on the process performance is then evaluated by conducting a parametric sensitivity analysis. Based on our previous studies, the 4-CBA concentration significantly affects the catalyst deactivation and consequently, the product quality [263]. CTA unit silo B with a high concentration of 4-CBA can be mixed with CTA unit silo A with a low concentration of 4-CBA. This mixing process is conducted to maintain the mass flowrate of TBR feed and the concentrations of TA and 4-CBA in the inlet stream corresponding to the normal operating conditions. Temperature is another influential parameter. The impact of H_2 on the reactor performance is analyzed, considering the influence of temperature on the H_2 solubility, TA solubility, and active surface area of the catalyst.

5.4 Dynamic Mathematical Model Development

A dynamic heterogenous model is developed for the performance analysis of the hydropurification system. Based on the reactor configuration and the operating conditions, reasonable assumptions are made. The mass balance for each component of the reaction system, and the energy balance for each phase are formulated. The key terms of the developed model, which are reaction kinetics and deactivation model, are discussed. Finally, the developed mathematical model solution is presented with detailed discussion.

Figure 5-5 illustrates the essential steps of the hydropurification process dynamic model development. Catalyst deactivation gives a dynamic behavior/nature to the hydropurification system. Calculation of the deactivation kinetics is carried out by the employment of the plant operating data, such as, inlet and outlet concentrations of the components, temperature, and the rates of reactions. The interrelation of the parameters involved in the deactivation phenomenon is merged in the conservation equations written for the components. The functionality of the deactivation rate (a) with time, catalyst active surface area, and catalyst residual catalytic activity are incorporated into general power law expression to obtain the deactivation rate model. Then, the catalyst deactivation rate (r_d) consisting of deactivation parameter (a), catalyst activation energy (E), deactivation model exponent (m), and temperature (T) represents the catalyst deactivation kinetics. Detailed discussion on the calculation of the catalyst deactivation rate is found in the published works [263, 271]. Conservation equations of the model are developed based on the reaction kinetics (three main reactions), catalyst deactivation kinetics, plant data, and model parameters, which are calculated using the proper correlations incorporating the real operating conditions. The set of partial differential equations containing the nonlinear equations of reaction kinetics and deactivation kinetics is solved using suitable numerical techniques. The numerical simulation of the system assessed under the fluctuation of the vital parameters produces the components' concentration and temperature profiles against time.

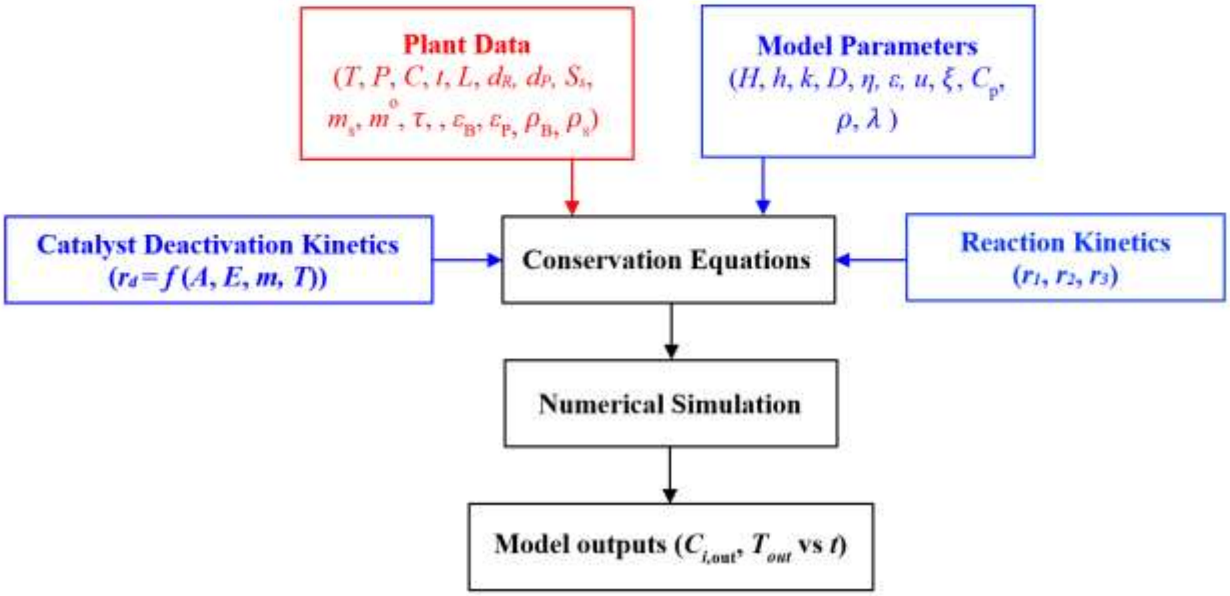

Figure 5-5: Main steps to develop the hydropurification process model.

5.4.1 Model Assumptions

The dynamic model developed in this study is complicated by the fluctuations in process variables along with the catalyst deactivation. Based on the process operating conditions, reactor dimensions, and catalyst specifications, we postulate our assumptions. The ratio of reactor dimeter (2.8 m) to the catalyst particle diameter (3.53 mm) is very high. This implies that there is no significant bypassing (e.g., wall effects) and effects of boundaries on heat transfer in the system. Given the high ratio of reactor diameter to particle diameter (> 25), radial diffusion coefficient can be considered constant over the radius of the fixed bed. Because of insignificant temperature changes in the reactor, its adiabatic operation, the radial heat dispersion can be ignored [20]. In addition, the contrast in reactor and catalyst dimensions leads to good liquid distribution even at high operating pressures [91]. Referring to the hydropurification operating conditions, the wetting efficiency of the catalytic bed is calculated to be 0.97, which can be assumed as unity [67]. The TBR is also well insulated, and the reactor pressure is higher than the saturation pressure of the reaction mixture. Therefore, the following main assumptions are made in this work:

- The wall effect on flowrate is insignificant [276].
- Mass [95] and energy [98] dispersions in the radial direction are minimal [20, 277].
- The reactor operation is adiabatic.
- Uniform flow in the catalyst bed is established [91].
- The components do not vaporize in the reactor under operating condition.
- The wetting efficiency of the catalyst particle is one [67].

5.4.2 Mass and Energy Balances

To predict the concentration profile of the reaction components and to evaluate the product quality change, a mass balance equation for each component is written in each phase in the three-phase catalytic TBR. The components of the reaction system are H_2, 4-CBA, pta, 4-hydroxymethylbenzoic acid (4-HMBA), BA, and CO. The mass balance equations of H_2 in the gas and liquid phases are given below:

$$\frac{\partial(\varepsilon_g C_{H_2,g})}{\partial t} = D_{H_2,g}\frac{\partial^2 C_{H_2,g}}{\partial z^2} - \frac{\partial(u_g C_{H_2,g})}{\partial z} - k_{H_2,gl}\xi_{gl}\,(\frac{C_{H_2,g}}{H_{H_2}} - C_{H_2,l}) \tag{5-1}$$

$$\frac{\partial(\varepsilon_l C_{H_2,l})}{\partial t} = D_{H_2,l}\frac{\partial^2 C_{H_2,l}}{\partial z^2} - \frac{\partial(u_l C_{H_2,l})}{\partial z} + k_{H_2,gl}\xi_{gl}\left(\frac{C_{H_2,g}}{H_{H_2}} - C_{H_2,l}\right) - k_{H_{2,ls}}\xi_{ls}(C_{H_2,l} - C^S_{H_2,s}) \tag{5-2}$$

The subscripts g, l, and s denote the gas phase, liquid phase, and solid phase, respectively. Superscript S signifies the catalyst surface; ε is the phase holdup in m^3/m^3; C represents the component concentration in kmol/m^3; D introduces the axial dispersion coefficient in m^2/s; z refers to the axial coordinate in m; k symbolizes the mass transfer coefficient in m/s; ξ stands for the specific interfacial surface area in m^2/m^3; H is the Henry's constant; t represents the time in s; and u resembles the superficial velocity in m/s. The following equation represents the mass balance of other components in the liquid phase:

$$\frac{\partial(\varepsilon_l C_{i,l})}{\partial t} = D_{i,l}\frac{\partial^2 C_{i,l}}{\partial z^2} - \frac{\partial(u_l C_{i,l})}{\partial z} - k_{i,ls}\xi_{ls}(C_{i,l} - C_{i,s}^S) \tag{5-3}$$

The mass balance of all components in the catalyst/solid phase is given by the following expression:

$$\varepsilon_P(1-\varepsilon_B)\frac{\partial C_{i,s}^S}{\partial t} = k_{i,ls}\xi_{ls}\left(C_{i,l} - C_{i,s}^S\right) \pm \sum_{k=1}^{3} r_k\,\eta_k\rho_B a(t) \tag{5-4}$$

in which, ε_B and ε_P refer to the catalyst bed voidage and catalyst particle porosity, respectively. ρ_B is the bed bulk density in kg/m^3; r_k signifies the rate of k^{th} reaction in kmol/kg_s.s; η_k denotes the k^{th} reaction effectiveness factor; and a indicates the catalyst activity with respect to time, affected by sintering mechanism of deactivation.

Although the temperature fluctuation is not significant, the reaction rates are strongly affected by temperature. Moreover, the operating parameters (e.g., flowrate and pressure) can change the system temperature considerably. Therefore, the energy exchange among the phases needs to be included in the model through the energy balance equations. The following equation expresses the energy balance in the gas phase:

$$\rho_g C_{p,g} \frac{\partial(\varepsilon_g T_g)}{\partial t} = \lambda_g \frac{\partial^2 T_g}{\partial z^2} - \rho_g C_{p,g} \frac{\partial(u_g T_g)}{\partial z} - h_{gl}\xi_{gl}(T_g - T_l) \tag{5-5}$$

In Equation (5-5), T is the temperature in K; ρ represents the phase density in kg/m^3; λ refers to the phase conductivity in W/m.K; C_P introduces the heat capacity in J/kg.K; and h is the convective heat transfer coefficient in W/m^2.K.

The energy balance in the liquid phase is as follows:

$$\rho_l C_{p,l} \frac{\partial(\varepsilon_l T_l)}{\partial t} = \lambda_l \frac{\partial^2 T_l}{\partial z^2} - \rho_l C_{p,l} \frac{\partial(u_l T_l)}{\partial z} + h_{gl}\xi_{gl}\left(T_g - T_l\right) - h_{ls}\xi_{ls}(T_l - T_s) \tag{5-6}$$

The energy balance in the solid/catalyst phase is introduced by the following relationship:

$$(1-\varepsilon_B)\rho_s C_{p,s} \frac{\partial T_s}{\partial t} = h_{ls}\xi_{ls}(T_l - T_s) + \sum_{k=1}^{3} r_k\,\eta_k \rho_B a(t)\,(-\Delta H_k) \tag{5-7}$$

where ΔH_k refers to the heat of k^{th} reaction in J/kmol.

5.4.3 Kinetics of Hydrotreating Reactions

Reaction kinetics plays a critical role in mathematical modeling of the catalytic system. There are numerous reactions, taking place in the process of TA hydropurification in the TBR [285]. Among the hydrorefining reactions, three most important/influential reactions are generally considered. Figure 5-6 illustrates the hydropurification reaction mechanisms [285]. Table 5-3 provides information on the relative reaction kinetics [273]. In the first reaction, 4-CBA is hydrogenated to 4-HMBA and is then converted to pta in the second reaction. These two reactions mostly determine the hydropurification reactions efficiency and 4-CBA content in the final product. In parallel with the main reactions, there is a possibility for decarbonylation of 4-CBA. In this reaction, 4-CBA is converted to BA and CO. BA can increase the product acidity, and CO is a common poison to the Pd catalysts. The chance of decarbonylation reaction increases with the O_2 dissolution in the reaction mixture [285].

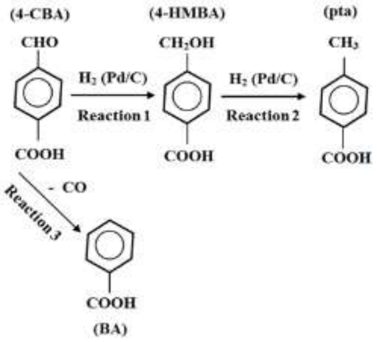

Figure 5-6: Mechanisms of 4-CBA hydropurification reactions [285].

Table 5-3: Kinetics data of hydropurification reactions [273].

Reaction Rate Expression	**Heat of Reaction**
$r_1 = 0.047\exp\left(\frac{-16.97}{RT}\right)\left(C_{C_8H_6O_3}\right)^{0.96}\left(C_{H_2}\right)^{0.24}$	$\Delta H_{r_1} = -83.82\ \ (\text{kJ/mol})$
$r_2 = 0.153\exp\left(\frac{-23.44}{RT}\right)\left(C_{C_8H_8O_3}\right)^{0.61}\left(C_{H_2}\right)^{0.75}$	$\Delta H_{r_2} = -121.88\ \ (\text{kJ/mol})$
$r_3 = 3406.6\exp\left(\frac{-88.87}{RT}\right)\left(C_{C_8H_6O_3}\right)^{0.54}$	$\Delta H_{r_3} = +18.73\ \ (\text{kJ/mol})$

5.4.4 Catalyst Deactivation Phenomenon

Catalyst deactivation is a serious concern in industrial catalytic processes. Catalyst replacement and process shutdown cost over billions of dollars to industry yearly [86]. The catalyst lifetime varies from a few seconds (e.g., cracking process) to a couple of years (e.g., ammonia synthesis). Although the catalyst deactivation is inevitable in most catalytic processes, some of its adverse impacts might be prevented, delayed, or even reversed [86]. The main mechanisms/causes for the catalyst deactivation are poisoning, fouling, and sintering (or thermal degradation) [372]. A better understanding of the catalyst deactivation mechanism can result in more sophisticated model of catalytic process, more stable catalyst design, and more accurate process optimization [86].

Pd/C catalysts that are used in TA hydropurification are deactivated through sintering mechanism [1, 2]. The Pd surface area decreases with increasing temperature. During the deactivation process, smaller Pd particles sinter (or agglomerate) into bigger particles, leading to the surface area reduction [1, 2]. We previously proposed the deactivation rate of the Pd/C catalyst from industrial hydropurification plant data as presented below [271]:

$$-r_d = -\frac{da}{dt} = A\,exp\left(\frac{-E}{R}\left(\frac{1}{T}-\frac{1}{T_R}\right)\right)a^m \tag{5-8}$$

In Equation (5-8), r_d refers to the deactivation rate in 1/h; A is a constant parameter, which is equal to 0.00092 1/h; E denotes the deactivation energy, which equals 5729 J/mol; R is the universal gas constant in J/mol.K; the exponent m is equal to 2.1; and T_R as a reference temperature equals 558 K. Parameter a relates the deactivation kinetics with the other operating parameters of the system by Equations (5-4) and (5-7).

5.4.5 Calculation of Model Parameters

The model parameters such as mass and heat transfer coefficients, phase holdup, and wetting efficiency depend on the physical properties (e.g., density, viscosity, and surface tension). The hydropurification system is operated under high pressure and temperature. Hence, the correlations and methods used to calculate the physical properties and the model parameters should be valid at the process operating conditions. The methods and correlations employed in this study are reported in the literature [271, 313].

5.4.6 Mathematical Solution

The developed model (Equations (5-1) to (5-7)) is a set of partial differential-algebraic equations, which include the nonlinear equations of reaction rates. The solution of the partial differential-algebraic equations requires the BCs and ICs, as listed below:

Condition	Spatial/Temporal	Concentration (C)	Temperature (T)	
BC1	at $z = 0$	$C_i = C_{i,in}$	$T_g = T_l = T_s = T_{in}$	
BC2	at $z = L$	$\frac{\partial C_i}{\partial z} = 0$	$\frac{\partial T_{out}}{\partial z} = 0$	(5-9)
IC	at $t = 0$	$C_i = C_i^{ss}$; $a = 1$	$T_g = T_g^{ss}$; $T_l = T_l^{ss}$; $T_s = T_s^{ss}$;	

The model needs to be solved in two steps. In the first step, the equations are solved assuming steady-state condition (e.g., the accumulation terms are set to zero). Then, the equations are discretized by backward finite difference method. The results obtained in this step are used as the ICs in the dynamic model which is solved by employing the backward finite difference method and method of lines. This solution approach converts the partial differential-algebraic equations to ordinary differential equations (ODEs). The obtained ODEs should be solved simultaneously. The solution procedure is coded into MATLAB 2017b environment. Further details about the mathematical model solution and the computer algorithm are found in Azarpour and Zendehboudi [313].

5.5 Results and Discussion

Hydropurification process is commonly employed to improve the product quality through removal of impurities in a catalytic reaction system with H_2. The product quality can be influenced by the operating parameters fluctuations, catalyst deactivation, and the process control procedure. Product quality is strongly related to the process efficiency and the operation costs. Therefore, control/monitoring of product quality is crucial in the industrial hydropurification processes. In this study, industrial TA catalytic hydropurification process is assessed through a dynamic mathematical three-phase heterogeneous model. The PTA product quality is analyzed by considering various factors including impurity concentration, reactor pressure, and temperature. The verification of hydropurification model is conducted using the operating data collected under normal operating conditions, which a normal practice for validation of simulation/modeling of a commercial production plant. To verify the control strategy for the product quality improvement, the process and production data at different operating conditions are required when fluctuations in the impurities concentrations and the amount of charged CTA powder are experienced. In most cases, it is not feasible to operate the plant at various conditions (other than normal operational) for data collection due to the safety, practical, and economic considerations/limitations as well as plant management policies. Thus, we have no available data to thoroughly assess the proposed control strategy; however, the developed model has been validated using normal operating data. The model is validated by comparing the model outputs with the industrial data, as demonstrated in Figure 5-7. The industrial data were collected during the lifetime of Pd/C catalyst, from its charge time (as the fresh catalyst) until the deactivation time. The model validation is made based on the 4-CBA concentration as the most important criterion of the product quality. The results reveal that the average and maximum absolute relative error percentages are 2.51% and 6.36%, respectively, implying the acceptable accuracy of the developed model. It also confirms that the model is reliable to be used for the system performance analysis and process optimization purposes.

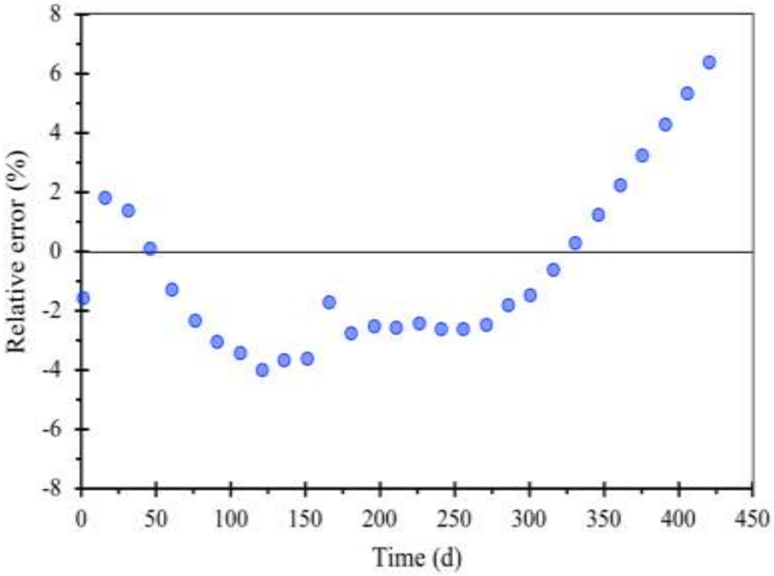

Figure 5-7: Validation phase of the developed hydropurification model.

The concentration of 4-CBA in the reactor feed is the most vital parameter affecting the PTA powder quality [32]. Figure 5-8 depicts the variation of 4-CBA concentration with time from the dynamic model. The model results and the industrial data of 4-CBA concentration in the product are in good agreement. According to Figure 5-8, the catalyst is entirely deactivated after 375 days of operation since at this particular time the 4-CBA content in the PTA powder is more than 25 ppm, which is the maximum allowable concentration in the final product. Based on the catalyst properties and operation conditions, the Pd/C catalyst lifetime is in the range of 6–18 months [2]. An increase in the 4-CBA concentration (in the product) with time implies a reduction in the catalyst activity. This reduction in the catalyst activity signifies that the hydropurification reactions in the TBR are not carried out efficiently for the conversion of 4-CBA to pta after passing a certain time.

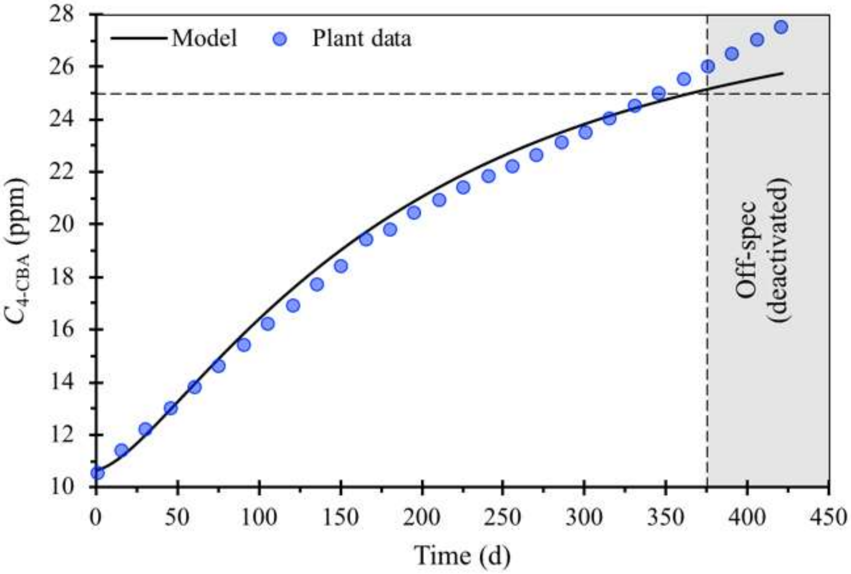

Figure 5-8: 4-CBA concentration during operation (Data taken from a PTA production plant [4]).

High fluctuations in the concentration of 4-CBA in the CTA powder charged into the feed mixing drum is a serious challenge in the hydropurification process. The engineering design of the reaction system considers the 4-CBA concentration in the CTA powder around 2500 ppm. Based on this specific concentration, the catalytic hydropurification reaction system is equipped with 0.5 wt.% Pd/C catalyst to convert the 4-CBA content in the TBR feed lower than 25 ppm.

5.5.1 Monitoring of CTA Impurity Concentration

The degree of catalyst activity is related to the active surface area that should be maintained at an acceptable level by controlling/monitoring concentration of 4-CBA in the CTA charged into the reaction system. The CTA powder produced in the first unit cannot be reprocessed even if the concentration of 4-CBA is high. Therefore, a suitable remedy is to effectively control the PX oxidation process. Figure 5-9 demonstrates a simple layout of the CTA powder charging system of the hydropurification process. The CTA powder having different concentrations of 4-CBA can be stored in either silo A or silo B; for example, low 4-CBA concentration in silo A and high 4-CBA concentration in silo B. The amount of powder charged into the reactor feed drum (RFD) can be controlled by a ratio controller to adjust the amounts of powder with low and high 4-CBA concentrations. Flowrate (W) from each silo can be set by altering the speed of the screw conveyor (SC). The produced mixture should provide a reactor feed stream having 23 wt.% of TA in the solution. The normal operating conditions of the feed flowrate and the 4-CBA concentration in the reactor inlet should be also maintained.

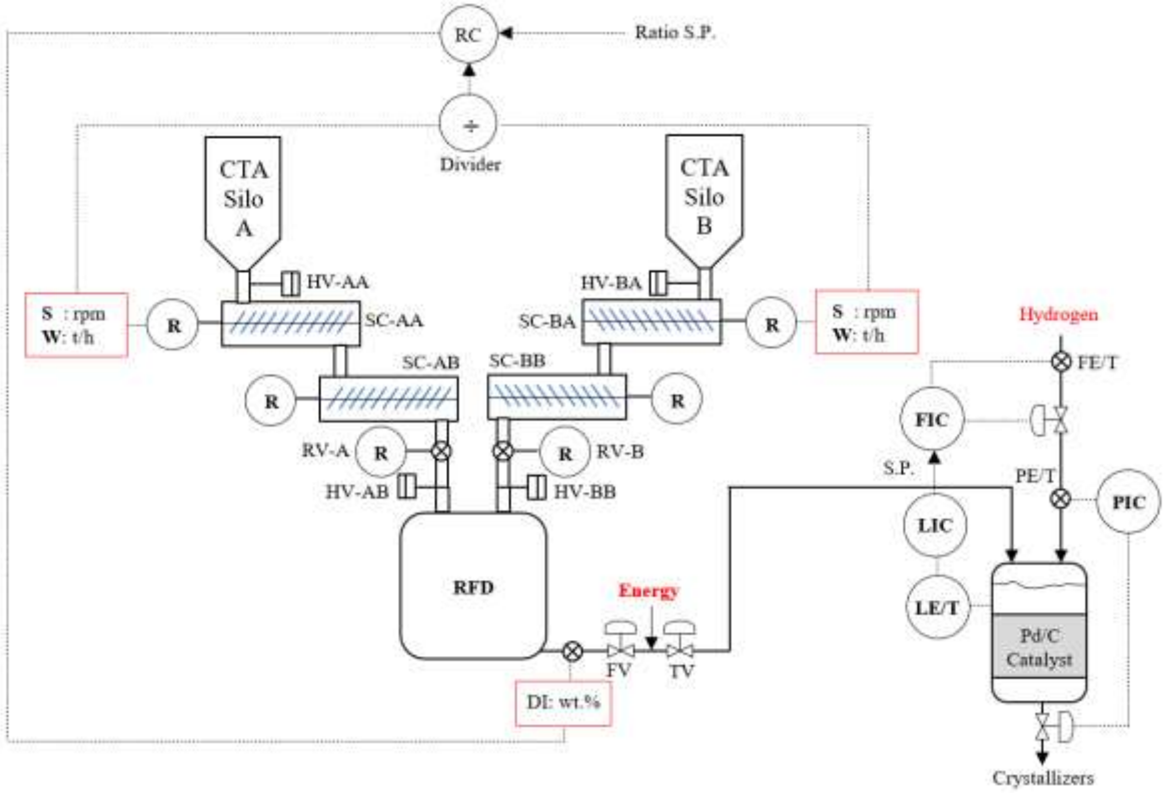

Figure 5-9: Simplified control layout of CTA powder charging system of PTA hydropurification unit (S: speed; DI: density indicator; HV: on-off valve; SC: screw conveyor; PIC: pressure indicator controller; FIC: flow indicator controller; RFD: reactor feed drum; LE/T: level element/transmitter; FV: flow valve; TV: temperature valve; RV: rotary valve; LIC: level indicator controller; R: running; rpm: round per minute; FE/T: flow element/transmitter; PE/T: pressure element/transmitter; RC: ratio controller; S.P.: set point; W: flowrate) [4].

Figure 5-10 shows the distribution of the 4-CBA concentration of the CTA powder produced in the CTA production unit during one year [4].

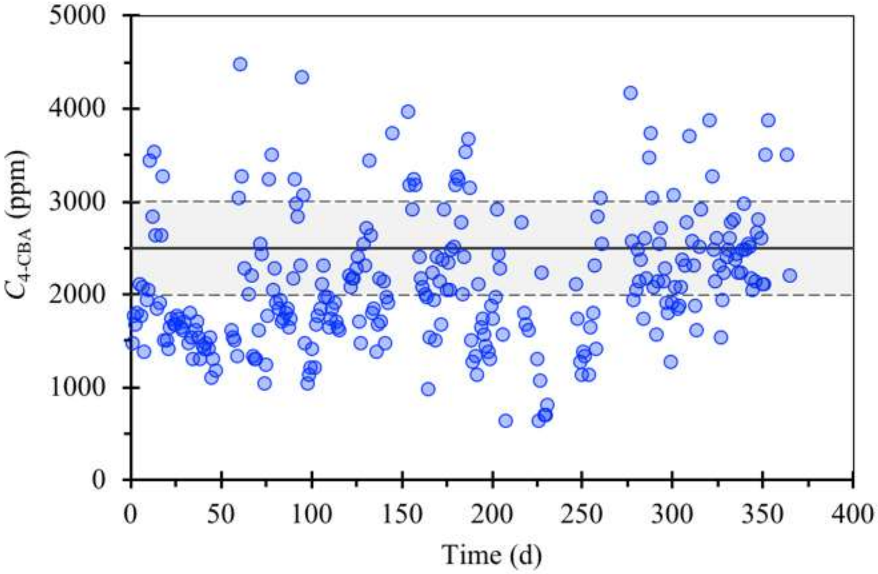

Figure 5-10: Variation of the 4-CBA content of the CTA powder over operation time [4].

Figure 5-10 reveals that the 4-CBA concentration of the CTA powder fluctuates considerably, and it sometimes exceeds the designed concentration limit (e.g., 2500 ppm). The concentration of 4-CBA between 2000 ppm and 3000 ppm is still considered normal. The powder containing the 4-CBA concentration exceeding the normal range noticeably affects the hydropurification system and eventually the PTA product quality. In addition, the CTA powder with a high concentration of 4-CBA accelerates the catalyst deactivation rate [263]. Figure 5-11 shows normal distribution of 4-CBA concentrations of the CTA powder within the acceptable range (e.g., between 2000 ppm and 3000 ppm), low range (e.g., less than 2000 ppm), and high range (e.g., more than 3000 ppm). The analysis is made based on the data collected from the industrial plant; samples are taken after each 8-hour operation (three samples per day). Therefore, each point is the daily average of three values of 4-CBA concentration. Based on Figure 5-11, around 48% of the impurity concentrations is less than the acceptable average (or 2000 ppm), and about 40% of the data is within the acceptable range, 2000–3000 ppm. Although the probability of the impurity concentration higher than the acceptable range is only 12%, it can adversely affect the process and catalyst performance. Therefore, mixing the CTA powder with low concentration of 4-CBA and that with high concentration of 4-CBA can lead to more efficient process in terms of product quality and catalyst lifetime. In this case, it is recommended to have two silos in the plant. Most of PTA production plants have such a flexibility. Implication of this strategy in the process design can help to control the plant more efficiently, leading to lower operation costs and higher product quality.

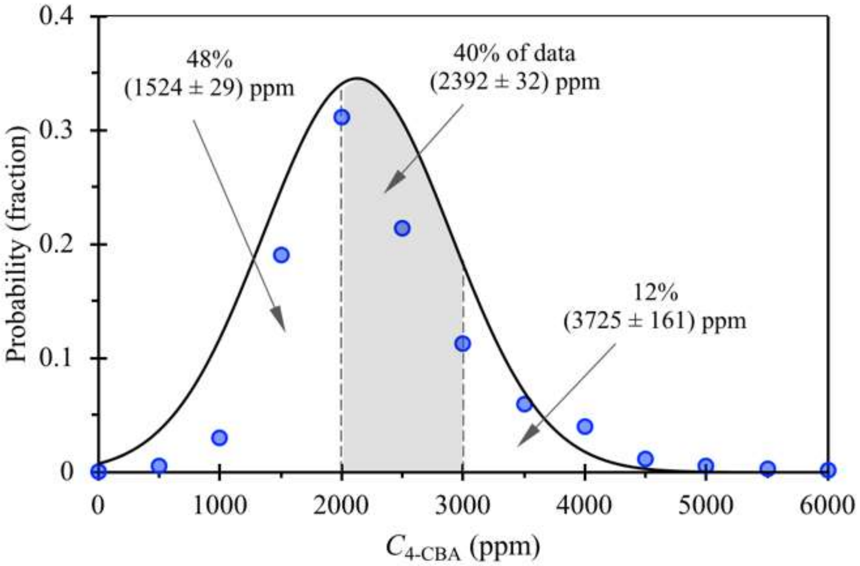

Figure 5-11: Statistical analysis for acceptable concentration range ($2000<C_{4\text{-CBA}}<3000$), low concentration range (<2000 ppm), and high concentration range (>3000 ppm) data. The solid line is normal distribution.

The scenario of mixing two CTA samples with different concentrations of 4-CBA is demonstrated in Figure 5-12 where the high concentrations of 4-CBA are 3000 ppm, 3500 ppm, 4000 ppm, and 4500 ppm.

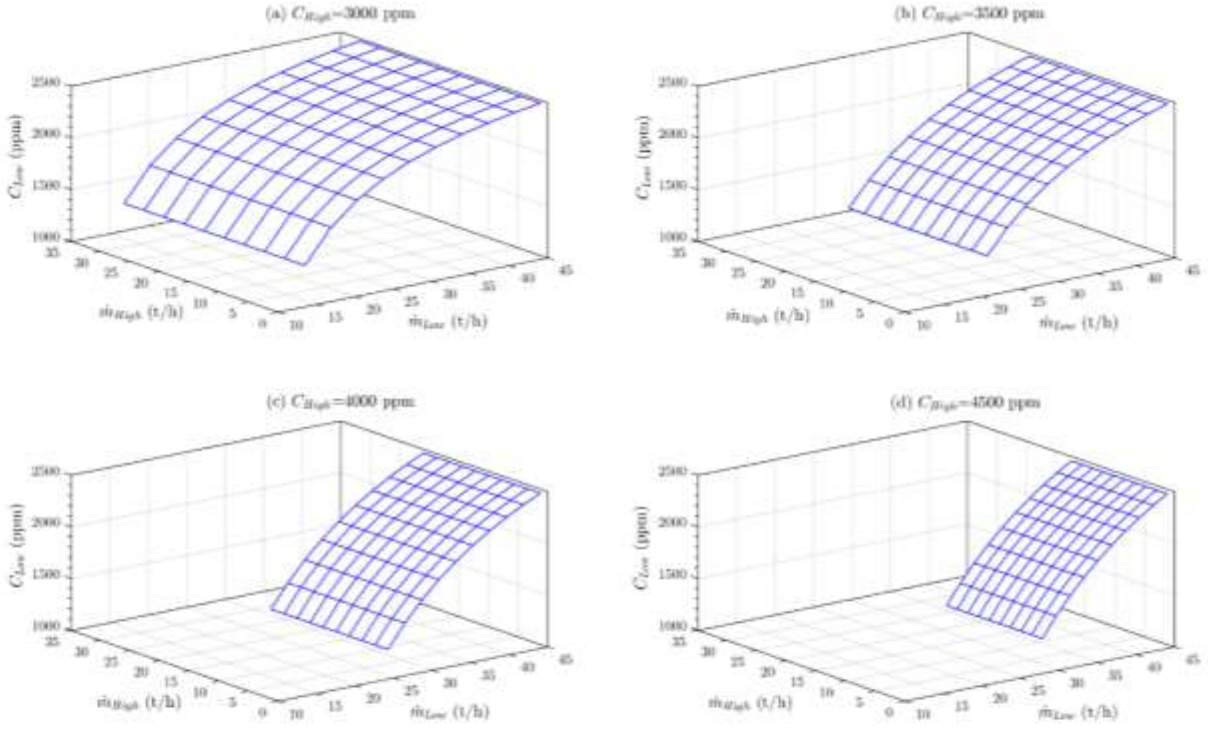

Figure 5-12: Mixing of the powder with low and high concentrations of 4-CBA at different high concentrations of 4-CBA.

Figure 5-12 reveals that lower mass flowrate of low-concentration 4-CBA powder and lower concentration of 4-CBA are required if the flowrate of powder with high concentration of 4-CBA increases. This behavior is valid if the TA concentration, 4-CBA concentration, and mass flowrate of the reactor feed are maintained at normal operating conditions (23 wt.%, 580 ppm, and 196 t/h, respectively). It is important that the mixing of the different levels of 4-CBA concentration should not affect the normal operating conditions.

Figure 5-13 depicts the mass flowrates ratio of the two CTA powder streams of low and high 4-CBA concentrations at various high 4-CBA concentrations.

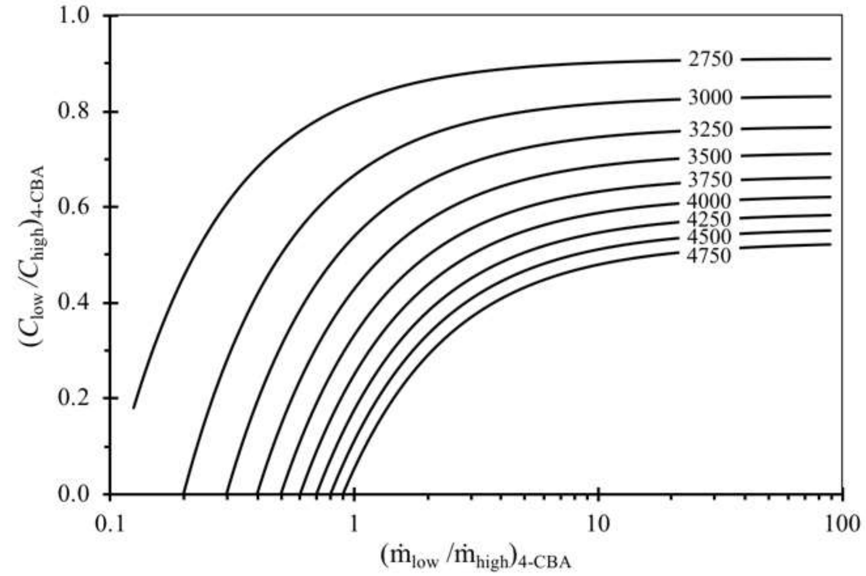

Figure 5-13: Mass flowrates ratio of low and high 4-CBA concentrations of the CTA powder at different high concentrations of 4-CBA in ppm.

When the concentration of 4-CBA in the silo increases, there is a limit for the mass flowrate of the high concentration 4-CBA stream to be mixed with the low-concentration 4-CBA stream. Because the flowrate of low-concentration 4-CBA stream cannot decrease the concentration of the mixed powder charged into the reactor considering the constraints of normal operating conditions (e.g., 580 ppm of 4-CBA in the reactor feed). For example, when the high concentration of 4-CBA powder stream is 3750 ppm, the maximum mass flowrate of the concentrated stream is 29.5 t/h, since the maximum mass flowrate of the low-concentration 4-CBA stream should be 15.5 t/h at a 4-CBA concentration of 1844 ppm.

5.5.2 Impact of Hydrogen Solubility

The solubility of the gas component(s) in gas-liquid systems is an important parameter in the design of hydroprocessing units [373]. The impact of pressure on the gas solubility in a liquid phase has been commonly evaluated by Henry's law since 1803 [374]. Dalton's extension of this law has been also successfully employed for numerous cases. These ideal laws can be effectively used where the association, chemical combination, polarity, and the deviation from the ideal gas law are not of importance [374]. In the design and analysis of multiphase reactors, the solubility of H_2 in organic liquids is a critical parameter [375]. Considering low solubility of H_2 in organic solvents, Henry's law is an acceptable solubility model for most binary systems [373]. However, design and modeling of hydroprocessing systems require more reliable and accurate data of H_2 solubility in the organic and/or inorganic mixtures. Solubility of H_2 in water is different from its solubility in the mixture of water and organic acid, though the mixture is mainly made of water (e.g., 75 wt.%). Most of the correlations for determination of the H_2 solubility in water and organic acid mixtures have been developed at very low temperatures and pressures. The H_2 solubility in TA and water solution is higher than that in water at the TBR operating conditions [285, 376].

Figure 5-14 illustrates the effect of H_2 on the product quality at normal operating pressure (73.5 barg) and TA solution concentration (23 wt.%) at various temperatures. The vapor pressure of the TA solution at 285 ^{o}C is 66 barg, leading to the H_2 partial pressure of 7.5 barg. When the temperature decreases by only one degree (e.g., 284˚C), the TA solution vapor pressure will be 65.2 barg; thus, the partial pressure of H_2 is 8.3 barg. It follows that the product quality improves, and the catalyst lifetime increases from 375 days to 405 days upon a reduction in temperature from 285 ºC to 284 ºC.

The vapor pressure of TA solution at 283˚C is 64.2 barg; hence, the partial pressure of H_2 becomes 9.3 barg. At this condition, the catalyst lifetime is extended to 445 days. It implies the positive effect of temperature reduction on the process efficiency. However, the process should be carefully (and safely) controlled because the low temperature limit is constrained by TA crystallization. An increase in the H_2 flowrate can also result in the reactor pressure fluctuation, which makes the process control difficult; the pressure fluctuation increases the Δy specification of PTA powder quality.

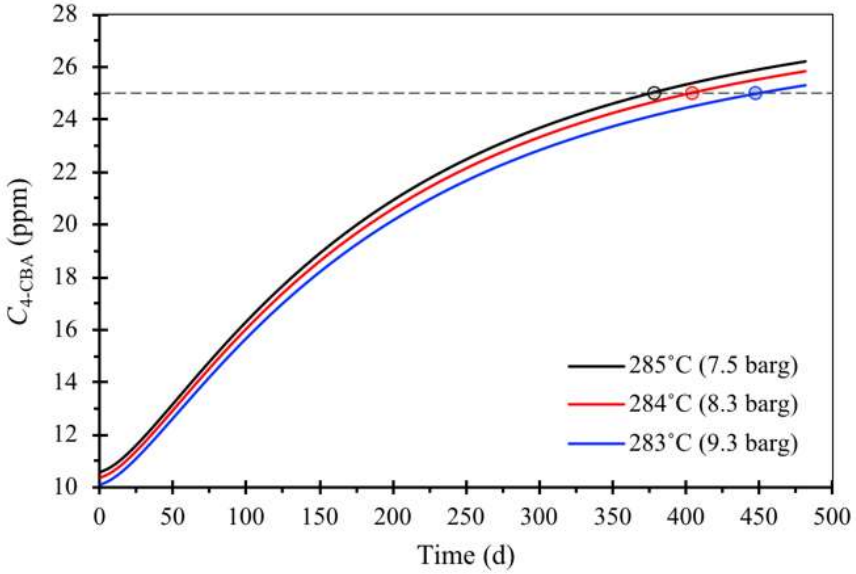

Figure 5-14: Effect of hydrogen partial pressure on the product quality upon change in temperature while maintaining the normal operating pressure of 73.5 barg and TA solution of 23 wt.%.

5.5.3 Off-Spec Product Reprocessing

In the hydropurification unit, off-spec product might be produced due to deviations in operating conditions and control system. The most important parameter, which makes the product off-spec, is the concentration of 4-CBA if it exceeds 25 ppm in the PTA product. Sometimes, the PTA powder with up to 55 ppm of 4-CBA can be utilized by the textile grade production factory. However, this level of contamination can cause serious operating difficulties (e.g., enhancement of PET polymerization side reactions, the polymer chain blockage, and the molecular weight reduction [377]). Therefore, 50 ppm of 4-CBA in the PTA powder product is generally considered undesirable as it leads to synthesis of an off-spec product. This low-quality powder should be recycled to the CTA silos and reprocessed. Alternatively, it is also possible to mix it with the CTA powder with very high concentration of 4-CBA. Figure 5-15 illustrates the amounts of off-spec PTA product and CTA powder with high concentration of 4-CBA produced under poor process control; the powder materials need to be mixed for maintaining the normal operating conditions of the hydropurification process. Although the off-spec PTA powder causes a reduction in the PTA production rate and sometime the CTA production rate, it is a good strategy to utilize the CTA powder having very high concentration of 4-CBA.

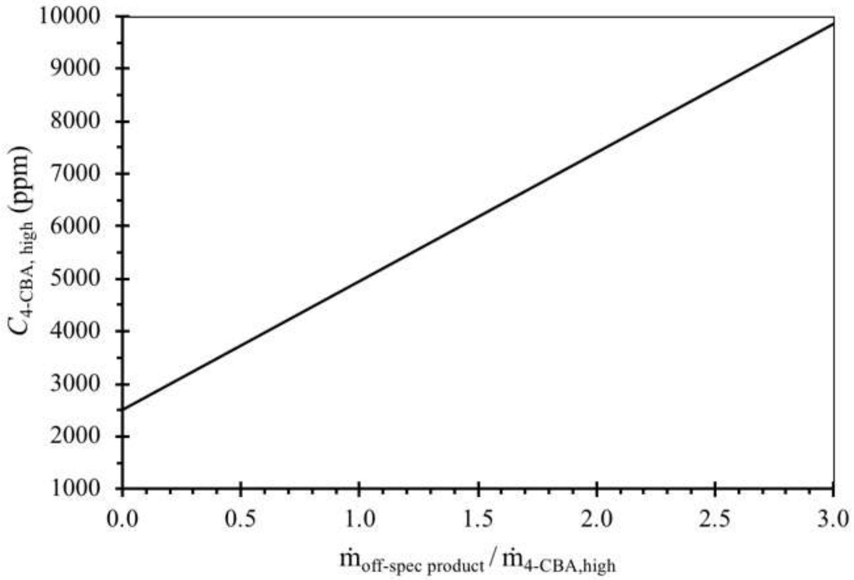

Figure 5-15: Mixing of recycled off-spec PTA powder with the CTA powder having a very high concentration of 4-CBA.

5.5.4 Reduction of Catalyst Surface Area

Catalyst activity loss occurs in a catalytic process. Hydroprocessing catalysts are continuously deactivated under industrial operating conditions [372]. Pd-supported catalysts are broadly employed in the hydrogenation processes for production of fine chemicals (e.g., pharmaceuticals) and bulk chemicals (e.g., PTA) [270]. The external Pd distribution leads to more accessible sites for the reactants. This results in a higher selectivity and less demand for the expensive metal catalyst content [2]. The dispersion and morphology of the metal phase and its electrostatic interactions with the support material considerably affect the catalyst activity and selectivity [270]. The average depth of Pd penetration is 15 μm. Higher external Pd distribution (lower Pd dispersion) might lead to a greater possibility for fast catalyst deactivation by abrasion, causing Pd loss [2]. Catalysts thermal degradation is a critical issue in high-temperature catalytic processes.

Thermal deactivation can be caused by a reduction in surface area due to the crystallite growth, a decrease in support area because of the support collapse, transformation of catalytic phase to non-catalytic phase, and a decrease in the active materials upon volatilization or vaporization [378]. Once the Pd/C catalyst is exposed to the industrial hydropurification conditions, it experiences a rapid Pd sintering. This might be due to the high Pd content in the external layer of the catalyst as well as weak interactions between the Pd and carbon support. It should be also noted that the Pd/C catalysts become ineffective at very high temperature. Hence, fresh Pd/C catalyst with large Pd dispersion is important from an industrial viewpoint. Metal sintering is the main reason for metal catalyst deactivation in industry. It was also found that the Pd surface area dramatically decreases with increasing temperature, implying Pd sintering is the major cause of Pd/C catalyst deactivation [2]. Figure 5-16 shows the influence of temperature on the catalyst deactivation (and/or total active surface area) for 0.5 wt.% Pd/C catalyst. It follows that an increase in temperature increases the rate of the catalyst surface area reduction and consequently lowers the catalyst lifetime. It should be mentioned that the temperatures of 315 ^{o}C and 255 ^{o}C for the reaction mixture are not practical in the industry. For instance, reducing the temperature below 273 ^{o}C results in crystallization of TA in the reaction mixture.

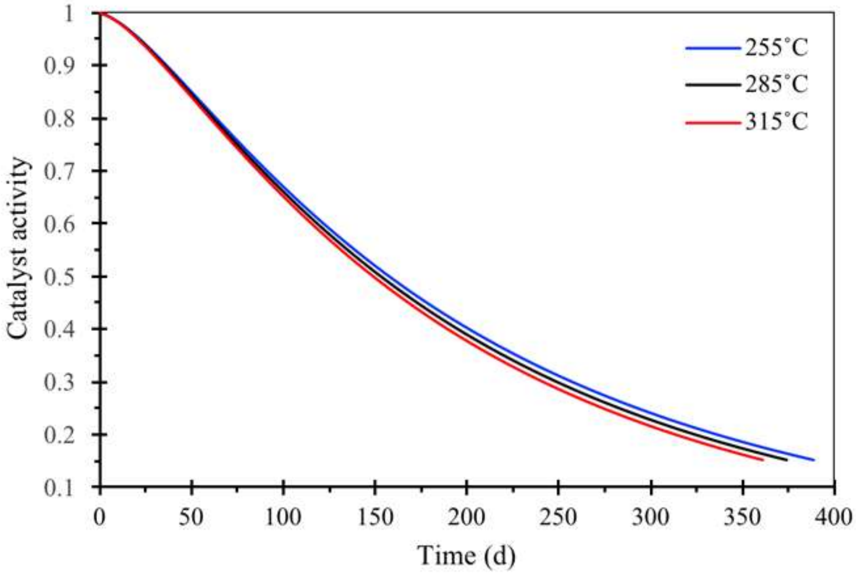

Figure 5-16: Active surface area of 0.5 wt.% Pd/C catalyst versus operation time at various temperatures.

Figure 5-17 shows the effect of temperature increase on declining rate of Pd/C catalyst surface area. It seems that there is a linear relationship between the catalyst surface area and temperature, for the temperature range shown in Figure 5-17. It is concluded that a temperature increase negatively affects the product quality and catalyst lifetime. The range of operating temperature in the industrial plant is usually narrow so that the temperature fluctuation is usually between 280 ^{o}C and 290 ^{o}C.

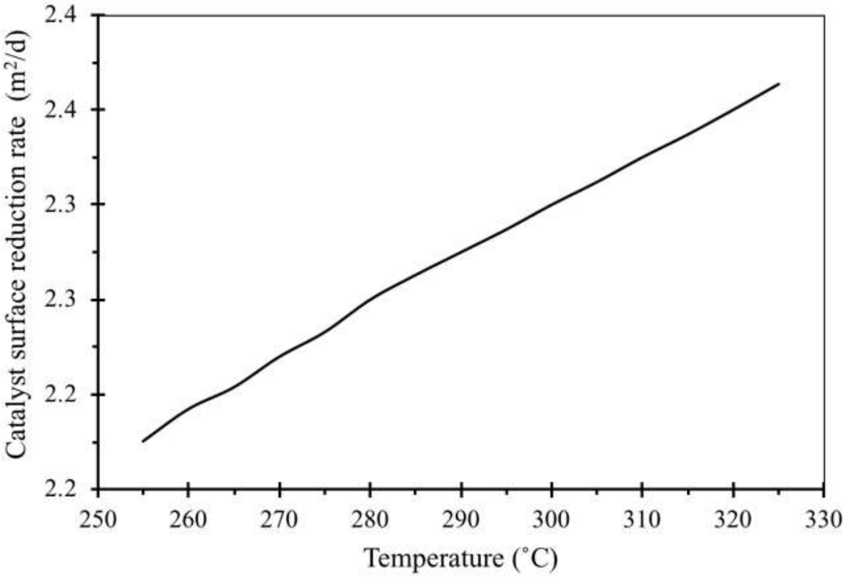

Figure 5-17: Variation of Pd/C catalyst surface area with temperature.

Figure 5-18 depicts a comparison between the catalyst surface area of the industrial Pd/C catalyst obtained from this work, and that for pure Pd surface area versus temperature based on the experimental results of Pernicone et al. [2]. Despite the difference in two systems, the results in Figure 5-18 show consistent trend/behavior; the catalyst surface area decreases when the temperature increases. To generate the experimental dataset for catalyst activity from raw data [2], we normalize the Pd surface area at different temperatures to that at the minimum temperature (285˚C). In fact, the *y*-axis shows the ratio of the catalyst surface area to the fresh catalyst surface area. As it is clear from Figure 5-18, the temperature has a little more impact on the Pd surface area, compared to Pd/C catalyst surface area. The difference is due to normalization at 285˚C and the fact that our deactivation model parameters are fitted to the operating conditions of the industrial reactor which is at 285˚C.

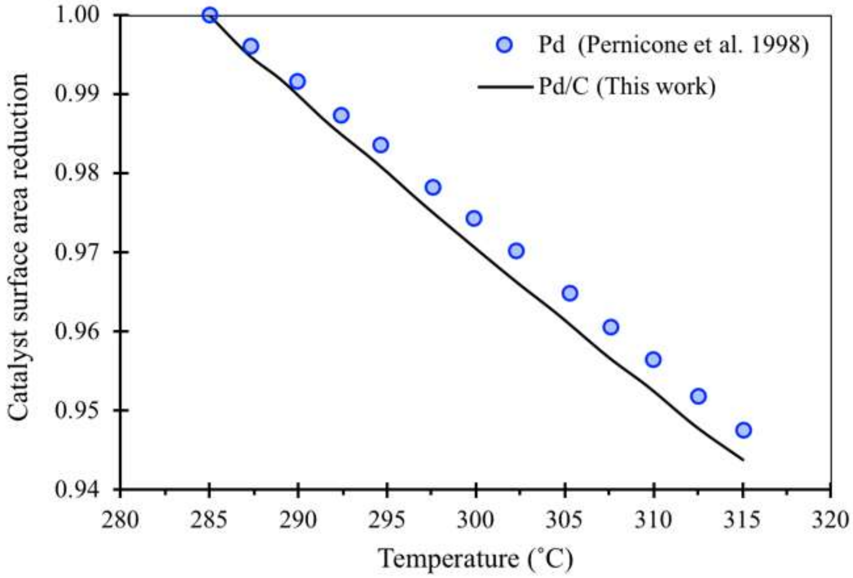

Figure 5-18: Effect of temperature on Pd/C catalyst and Pd surface area.

In an industrial operation, there are various factors affecting the process performance. A high process efficiency is usually linked to high product quality and low operating costs. In the hydropurification process, the most important parameter affecting the process efficiency is the quality of the feedstock. The quality of the CTA powder produced in the oxidation process cannot be improved, even if the quality is low. The unit does not allow for such flexibility to reprocess it. Therefore, a practical strategy is to properly control the oxidation process. High selectivity in the PX oxidation can be achieved by controlling the side reactions, reducing the PX over-oxidation to CO_2, and using optimal catalyst formulation [358]. Operating temperature and pressure have also appreciable impacts on the PX oxidation. 4-CBA concentration decreases with increasing temperature in the oxidation reactor (temperature is controlled by the reactor pressure). However, the PX reactivity does not increase when temperature exceeds a threshold value. Optimal temperature can be established by the control/adjustment of the catalyst composition and water concentration [7]. Utilization of higher amount of the catalyst in the process of PX oxidation can decrease the 4-CBA concentration in the CTA powder. However, this causes higher cost of operation and more operating challenges (e.g., difficulties in the catalyst recovery unit operation). A minor amount of water improves the PX oxidation rate, but high water content decreases the overall reaction rate [7]. The catalyst composition is also important. For example, the ratio of Co^{2+}/Mn^{2+} considerably affects each reaction steps for PX oxidation [7]. O_2 partial pressure can have a positive impact on the PX oxidation selectivity [357]. CO_2-assisted oxidation of PX can increase the selectivity since CO_2 can improve the O_2 solubility in the reaction mixture [359]. The impurities present in the PX and acetic acid can lead to production of unwanted byproducts [7]. The other important parameter is the reaction residence time to properly control the PX oxidation process. An increase in the residence time increases the byproducts production rate. There are several research investigations on the PX catalytic oxidation system in the literature. It was reported that zirconium [6, 379] and guanidine [365] can improve the process efficiency. Another research claims that TA can be directly produced upon the use of ionic liquids (e.g., $NHPI/O_2/HNO_3$) as an oxidative system in [bmim][OMs] with a selectivity of 98% [380]. Heterogeneous catalyst (e.g., μ_3-Oxo-Bridged Co/Mn cluster complexes encapsulated in zeolite-Y) is used to oxidize PX (100% conversion of PX) [381].

In the hydropurification process, there are some remedies to cope with the CTA powder with high concentration of 4-CBA. As mentioned earlier, an effective procedure can be employed to monitor the 4-CBA concentrations in the CTA powder. In addition, the production duration of the CTA powder with particular qualities is a vital aspect. In fact, the reactor pressure can be controlled to improve the process efficiency and catalyst utilization. Furthermore, accurate control of the reaction temperature can enhance the process performance.

5.6 Conclusions

In this study, a technoeconomic strategy is proposed to effectively control the PTA plant hydropurification process, leading to the significant reduction in its operating expenses. To achieve this goal, a dynamic dispersion model is developed based on theoretical transport phenomena, and reaction kinetics, and using an industrial-scale plant data. The validated model is used to evaluate the effects of vital operating parameters on the process performance. The negative impact of the CTA powder having high concentration of 4-CBA (as the process feedstock) on the process efficiency can be lowered/managed through using the feedstock with low concentration of 4-CBA. In this case, the mass flowrates of the two streams can be regulated to achieve design feed composition. It is concluded that increasing the H_2 partial pressure (by decreasing temperature) can enhance the process performance, resulting in better product quality with longer catalyst lifetime. Off-spec PTA powder can be mixed with the CTA powder having a very high concentration of 4-CBA to eliminate its impact on the shut-down time for the catalyst replacement. An increase in temperature can accelerate the sintering phenomenon of the Pd/C catalyst. The strategy proposed in this study can be efficiently applied in feedback control loop, and in operating procedures of the industrial plant to improve the process economy. The possible vulnerability potentials of the model include fluctuation in the 4-CBA concentration in the CTA powder, difficulty in separately storing the CTA powder with different levels of impurities, and possessing at least two CTA powder silos for achieving the product quality with a higher flexibility. Future research topics can be dedicated to the development of a stochastic model for the product quality control, employing a hydrodynamic model for the periodic operation of the hydropurification process, and conducting effective exergy and optimization approaches for attaining a greater performance from the production plant.

NOMENCLATURES

Acronyms

4-CBA - 4-carboxybenzaldehyde

4-HMBA - 4-hydroxymethylbenzoic acid

BA - benzoic acid

BC - boundary condition

CTA - crude terephthalic acid

DI - density indicator

FE/T - flow element/transmitter

FIC - flow indicator controller

FV - flow valve

HDN - hydrodenitrogenation

HDS - hydrodesulfurization

HPLC - high-performance liquid chromatography

HV - on-off valve

IC - initial condition

LE/T - level element/transmitter

LIC - level indicator controller

ODE - ordinary differential equation

Pd/C - palladium supported on carbon

PE/T - pressure element/transmitter

PET - polyethylene terephthalate

PIC - pressure indicator controller

PTA - purified terephthalic acid

pta - para-toluic acid

PTLD - p-tolualdehyde

PX - para-xylene

R - running

RC - ratio controller

RFD - reactor feed drum

rpm - round per minute

RV - rotary valve

S - speed

SC - screw conveyor

SimDis - simulated distillation

S.P. - set point

SS - steady-state

TA - terephthalic acid

TBR - trickle-bed reactor

TV - temperature valve

W - flowrate

List of Variables/Symbols

A - parameter of dynamic deactivation model (h^{-1})

a - metallic sintering dispersion parameter (-)

C - concentration ($kmol\ m^{-3}$)

C_P - heat capacity ($J\ kg^{-}1\ K^{-1}$)

D - axial dispersion coefficient ($m^2\ s^{-1}$)

d_P - diameter of catalyst particle (m)

d_R - diameter of reactor (m)

E - catalyst activation energy ($J\ mol^{-1}$)

H	-	Henry’s constant	(m^{3} MPa mol^{-1})
ΔH	-	heat of reaction	(kJ mol^{-1})
h	-	heat transfer coefficient	(W m^{-2} K^{-1})
k	-	mass transfer coefficient	(m s^{-1})
L	-	length of reactor	(m)
m	-	exponent in catalyst deactivation model	(-)
m^{o}	-	mass flowrate	(kg h^{-1})
m_{s}	-	mass of catalyst	
R	-	universal gas constant	(J mol^{-1} K^{-1})
r	-	reaction rate	(kmol kg$_{s}^{-1}$ s^{-1})
r_{d}	-	deactivation rate	(h^{-1})
S	-	catalyst active surface area	(m^{2} g^{-1})
T	-	temperature	(K)
T_{R}	-	reference temperature	(K)
t	-	time	(s)
u	-	superficial velocity	(m s^{-1})
z	-	axial coordinate	(m)

Greek Symbols

ε	-	hold up	(-)
ε_{B}	-	porosity of bed	(-)
ε_{P}	-	porosity of particle	(-)
η	-	effectiveness factor	(-)
λ	-	conductivity	(W m^{-1} K^{-1})
ξ	-	phase interface specific surface area	(m^{2} m^{-3})
ρ	-	density	(kg m^{-3})

ρ_B - bulk density (kg m^{-3})

τ - residence time (d)

Subscripts

g - gas phase

gl - gas to liquid

i - index of components

in - inlet to reactor

k - index of reaction

l - liquid phase

ls - liquid to solid

out - outlet from reactor

s - solid/catalyst phase

Superscripts

S - surface of the catalyst

ss - steady-state

6 CHAPTER SIX: Systematic Energy and Exergy Assessment of a Hydropurification Process: Theoretical and Practical Insights

Preface

A version of this chapter was submitted to Energy Journal. I collected the data, conducted the literature review, and wrote the first draft of the manuscript. I shared my process knowledge and experience with all co-authors. All co-authors were involved in the modeling and simulation phase. Mohamad Mohamadi-Baghmolaei also provided comments and inputs for the methodology section. In addition, Abdollah Hajizadeh had comments on the simulation phase and results and discussion section. Sohrab Zendehboudi also provided me with comments and feedback on all sections of the manuscript; he also edited the entire text.

Abstract

Improvement of a process efficiency and reduction of its operation costs are of the significant importance in chemical industrial plants. In this study, an effective approach is presented to analyze a hydropurification process, with focus on its energy utilization, operating costs, environmental impact in terms of CO_2 emissions, and exergy performance. The hydropurification process includes heat exchangers, pumps, crystallizers, reactor, and furnace. The vital operating parameters affecting the system performance are chosen by employing the Taguchi method. The process simulation is carried out in the environment of Aspen Plus® software, and the codes for the exergy calculation are written in MATLAB software environment. The results are in a satisfactory agreement with the industrial data (e.g., an error percentage of 3.73% based on the heat duty data of the steam preheaters for the reactor feed). The results verify that the optimal conditions lead to 15% reduction in the exergy destruction. Furthermore, the performance of the fourth and sixth heat exchangers can be enhanced by about 33.3%. In addition, the performance of the fourth crystallizer operation can be improved up to 18.7%. The furnace using expensive Therminol® 66 (as the heat transfer fluid) experiences a significant exergy destruction, and the combustion process can be controlled more accurately. Implementation of the proposed optimal conditions can lower the operation costs and the carbon tax by 9.96% ($20.5/h) and 14.75% ($14.54/h), respectively; and the CO_2 emission rate can be declined at the amount of 0.582 t/h. The results of this research can be applied to the relevant industrial sectors toward process performance improvement.

6.1 Introduction

Tremendous growth in the population and significant development in chemical and energy industries are the key factors for energy demand escalation [382]. Moreover, development of a nation is strongly dependent on energy [383]. The world is still dependent on the fossil fuels and their derivatives for the production of required energy, though they are considered as the most harmful energy resources [382]. In the past decades, the main environmental concerns of global warming and climate change have resulted in critical issues worldwide. High CO_2 concentration in the atmosphere is the major cause of greenhouse effects. CO_2 emissions are essentially resulted from the combustion of fossil fuels and the industrial processes [384]. Increase in the cost of primary energy, urgency of environmental concerns, and reduction in the use of fossil fuels have shifted the energy approach from the process performance to the efficient utilization of energy (reduction of required energy). Improvement in the process efficiency in terms of energy consumption leads to the cost-effective operation and more environmentally friendly system. Process efficiency and waste reduction in energy systems have gained considerable attention during the past two decades owing to the increase in energy demand and consumption, natural resources depletion, and environmental concerns [385-387]. The literature review shows that industrial sectors consume 37% of the world's total supplied energy [388]. The energy consumption share of the industrial plants fluctuates within the range of 30% to 70%, depending on the locations and applications (e.g., 70% for China) [389]. The industrial operation costs are significantly affected by the energy utilization and fuel compositions [390]. It was predicted that the world's energy consumption will be three-fold in the next 30 years [391]. The relationship between the sustainability and energy analysis verifies that the energy quality loss leads to an increase in the energy utilization sustainability [392].

Increase in the polyester utilization has dramatically increased the demand for purified terephthalic acid (PTA) [393]. PTA is a petrochemical product, which is used in the textile and polyester industries as a raw material [394]. It is also utilized for the production of polymer stabilizer, pesticides, light sensitive compounds, and animal feed supplements [395]. Even though PTA is an important raw chemical in industries, unfortunately, the overall efficiency of the process energy has declined due to the high costs of constructing/adding a new plant [396]. However, there is still a high potential for the enhancement of energy saving and the reduction of CO_2 emissions in the chemical plant [397]. Thus, improvement of productivity and energy efficiency of such a complicated petrochemical process by a proper energy optimization and analysis model can be essential [396]. Considering the AMOCO-MC process, PTA production is carried out in two different process units. In the first unit, p-xylene oxidation takes place in the acetic acid solvent and the catalyst system of Co, Mn, and Br [1]. The acetic acid recovery system is one of the most energy consuming units in the first PTA production unit [394]. In the second unit as the hydropurification process, the crude terephthalic acid (CTA) produced in the first unit is purified in a catalytic reactor equipped with 0.5% palladium over carbon (Pd/C) catalysts [2]. The most challenging task in the hydropurification process is to maintain the energy consumption at an optimum level. Optimization of the PTA process plays a key role in energy savings and emission reduction in the petrochemical industry [398]. In a research work on the pollution sources of PTA production plant, an environmental flow diagram method was used to assess and manage the environmental pollutants [399]. According to the results, the emission factors of acetic acid, PTA powder, hot oil, and CO_2 were 219.05, 44.6, 0.9, and 54661355.3 mg/ton of PTA product [399]. In a recent study, Chen et al. [400] conducted the assessment of energy efficiency and the optimization of the resource allocation to improve the production process of the complex chemical plants and to reduce CO_2 emissions. They employed an advanced technique of data envelopment analysis in combination with the cosine similarity. They applied the developed technique to the PTA production plant, which resulted in 1.22% energy saving in the process [400]. An energy optimization and production capacity model was presented by employing extreme learning machine (ELM) and incorporating affinity propagation clustering [397]. The affinity propagation method helps obtain the cluster of data to decrease multi-dimensional data and merge the data with high similarity. The case studies were ethylene and PTA production plants. It was found that there is a 99% accuracy in the production prediction. Moreover, the model could improve the energy efficiency and lower CO_2 emissions [397]. In another study on PTA plant, hierarchical-indicator comparison (HIC) method, which is based on the construction of energy efficiency indicators (EEIs) and an appropriate technique to utilize the indicators, was developed to evaluate the energy efficiency of the industrial plants (industrial energy conservative programs). PTA plant was chosen as a case study due to its diverse production technologies, moderate complexity of the production process, diverse energy consumption resources, and comparatively full coverage extent of EEIs types. They discussed about the correction of indicators' reference values, and implemented the method in accordance with the EEI system [401]. In another research, benchmarking was used as an analytical tool to predict EEIs of the key energy intensive industries. The research revealed that the average specific energy consumption of PTA plant is 5.3 GJ/ton. It was claimed that the results could be utilized as a benchmark for more efficiently use of the energy [402]. The literature shows that the energy evaluation of the industrial plants is of great importance. This assessment plays more crucial role for the processes that are operated under high temperature and pressure conditions, and utilize a significant amount of energy (e.g., PTA plant). This important aspect is more highlighted when such processes emit a considerable amount of CO_2 into atmosphere.

The energy balance is a basic technique in a process energy analysis. Also, it is essential for the process optimization and for the development of more sophisticated energy models, such as exergy analysis [403]. The energy analysis results determine the energy utilization efficiency. The classical energy analysis only provides basic information on the energy utilization in a thermal system. Such a method is unable to evaluate the energy quality. On the other hand, exergy analysis expresses a real efficiency, and is considered as a powerful tool in energy analysis of industrial sectors [390]. Exergy is introduced as the maximum theoretical work that a system can accomplish when it reaches equilibrium with the environment or the dead state [404, 405]. Exergy consumption takes place during actual process owing to irreversibility and conserved ideal process [405]. The accurate identification of the thermodynamic losses cannot be carried out by the energy analysis [405]. Exergy analysis can identify and quantify exergy destruction within a process due to irreversibility (i.e., cannot be utilized to produce work and should be probably eliminated) and the exergy losses (e.g., energy transfer to the environment) [406]. Exergy analysis is an advanced thermodynamic technique, which is employed as a modern tool for the evaluation of engineering processes in terms of energy and exergy efficiency [403]. Studies on the exergy-based analysis of PTA plant are scarce. The latest investigation was conducted by Ghannadzadeh and Sadeqzadeh

[407]. They conducted an overall exergy analysis for the identification of low exergy efficient units of a PTA plant. They reported that the oxidation unit has the largest exergy loss; they suggested using a few reactors in series with the gradual decrease in temperature to reduce the losses [407]. Mingyan et al. [408] simulated two PTA production technologies using Aspen Plus. Exergy analysis of the units in the two PTA production plants was carried out. The results revealed that the main exergy losses are observed/identified in air compressor unit, oxidation reaction system, energy recovery, and solvent dehydration [408]. There are numerous studies in the literature, focusing on the exergy-energy analysis of other industrial process systems. One of the most recent studies was performed by Mohamadi-Baghmolaei et al. [385]. They conducted exergy, energy, economic, and environmental (4E) analysis of a gas sweetening plant. Different concentrations of methyl-di-ethanolamine and di-ethanolamine were considered in the simulation phase and 4E analysis. The results indicated a considerable reduction in CO_2 emissions at the amount of 2894 t/y in comparison with the existing working/operating conditions [385]. In another study, the exergy analysis of a biomass-fueled steam power plant for industrial combined heat and power plant with district cooling and heating media was performed. The exergy-energy analysis, which was fulfilled by different indexes in accordance with the first and second thermodynamic laws, revealed that the maximum exergy destruction occurs during the processes of combustion and steam generation [409]. Conventional and advanced exergy analyses of an industrial ethylene cracking furnace were performed by Yuan et al. [410]. The steady-state simulation and conventional exergy analysis showed the high exergy destruction in the radiation section of the combustion process. However, the advanced exergy analysis, which is accomplished by the incorporation of exogenous/endogenous and unavoidable/avoidable parts in the analysis, indicated

that the largest exergy destruction happens in the tube reactors in the radiation section [410]. Zhang et al. [411] implemented an exergy-energy analysis of coal-fired industrial boilers using thermal data of 141 units. The exergy model was developed by employing the first and second laws of thermodynamics. The results showed that the main heat loss takes place in the flue gas and unburnt carbon, and the greatest destruction of exergy is attained in the coal combustion and heat transfer system due to the process irreversibility. They also reported the average CO_2 emissions of 147.13 kgCO_2/GJ from the 141 units, which can be reduced significantly if the efficiency of the boilers reaches the target level suggested in the standard [411]. Focusing on food industries, Soufiyan and Aghbashlo [412] performed an interesting exergy analysis on a yogurt drink production plant. Using the thermodynamic laws, the exergy efficiency and destruction of different units in the plant (e.g., steam generation, milk pasteurization, and above-zero refrigeration) were analyzed. The highest exergy destruction happens in the boiler-compressor unit of steam generation process [412]. Considerable energy consumption and significant pollution emissions in the iron and steel industry motivated Wu et al. [413] to conduct an integrated evaluation of energy, exergy, and CO_2 emissions in a typical relevant industry. They found that there is an urgent need in the improvement of the sinter stand and in the redesign of the wet quenching process. Through adopting the industrial symbiosis measures, the overall exergy and energy efficiencies can be also improved. Moreover, CO_2 emissions can be dramatically decreased if the use of renewable energy and solid waste recycling are implemented in the energy system structure [413]. In another energy-exergy analysis, an industrial fluidized bed drying process of puddy was assessed. The results obtained from the developed model revealed that only about 34% of the exergy is utilized in the puddy drying, and the remaining amount of exergy is wasted. They claimed that the insulation of the dryer and the exhaust air recycle can improve the exergy efficiency [414].

After careful review of the energy and exergy-based studies on PTA plant, it is understood that there is no detailed techno-economic and exergy-based study, which aims to evaluate the energy analysis of the system through hybridized strategies of process economy, energy assessment, and exergy analysis. Therefore, the process efficiency can be evaluated by the incorporation of the operating parameters with the cost metrics/measurements. The employment of the industrial data for the analysis enhances the reliability of the developed model and the obtained results. By implementing the hybridized techno-economic and exergy-based evaluation of PTA unit, the energy consumption of the system can be optimized, leading to a cost-effective and environmentally friendly process. Hence, an optimization methodology is required by considering the most vital operating parameters that influence the process economy, process energy utilization, and pollution generation. The employment of the mentioned techniques leads to the identification of thermodynamic imperfection and the consideration of work and energy separately. The literature review shows that the studies carried out on PTA production plant mainly focus on a small part of an operation unit (e.g., solvent recovery of CTA unit).

In this study, an exergy-based concept is applied to extend the energy/thermodynamic analysis of an industrial plant. PTA hydroprocessing unit is chosen as a case study. The main contribution of the current study is the exergy-based techno-economic evaluation of the PTA unit, and to suggest the solutions/remedies to improve the system efficiency, demonstrating the capacity of exergy analysis as an analytical tool. The simulation of the hydropurification process is carried out by the

Aspen Plus® process simulator, which is extended carefully to incorporate real-time computation of chemical and physical exergy. Eventually, a comparison between the energy efficiency of the current hydropurification process and that of the modified process is made to determine the feasibility of the proposed suggestions in terms of application to the relevant industrial sector.

6.2 Theory and Background

This section includes the theoretical and practical aspects of the PTA production plant as well as previous related research investigations to provide a proper workflow for the performance evaluation of the case study.

6.2.1 Literature Review

There have been numerous research investigations on the PTA process plant [415-421]. For instance, Han et al. [422] used partial least square methods to analyze the product quality fluctuation in an industrial PTA production process. The goal was to detect and eliminate the main sources of changes in the product quality, using the process historical data and quality variables. It was concluded that the catalyst concentration and the production flow rate considerably affect the product quality. They proposed a novel control system to stabilize the catalyst concentration and operating conditions based on a simple linear equation while encountering the variations in the process throughput of PTA production [422]. In another study, a dynamic model for simulation of the PTA solvent dehydration process was developed to analyze and characterize the process [423]. The developed model as a temperature differential equation was applied to an azeotropic distillation column that separates acetic acid and water with n-butyl acetate as an entrainer. The simulation was carried out with focus on the flowrates of feed and aqueous reflux. The results revealed that the reflux flowrate is a highly effective parameter, and the temperature is also a determinant factor in the concentration of acetic acid [423]. In the solvent (acetic acid) recovery unit of PTA production plant, a small amount of p-xylene and methyl acetate (byproduct) may enter the acetic acid dehydration system [424]. A research work was carried out to obtain the UNIQUAC model of the quinary system (water, acetic acid, p-xylene, methyl acetate, and n-propyl acetate) of acetic acid dehydration through correlating the phase equilibrium data collected from the literature and the experimental data. The accuracy of the dehydration model built in Aspen Plus® was ±6%. The sensitivity analysis showed that reduction in the water content of the bottom product of the distillation column as well as decrease in the column reflux flowrate can lead to the significant energy saving [424]. The dynamic behavior of the hydropurification process in the PTA production plant was assessed by developing a new model for deactivation of Pd/C catalyst. The proposed dynamic mathematical model of the hydropurification process confirmed that an increase in hydrogen flowrate and reactor feed concentration of TA can enhance the system efficiency in terms of production rate and catalyst lifetime. However, effective monitoring of 4-carboxybenzaldehyde (4-CBA) concentration in the feed is critical to achieve the targeted performance [271]. Li et al. [267] proposed a control strategy/structure to improve the hydropurification efficiency of the PTA plant through employing the data obtained from the dynamic model of the work conducted by Azarpour and Zahedi [263] and the results from Aspen Dynamics software. It was found that the proposed control loops, which are designed based on stepwise heuristic simulation and analysis, could result in the higher production profit [267]. Development of an accurate simulation and optimization model for a petrochemical plant with focus on energy consumption is a challenge due to the small datasets [398]. A virtual sample generation procedure by using the Monte Carlo algorithm and particle swarm optimization (PSO) algorithm was proposed to enhance the precision of the energy efficiency analysis. Then, an accurate model was presented with the extreme learning machine (ELM) by using the synthetic data. The model validation was carried out based on the data of the PTA solvent recovery system and the ethylene production system. It was revealed that the model could be used to reduce the acetic acid consumption [398]. Energy analysis and optimization play a crucial role in the sustainable development of a chemical process [396]. Geng et al. [396] suggested an energy analysis and optimization procedure on the basis of ELM to tackle the high-dimensional and noise data in the complicated chemical process. Index decomposition analysis was used to group the high-dimensional data to three performance indexes of the structure effect, activity effect, and intensity. The developed model was used to conduct the energy analysis of PTA solvent dehydration system and the ethylene production plant, verifying that the method has excellent features such as fast learning, high accuracy, and stable outputs [396]. In another study by Geng et al. [425], they used fuzzy C-Means algorithm to cluster the input attributes of the high-dimensional data and the analytic hierarchy process to filter the redundant data. Thereafter, the selected/fusion data was considered as the input of ELM. The developed model had a higher performance with regard to the convergence speed, accuracy, and generalization. The model was applied to the PTA solvent recovery system and the ethylene production plant. It was found that the model could be used to increase the energy utilization efficiency and decrease CO_2 emissions [425]. Azarpour and Zendehboudi [313] developed a dynamic heterogeneous model for the PTA hydropurification process unit considering the flow non-ideality. The model results revealed that a decrease in the Pd/C catalyst particle size and an increase in its porosity can improve the system efficiency in terms of product quality and catalyst lifetime [313]. Accurate energy modeling of petrochemical processes is a demanding task due to the high nonlinearity and uncertainty characteristics. Xu et al. [426] proposed a novel prediction intervals method, which is usually used to deal with the uncertainty prediction along with the confidence intervals method, by incorporating error and self-feedback ELM and PSO. The developed model was applied to the PTA solvent dehydration system. It was concluded that the proposed procedure can be used as an efficient tool for energy consumption prediction to make better plans for energy saving [426]. In a research work, a model using a latent variable-based efficient functional link learning machine was proposed. The model was structured based on three features: extension of the energy modeling data to highly nonlinear space using a nonlinear function expansion block; utilization of the extended space to remove the redundant data; and employment of ELM to train the model for faster learning speed. The validation of the model was done using the data of the PTA solvent recovery system. They concluded that the proposed model is more accurate with a higher training speed, and it can be used for effective energy analysis of the petrochemical processes [364]. Geng et al. [362] developed an energy-saving model with ELM, through employing interpretative structural modeling and analytic hierarchy process. The developed model was applied to the solvent recovery of PTA plant and ethylene production process. It was concluded that the model could predict the PTA and ethylene production rates at the accuracy of 99% and improve the efficiency of energy utilization [362]. In another energy modeling study, an energy saving model was proposed by utilizing long short-term memory on the basis of attention mechanism. The effectiveness and reliability of the model were validated using the dataset of University of

California Irvine. Then, the model was used to simulate the PTA solvent recovery system and ethylene production system. The model could be employed to reduce the energy consumption of the relevant industrial sectors [427].

6.2.2 Hydropurification Process Challenges

Operation of hydropurification process is challenging since it deals with the control of a slurry system under high temperature and pressure. Slurry phase poses critical operating issues, such as the transfer lines blockage and the equipment performance reduction. Another important stage of the process is the effective dissolution of the solid phase into the liquid/solvent phase before introducing the feed to the reaction system filled with the solid catalysts. Therefore, temperature control is a crucial matter in the hydropurification process. The temperature of reactor feed mixture is increased by the utilization of high pressure steam and hot oil. The steam is generated in the crystallization process, and a relatively expensive oil is required to run the process furnace. The most commonly oils used in the hot oil furnace are Therminol® 66 and Jarytherm® DBT. They generally encounter the risk of degradation under high temperature conditions. It should be noted that although the oil is purchased based on the process design and operation needs, improper control of the process and exposure to high temperature for a long period can deteriorate the oil quality. In the AMOCO process, the temperature of the hot oil supply is controlled at 316 ^{o}C. If the oil degradation takes place, its replacement and the system cleaning take a significant amount of time. In this condition, the production process should be stopped, and cleaning process could be costly. Therefore, controlling the process at a safe energy level is crucial. The other concern of the process is the deactivation of the expensive Pd/C catalyst. The main cause of the catalyst deactivation is sintering (thermal degradation) [1, 2]. These two operating concerns further highlight how crucial the process temperature control is. Therefore, possible reduction in the process temperature can lead to a considerable decrease in the process costs and more efficient control of the process. Exergy and energy analysis of the hydropurification process can offer the practical solutions to a more energy-efficient process.

6.2.3 Reaction Mechanisms

Reaction kinetics is an important factor in the analysis of a process system. This parameter is included in the mass balance equation to compute the conversion of components. It is also incorporated into the energy balance to determine the reaction heat and examine its impact on the temperature of the reaction mixture. The reaction rates are expressed in the form of empirical models that are obtained from the experimental observations. It is crucial to establish the real operating conditions in the lab so that the obtained reaction rates can be used for the actual/industrial process whose operating conditions are close to the experimental conditions. There are some reactions, occurring in the hydropurification reaction mixture [285]. The expressions of the reaction rates of 4-CBA hydrogenation taking place in the reaction mixture of the hydropurification process trickle-bed reactor (TBR) are given below [273]:

$$r_1 = 0.047\, exp\left(-\frac{16.97}{RT}\right) C_{4-CBA}^{0.96}\, C_{H2}^{0.24} \qquad ; \Delta H_1 = -83.82\ kJ\ mol^{-1} \tag{6-1}$$

$$r_2 = 0.153\, exp\left(-\frac{23.44}{RT}\right) C_{4-HMBA}^{0.61}\, C_{H2}^{0.75} \qquad ; \Delta H_2 = -121.88\; kJ\; mol^{-1} \tag{6-2}$$

$$r_3 = 3406.6\, exp\left(-\frac{88.87}{RT}\right) C_{4-CBA}^{0.54} \qquad ; \Delta H_3 = 18.73\; kJ\; mol^{-1} \tag{6-3}$$

where *r* is the rate of reaction in kmol/kg$_c$.s; *R* represents the universal gas constant in J/mol.K; C denotes the concentration in kmol/m^3; and *T* signifies the temperature in K. Figure 6-1 shows the mechanisms of the most important hydropurification reactions [285]. According to the mechanisms, 4-CBA is initially hydrogenated to 4-hydroxymethyl benzoic acid (4-HMBA) and is then synthesized to para-toluic acid (pta). These two reactions greatly determine the efficiency of the hydropurification reactions and the magnitude of the 4-CBA concentration in the final product. In parallel with the major reactions, the decarbonylation of 4-CBA might take place. In the 4-CBA decarbonylation reaction, benzoic acid (BA) and CO are formed. CO is a common poison to the Pd catalysts, and BA can enhance the product acidity. The possibility of decarbonylation reaction increases with oxygen dissolution in the reaction mixture [285]. These three reactions are incorporated in the simulation phase.

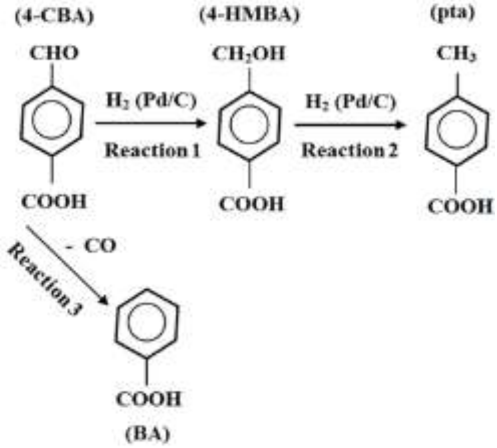

Figure 6-1: Kinetics of hydropurification reactions [285].

6.3 Process Description

Knowledge on the process operation is required to develop suitable models in terms of practical and theoretical aspects. It helps understand the process details and develop more reliable and accurate model, representing the process. Terephthalic acid (TA) is an important chemical in the industries of modern polymer and textile [428]. Purified terephthalic acid (PTA) is utilized as a raw material in the production of various petrochemicals, such as polyethylene terephthalate (PET), dye, and polyester film [429]. AMOCO is the most commonly used process technology for the production of PTA [7, 357]. PTA is processed in two different units. In the first unit as the production of crude terephthalic acid (CTA), p-xylene is oxidized to TA in a CSTR reactor, filled with acetic acid as a solvent and a homogeneous mixture of Co, Mn, and Br as a catalyst. The CTA obtained in this unit has about 3000 ppm of 4-carboxybenzaldehyde (4-CBA) and some colored polyaromatic compounds as the impurities. These impurities, especially 4-CBA, have an adverse impact on the polymerization process. Therefore, in the second unit as the hydropurification process, CTA is purified in a trickle-bed reactor (TBR), packed with 0.5 wt.% palladium supported on carbon (Pd/C) catalyst. 4-CBA is hydrogenated to para-toluic acid (pta) in a reaction mixture whose main component is water as the solvent within a temperature range of 270-290 ^{o}C [1]. The most important section of the hydropurification process is the TBR. A proper control of the reactor is not restricted to only controlling the reactor itself since its process behavior is affected by the performance of other equipment and process units (e.g., preheaters). A simplified structure of the hydropurification system is illustrated in Figure 6-2. The CTA powder is charged into a slurry feed drum (SFD) mixed with the filtrate coming from rotary vacuum filter (RVF) and the condensate from the condensation system. The reactor feed is heated up in two sets of heat exchangers. In the first series of the heat exchangers, the heat transfer medium is the steam generated in the crystallizers. The amount of energy existed in the steam cannot enhance the reactor feed temperature to a required level. Thus, the second set of the heat exchangers is supplied with a hot oil medium, which is heated up in a furnace. The temperature of the outlet stream of the heat exchangers is about 285 ^{o}C, which ensures the complete dissolution of the CTA powder into water. The hydrogenation reactions of 4-CBA occur in the TBR packed with Pd/C catalyst under a pressure of 73.5 barg with hydrogen. The reactor outlet mixture is introduced into five crystallizers. In the crystallizers, the produced pta remains in the liquid phase. Then, the slurry is transferred to a few centrifuges to separate the solid TA. The separated solid TA is mixed with water again and filtered in a rotary vacuum filter (RVF). The wet TA is dried in a rotary dryer using low-pressure steam. The powder quality is determined in the plant laboratory. The sample is taken at the end of the drier. The powder is transferred to the checking silos by a powder conveying system (PCS). If the product is on-spec, the powder is transferred to the final silos by a PCS. The product is recycled to the beginning of the process (CTA silos) in case of off-spec powder production.

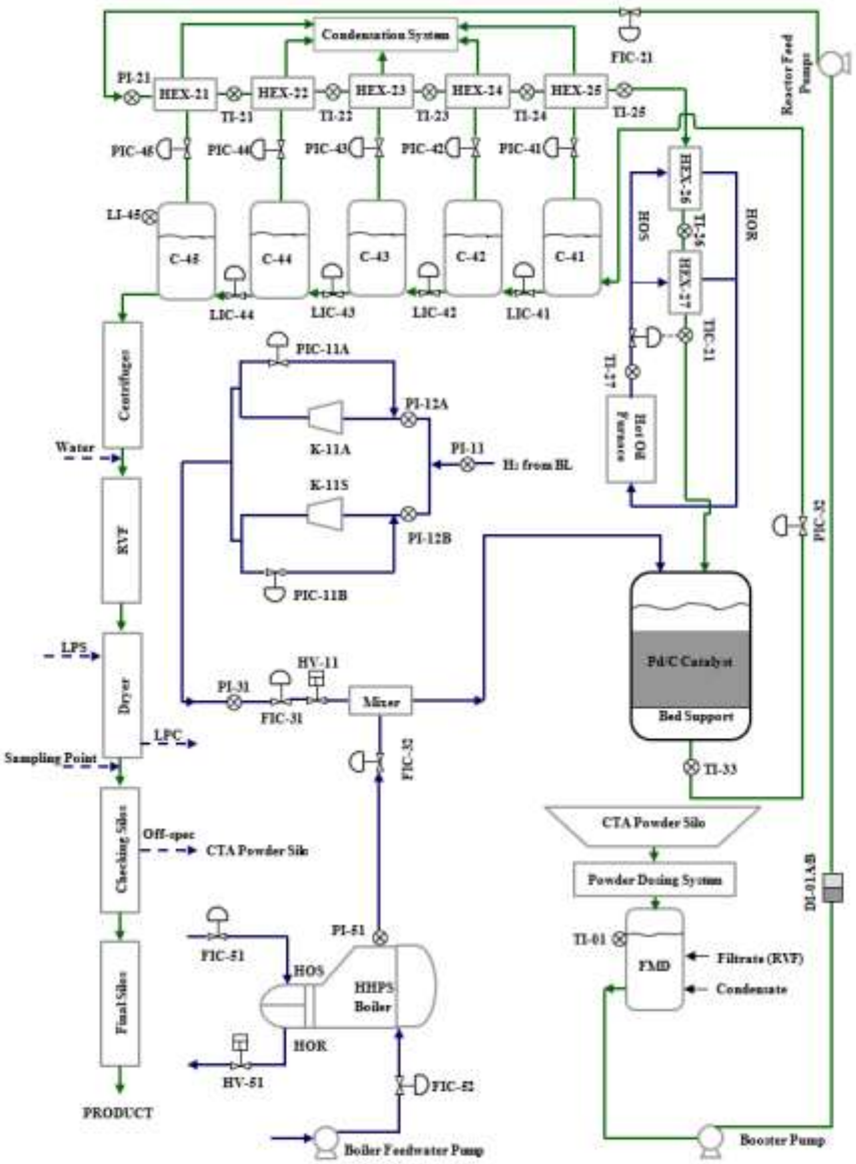

Figure 6-2: Simplified layout of PTA hydropurification unit (FMD: feed mixed drum; HEX: heat exchanger; PI: pressure indicator; TI: temperature indicator; TIC: temperature indicator controller; C: crystallizer; PIC: pressure indicator controller; FIC: flow indicator controller; HV: on/off valve; RVF: rotary vacuum filter; LPS: low pressure

steam; LPC: low pressure condensate; HOS: hot oil supply; HOR: hot oil return; LI: level indicator; LIC: level indicator controller; K: compressor; DI: density indicator; BL: battery limit; HHPS: high-high pressure steam) [4].

Table 6-1 presents the operating conditions of the hydropurification process, the catalyst specifications, reactor characteristics, and the designed set-points of operating variables [271].

Table 6-1: Process information of the PTA hydropurification unit [271].

Attribute	**Parameters**	**Values**	**Unit**
Operating conditions	Pressure	73.5	barg
	Temperature	285	˚C
	TA concentration in feed	23	wt %
	Feed flowrate	196	t/h
	H_2 flowrate	13.2	kg/h
Catalyst bed (Reactor)	Length	7.4	m
	Diameter	2.8	m
	Porosity	0.44	m^3/m^3
Catalyst	Bulk density	475	kg/m^3
	Particle diameter	3.53	mm
	Particle porosity	0.61	m^3/m^3
	Total surface area	900-1100	m^2/g
	Pd content	0.5±0.02	wt.%
	Activated carbon	99.5	wt.%
	Water in wet catalyst	38±2	wt.%

6.4 Methodology

This section includes the steps required to conduct the exergy-based evaluation of a PTA unit. The thermodynamic modeling, physical exergy, and chemical exergy analyses are presented in the following subsections:

6.4.1 Thermodynamic Modeling

While the energy analysis is based on the first law of thermodynamics, the exergy analysis involves both the first and second laws of thermodynamics. Both energy and exergy assessment phases use the mass balance for the proposed process/system [403]. The first law of thermodynamics determines the amount of energy wasted or generated in the system (i.e., energy can be not created nor destroyed) [404]. The first law of thermodynamics is not capable of quantitatively determining the energy quality [390] since it cannot account the dissipated energy and the amount of potential work available [404]. The second law of thermodynamics supersedes the limitation, and it presents the exergy analysis, quantifying the potential useful work for a provided amount of energy. It is vital to use both the quality and quantity of energy for obtaining the effective utilization of energy [390]. Figure 6-3 illustrates the fundamental concept of the overall energy and exergy balances [405, 430]. The key purpose of exergy analysis is to quantitatively predict the deficiency extent of a thermal or chemical process. Exergy as an indicator of energy quality can be employed to evaluate and optimize the industrial processes in terms of energy and exergy efficiency [389]. Collection of the industrial data under stable/normal operating conditions and the assessment of the collected data reliability are the key steps for performing exergy analysis [403]. Assessment of a system performance on the basis of the exergy analysis is more practical, compared to the energy analysis [389].

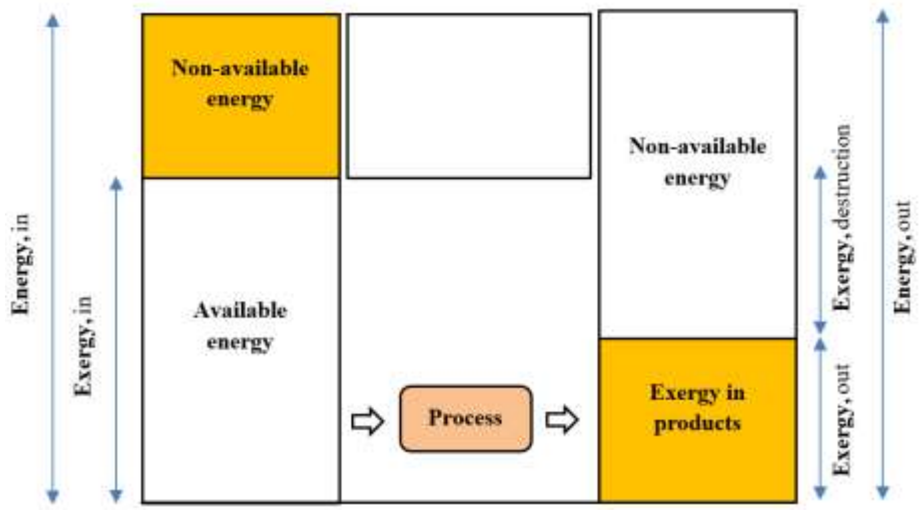

Figure 6-3: Base concept of total energy and exergy balances [405, 430].

The exergy calculation is made based on the physical exergy (pressure, thermal, elevation, and velocity) and chemical exergy, which is related to the exergy flows of the process [431]. The mass and energy balance equations combined with the first and second laws of thermodynamics are used to obtain the exergy balance of a control volume, as expressed below:

$$\frac{d(Ex)}{dt} = \sum_{j}(1 - \frac{T_0}{T_j})\dot{Q}_j - \dot{E}x_{work} + \sum_{in}\dot{E}x_{in.j} - \sum_{out}\dot{E}x_{out.j} - \dot{E}x_D \qquad (6\text{-}4)$$

where Ex introduces the amount of exergy in J; t represents the time in s; T_0 and T_j are the ambient air temperature and the surrounded boundary temperature in K, respectively; $\dot{Q}_j$ indicates the heat source in W; $\dot{E}x_{work}$ describes the output work (mechanical work and electrical work) in W; $\dot{E}x_{in.j}$ and $\dot{E}x_{out.j}$ refer to the input and output exergy rates in W, respectively; and $\dot{E}x_D$ signifies the exergy destruction flow in W. The term on the left side of Equation (6-4) is equal to zero at steady-state condition. Therefore, Equation (6-4) changes to the following expression:

$$\dot{E}x_D = \sum_j (1 - \frac{T_0}{T_j})\dot{Q}_j \; - \dot{E}x_{work} + \sum_{in} \dot{E}x_{in.j} - \sum_{out} \dot{E}x_{out.\mathrm{j}} \tag{6-5}$$

The amount of exergy destruction is strongly dependent on the irreversibility of the process. The system experiences greater exergy destruction when the irreversibility degree is higher. It should be emphasized that $\dot{E}x_{in,j}$ and $\dot{E}x_{out.j}$ contain both physical and chemical exergy. The exergetic efficiency (η) is defined as follows:

$$\eta = \frac{\dot{E}x_{out.j}}{\dot{E}x_{in.j}} = 1 - \frac{\dot{E}x_D}{\dot{E}x_{in.j}} \tag{6-6}$$

6.4.1.1 Physical Exergy

This type of exergy represents the maximum work that can be produced from the interactions of a control volume with a particular temperature, pressure, velocity, and potential energy with the environment or surrounding [385]. In other words, physical exergy is associated with the differences in pressure, temperature, elevation, and velocity between the maintained thermodynamic state and the dead state at a fixed composition [431]. The following expression introduces the physical exergy (ex_{ph}):

$$ex_{ph} = (h - h_0) - T_0(s - s_0) + \frac{V^2}{2} + gz \tag{6-7}$$

where h, s, V, g, and z signify the enthalpy in J/mol, entropy in J/mol.K, velocity in m/s, gravitational acceleration in m/s^2, and height in m, respectively. The ambient condition is specified by zero subscript. Both enthalpy and entropy depend on the gas compressibility factor and the specific heat capacity for compressible fluids [385].

6.4.1.2 Chemical Exergy

The exergy, which is released through a chemical reaction at a reference temperature and pressure until the chemical equilibrium condition, is called chemical exergy. If a thermodynamic system undergoes a chemical reaction, the chemical exergy needs to be incorporated in the model development [385].

If the standard chemical exergy of components is not provided in the literature, the following equation can be used to calculate the standard chemical exergy:

$$\sum_i \nu_i (ex^0_{ch.i} - g_{f0.i}) = 0 \tag{6-8}$$

In Equation (6-8), $ex^o_{ch.i}$ stands for the reactants' standard chemical exergy in J/mol; $g_{f0.i}$ represents the Gibbs free energy standard formation in J/mol; and ν_i symbolizes the stoichiometric coefficient of reactants and products. The ν_i is positive for the products and negative for the reactants. It is worth noting that the amount of $g_{f0.i}$ is zero for elements.

The molar chemical exergy of gas mixtures or ideal liquids is computed using the following equation:

$$ex_{ch}^{ig} = \sum_i x_i ex_{ch,i}^0 + RT_0 \sum_i x_i ln(x_i) \tag{6-9}$$

In Equation (6-9), x_i is the molar fraction of component i; $ex_{ch.i}^0$ represents the standard chemical exergy of component *i* in J/mol; and *R* denotes the universal gas constant in J/mol.K. In order to calculate the amount of chemical exergy of a component, the component's chemical reaction with one of the air constituents or any component with an identified standard chemical exergy needs to be considered. The standard chemical exergy of air components with a specified mole fraction (e.g., 0.7803 N_2, 0.2099 O_2, and 0.0098 Ar) is regarded as the reference composition of air. An unknown standard exergy of any component ($ex_{ch.j}^0$) can be calculated through rearranging Equation (6-8) as follows:

$$ex_{ch.j}^0 = g_{f0.j} - \frac{1}{v_j}\sum_{i\neq j} v_i(ex_{ch.i}^0 - g_{f0.i}) \tag{6-10}$$

where $ex^{o}_{ch.j}$ and $g_{f0.j}$ stand for the standard exergy and the formation Gibbs free energy of the component *j* in J/mol, respectively. Table 6-2 the magnitudes of standard chemical exergy for the components used in this study.

Table 6-2: The calculated values of standard chemical exergy for the components.

Component ID	Type	Alias	$g_{f0.j}$ (kJ/mol)	$ex^{o}_{ch.j}$ (kJ/mol)
TA	Conventional	$C_8H_6O_4$-D3	-550.1	3482.011
TA-SOLID	Solid	$C_8H_6O_4$-D3	-3189.3	842.811
4-CBA	Conventional	$C_8H_6O_3$	-342	3664.306
4-HMBA	Conventional	$C_8H_8O_3$-D2	-265.8	0
PTA	Conventional	$C_8H_8O_2$-D2	-212	0
BA	Conventional	$C_7H_6O_2$	-214.2	0
H_2O	Conventional	H_2O	-228.572	0.9
H_2	Conventional	H_2	0	236.12
CO	Conventional	CO	-137.15	279.075
CO_2	Conventional	CO_2	-394.37	19.87
O_2	Conventional	O_2	0	3.97
N_2	Conventional	N_2	0	0.72
Therminol® 66	Conventional	$C_{18}H_{22}$ (82.6 wt.%) $C_{24}H_{18}$ (12.06 wt.%) $C_{18}H_{14}$ (5.35 wt.%)	294.7 581.5 423	10368.507 12701.653 9570.979
				10607.32068

To calculate the chemical exergy of non-ideal and ionic mixtures (salts and water), the following relationship is employed:

$$ex_{ch} = \sum_{i} n_i(ex^{a}_{ch.i} + RT_0Ln(M_i\gamma_i)) + n_w(ex^{0}_{ch.w} + RT_0Ln(x_w\gamma_w)) \qquad (6\text{-}11)$$

In the above equation, $ex^{a}_{ch.i}$ is the standard chemical exergy of component *i* in the aqueous solution in J/mol; M_i refers to the molarity of component *i* in mol/l; γ_i denotes the activity coefficient of component i; n_i represents the number of moles of component i; n_w indicates the number of moles of water in the solution; x_w symbolizes the water mole fraction; γ_w resembles the water activity coefficient; and $ex^o_{ch.w}$ introduces the standard chemical exergy of water in J/mol. The ELECNRTL model built in the Aspen Plus® can calculate the activity coefficients of the components with high precision. $ex^a_{ch,i}$ is obtained by the following equation:

$$ex^a_{ch.i} = ex^0_{ch.i} + \Delta_f G_{aq.i} - \Delta_f G^0_i \qquad (6\text{-}12)$$

where $\Delta_f G^o_i$ represents the formation Gibbs free energy of pure component *i* in J/mol; and $\Delta_f G_{aq.i}$ is the formation Gibbs free energy of component *i* in the solution in J/mol. It should be noted that the formation Gibbs free energy of component i in the solution is smaller than that of pure component i. As a general rule, the formation Gibbs free energy of a pure organic salt is around 10 kJ/mol larger than that of the salt in the solution.

6.4.2 Taguchi Method

In the current study, a set of simulation runs, which are identified by the Taguchi method are conducted. Taguchi method employs an experimental design to find optimal conditions. Standard sets of orthogonal arrays along with the results analysis in accordance with signal-to-noise ratio are provided by this method. One of the benefits of the Taguchi method is reproducibility of the optimum operating conditions from laboratory in actual environment [432]. Taguchi method has been used in many energy cases. The details of this method implementation and the relevant information can be found in open sources [252, 433-435].

6.4.3 Exergy, Energy, Economic, and Environmental Evaluation

A hybridized modeling and simulation approach is implemented by employing the governing equations. As the first step, the industrial data are collected from the relevant process. Thereafter, simulation of the hydropurification process is conducted by following a detailed framework/strategy in the environment of Aspen Plus® (Version 11). Before using the simulated process conditions, the validation phase is carried out through the comparison of the simulation results and the plant data [4]. The simulated thermodynamic parameters and process variables are fine-tuned in such a way that the obtained results can be reliable. In order to optimize the process conditions, different scenarios (by changing/adjusting the vital operating parameters) are suggested based on the Taguchi method. In the next phase, the calculation of chemical and physical exergies is performed for all hydropurification process streams through programming in MATLAB software environment.

The physical exergy of fluids is computed using Equation (6-7) and Aspen Plus® simulation results. The standard chemical exergy of the components is determined by Equation (6-10), and the components' activity coefficients are calculated by employing Aspen Plus®. Thereafter, the exergy destruction and efficiency are obtained for each equipment of the process using Equations (6-5) and (6-6), respectively. Eventually, assessment of each case simulation is performed in terms of economic and environmental prospects. Figure 6-4 illustrates the procedure to conduct the exergy analysis.

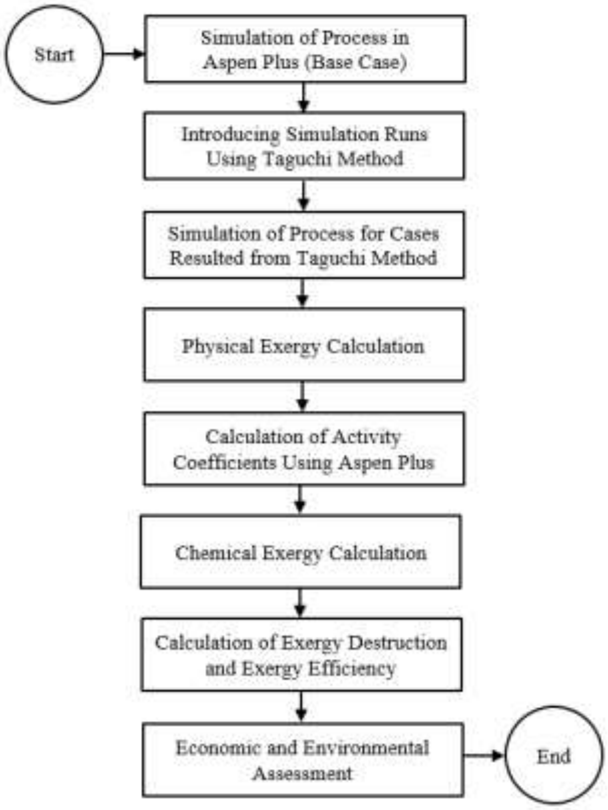

Figure 6-4: Steps of the modeling and simulation in this study.

A term known as specific energy consumption (SEC) is introduced for the effective evaluation of process energy. SEC is the energy utilized in a process to produce one unit of product, as defined below [436, 437]:

$$SEC = \frac{Q_c}{F - L} \tag{6-13}$$

in which, Q_c denotes the total energy consumption of process in GJ/h; F indicates the mass flowrate of feed stream in t/h; and L represents the loss stream flowrate in t/h.

A low SEC indicates smaller consumption of energy with reference to one unit of product. In addition to economic advantage through lowering the amount of SEC, the minimization of energy can be accomplished by reducing SEC. Loss stream is not considered as a useful stream or mainstream.

Regarding the environmental concerns, numerous efforts should be made to find effective solutions for the reduction of the relevant hazards. For instance, fossil fuels consumption significantly increases the CO_2 emission [438]. An increase in the greenhouse gases (GHGs) , particularly CO_2, adds negative environmental impacts such as climate change and temperature rise. Hydropurification process can be optimized to considerably lower the concentration of emitted GHGs. Since the carbon management is highly recommended in energy sectors, this highlights the significance of this research.

In this study, the energy consumption is the amount of energy which is utilized by the process equipment, such as heat exchangers, crystallizers, and reactor. It should be noted that the time needed to produce product and the time required for the energy consumption should be equal in the calculations of SEC. The carbon tax is determined on the basis of the average tax rate of CO_2 emissions (e.g., \$25/ton of CO_2 emitted) [439].

6.4.4 Process Modeling and Simulation Assumptions

There are some reasonable assumptions that can be made to carry out the simulation phase without lowering the results accuracy. Reactor and crystallizers are the two key components of the hydropurification unit. The assumptions for the reaction system are summarized below:

- Plug flow model is employed to simulate the reactor in Aspen Plus®. The RPlug block is a rigorous model for plug flow reactors.

- There is a constant temperature along the reactor bed.

- The mode of the reactor operation is adiabatic.

- Perfect mixing in the radial direction is established, and no mixing in the axial direction takes place.

- Only vapor and liquid phases are considered in the process.

- Pressure drop along the reactor length is minimal.

- There is no slip between phases; the holdup fraction of a phase is the same as the fractional volumetric flow of that phase.

A key parameter in the crystallization process (as the main separation stage) is the solubility of TA in water. The solubility data are extracted from the study performed by Lijin et al. [440]. The assumptions considered for the crystallization process are given below:

- The product magma leaves the crystallizer in equilibrium; therefore, the mother liquor in the product magma is saturated.

- The feed to the crystallizer is mixed with the recirculated magma and passes through a heat exchanger before entering the crystallizer.

- The product stream from the crystallizer contains liquid and solid.

- Only TA is crystallized.
- There is no recycle stream for the crystallizer.
- The pressure and outlet vapor flowrate are chosen as the operating variables of each crystallizer. In order to calculate the outlet vapor flowrate, an initial guess is needed, and the final value of the vapor flowrate is calculated based on the temperature of the outlet vapor stream.

The simulation results based on the above-mentioned assumptions need to be validated for further analysis of the process.

6.5 Results and Discussion

In chemical processes, operational and energy issues can be rectified by employing proper practical approaches and troubleshooting. For example, the energy utilization, catalyst deactivation, solvent consumption, and control loops of the equipment/units can be optimized by various practical actions/strategies. In this study, the energy consumption and exergy analysis of the hydropurification process of a PTA plant are assessed through mathematical modeling and use of simulation packages and actual plant data. The process simulation is performed in Aspen Plus® environment. Figure 6-5 illustrates the process flow diagram of the hydropurification process constructed in Aspen Plus® environment.

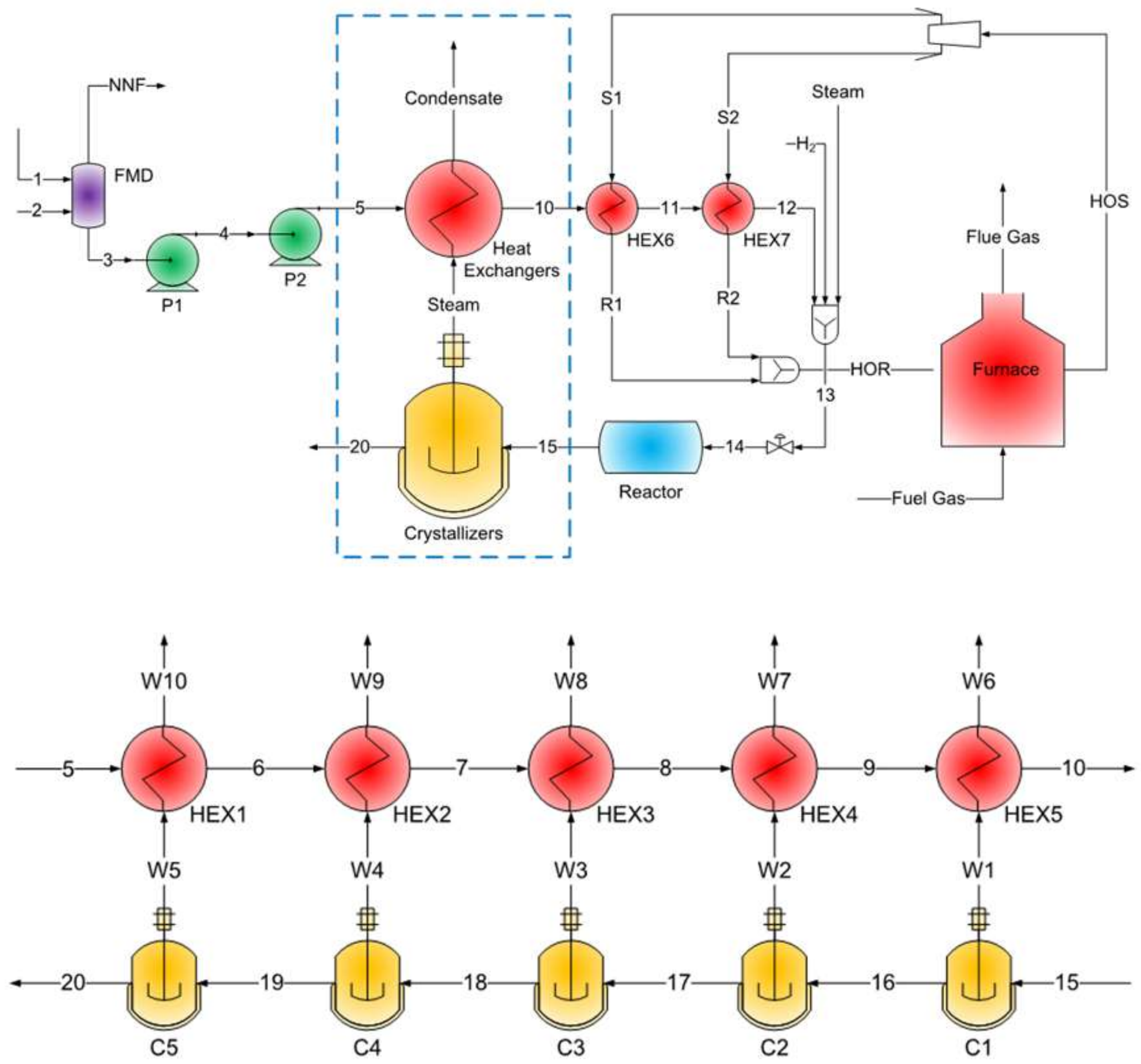

Figure 6-5: Process flow diagram of the hydropurification process established in Aspen plus® (NNF: normally no flow; FMD: feed mixed drum; P1: booster pump; P2: reactor feed pump; HEX: heat exchanger; HOS: hot oil supply; HOR: hot oil return; S1 and S2: hot oil supply; R1 and R2: hot oil return; W: steam or condensate; and C: crystallizer).

Table 6-3 includes the results of the process simulation and exergy analysis based on the streams shown in Figure 6-5.

Table 6-3: Simulation results and the outputs of the exergy calculations.

Stream No.	Temperature (ºC)	Pressure (bar)	Flowrate (kmol/h)	Phys Exergy (kW)	Chem Exergy (kW)	Total Exergy (kW)
1	90	1.01	271.80	119.18	262656.78	262775.96
2	90	1.01	8373.39	1181.08	2093.35	3274.43
3	90	1.01	8645.19	1288.11	263919.10	265207.20
4	90.15	11.51	8645.19	1359.38	263919.10	265278.48
5	91.27	91.01	8645.19	1898.82	263919.10	265817.91
6	110	88.65	8645.19	2679.90	263919.10	266599.00
7	141	86.29	8645.19	4336.48	263919.10	268255.58
8	175	83.93	8645.19	6640.45	263919.10	270559.55
9	215	81.57	8645.19	10014.16	263919.10	273933.26
10	251	79.21	8645.19	13747.15	263919.10	277666.24
11	268.00	76.85	8645.19	15799.55	263919.10	279718.65
12	285.00	74.49	8645.19	18114.75	263919.10	282033.84
13	283.62	74.49	8702.36	18096.02	264354.15	282450.17
14	283.62	74.49	8702.36	18096.02	264354.15	282450.17
15	283.62	74.49	8701.63	18049.08	263458.77	281507.85
16	260.72	47.71	7741.74	13245.39	173386.03	186631.42
17	227.17	26.51	6858.63	8667.57	90914.79	99582.36
18	197.37	14.61	6192.35	5799.90	71807.85	77607.75
19	169.07	7.61	5631.83	3785.30	66618.25	70403.55
20	144.84	4.01	5307.01	2534.97	65209.70	67744.66
H_2	90	96.01	6.55	21.06	429.48	450.54
Steam	90	96.01	50.62	9.94	12.66	22.60
HOR	302	14.01	2878.06	34434.42	8478783.46	8513217.88
R1	302	14.01	1380.55	16517.57	4067118.60	4083636.16
R2	302	14.01	1497.51	17916.86	4411664.86	4429581.72
S1	322	14.01	1380.55	18816.33	4067118.60	4085934.92

S2	322	14.01	1497.51	20410.36	4411664.86	4432075.22
HOS	322	14.01	2878.06	39226.68	8478783.46	8518010.14
W1	260.72	47.71	959.89	5139.83	3260.66	8400.49
W2	227.17	26.51	883.11	4421.76	2570.42	6992.18
W3	197.37	14.61	666.29	3051.81	1844.44	4896.25
W4	169.07	7.61	560.52	2294.73	1512.57	3807.30
W5	144.84	4.01	324.81	1173.61	867.32	2040.92
W6	224.97	47.21	959.89	1152.39	1011.68	2164.07
W7	185.31	26.01	883.11	681.53	464.63	1146.17
W8	150.59	14.11	666.29	326.50	255.54	582.04
W9	119.91	7.11	560.52	162.90	175.90	338.80
W10	100.94	3.51	324.81	61.92	92.64	154.57

As the first step, we need to make sure about the reliability of the results so that they can be used for the optimization purpose. The main challenges of the modeling and simulation of industrial processes are the lack of data for some units as well as the fluctuations of the operating parameters whose setpoints are to be maintained at fixed points. Based on the process data for the TBR, the 4-CBA flowrate, which is the main impurity of the product and the most important criterion of PTA powder quality, is 0.1 kg/h at the reactor exit. The simulation provides this value as the trace, implying that the simulator performs acceptably for the reaction part. Focusing on the crystallization process, the TA concentration at the fifth crystallizer outlet is 33.53 wt.% based on the industrial plant data. The simulation gives the value of 32.93 wt.%, revealing an absolute error percentage of 1.79 %. Thus, there is an acceptable match between the simulation results and the real data. To systematically assess the process simulation, the results are presented in the form of figures and tables. Figure 6-6 illustrates the crystallization process progress, which takes place in five crystallizers. The temperature of each crystallizer is reduced upon pressure reduction by two pressure split-range control valves. In this condition, the temperature goes down to a temperature lower than the TA equilibrium solubility in water.

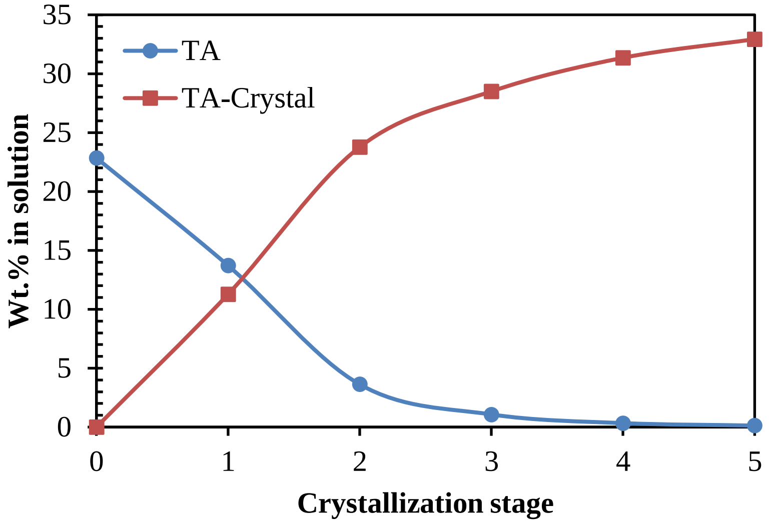

(a)

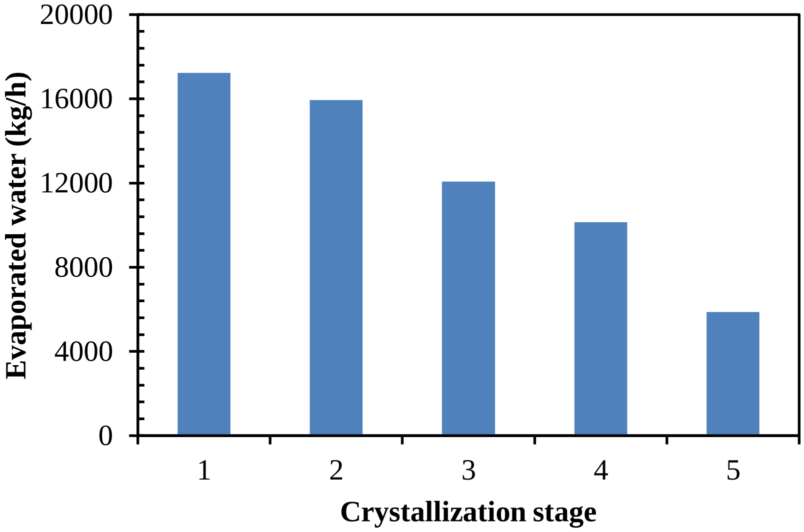

(b)

Figure 6-6: Crystallization process: (a) TA crystal concentration in the solution and the crystallization progress through the five crystallizers; and (b) The amount of water vaporized in the five crystallization steps.

Figure 6-6 (a) depicts the TA concentration in the liquid phase and the TA crystallization progress in the five crystallizers, and Figure 6-6 (b) shows the rate of water evaporation affected by the cooling-evaporation mechanism of crystallization. The TA crystal concentration increases, and the rate of steam generation decreases over the crystallization process through the five crystallizers in series. Figure 6-7 demonstrates the heat released from each crystallizer through the steam generation. It reveals that the highest amount of energy is generated in the first crystallizer having a higher saturation pressure. In addition, the highest rate of crystallization takes place in the first crystallizer due to the significant reduction in pressure at the amount of 26.8 bar, compared to the other crystallization stages. It can be concluded that TA crystals are produced in the first and second crystallizers, and the crystal size distribution is dominant in the third, fourth, and fifth crystallizers. The crystal size distribution is maintained through the agitation made by the mixers. However, control of the pressure and the level of the contents in the crystallizers play a significant role in the desired crystal size distribution.

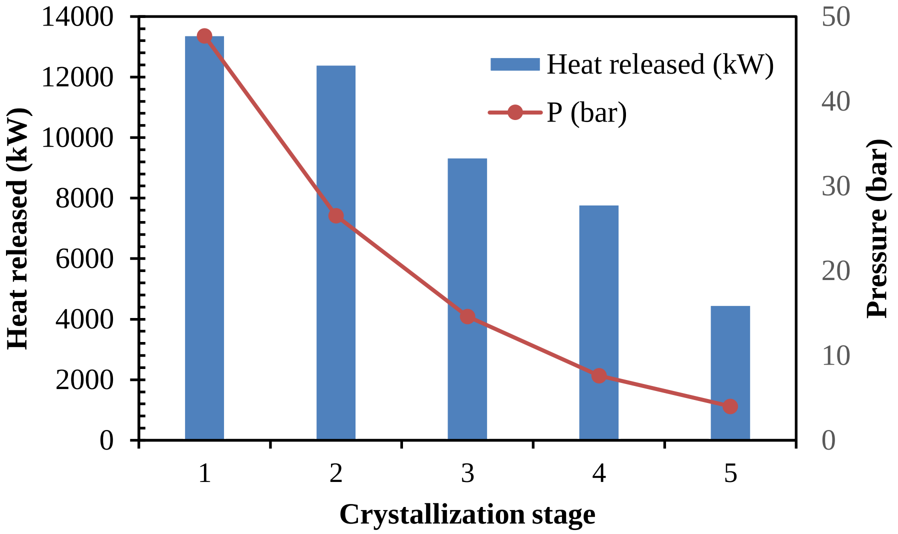

Figure 6-7: The magnitudes of the heat released via water vaporization and the pressure values of all crystallizers.

Figure 6-8 displays the amount of heat duty for the heat exchangers operating with steam generated in the crystallizers as the heat transfer medium. It is found that the heat duties of the fourth and the fifth heat exchangers are greater than the other ones since they operate with higher-pressure saturated steam coming from the high-pressure crystallizers. It is obvious that the amounts of heat duties determined by the simulation software are satisfactorily close to those calculated using the operating data. The average percentage error is obtained to be 3.73%.

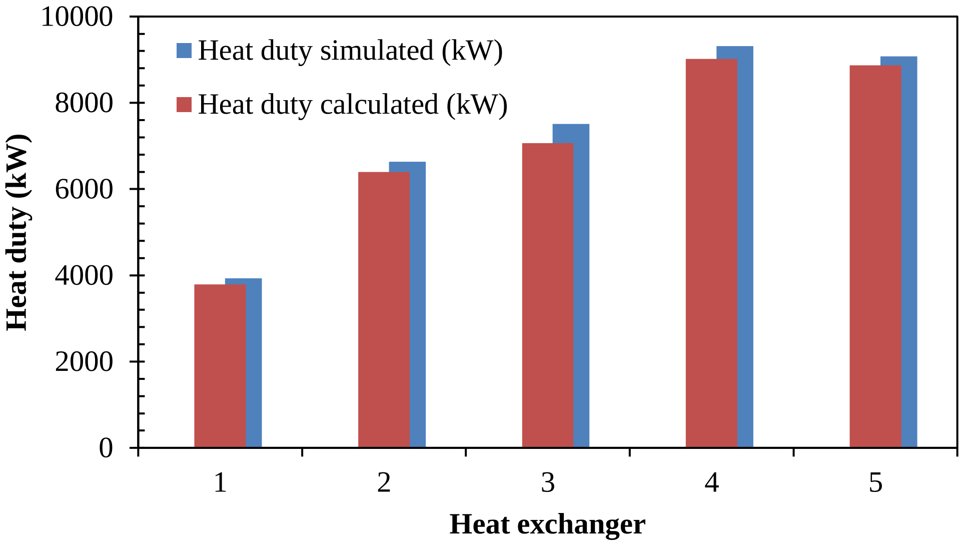

Figure 6-8: Comparison of the heat duty values of heat exchangers using steam as the heat transfer medium based on the plant data [4] and simulation results.

In order to find an optimum condition of the process considering various factors such as operation costs, CO_2 emissions, energy consumption, and exergy destruction, the Taguchi method is used to determine the most influential operating parameters. Table 6-4 lists the key operating parameters along with their corresponding values.

Table 6-4: Parameters and operating conditions selected for the optimization phase and energy/exergy analysis.

Run	**Outlet temperature of sixth heat exchanger**	**ΔT_{min} of heat exchangers**	**Reactor feed pump pressure**
	^{o}C	^{o}C	bar
1	266	5	86
2	266	10	91
3	266	15	96
4	268	5	91
5	268	10	96
6	268	15	86
7	270	5	96
8	270	10	86
9	270	15	91

The temperature considerably impacts the hydropurification process. Based on the plant operation procedure, the temperature needs to reach 285 ^{o}C before entering the reaction system [271, 440]. This temperature guarantees the complete dissolution of TA into water and ensures the effective operation of the furnace. Since the catalytic TBR system suffers from the sintering mechanism of catalyst deactivation, the temperature plays a critical role in this process in terms of efficiency and energy aspects. In addition, temperature gradient in the preheaters/heat exchangers determines the heat transfer rate, affecting the flowrate of the hot oil used and the fuel consumption in the furnace. Therefore, heat transfer in the heat exchangers noticeably impacts the process energy consumption. The pressure can effectively influence the heat transfer rate and control of the reaction system due to its impact on the product quality.

Figure 6-9 summarizes the exergy destruction values of the selected cases and the base case, which reflects the current/normal operating conditions of the hydropurification unit of the PTA plant. It reveals that Case 7 is the best one, which is chosen based on the calculated values of exergy destruction. Case 6 has the highest exergy destruction, implying that the corresponding operating conditions result in inefficient plant operation (or operational problems). Operating conditions of Case 7 suggest that controlling the exit temperature of the heat exchangers is of high significance. This can be achieved by proper control of the flowrate of the reactor feed pump, TA concentration in the feed, and efficient control of the furnace. Thus, Case 7 conditions further explain that the heat transfer efficiency of the heat exchangers is critical. Moreover, maintaining proper pressure in the heat exchangers is central; this can be accomplished by the suitable control of the discharge pressure of the reactor feed pumps and frequent flushing of the system by following the process procedure. To further emphasize the superiority of Case 7 to the other cases, Case 7 has around 15.7% less exergy destruction compared to the base case.

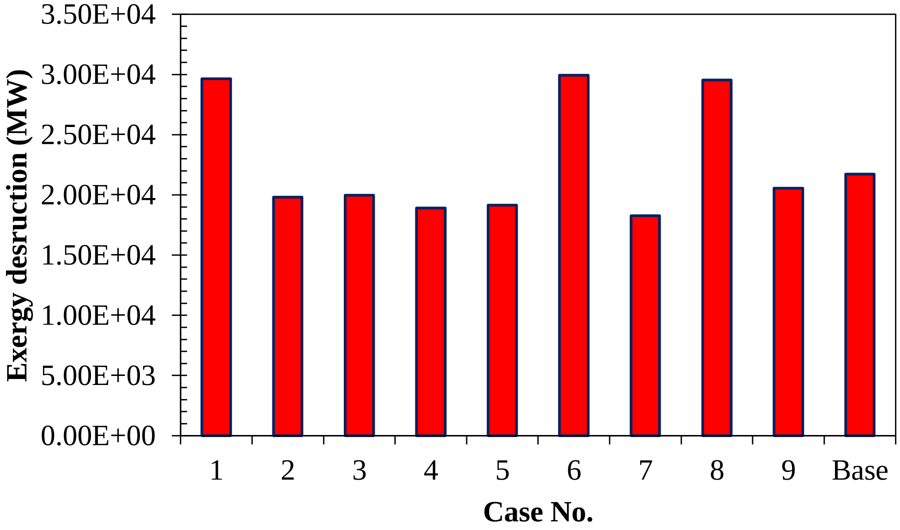

Figure 6-9: Exergy destruction values of the nine cases and the base case (as the normal operating scenario).

The exergy destruction values for the different process units of the hydropurification system, including pumps, heat exchangers, crystallizers, reactor, and furnace are calculated, as shown in Figure 6-10 for the best case (Case 7) and the base case (normal operating conditions). In fact, Figure 6-10 lists the exergy destruction extent for the units of the reactor feed preparation and the reactor itself. As it is clear, HEX4 and HEX6 performance can be improved by about 33.3% if they work under the best operating conditions (Case 7). The results show that the reactor exhibits an efficient performance under the normal operating conditions. Moreover, the reactor feed pumps (which are high manometric vertical centrifugal pumps), and their performance is of great significance towards efficient plant operation.

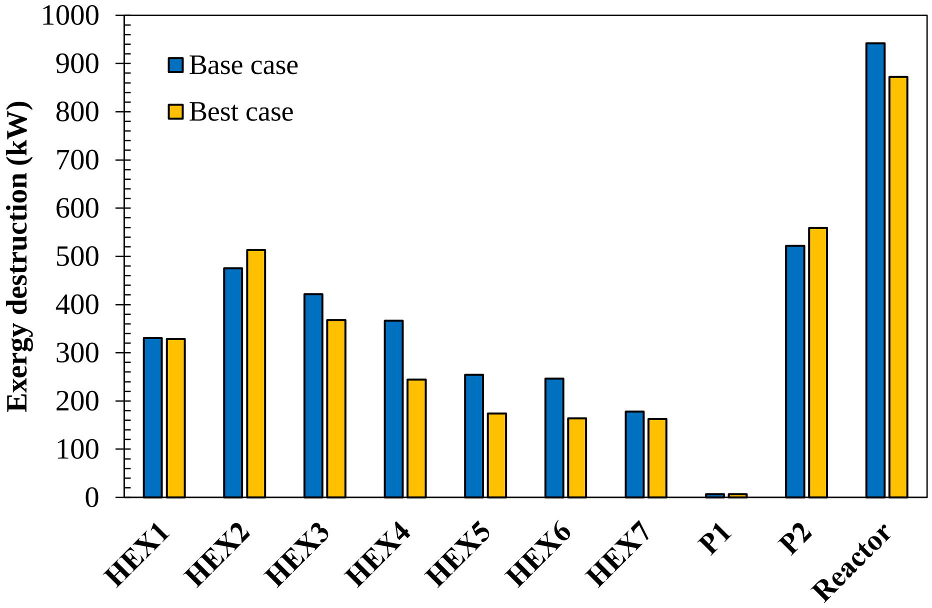

Figure 6-10: Exergy destruction values for the reaction system (HEX: feed preheater; P1: booster pump; P2: feed pump; and reactor).

Figure 6-11 displays the exergy destruction values for the most important unit of the separation process (i.e., crystallization). The exergy destruction values are calculated for the five crystallizers.

The results imply that the performance of the fourth crystallizer (C4) can be improved by about 18.7%, considering the changes in the exergy destruction after implementing Case 7 conditions. Also, it is found that the fifth crystallizer (C5) works efficiently under normal operating conditions. It is worth noting that the first and the second crystallizers, which play the most important role in the crystallization process, perform efficiently.

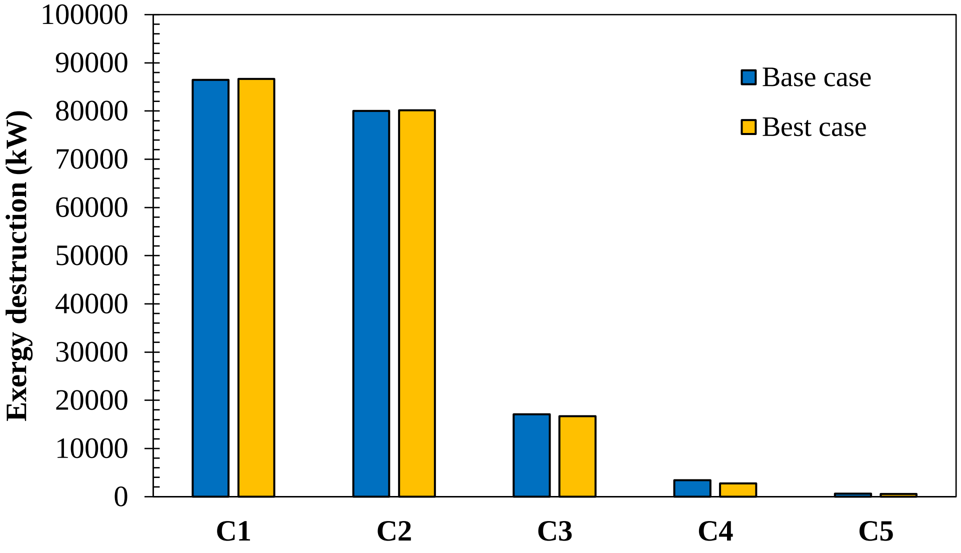

Figure 6-11: Exergy destruction values for the five crystallizers (as the most important separation process unit) of the hydropurification plant (C stands for the crystallizer).

Figure 6-12 illustrates the exergy efficiency and the exergy destruction of the furnace for the base and the best cases. According to Figure 6-12, the exergy efficiency is increased while operating the furnace under the optimal conditions (Case 7). Moreover, there is a decrease in the exergy destruction of the furnace by about 16% if Case 7 is selected. The hot oil furnace has a significant effect on the energy/exergy state of the entire plant. The order of the furnace's exergy destruction is substantially larger than the other components of the process. Significant and rapid fluctuations in temperature lead to the substantial exergy destruction in the furnace. The irreversibilities in the combustion reaction/process also cause extensive exergy destruction. In addition, considerable energy is lost through the flue gas. Even though an economizer (to preheat the combustion air) is designed to decrease the energy loss, the furnace operation and its efficiency should be still improved.

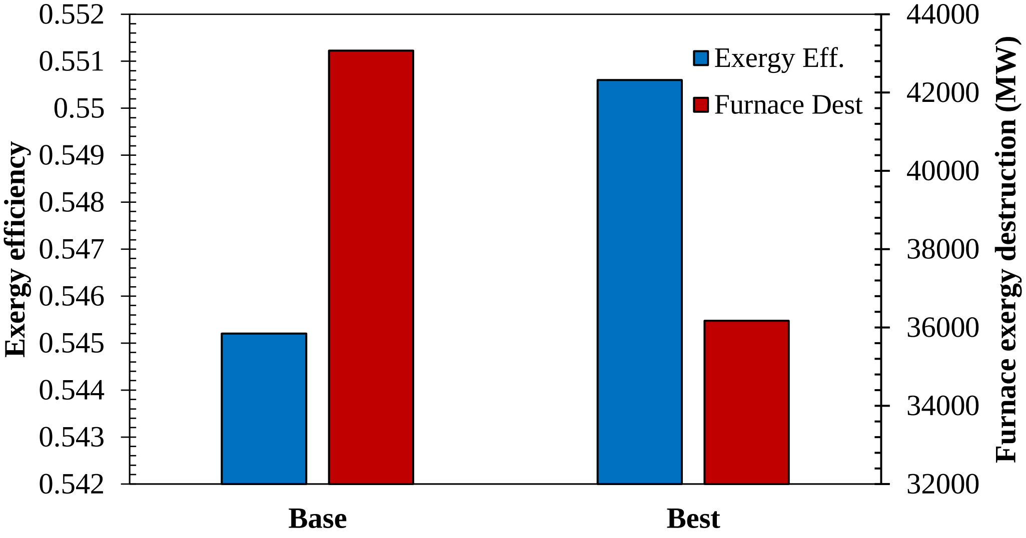

Figure 6-12: Exergy efficiency and the furnace exergy destruction for the base and the best scenarios.

Figure 6-13 summarizes the SEC index results for the optimal operating conditions (Best Case) and the normal operating conditions (Base case). The SEC can be used to specify the potential improvements in the energy efficiency as a significant measure of the energy management. The SEC index of the best case is considerably lower than that of the base case (e.g., 14.14%). This improvement occurs upon lower energy consumption of some preheaters and better performance of the hot oil furnace. This can be achieved by more accurate control of the crystallizers' pressure and improvement in the combustion process in the furnace.

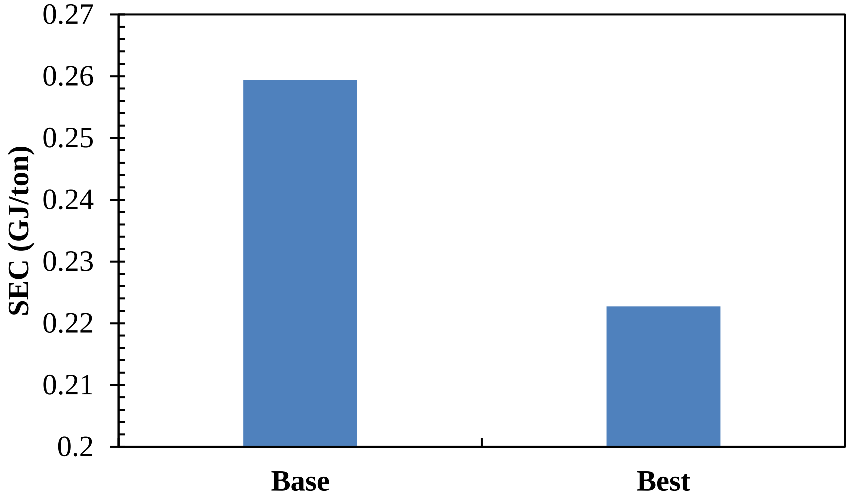

Figure 6-13: SEC index for the optimal and normal operating conditions.

Different process simulation runs (Cases 1 through 9) are carried out, and the results of the electricity consumption and fuel consumption in terms of duty, usage, and CO_2 emission rate are compared (see Table 6-5). In addition, Table 6-5 includes the carbon tax and the total costs for all runs. Based on Table 6-5, considering the total costs and the carbon tax Case 7 introduces the most optimal operating conditions, though it does not have the minimum cost and CO_2 emission rate under the category of electricity consumption. Implementing the operating conditions of Case 7 leads to 9.96% reduction in the total operation costs, 14.75% decrease in the carbon tax, and 0.582 t/h (14.75%) drop in the CO_2 emission rate. The results obtained from the economic and environmental evaluation verify the outcome of the energy and exergy analysis of the hydropurification process.

Table 6-5: Systematic evaluation in terms of electricity and fuel consumption, total expenses, and carbon tax for selected cases.

Case	**Electricity**				**Fuel**				**$25/ton of CO$_2$ emitted**	**Total Cost**
	Duty	Usage	Cost	CO$_2$ emission rate	Duty	Usage	Cost	CO$_2$ emission rate	Carbon tax	
	kW	kW	$/h	kg/h	kW	kg/h	$/h	kg/h	$/h	$/h
0	671.04	671.04	52.01	232.78	9771.02	732.83	55.23	3709.37	98.55	205.78
1	633.76	633.76	49.12	219.85	13364.90	1002.37	75.54	5073.72	132.34	256.99
2	671.04	671.04	52.01	232.78	8898.85	667.41	50.30	3378.27	90.28	192.58
3	708.32	708.32	54.89	245.72	8974.90	673.12	50.73	3407.14	91.32	196.94
4	671.04	671.04	52.01	232.78	8488.80	636.66	47.98	3222.60	86.38	186.37
5	708.32	708.32	54.89	245.72	8606.20	645.47	48.64	3267.17	87.82	191.36
6	633.76	633.76	49.12	219.85	13500.90	1012.56	76.31	5125.33	133.63	259.05
7	708.32	708.32	54.89	245.72	8204.68	615.35	46.37	3114.74	84.01	185.28
8	633.76	633.76	49.12	219.85	13308.90	998.17	75.22	5052.44	131.81	256.14
9	671.04	671.04	52.01	232.78	9243.59	693.27	52.24	3509.14	93.55	197.80

The results reveal that the hydropurification process of the PTA plant can be significantly improved under the proposed operating conditions. However, there are some challenges that need to be addressed for the effective implementation of the optimal operating conditions. It should be noted that an industrial chemical process is not flexible enough to considerably change the operating conditions, because numerous operational problems including the reduction in the product quality and the catalyst lifetime might occur upon significant variations in operating conditions. However, it is feasible to effectively control the process under acceptable changes/deviations in the operating conditions toward optimal performance in terms of energy, cost, safety, and environmental aspects. The operating conditions modifications suggested in this research can be applied to the similar chemical processes by proper control of the reactor pumps and feed pumps, routine flush procedure, hot oil furnace, and crystallizer pressure and liquid phase level. However, more expensive preheaters might be required.

6.6 Conclusions

Energy crisis and environmental concerns are the most intriguing topics in engineering and research sectors, nowadays. In this research, the hydropurification process of a PTA production plant is analyzed in terms of exergy, energy, environmental, and economic aspects. The key process equipment such as catalytic reaction system, separation process of crystallization, and hot oil furnace are assessed to find the optimal operating conditions. This important objective is met by the process simulation in the environment of Aspen Plus and programming in the MATLAB environment where various operating conditions are suggested by the Taguchi method for energy and exergy evaluation. The results of the simulation runs are validated against the industrial data and acceptable agreement is attained. The process simulation reveals that some process units and equipment have high exergy destruction; therefore, their performance can be improved by the remedial process actions. The findings of the current research are summarized as follows:

- The outlet temperature of the sixth heat exchanger, the outlet pressure of the reactor feed pumps, and ΔT_{min} of the heat exchangers are the vital operating condition in the energy and exergy analysis toward optimal operation.
- Case 7 (optimal operating conditions) has 15% less exergy destruction in comparison with the base case (normal operating conditions).

- Performance of the fourth and sixth heat exchangers can be significantly improved (33.3%).
- The exergy destruction of the fourth crystallizer can be decreased from 3400 kW at normal operating conditions to 2760 kW at optimal operating conditions.
- The hot oil furnace has a considerable exergy destruction, and its performance can be improved substantially.
- The cost of operation and carbon tax can be decreased up to 9.96% ($20.5/h) and 14.75% ($14.54/h), respectively, under optimal operating conditions.
- The reduction rate of CO_2 emissions is 0.582 t/h if the optimal operating conditions are established in the hydropurification process.
- The SEC index of the optimal operating conditions is 14.14% lower than that of the normal operating conditions.

Since the studied process is operated under high pressure and temperature, even minor changes in some operating parameters (e.g., temperature) can considerably influence the process performance. For instance, small reduction in temperature can lengthen the lifetime of the expensive catalyst and delay the degradation of the costly oil used in the furnace. In addition, the hydropurification process can be more effectively controlled, leading to less energy utilization, more friendly environment process, lower operation costs, and generation of higher work quality (less exergy destruction). A research study can be conducted to optimize the furnace operation and the combustion process using the relevant industrial data. Furthermore, the process evaluation based on the endogenous and exogenous exergy destruction can be done. The possible improvement in the product quality and catalyst lifetime, and increase in the production rate can be investigated under the optimal conditions proposed in this research. It is believed that our results can be applied to the relevant industrial processes.

NOMENCLATURES

Acronyms

4-CBA	-	4-carboxybenzaldehyde
4-HMBA	-	4-hydroxymethylbenzoic acid
BA	-	benzoic acid
BL	-	battery limit
C	-	crystallizer
CTA	-	crude terephthalic acid
DI	-	density indicator
HEX	-	heat exchanger
EEI	-	energy efficiency indicators
ELM	-	extreme learning machine
FIC	-	flow indicator controller
FMD	-	feed mixed drum
GHG	-	greenhouse gas
HHPS	-	high-high pressure steam
HIC	-	hierarchical-indicator comparison
HOS	-	hot oil supply
HOR	-	hot oil return
HV	-	on-off valve
K	-	compressor
LI	-	level indicator
LIC	-	level indicator controller
LPC	-	low pressure condensate
LPS	-	low pressure steam

NNF - normally no flow
P - pump
PCS - powder conveying system
Pd/C - palladium supported on carbon
PET - polyethylene terephthalate
PI - pressure indicator
PIC - pressure indicator controller
PSO - particle swarm optimization
PTA - purified terephthalic acid
pta - para-toluic acid
R - hot oil exit from HEX (stream)
RVF - rotary vacuum filter
S - hot oil inlet to HEX (stream)
SEC - specific energy consumption
TA - terephthalic acid
TBR - trickle-bed reactor
TI - temperature indicator
TIC - temperature indicator controller
W - steam or condensate (stream)

List of Variables/Symbols

Ex - exergy (J)
$\dot{Ex}/\dot{ex}$ - exergy flow (W)
$\dot{Ex}_D$ - exergy destruction flow (W)
$\dot{Ex}_{work}$ - output work (W)
ex - specific exergy (J mol^{-1})
F - mass flowrate (t h^{-1})
$\Delta_f G$ - Gibbs free energy of formation (J mol^{-1})
G - Gibbs free energy (J mol^{-1})
g - gravitational acceleration (m s^{-2})
g_{f0} - standard Gibbs free energy of formation (J mol^{-1})
ΔH - heat of reaction (kJ mol^{-1})

h - specific heat enthalpy (J mol^{-1})

L - loss stream mass flowrate (t h^{-1})

M - molarity (mol l^{-1})

n - number of moles (mol)

Q_c - total energy consumption (GJ h^{-1})

$\dot{Q}_J$ - heat source (W)

R - universal gas constant (J mol^{-1} K^{-1})

r - reaction rate (kmol kg$_c^{-1}$ s^{-1})

s - specific entropy (J mol^{-1} K^{-1})

T - temperature (K)

T_0 - ambient temperature (K)

T_j - surrounded boundary temperature (K)

t - time (s)

V - fluid velocity (m s^{-1})

x - mole fraction (-)

z - height (m)

Greek Symbols

γ - activity coefficient (-)

η - exergetic efficiency (-)

ϑ - stoichiometric coefficient (-)

Subscripts

0 - reference

aq - aqueous state

ch - chemical

D - destruction

f - formation

i,j - index of components

in - input

out - output

ph - physical

c - catalyst

w - water

Superscripts

0 - standard state

a - solution

ig - ideal gas

7 CHAPTER SEVEN: Summary and Recommendations for Future Work

In this research, the performance of the industrial hydroprocessing process is analyzed using advanced and accurate mathematical models. The industrial data, which were collected from the hydropurification process of PTA production plant, are used to validate the results of the developed models.

As the first phase, the literature review chapter summarizes the past studies on the hydroprocessing processes. In this phase, the application of the TBRs used in the hydroprocessing processes is extensively analyzed. The literature review reveals that most of the previous studies are experimental, and they do not consider the catalyst deactivation in the process, which is a serious concern in the industrial hydroprocessing plants.

In the third and fourth chapters, a dynamic mathematical model is developed considering the non-linear reaction rate expressions and the catalyst deactivation rate. The developed mathematical model, which is a set of partial differential equations, considers the critical operating parameters, especially the hydrodynamic ones. Suitable numerical techniques are selected to simultaneously solve the equations. The model predictions are in a good agreement with the industrial data. A systematic parametric sensitivity analysis is then conducted to recognize the most important operating parameters, affecting the product quality and catalyst lifetime. According to the results, the traditional synthesis of the catalyst can be modified to lengthen its lifetime and also to produce the product with a higher quality. The optimal operational conditions of the process are also determined.

Moreover, a novel strategy is proposed in the fifth chapter to efficiently utilize the feedstock with high concentration of the impurities (mixed with the feed with low impurity content), which are detrimental to the process operation, product quality control, and the catalyst lifetime. Since the process is operated at high temperatures and pressures, and it also includes several high consuming energy equipment (e.g., furnace), the energy utilization can be carefully optimized. In addition, there are many sources of the irreversibility that can be reduced as much as possible, toward achieving more high quality work. The energy-exergy model is developed in the last phase of the research, and the operational costs and the CO_2 emissions rate are quantified at various process and thermodynamic conditions. It is found that the process can be more properly operated and controlled if the optimal operating conditions are maintained in the process. In this case, the process is more efficient in terms of energy consumption, operating expenses, process safety, and environmental impacts. The results of this research can be applied to the relevant industrial plants for design, operation, and optimization purposes.

7.1 Literature Review (Chapter 2)

There have been many studies focusing on the hydroprocessing units and their reaction systems. After a comprehensive literature review, the following main points can be summarized:

- Incorporation of the deactivation rate in the dynamic model is an important step to better analyze the performance of a catalytic hydroprocessing unit. The catalyst deactivation rate should be obtained using the industrial operating data for attaining a more reliable rate.
- The extent of the wetting area of the catalyst particle is a critical parameter for the analysis of the catalytic reaction system. A model/technique might be useful to accurately determine/estimate the wetting efficiency of the particles.

- Flow regime transition takes place upon the fluctuations in the operating parameters. Since this occurs frequently in the industrial operation, a model should be developed to detect the flow regime transition so that the process analysis can be performed more precisely.
- Adequate knowledge on the characteristics of catalyst particles and the procedure selected for their loading into the reactor bed are essential for better assessment of the catalytic hydroprocessing units. An appropriate model considering the catalyst particle characteristics (e.g., particle size and particle porosity) and the catalyst charge technique can lead to a more cost-effective process in terms of the product quality and catalyst lifetime.
- A CFD model can be employed to determine the most suitable locations for the reactor feed nozzles. In addition, a CFD model can be developed for the most effective arrangement of the catalyst particles along with proper proposed modifications/changes in the internal design of the catalyst bed.
- An energy-exergy model is required to identify the sources of irreversibility in the process. In this case, the developed model can be used to optimize the process in terms of operation costs, product quality, and environmental impacts.

7.2 Dispersion Dynamic Model (Chapters 3 and 4)

The hydrodynamic parameters are of significant importance in the proper operation of the catalytic processes, especially the hydroprocessing units. The main objective of this research phase is to determine the most influential parameters in the hydropurification process. A dynamic model is developed by incorporating the catalyst deactivation phenomenon where a sensitivity analysis based on the hydrodynamic parameters is conducted. The partial differential equations are simultaneously solved using the method of lines and backward difference technique. The results are validated using the industrial data. The results of sensitivity analysis reveal that the main impurity (or 4-CBA) adversely affects the product quality and catalyst lifetime. The process can be improved through using small size of the catalyst particles and more porous particles. Moreover, liquid hourly space velocity plays a major role in the production process. The partial pressure of hydrogen can be increased to improve the product quality and prolong the catalyst lifetime. Also, the structured packing of the catalyst particles can help improve the process performance. The mass transfer coefficients do not have an appreciable impact on the process efficiency.

7.3 Mathematical Model and Process Control Procedure (Chapters 3, 4, and 5)

The majority of the hydroprocessing processes suffer from the catalyst deactivation. One of the important factors affecting the catalyst deactivation is the presence of the impurity in the reactor feed. The concentration of the impurity needs to be controlled to limit its harmful impact on the reaction system. The hydropurification process of PTA plant is considerably affected by the concentration of the main impurity (4-CBA) in the feedstock. In this research phase, a new strategy is proposed to effectively utilize the feedstocks having different concentrations of 4-CBA. A dynamic mathematical model is developed to simulate this mixing operation. The proposed approach can be used by the relevant industry so that a procedure is provided for proper use of the silos and accurate control of the ratio of the feed streams to the reactor feed mix drum. In this case, the mixing of the feedstock is performed based on a particular procedure so that the normal operating conditions of terephthalic acid concentration, flowrate, and main impurity concentration in the reactor feed are maintained. Moreover, the effect of temperature on the Pd dispersion and the catalyst deactivation is examined, revealing its crucial role in the catalyst deactivation phenomenon.

7.4 Energy, Exergy, Economic, and Environmental Assessment (Chapter 6)

In the last phase, the hydropurification unit of PTA plant is assessed in terms of energy, operating costs, and exergy performance. The process is simulated in Aspen plus® software environment, and the exergy calculations are conducted through computer coding in MATLAB software environment. The validation phase is performed by employing the industrial data. Different operating conditions/cases suggested by Taguchi method are run in the simulator, and the results of the cases are compared where the energy utilization, operation costs, CO_2 emission rate, and the exergy destruction are obtained. It is concluded that the optimal operating conditions lead to less energy consumption, lower operation costs, and decreased CO_2 emissions. The results also reveal that the process performance can be enhanced by improving the operation of some heat exchangers and crystallizers. The exergy destruction can be significantly reduced if the operation of the hot oil furnace is improved. The exergy destruction of the process can be reduced by 15% if the optimal operating conditions are established.

7.5 Recommendations for Future Work

Based on the mathematical models, proposed process strategies, and analysis of the results, the following recommendations can be made for future research investigations:

- Since the pressure has a significant impact on the final product quality (e.g., turbidity), it is suggested to introduce a model that can relate the reactor pressure to the product quality. It should be noted that the pressure fluctuations can break the fragile structure of the catalyst particles, leading to the diffusion of the carbon powder into the product.
- It would be a good recommendation to develop a mathematical model, representing the Pd/metal dispersion in the catalyst phase as a function of active surface area and the final product quality. In other words, the amount of the dispersion can be quantified to optimize the catalyst lifetime and product quality.
- A CFD model can be developed to compare different procedures of catalyst charge into the reactor bed in order to find the best strategy, leading to an increase in the catalyst lifetime and the product quality improvement.
- A multiple bed reactor can be considered to explore the effect of various configurations of reaction systems on the process performance. This is crucial since most of the hydroprocessing units suffer from the poor distribution of the heat as well as the hotspot formation.
- A new model can be developed to relate the flow regime transition to the fluctuation of operating variables (e.g., liquid flowrate). This can be quantified to evaluate the influence of each flow regime on the process performance in terms of the catalyst lifetime and product quality.
- The wetting efficiency of the catalyst particles can be correlated to the catalyst deactivation and the product quality.

- Flow distribution in the catalyst bed and the degree of maldistribution can be examined by incorporating the catalyst deactivation and the flowrate of the phases in a dynamic model to figure out the influence of the fluctuations in the reactor feed pump flowrate on the process performance.
- A dispersion model can be proposed to take into account the flow regime transition and flow non-ideality.
- Vapor-liquid equilibrium data of the reaction system can be incorporated in the proposed dynamic model to highlight the impact of the phase equilibria on the process behavior.
- Since the crystal size distribution of the product is a key criterion, a research investigation can be conducted to determine the influence of the crystallizers’ pressure and residence time on the product quality.

References

1. Pellegrini, R., G. Agostini, E. Groppo, A. Piovano, G. Leofanti, and C. Lamberti, *0.5 wt.% Pd/C catalyst for purification of terephthalic acid: Irreversible deactivation in industrial plants.* Journal of Catalysis, 2011. **280**(2): p. 150-160.

2. Pernicone, N., M. Cerboni, G. Prelazzi, F. Pinna, and G. Fagherazzi, *An investigation on Pd/C industrial catalysts for the purification of terephthalic acid.* Catalysis Today, 1998. **44**(1-4): p. 129-135.

3. Sun, W. and L. Zhao, *Simulation of secondary oxidation of p-xylene in liquid phase.* Industrial & Engineering Chemistry Research, 2010. **50**(5): p. 2548-2553.

4. STPC, *Operating Manual of PTA/PET Production Plant.* Shahid Tondgooyan Petrochemical Company (Iran), 2010.

5. Sheehan, R.J., *Terephthalic acid, dimethyl terephthalate, and isophthalic acid*. Ullmann's Encyclopedia of Industrial Chemistry. 2000, New York: WileyVCH Verlag GmbH & Co. KGaA.

6. Lin, R., R.S. O'meadhra, and R.B. Sheppard, *Process for the production of purified terephthalic acid*. 2007, US Patent and Trademark Office: USA.

7. Tomas, R.A., J.C. Bordado, and J.F. Gomes, *p-Xylene oxidation to terephthalic acid: a literature review oriented toward process optimization and development.* Chemical Reviews, 2013. **113**(10): p. 7421-7469.

8. Roy, S., T. Bauer, M. Al-Dahhan, P. Lehner, and T. Turek, *Monoliths as multiphase reactors: a review.* AIChE Journal, 2004. **50**(11): p. 2918-2938.

9. Kelkar, V.V. and K.M. Ng, *Screening multiphase reactors for nonisothermal multiple reactions.* AIChE Journal, 2000. **46**(2): p. 389-406.

10. Kashid, M.N. and L. Kiwi-Minsker, *Microstructured reactors for multiphase reactions: state of the art.* Industrial & Engineering Chemistry Research, 2009. **48**(14): p. 6465-6485.

11. Mederos, F.S. and J. Ancheyta, *Mathematical modeling and simulation of hydrotreating reactors: Cocurrent versus countercurrent operations.* Applied Catalysis A: General, 2007. **332**(1): p. 8-21.

12. Al-Dahhan, M.H., F. Larachi, M.P. Dudukovic, and A. Laurent, *High-pressure trickle-bed reactors: a review.* Industrial & Engineering Chemistry Research, 1997. **36**(8): p. 3292-3314.

13. Ranade, V.V., R. Chaudhari, and P.R. Gunjal, *Trickle Bed Reactors: Reactor Engineering & Applications*. 2011, UK: Elsevier.

14. Lämmermann, M., G. Horak, W. Schwieger, and H. Freund, *Periodic open cellular structures (POCS) for intensification of multiphase reactors: Liquid holdup and two-phase pressure drop.* Chemical Engineering and Processing-Process Intensification, 2018. **126**: p. 178-189.

15. Al-Dahhan, M., M. Khadilkar, Y. Wu, and M. Duduković, *Prediction of pressure drop and liquid holdup in high-pressure trickle-bed reactors.* Industrial & Engineering Chemistry Research, 1998. **37**(3): p. 793-798.

16. Boyer, C., C. Volpi, and G. Ferschneider, *Hydrodynamics of trickle bed reactors at high pressure: Two-phase flow model for pressure drop and liquid holdup, formulation and experimental validation.* Chemical Engineering Science, 2007. **62**(24): p. 7026-7032.

17. Iliuta, I., F.ç. Larachi, B.P. Grandjean, and G. Wild, *Gas–liquid interfacial mass transfer in trickle-bed reactors: state-of-the-art correlations.* Chemical Engineering Science, 1999. **54**(23): p. 5633-5645.

18. Mewes, D., T. Loser, and M. Millies, *Modelling of two-phase flow in packings and monoliths.* Chemical Engineering Science, 1999. **54**(21): p. 4729-4747.

19. Losey, M.W., M.A. Schmidt, and K.F. Jensen, *Microfabricated multiphase packed-bed reactors: characterization of mass transfer and reactions.* Industrial & Engineering Chemistry Research, 2001. **40**(12): p. 2555-2562.

20. Mederos, F.S., J. Ancheyta, and J. Chen, *Review on criteria to ensure ideal behaviors in trickle-bed reactors.* Applied Catalysis A: General, 2009. **355**(1-2): p. 1-19.

21. Ng, K., *A model for flow regime transitions in cocurrent down-flow trickle-bed reactors.* AIChE Journal, 1986. **32**(1): p. 115-122.

22. Burghardt, A., G. Bartelmus, M. Jaroszyński, and A. Kołodziej, *Hydrodynamics and mass transfer in a three-phase fixed-bed reactor with cocurrent gas—liquid downflow.* The

Chemical Engineering Journal and the Biochemical Engineering Journal, 1995. **58**(2): p. 83-99.

23. Narasimhan, C., R. Verma, A. Kundu, and K. Nigam, *Modeling hydrodynamics of trickle-bed reactors at high pressure.* AIChE Journal, 2002. **48**(11): p. 2459-2474.

24. Al-Naimi, S.A., F.T.J. Al-Sudani, and E.K. Halabia, *Hydrodynamics and flow regime transition study of trickle bed reactor at elevated temperature and pressure.* Chemical Engineering Research and Design, 2011. **89**(7): p. 930-939.

25. Urseanu, M., J. Boelhouwer, H. Bosman, J. Schroijen, and G. Kwant, *Estimation of trickle-to-pulse flow regime transition and pressure drop in high-pressure trickle bed reactors with organic liquids.* Chemical Engineering Journal, 2005. **111**(1): p. 5-11.

26. García-Serna, J., G. Gallina, P. Biasi, and T. Salmi, *Liquid holdup by gravimetric recirculation continuous measurement method. Application to trickle bed reactors under pressure at laboratory scale.* Industrial & Engineering Chemistry Research, 2017. **56**(45): p. 13294-13300.

27. McIlvried, H.G., *Mass Transfer in Cocurrent Gas-Liquid Flow through a Packed Column*. 1956, Carnegie Institute of Technology.

28. Larkins, R.P., *Two-phase cocurrent flow in packed beds.* AIChE Journal, 1959. **7**(2): p. 231-239.

29. Saez, A.E. and R. Carbonell, *Hydrodynamic parameters for gas-liquid cocurrent flow in packed beds.* AIChE Journal, 1985. **31**(1): p. 52-62.

30. Weber, M.E., A. Alarie, and M.E. Ryan, *Velocities of extended bubbles in inclined tubes.* Chemical Engineering Science, 1986. **41**(9): p. 2235-2240.

31. Ramachandran, P. and R. Chaudhari, *Three-Phase Catalytic Reactors*. Vol. 2. 1983, Netherlands: Gordon & Breach Science Publishers. 427.

32. Azarpour, A., N. Rezaei, and S. Zendehboudi, *Dynamic Modeling Strategy To Assess Impacts of Hydrodynamic Parameters on Industrial Hydropurification Process by Considering Catalyst Deactivation.* Industrial & Engineering Chemistry Research, 2018. **57**(41): p. 13671-13688.

33. Xiao, Q., A. Anter, Z. Cheng, and W. Yuan, *Correlations for dynamic liquid holdup under pulsing flow in a trickle-bed reactor.* Chemical Engineering Journal, 2000. **78**(2-3): p. 125-129.

34. Duchowicz, P.R., J.F. Aranda, D.E. Bacelo, and S.E. Fioressi, *QSPR study of the Henry's law constant for heterogeneous compounds.* Chemical Engineering Research and Design, 2020. **154**: p. 115-121.

35. Ferrando, N., R. Lugo, and P. Mougin, *Coupling activity coefficient models, Henry constant equations, and equations of state to calculate vapor–liquid and solid–liquid equilibrium data.* Chemical Engineering and Processing: Process Intensification, 2006. **45**(9): p. 773-782.

36. Faúndez, C.A., J.O. Valderrama, and R.A. Campusano, *Henry's law constant as a function of temperature and pressure to calculate the solubility of difluoromethane (R-32) in ionic liquids.* International Journal of Refrigeration, 2020. **119**: p. 401-409.

37. Sander, R., *Compilation of Henry's law constants (version 4.0) for water as solvent.* Atmospheric Chemistry and Physics, 2015. **15**(8): p. 4399-4981.

38. Malviya, A. and J. Vrabec, *Henry's law constant of nitrogen, oxygen, and argon in ternary aqueous alcoholic solvent mixtures.* Journal of Chemical & Engineering Data, 2019. **65**(3): p. 1189-1196.

39. Giri, A.K. and S.K. Majumder, *Pressure drop and its reduction of gas–non-Newtonian liquid flow in downflow trickle bed reactor (DTBR).* Chemical Engineering Research and Design, 2014. **92**(1): p. 34-42.

40. Benkrid, K., S. Rode, and N. Midoux, *Prediction of pressure drop and liquid saturation in trickle-bed reactors operated in high interaction regimes.* Chemical Engineering Science, 1997. **52**(21-22): p. 4021-4032.

41. Al-Ani, M. and M. Al-Dahhan, *Effect of catalyst shape on pressure drop and liquid holdup in a pilot plant trickle bed reactor.* Fuel, 2021. **284**: p. 118860.

42. Qi, B., S. Uribe, O. Farid, and M. Al-Dahhan, *Development of a hybrid pressure drop and liquid holdup phenomenological model for trickle bed reactors based on two-phase volume averaged equations.* The Canadian Journal of Chemical Engineering, 2020.

43. Whitaker, S., *Flow in porous media II: The governing equations for immiscible, two-phase flow.* Transport in Porous Media, 1986. **1**(2): p. 105-125.

44. Lange, R., M. Schubert, and T. Bauer, *Liquid holdup in trickle-bed reactors at very low liquid Reynolds numbers.* Industrial & Engineering Chemistry Research, 2005. **44**(16): p. 6504-6508.

45. Singh, B.K., E. Jain, and V.V. Buwa, *Feasibility of Electrical Resistance Tomography for measurements of liquid holdup distribution in a trickle bed reactor.* Chemical Engineering Journal, 2019. **358**: p. 564-579.

46. Lopes, R.J. and R.M. Quinta-Ferreira, *Three-dimensional numerical simulation of pressure drop and liquid holdup for high-pressure trickle-bed reactor.* Chemical Engineering Journal, 2008. **145**(1): p. 112-120.

47. Bazmi, M., S. Hashemabadi, and M. Bayat, *Extrudate trilobe catalysts and loading effects on pressure drop and dynamic liquid holdup in porous media of trickle bed reactors.* Transport in Porous Media, 2013. **99**(3): p. 535-553.

48. Fu, M.-S. and C.-S. Tan, *Liquid holdup and axial dispersion in trickle-bed reactors.* Chemical Engineering Science, 1996. **51**(24): p. 5357-5361.

49. Liu, G., J.-a. Lan, Y. Cao, Z. Huang, Z. Cheng, and Z. Mi, *New insights into transient behaviors of local liquid-holdup in periodically operated trickle-bed reactors using electrical capacitance tomography (ECT).* Chemical Engineering Science, 2009. **64**(14): p. 3329-3343.

50. Ayude, M.A., O.M. Martinez, and M. Cassanello, *Modulation of liquid holdup along a trickle bed reactor with periodic operation.* Chemical Engineering Science, 2007. **62**(21): p. 6002-6014.

51. Nemec, D., G. Berčič, and J. Levec, *Gravimetric method for the determination of liquid holdup in pressurized trickle-bed reactors.* Industrial & Engineering Chemistry Research, 2001. **40**(15): p. 3418-3422.

52. McManus, R.L., G.A. Funk, M.P. Harold, and K.M. Ng, *Experimental study of reaction in trickle-bed reactors with liquid maldistribution.* Industrial & Engineering Chemistry Research, 1993. **32**(3): p. 570-574.

53. Atta, A., S. Roy, and K.D. Nigam, *Investigation of liquid maldistribution in trickle-bed reactors using porous media concept in CFD.* Chemical Engineering Science, 2007. **62**(24): p. 7033-7044.

54. Boelhouwer, J.G., *Nonsteady operation of trickle-bed reactors: Hydrodynamics, mass and heat transfer*, in *Department of Chemical Engineering and Chemistry*. 2001, Technische Universiteit Eindhoven: Eindhoven.

55. Lutran, P.G., K.M. Ng, and E.P. Delikat, *Liquid distribution in trickle-beds. An experimental study using computer-assisted tomography.* Industrial & Engineering Chemistry Research, 1991. **30**(6): p. 1270-1280.

56. Hanratty, P. and M. Duduković, *Detection of flow maldistribution in trickle-bed reactors via tracers.* Chemical Engineering Science, 1992. **47**(12): p. 3003-3014.

57. Dashliborun, A.M., A. Füssel, and F. Larachi, *Prospect of open-cell solid foams for floating-platform multiphase reactor applications–Maldistribution susceptibility and hydrodynamic behavior.* Chemical Engineering Journal, 2018. **332**: p. 596-607.

58. Llamas, J.-D., C. Pérat, F. Lesage, M. Weber, U. D'Ortona, and G. Wild, *Wire mesh tomography applied to trickle beds: A new way to study liquid maldistribution.* Chemical Engineering and Processing: Process Intensification, 2008. **47**(9-10): p. 1765-1770.

59. Tsochatzidis, N., A. Karabelas, D. Giakoumakis, and G. Huff, *An investigation of liquid maldistribution in trickle beds.* Chemical Engineering Science, 2002. **57**(17): p. 3543-3555.

60. Van Houwelingen, A.J. and W. Nicol, *Parallel hydrogenation for the quantification of wetting efficiency and liquid–solid mass transfer in a trickle-bed reactor.* AIChE Journal, 2011. **57**(5): p. 1310-1319.

61. Ruecker, C.M. and A. Akgerman, *Determination of wetting efficiencies for a trickle-bed reactor at high temperatures and pressures.* Industrial & Engineering Chemistry Research, 1987. **26**(1): p. 164-166.

62. Julcour-Lebigue, C., F. Augier, H. Maffre, A.-M. Wilhelm, and H. Delmas, *Measurements and modeling of wetting efficiency in trickle-bed reactors: liquid viscosity and bed packing effects.* Industrial & Engineering Chemistry Research, 2009. **48**(14): p. 6811-6819.

63. Augier, F., A. Koudil, A. Royon-Lebeaud, L. Muszynski, and Q. Yanouri, *Numerical approach to predict wetting and catalyst efficiencies inside trickle bed reactors.* Chemical Engineering Science, 2010. **65**(1): p. 255-260.

64. Llano, J.J., R. Rosal, H. Sastre, and F.V. Díez, *Determination of wetting efficiency in trickle-bed reactors by a reaction method.* Industrial & Engineering Chemistry Research, 1997. **36**(7): p. 2616-2625.

65. Wu, Q., X. Hu, P.L. Yue, and D. Wang, *Measurement of wetting efficiency in a trickle-bed reactor*, in *17th Symposium of Chemical Reaction Engineering*. 2002, Chemical Engineering Science: Hong Kong.

66. Baussaron, L., C. Julcour-Lebigue, A.-M. Wilhelm, C. Boyer, and H. Delmas, *Partial wetting in trickle bed reactors: measurement techniques and global wetting efficiency.* Industrial & Engineering Chemistry Research, 2007. **46**(25): p. 8397-8405.

67. Al-Dahhan, M.H. and M.P. Duduković, *Catalyst wetting efficiency in trickle-bed reactors at high pressure.* Chemical Engineering Science, 1995. **50**(15): p. 2377-2389.

68. Mogalicherla, A.K., G. Sharma, and D. Kunzru, *Estimation of wetting efficiency in trickle-bed reactors for nonlinear kinetics.* Industrial & Engineering Chemistry Research, 2009. **48**(3): p. 1443-1450.

69. Sederman, A. and L. Gladden, *Magnetic resonance imaging as a quantitative probe of gas–liquid distribution and wetting efficiency in trickle-bed reactors.* Chemical Engineering Science, 2001. **56**(8): p. 2615-2628.

70. Dietz, A., C. Julcour, A.-M. Wilhelm, and H. Delmas, *Selective hydrogenation in trickle-bed reactor: experimental and modelling including partial wetting.* Catalysis Today, 2003. **79**: p. 293-305.

71. Highfill, W. and M. Al-Dahhan, *Liquid-solid mass transfer coefficient in high pressure trickle bed reactors.* Chemical Engineering Research and Design, 2001. **79**(6): p. 631-640.

72. Mills, P. and R. Chaudhari, *Multiphase catalytic reactor engineering and design for pharmaceuticals and fine chemicals.* Catalysis Today, 1997. **37**(4): p. 367-404.

73. Cassanello, M., F. Larachi, A. Laurent, G. Wild, and N. Midoux, *Gas-liquid mass transfer in high pressure trickle-bed reactors: Experiments and modelling.* Process Technology Proceedings, 1996. **12**: p. 493-498.

74. Larachi, F., M. Cassanello, and A. Laurent, *Gas− liquid interfacial mass transfer in trickle-bed reactors at elevated pressures.* Industrial & Engineering Chemistry Research, 1998. **37**(3): p. 718-733.

75. Wammes, W.J. and K.R. Westerterp, *Hydrodynamics in a pressurized cocurrent gas-liquid trickle-bed reactor.* Chemical Engineering & Technology, 1991. **14**(6): p. 406-413.

76. Goto, S. and J. Smith, *Trickle-bed reactor performance. Part I. Holdup and mass transfer effects.* AIChE Journal, 1975. **21**(4): p. 706-713.

77. Wammes, W., J. Middelkamp, W. Huisman, C. DeBass, and K. Westerterp, *Hydrodynamics in a cocurrent gas-liquid trickle bed at elevated pressures.* AIChE Journal, 1991. **37**(12): p. 1849-1862.

78. Lakota, A. and J. Levec, *Solid-liquid mass transfer in packed beds with cocurrent downward two-phase flow.* AIChE Journal, 1990. **36**(9): p. 1444-1448.

79. Tan, C. and J. Smith, *A dynamic method for liquid-particle mass transfer in trickle beds.* AIChE Journal, 1982. **28**(2): p. 190-195.

80. Satterfield, C.N., M.W. Van Eek, and G.S. Bliss, *Liquid-solid mass transfer in packed beds with downward concurrent gas-liquid flow.* AIChE Journal, 1978. **24**(4): p. 709-717.

81. Shah, Y.T., *Gas-Liquid-Solid Reactor Design*. 1979, USA: McGraw-Hill International Book Company. 373.

82. Önsan, Z.I. and A.K. Avci, *Multiphase Catalytic Reactors: Theory, Design, Manufacturing, and Applications*. First ed. 2016, New Jersey: John Wiley & Sons. 400.

83. Jana, A.K., *Chemical Process Modelling and Computer Simulation*. Third ed. 2018, Delhi: PHI Learning Pvt. Ltd. 468.

84. Zendehboudi, S., N. Rezaei, and A. Lohi, *Applications of hybrid models in chemical, petroleum, and energy systems: A systematic review.* Applied Energy, 2018. **228**: p. 2539-2566.

85. Ranade, V.V., *Computational Flow Modeling for Chemical Reactor Engineering*. First ed. Vol. 5. 2001, USA: Elsevier. 480.

86. Argyle, M.D. and C.H. Bartholomew, *Heterogeneous catalyst deactivation and regeneration: a review.* Catalysts, 2015. **5**(1): p. 145-269.

87. Prchlik, J., J. Soukup, V. Zapletal, and V. Růžička, *Liquid distribution in reactors with randomly packed porous beds.* Collection of Czechoslovak Chemical Communications, 1975. **40**(3): p. 845-855.

88. Prchlik, J., J. Soukup, V. Zapletal, V. Růžička, and P. Kovařík, *Wall flow in trickle bed reactor.* Collection of Czechoslovak Chemical Communications, 1975. **40**(10): p. 3145-3152.

89. Herskowitz, M. and J. Smith, *Liquid distribution in trickle-bed reactors: Part I. Flow measurements.* AIChE Journal, 1978. **24**(3): p. 439-450.

90. Al-Dahhan, M.H., *Pressure drop and liquid holdup in high pressure trickle-bed reactors.* Chemical Engineering Science, 1994. **49**(24): p. 5681-5698.

91. Doraiswamy, L. and D. Tajbl, *Laboratory catalytic reactors.* Catalysis Reviews - Science and Engineering, 1974. **10**(1): p. 177-219.

92. Mears, D.E., *The role of axial dispersion in trickle-flow laboratory reactors.* Chemical Engineering Science, 1971. **26**(9): p. 1361-1366.

93. Kumar, V.R., K. Balaraman, V.R. Rao, and M. Ananth, *Performance study of certain commercial catalysts in hydrodesulfurization of diesel oils.* Petroleum Science and Technology, 2001. **19**(9-10): p. 1029-1038.

94. Perego, C. and S. Peratello, *Experimental methods in catalytic kinetics.* Catalysis Today, 1999. **52**(2): p. 133-145.

95. Bischoff, K. and O. Levenspiel, *Fluid dispersion-generalization and comparison of mathematical models-I generalization of models.* Chemical Engineering Science, 1962. **17**(4): p. 245-255.

96. Mears, D.E., *Diagnostic criteria for heat transport limitations in fixed bed reactors.* Journal of Catalysis, 1971. **20**(2): p. 127-131.

97. Froment, G.F., K.B. Bischoff, and J. De Wilde, *Chemical Reactor Analysis and Design*. Second ed. 1990, USA: John Wiley & Sons.

98. Butt, J.B. and V.W. Weekman, *Catalyst Deactivation*. 1974, USA: American Institute of Chemical Engineers.

99. Mears, D.E., *Tests for transport limitations in experimental catalytic reactors.* Industrial & Engineering Chemistry Process Design and Development, 1971. **10**(4): p. 541-547.

100. Jakobsen, H.A., *Chemical Reactor Modeling*. First ed. 2008, Berlin: Springer-Verlag. 1244.

101. Zamaniyan, A., A.A. Khodadadi, Y. Mortazavi, and H. Manafi, *Comparative model analysis of the performance of tube fitted bulk monolithic catalyst with conventional pellet shapes for natural gas reforming.* Journal of Industrial and Engineering Chemistry, 2011. **17**(4): p. 767-776.

102. Moulijn, J.A., A. Van Diepen, and F. Kapteijn, *Catalyst deactivation: is it predictable?: What to do?* Applied Catalysis A: General, 2001. **212**(1-2): p. 3-16.

103. Butt, J.B. and E.E. Peterson, *Activation, Deactivation, and Poisoning of Catalysts*. 1st ed. 1988, USA: Academic Press Inc.

104. Bartholomew, C.H., *Mechanisms of catalyst deactivation.* Applied Catalysis A: General, 2001. **212**(1-2): p. 17-60.

105. Aguinaga, A., M. Montes, J.C. De la Cal, and J.M. Asua, *Kinetics of the poisoning by thiophene of supported nickel catalysts.* Industrial & Engineering Chemistry Research, 1992. **31**(1): p. 155-163.

106. Hwang, S. and R. Smith, *Heterogeneous catalytic reactor design with non-uniform catalyst considering shell-progressive poisoning behavior.* Chemical Engineering & Technology, 2008. **31**(3): p. 384-397.

107. Mäki-Arvela, P., et al., *Kinetics, catalyst deactivation and modeling in the hydrogenation of β-sitosterol to β-sitostanol over microporous and mesoporous carbon supported Pd catalysts.* Chemical Engineering Journal, 2009. **154**(1-3): p. 45-51.

108. Pina, J., V. Bucala, and D.O. Borio, *Influence of the sulfur poisoning on the performance of a primary steam reformer.* International Journal of Chemical Reactor Engineering, 2003. **1**(1).

109. Salmi, T., D.Y. Murzin, J. Wärnå, P. Mäki-Arvela, and G. Martin, *Integrated modelling of reaction and catalyst deactivation kinetics—Hydrogenation of sitosterol to sitostanol over a palladium catalyst.* Chemical Engineering Science, 2013. **104**: p. 156-165.

110. Barghi, B., M. Fattahi, and F. Khorasheh, *The modeling of kinetics and catalyst deactivation in propane dehydrogenation over Pt-Sn/γ-*Al_2O_3 *in presence of water as an oxygenated additive.* Petroleum Science and Technology, 2014. **32**(10): p. 1139-1149.

111. Diglio, G., P. Bareschino, E. Mancusi, and F. Pepe, *Numerical assessment of the effects of carbon deposition and oxidation on chemical looping combustion in a packed-bed reactor.* Chemical Engineering Science, 2017. **160**: p. 85-95.

112. Froment, G., *Modeling of catalyst deactivation.* Applied Catalysis A: General, 2001. **212**(1-2): p. 117-128.

113. Garcia-Dopico, M., A. Garcia, and A.S. García, *Modelling coke formation and deactivation in a FCCU.* Applied Catalysis A: General, 2006. **303**(2): p. 245-250.

114. Grewal, T.P.K. and S. Roy, *Modeling the effect of coke deposition in a heat integrated ethanol reformer.* International Journal of Hydrogen Energy, 2016. **41**(44): p. 19863-19880.

115. Hardiman, K.M., F.J. Trujillo, and A.A. Adesina, *Deactivation-influenced propane steam reforming: reactor analysis and parameter estimation.* Chemical Engineering and Processing: Process Intensification, 2005. **44**(9): p. 987-992.

116. Rahimpour, M.R., *Operability of an industrial catalytic naphtha reformer in the presence of catalyst deactivation.* Chemical Engineering & Technology, 2006. **29**(5): p. 616-624.

117. Rodríguez, E., G. Félix, J. Ancheyta, and F. Trejo, *Modeling of hydrotreating catalyst deactivation for heavy oil hydrocarbons.* Fuel, 2018. **225**: p. 118-133.

118. Sørensen, M.D.P., *Deactivation models by fitting the progression of temperature profiles–Coking model for the MTG process in adiabatic reactors.* Chemical Engineering Science, 2014. **106**: p. 126-135.

119. Bayat, M., Z. Dehghani, M. Hamidi, and M. Rahimpour, *Dynamic mathematical modeling of a novel dual-type industrial ethylene oxide (EO) reactor.* Chemical Engineering Research and Design, 2013. **91**(6): p. 1123-1132.

120. Finol, C., M. Menéndez, and J. Santamaría, *Regeneration of coked catalysts in a polytropic reactor.* Industrial & Engineering Chemistry Research, 2005. **44**(14): p. 5373-5379.

121. Giunta, P., N. Amadeo, and M. Laborde, *Simulation of a low temperature water gas shift reactor using the heterogeneous model/application to a pem fuel cell.* Journal of Power Sources, 2006. **156**(2): p. 489-496.

122. Gudlavalleti, S., T. Ros, and D. Lieftink, *Thermal sintering studies of an autothermal reforming catalyst.* Applied Catalysis B: Environmental, 2007. **74**(3-4): p. 251-260.

123. Rahimpour, M. and M. Lotfinejad, *A comparison of auto-thermal and conventional methanol synthesis reactor in the presence of catalyst deactivation.* Chemical Engineering and Processing: Process Intensification, 2008. **47**(12): p. 2121-2130.

124. Rajkhowa, T., G.B. Marin, and J.W. Thybaut, *Quantifying the dominant factors in Cu catalyst deactivation during glycerol hydrogenolysis.* Journal of Industrial and Engineering Chemistry, 2017. **54**: p. 270-277.

125. Sadeqzadeh, M., et al., *Effect of different reaction conditions on the deactivation of alumina-supported cobalt Fischer–Tropsch catalysts in a milli-fixed-bed reactor: experiments and modeling.* Industrial & Engineering Chemistry Research, 2014. **53**(17): p. 6913-6922.

126. Sadeqzadeh, M., et al., *Mechanistic modeling of cobalt based catalyst sintering in a fixed bed reactor under different conditions of Fischer–Tropsch synthesis.* Industrial & Engineering Chemistry Research, 2012. **51**(37): p. 11955-11964.

127. Tavasoli, A., R.M.M. Abbaslou, and A.K. Dalai, *Deactivation behavior of ruthenium promoted* $Co/\gamma\text{-}Al_2O_3$ *catalysts in Fischer–Tropsch synthesis.* Applied Catalysis A: General, 2008. **346**(1-2): p. 58-64.

128. Xaba, B. and J. De Villiers, *Sintering behavior of* TiO_2*-supported model cobalt Fischer–Tropsch catalysts under* H_2 *reducing conditions and elevated temperature.* Industrial & Engineering Chemistry Research, 2016. **55**(35): p. 9397-9407.

129. Liu, P., Z.B. Huang, J. Zhu, K. Yu, and Z.M. Cheng, *A Stochastic model for liquid dispersion in a trickle-bed reactor.* Chemical Engineering & Technology, 2014. **37**(12): p. 2056-2064.

130. Rastegar, S.O. and T. Gu, *Empirical correlations for axial dispersion coefficient and Peclet number in fixed-bed columns.* Journal of Chromatography A, 2017. **1490**: p. 133-137.

131. Gheni, S.A., S.A. Awad, S.M. Ahmed, G.H. Abdullah, and M. Al Dahhan, *Nanoparticle catalyzed hydrodesulfurization of diesel fuel in a trickle bed reactor: experimental and optimization study.* RSC Advances, 2020. **10**(56): p. 33911-33927.

132. Bartelmus, G.y., *Local solid—liquid mass transfer coefficients in a three-phase fixed bed reactor.* Chemical Engineering and Processing: Process Intensification, 1989. **26**(2): p. 111-120.

133. van Swaaij, W.P.M., *Residence time distributions in Raschig ring columns at trickle flow*, in *Chemical Engineering and Chemistry*. 1967, Eindhoven University of Technology: Eindhoven.

134. Lamine, A., L. Gerth, H. Le Gall, and G. Wild, *Heat transfer in a packed bed reactor with cocurrent downflow of a gas and a liquid.* Chemical Engineering Science, 1996. **51**(15): p. 3813-3827.

135. Taulamet, M.J., N.J. Mariani, G.F. Barreto, and O.M. Martínez, *A critical review on heat transfer in trickle bed reactors.* Reviews in Chemical Engineering, 2015. **31**(2): p. 97-118.

136. Mariani, N.J., O. Martınez, and G.F. Barreto, *Evaluation of heat transfer parameters in packed beds with cocurrent downflow of liquid and gas.* Chemical Engineering Science, 2001. **56**(21-22): p. 5995-6001.

137. Mariani, N.J., *Transferencia de calor en sistemas multifásicos*. 2000, Universidad Nacional de La Plata.

138. Rasmuson, A., B. Andersson, L. Olsson, and R. Andersson, *Mathematical Modeling in Chemical Engineering*. First ed. 2014, UK: Cambridge University Press.

139. Oh, M., *Modelling and Simulation of Combined Lumped and Distributed Processes*, in *Department of Chemical Engineering and Chemical Technology* 1995, University of London: London. p. 183.

140. Singh, S.K., *Process Control: Concepts Dynamics and Applications*. First ed. 2009, New Delhi: PHI Learning Pvt. Ltd. 748.

141. He, Y., *Simulation Studies on a Non-Isothermal, Non-Adiabatic, Fixed-Bed Reactor*, in *Chemical and Petroleum Engineering*. 2004, University of Kansas: USA.

142. Tsamatsoulis, D. and N. Papayannakos, *Investigation of intrinsic hydrodesulphurization kinetics of a VGO in a trickle bed reactor with backmixing effects.* Chemical Engineering Science, 1998. **53**(19): p. 3449-3458.

143. Alicilar, A., A. Bicer, and A. Murathan, *The relation between wetting efficiency and liquid holdup in packed columns.* Chemical Engineering Communications, 1994. **128**(1): p. 95-107.

144. Henry, H.C. and J.B. Gilbert, *Scale up of pilot plant data for catalytic hydroprocessing.* Industrial & Engineering Chemistry Process Design and Development, 1973. **12**(3): p. 328-334.

145. Ramírez-Castelán, C.E., A. Hidalgo-Vivas, J. Brix, A.D. Jensen, and J.K. Huusom, *Modelling of an adiabatic trickle-bed reactor with phase change*, in *Computer Aided Chemical Engineering*. 2017, Elsevier: Spain. p. 115-120.

146. Azarpour, A., T.N. Borhani, S.R.W. Alwi, Z.A. Manan, and M.I.A. Mutalib, *A generic hybrid model development for process analysis of industrial fixed-bed catalytic reactors.* Chemical Engineering Research and Design, 2017. **117**: p. 149-167.

147. Bell, N.H., *Steady state and dynamic modeling of a fixed-bed water-gas shift reactor*, in *Faculty of Graduate School*. 1990, The University of Texas at Austin: USA.

148. Munteanu, M.C. and J. Chen, *Vapor–liquid equilibrium (VLE)-based modeling for the prediction of operating regimes in a heavy gas oil hydrotreater.* Energy & Fuels, 2012. **26**(2): p. 1230-1236.

149. Alvarez-Majmutov, A. and J. Chen, *Modeling and simulation of a multibed industrial hydrotreater with vapor–liquid equilibrium.* Industrial & Engineering Chemistry Research, 2014. **53**(26): p. 10566-10575.

150. Murali, C., R. Voolapalli, N. Ravichander, D. Gokak, and N. Choudary, *Trickle bed reactor model to simulate the performance of commercial diesel hydrotreating unit.* Fuel, 2007. **86**(7-8): p. 1176-1184.

151. Chen, J., V. Mulgundmath, and N. Wang, *Accounting for vapor− liquid equilibrium in the modeling and simulation of a commercial hydrotreating reactor.* Industrial & Engineering Chemistry Research, 2011. **50**(3): p. 1571-1579.

152. Mijatović, I.M., S.B. Glisic, and A.M. Orlović, *Modeling a catalytic reactor for hydrotreating of straight-run gas oil blended with fluid catalytic cracking naphtha and light cycle oil: Influence of vapor–liquid equilibrium.* Industrial & Engineering Chemistry Research, 2014. **53**(49): p. 19104-19116.

153. Kulikov, A., N. Kuzin, A. Shigarov, V. Kirillov, A.E. Kronberg, and K. Westerterp, *Experimental study of vaporization effect on steady state and dynamic behavior of catalytic pellets.* Catalysis Today, 2001. **66**(2-4): p. 255-262.

154. Chávez, L.M., F. Alonso, and J. Ancheyta, *Vapor–liquid equilibrium of hydrogen–hydrocarbon systems and its effects on hydroprocessing reactors.* Fuel, 2014. **138**: p. 156-175.

155. Pellegrini, L.A., S. Gamba, V. Calemma, and S. Bonomi, *Modelling of hydrocracking with vapour–liquid equilibrium.* Chemical Engineering Science, 2008. **63**(17): p. 4285-4291.

156. Chen, J., N. Wang, F. Mederos, and J. Ancheyta, *Vapor−liquid equilibrium study in trickle-bed reactors.* Industrial & Engineering Chemistry Research, 2009. **48**(3): p. 1096-1106.

157. de Jong, K.P., *Effects of vapor-liquid equilibria on coke deposition in trickle-bed reactors during heavy oil processing. 1. Experimental results.* Industrial & Engineering Chemistry Research, 1994. **33**(4): p. 821-824.

158. de Jong, K.P., *Effects of vapor-liquid equilibria on coke deposition in trickle-bed reactors during heavy oil processing. 2. Modeling.* Industrial & Engineering Chemistry Research, 1994. **33**(12): p. 3141-3145.

159. LaVopa, V. and C.N. Satterfield. *Some effects of vapor-liquid equilibria on performance of a trickle-bed reactor*. in *Tenth International Symposium on Chemical Reaction Engineering*. 1988. Elsevier.

160. Hoekstra, G., *The effects of gas-to-oil rate in ultra low sulfur diesel hydrotreating.* Catalysis Today, 2007. **127**(1-4): p. 99-102.

161. Bellos, G. and N. Papayannakos, *The use of a three phase microreactor to investigate HDS kinetics.* Catalysis Today, 2003. **79**: p. 349-355.

162. Avraam, D.G. and I.A. Vasalos, *HdPro: a mathematical model of trickle-bed reactors for the catalytic hydroprocessing of oil feedstocks.* Catalysis Today, 2003. **79**: p. 275-283.

163. Khadilkar, M., P. Mills, and M. Dudukovic, *Trickle-bed reactor models for systems with a volatile liquid phase.* Chemical Engineering Science, 1999. **54**(13-14): p. 2421-2431.

164. Akgerman, A., G.M. Collins, and B.D. Hook, *Effect of feed volatility on conversion in trickle bed reactors.* Industrial & Engineering Chemistry Fundamentals, 1985. **24**(3): p. 398-401.

165. Tirado, A., J. Ancheyta, and F. Trejo, *Kinetic and reactor modeling of catalytic hydrotreatment of vegetable oils.* Energy & Fuels, 2018. **32**(7): p. 7245-7261.

166. Kilpiö, T., A. Aho, D. Murzin, and T. Salmi, *Experimental and modeling study of catalytic hydrogenation of glucose to sorbitol in a continuously operating packed-bed reactor.* Industrial & Engineering Chemistry Research, 2013. **52**(23): p. 7690-7703.

167. Kiss, A.A., C.S. Bildea, and J. Grievink, *Dynamic modeling and process optimization of an industrial sulfuric acid plant.* Chemical Engineering Journal, 2010. **158**(2): p. 241-249.

168. Pintar, A., G. Bercˇicˇ, and J. Levec, *Catalytic liquid-phase oxidation of aqueous phenol solutions in a trickle-bed reactor.* Chemical Engineering Science, 1997. **52**(21-22): p. 4143-4153.

169. Kostyniuk, A., D. Bajec, and B. Likozar, *Catalytic hydrocracking reactions of tetralin as aromatic biomass tar model compound to benzene/toluene/xylenes (BTX) over zeolites under ambient pressure conditions.* Journal of Industrial and Engineering Chemistry, 2021.

170. Fernandez-Puertas, E., A.J. Robinson, H. Robinson, S. Sathiyalingam, H. Stubbs, and L.J. Edwards, *Evaluation and Screening of Spherical Pd/C for Use as a Catalyst in Pharmaceutical-Scale Continuous Hydrogenations.* Organic Process Research & Development, 2020. **24**(10): p. 2147-2156.

171. Kostyniuk, A., D. Bajec, and B. Likozar, *Catalytic hydrogenation, hydrocracking and isomerization reactions of biomass tar model compound mixture over Ni-modified zeolite catalysts in packed bed reactor.* Renewable Energy, 2021. **167**: p. 409-424.

172. Kostyniuk, A., D. Bajec, and B. Likozar, *Hydrocracking, Hydrogenation and Isomerization of Model Biomass Tar in a Packed Bed Reactor over Bimetallic NiMo Zeolite Catalysts: Tailoring Structure/Acidity.* Applied Catalysis A: General, 2021: p. 118004.

173. Rice, R.G. and D.D. Do, *Applied Mathematics and Modeling for Chemical Engineers*. Second ed. 2012, New Jersey: John Wiley & Sons.

174. Liotta, F., P. Chatellier, G. Esposito, M. Fabbricino, E.D. Van Hullebusch, and P.N. Lens, *Hydrodynamic mathematical modelling of aerobic plug flow and nonideal flow reactors: a critical and historical review.* Critical Reviews in Environmental Science and Technology, 2014. **44**(23): p. 2642-2673.

175. Wang, Y., J. Chen, and F. Larachi, *Modelling and simulation of trickle-bed reactors using computational fluid dynamics: A state-of-the-art review.* The Canadian Journal of Chemical Engineering, 2013. **91**(1): p. 136-180.

176. Azarpour, A., N. Rezaei, and S. Zendehboudi, *Product quality control in hydropurification process by monitoring reactor feed impurities: Dynamic mathematical modeling.* Journal of Industrial and Engineering Chemistry, 2020. **92**: p. 62-76.

177. Limtrakul, S., P. Bannatham, S. Teeraboonchaikul, T. Vatanatham, and P.A. Ramachandran, *Modeling and evaluation of hydrodesulfurization and deactivation rates for partially wetted Trilobe catalyst using finite element method.* Powder Technology, 2019. **354**: p. 779-791.

178. Al-Obaidi, M., A.T. Jarullah, C. Kara-Zaitri, and I.M. Mujtaba, *Simulation of hybrid trickle bed reactor–reverse osmosis process for the removal of phenol from wastewater.* Computers & Chemical Engineering, 2018. **113**: p. 264-273.

179. Ahmadi, A., F. Samimi, and M. Rahimpour, *Three-phase reactor model for simulation of methylacetylene and propadiene selective hydrogenation process.* Chemical Product and Process Modeling, 2018. **144**(2).

180. Iliuta, I. and F. Larachi, *Fischer-Tropsch synthesis in vertical, inclined and oscillating trickle-bed reactors for offshore floating applications.* Chemical Engineering Science, 2018. **177**: p. 509-522.

181. Patil, R.C., P. Patra, A. Gupta, and A. Das, *Effect of reactor configuration on performance of vacuum gas oil (VGO) hydrotreater: Modelling studies.* Computers & Chemical Engineering, 2017. **104**: p. 89-106.

182. Azarpour, A., M.I.A. Mutalib, S. Mahadzir, and A. Ramli, *Analysis of hydrodynamic parameters effect on the hydropurification reactor operation through numerical simulation.* Procedia Engineering, 2017. **184**: p. 318-325.

183. Lee, S., N. Zaborenko, and A. Varma, *Acetophenone hydrogenation on Rh/Al2O3 catalyst: Flow regime effect and trickle bed reactor modeling.* Chemical Engineering Journal, 2017. **317**: p. 42-50.

184. Sadighi, S., *A two-dimensional discrete lumped model for a trickle-bed vacuum gas oil hydrocracking reactor.* Korean Journal of Chemical Engineering, 2016. **33**(9): p. 2538-2546.

185. Mary, G., A. Esmaeili, and J. Chaouki, *Simulation of the selective hydrogenation of C3-Cut in the liquid phase.* International Journal of Chemical Reactor Engineering, 2016. **14**(4): p. 859-874.

186. Mohammed, A.E., A.T. Jarullah, S.A. Gheni, and I.M. Mujtaba, *Optimal design and operation of an industrial three phase reactor for the oxidation of phenol.* Computers & Chemical Engineering, 2016. **94**: p. 257-271.

187. Iliuta, I. and F. Larachi, *Hydrocarbon hydrodesulfurization in vertical, inclined and oscillating trickle beds–Hydrodynamics & reactor performance for offshore petroleum marine applications.* Fuel, 2016. **186**: p. 35-49.

188. Nawaf, A.T., S.A. Gheni, A.T. Jarullah, and I.M. Mujtaba, *Optimal design of a trickle bed reactor for light fuel oxidative desulfurization based on experiments and modeling.* Energy & Fuels, 2015. **29**(5): p. 3366-3376.

189. Tohidian, T., O. Dehghani, and M. Rahimpour, *Modeling and simulation of an industrial three phase trickle bed reactor responsible for the hydrogenation of 1, 3-butadiene: A case study.* Chemical Engineering Journal, 2015. **275**: p. 391-404.

190. Durante, D., T. Kilpiö, P. Suominen, V.S. Herrera, J. Wärnå, P. Canu, and T. Salmi, *Modeling and simulation of a small-scale trickle bed reactor for sugar hydrogenation.* Computers & Chemical Engineering, 2014. **66**: p. 22-35.

191. Lee, B., et al., *Kinetic modeling of hydrocracking reaction in a trickle-bed reactor with Pt/Y-zeolite catalysts.* Korean Journal of Chemical Engineering, 2014. **31**(3): p. 419-426.

192. Brunner, K.M., J.C. Duncan, L.D. Harrison, K.E. Pratt, R.P. Peguin, C.H. Bartholomew, and W.C. Hecker, *A trickle fixed-bed recycle reactor model for the Fischer-Tropsch synthesis.* International Journal of Chemical Reactor Engineering, 2012. **10**(1).

193. Schwidder, S. and K. Schnitzlein, *A new model for the design and analysis of trickle bed reactors.* Chemical Engineering Journal, 2012. **207**: p. 758-765.

194. Lopes, R.J., V.S. de Sousa, and R.M. Quinta-Ferreira, *Numerical simulation of reactive pulsing flow for the catalytic wet oxidation in TBR using a VOF technique.* AIChE Journal, 2012. **58**(2): p. 493-504.

195. Lopes, R.J., R.M. Quinta-Ferreira, and F. Larachi, *ECT imaging and CFD simulation of different cyclic modulation strategies for the catalytic abatement of hazardous liquid pollutants in trickle-bed reactors.* Chemical Engineering Journal, 2012. **211**: p. 270-284.

196. Lopes, R.J., V.S. De Sousa, and R.M. Quinta-Ferreira, *CFD and experimental studies of reactive pulsing flow in environmentally-based trickle-bed reactors.* Chemical Engineering Science, 2011. **66**(14): p. 3280-3290.

197. Bazer-Bachi, F., F. Augier, and B. Santos, *1D and 2D simulations of partially wetted catalyst particles: A focus on heat transfer limitations.* Chemical Engineering Science, 2011. **66**(9): p. 1953-1961.

198. Xi, Y., J.E. Jackson, and D.J. Miller, *Characterizing lactic acid hydrogenolysis rates in laboratory trickle bed reactors.* Industrial & Engineering Chemistry Research, 2011. **50**(9): p. 5440-5447.

199. Jarullah, A.T., I.M. Mujtaba, and A.S. Wood, *Kinetic model development and simulation of simultaneous hydrodenitrogenation and hydrodemetallization of crude oil in trickle bed reactor.* Fuel, 2011. **90**(6): p. 2165-2181.

200. Lopes, R.J. and R.M. Quinta-Ferreira, *Assessment of CFD Euler–Euler method for trickle-bed reactor modelling in the catalytic wet oxidation of phenolic wastewaters.* Chemical Engineering Journal, 2010. **160**(1): p. 293-301.

201. Lopes, R.J. and R.M. Quinta-Ferreira, *Numerical studies of catalyst wetting and total organic carbon reaction on environmentally based trickle-bed reactors.* Industrial & Engineering Chemistry Research, 2010. **49**(21): p. 10730-10743.

202. Xi, Y., J.E. Holladay, J.G. Frye, A.A. Oberg, J.E. Jackson, and D.J. Miller, *A kinetic and mass transfer model for glycerol hydrogenolysis in a trickle-bed reactor.* Organic Process Research & Development, 2010. **14**(6): p. 1304-1312.

203. Wu, Q., X. Hu, P.L. Yue, J. Feng, X. Chen, H. Zhang, and S. Qiao, *Modeling of a pilot-scale trickle bed reactor for the catalytic oxidation of phenol.* Separation and Purification Technology, 2009. **67**(2): p. 158-165.

204. Abbasi, R. and S. Fatemi, *Mathematical modeling of gas oil hds and optimization of operational conditions in trickle bed reactor by genetic algorithm.* International Journal of Chemical Reactor Engineering, 2009. **7**(1): p. A8.

205. Liu, G., X. Zhang, L. Wang, S. Zhang, and Z. Mi, *Unsteady-state operation of trickle-bed reactor for dicyclopentadiene hydrogenation.* Chemical Engineering Science, 2008. **63**(20): p. 4991-5002.

206. Lopes, R.J., A.M. Silva, and R.M. Quinta-Ferreira, *Kinetic modeling and trickle-bed CFD studies in the catalytic wet oxidation of vanillic acid.* Industrial & Engineering Chemistry Research, 2007. **46**(25): p. 8380-8387.

207. Liu, G., Z. Mi, L. Wang, X. Zhang, and S. Zhang, *Hydrogenation of dicyclopentadiene into e ndo-tetrahydrodicyclopentadiene in trickle-bed reactor: Experiments and modeling.* Industrial & Engineering Chemistry Research, 2006. **45**(26): p. 8807-8814.

208. Guo, J. and M. Al-Dahhan, *Modeling catalytic trickle-bed and upflow packed-bed reactors for wet air oxidation of phenol with phase change.* Industrial & Engineering Chemistry Research, 2005. **44**(17): p. 6634-6642.

209. Khadilkar, M., M. Al-Dahhan, and M. Duduković, *Multicomponent flow-transport-reaction modeling of trickle bed reactors: application to unsteady state liquid flow modulation.* Industrial & Engineering Chemistry Research, 2005. **44**(16): p. 6354-6370.

210. Bhaskar, M., G. Valavarasu, B. Sairam, K. Balaraman, and K. Balu, *Three-phase reactor model to simulate the performance of pilot-plant and industrial trickle-bed reactors sustaining hydrotreating reactions.* Industrial & Engineering Chemistry Research, 2004. **43**(21): p. 6654-6669.

211. Singh, A., K. Pant, and K. Nigam, *Catalytic wet oxidation of phenol in a trickle bed reactor.* Chemical Engineering Journal, 2004. **103**(1-3): p. 51-57.

212. Eftaxias, A., F. Larachi, and F. Stüber, *Modelling of trickle bed reactor for the catalytic wet air oxidation of phenol.* The Canadian Journal of Chemical Engineering, 2003. **81**(3-4): p. 784-794.

213. Chowdhury, R., E. Pedernera, and R. Reimert, *Trickle-bed reactor model for desulfurization and dearomatization of diesel.* AIChE Journal, 2002. **48**(1): p. 126-135.

214. Bhaskar, M., G. Valavarasu, A. Meenakshisundaram, and K. Balaraman, *Application of a three phase heterogeneous model to analyse the performance of a pilot plant trickle bed reactor.* Petroleum Science and Technology, 2002. **20**(3-4): p. 251-268.

215. Rajashekharam, M.V., R. Jaganathan, and R.V. Chaudhari, *A trickle-bed reactor model for hydrogenation of 2, 4 dinitrotoluene: experimental verification.* Chemical Engineering Science, 1998. **53**(4): p. 787-805.

216. Devetta, L., P. Canu, A. Bertucco, and K. Steiner, *Modelling of a trickle-bed reactor for a catalytic hydrogenation in supercritical* CO_2. Chemical Engineering Science, 1997. **52**(21-22): p. 4163-4169.

217. Bergault, I., M. Rajashekharam, R. Chaudhari, D. Schweich, and H. Delmas, *Modeling and comparison of acetophenone hydrogenation in trickle-bed and slurry airlift reactors.* Chemical Engineering Science, 1997. **52**(21-22): p. 4033-4043.

218. Valerius, G., X. Zhu, H. Hofmann, D. Arntz, and T. Haas, *Modelling of a trickle-bed reactor II. The hydrogenation of 3-hydroxypropanal to 1, 3-propanediol.* Chemical Engineering and Processing: Process Intensification, 1996. **35**(1): p. 11-19.

219. Toppinen, S., J. Aittamaa, and T. Salmi, *Interfacial mass transfer in trickle-bed reactor modelling.* Chemical Engineering Science, 1996. **51**(18): p. 4335-4345.

220. Hanika, J. and J. Růžička, *Modelling of a trickle bed reactor with strong exothermal reaction.* Catalysis Today, 1995. **24**(1-2): p. 87-93.

221. Zheng, Q., F.J. Russo-Abegao, A.J. Sederman, and L.F. Gladden, *Operando determination of the liquid-solid mass transfer coefficient during 1-octene hydrogenation.* Chemical Engineering Science, 2017. **171**: p. 614-624.

222. Haßelberg, J., A. Behr, C. Weiser, J. Bially, and I. Sinev, *Process development for the synthesis of saturated branched fatty derivatives: Combination of homogeneous and heterogeneous catalysis in miniplant scale.* Chemical Engineering Science, 2016. **143**: p. 256-269.

223. Haase, S., M. Weiss, R. Langsch, T. Bauer, and R. Lange, *Hydrodynamics and mass transfer in three-phase composite minichannel fixed-bed reactors.* Chemical Engineering Science, 2013. **94**: p. 224-236.

224. Safinski, T. and A.A. Adesina, *Two-phase flow countercurrent operation of a trickle bed reactor: hold-up and mixing behavior over raschig rings fixed bed and structured bale packing.* Industrial & Engineering Chemistry Research, 2011. **51**(4): p. 1647-1662.

225. Son, S.M. and K. Kusakabe, *Transesterification of sunflower oil in a countercurrent trickle-bed reactor packed with a CaO catalyst.* Chemical Engineering and Processing: Process Intensification, 2011. **50**(7): p. 650-654.

226. Bauer, T. and S. Haase, *Comparison of structured trickle-bed and monolithic reactors in Pd-catalyzed hydrogenation of alpha-methylstyrene.* Chemical Engineering Journal, 2011. **169**(1-3): p. 263-269.

227. Atta, A., M. Hamidipour, S. Roy, K. Nigam, and F. Larachi, *Propagation of slow/fast-mode solitary liquid waves in trickle beds via electrical capacitance tomography and computational fluid dynamics.* Chemical Engineering Science, 2010. **65**(3): p. 1144-1150.

228. Atta, A., S. Roy, and K. Nigam, *A two-phase Eulerian approach using relative permeability concept for modeling of hydrodynamics in trickle-bed reactors at elevated pressure.* Chemical Engineering Research and Design, 2010. **88**(3): p. 369-378.

229. Trivizadakis, M., D. Giakoumakis, and A. Karabelas, *Induced pulsing in trickle beds—particle shape and size effects on pulse characteristics.* Chemical Engineering Science, 2006. **61**(22): p. 7448-7462.

230. Callejas, M.A. and M.T. Martínez, *Evaluation of kinetic and hydrodynamic models in the hydroprocessing of a trickle-bed reactor.* Energy & Fuels, 2002. **16**(3): p. 647-652.

231. Iliuta, I. and F. Larachi, *Onset of pulsing in gas–liquid trickle bed filtration.* Chemical Engineering Science, 2004. **59**(6): p. 1199-1211.

232. Gray, M.R., N. Srinivasan, and J.H. Masliyah, *Pressure buildup in gas-liquid flow through packed beds due to deposition of fine particles.* The Canadian Journal of Chemical Engineering, 2002. **80**(3): p. 346-354.

233. Janecki, D., A. Szczotka, A. Burghardt, and G. Bartelmus, *Modelling wet-air oxidation of phenol in a trickle-bed reactor using active carbon as a catalyst.* Journal of Chemical Technology & Biotechnology, 2016. **91**(3): p. 596-607.

234. Erjavec, B., R. Kaplan, P. Djinović, and A. Pintar, *Catalytic wet air oxidation of bisphenol A model solution in a trickle-bed reactor over titanate nanotube-based catalysts.* Applied Catalysis B: Environmental, 2013. **132**: p. 342-352.

235. Silva, J., *Dynamic modelling for a trickle-bed reactor using the numerical inverse Laplace transform technique.* Procedia Engineering, 2012. **42**: p. 454-470.

236. Nijhuis, T., F. Dautzenberg, and J. Moulijn, *Modeling of monolithic and trickle-bed reactors for the hydrogenation of styrene.* Chemical Engineering Science, 2003. **58**(7): p. 1113-1124.

237. Ferdous, D., A. Dalai, and J. Adjaye, *Comparison of hydrodenitrogenation of model basic and nonbasic nitrogen species in a trickle bed reactor using commercial NiMo/Al_2O_3 Catalyst.* Energy & Fuels, 2003. **17**(1): p. 164-171.

238. Khadilkar, M., Y. Wu, M. Al-Dahhan, M. Duduković, and M. Colakyan, *Comparison of trickle-bed and upflow reactor performance at high pressure: model predictions and experimental observations.* Chemical Engineering Science, 1996. **51**(10): p. 2139-2148.

239. Maiti, R., R. Khanna, and K. Nigam, *Hysteresis in trickle-bed reactors: a review.* Industrial & Engineering Chemistry Research, 2006. **45**(15): p. 5185-5198.

240. Kuzeljevic, Z.V., W.v.d. Merwe, M.H. Al-Dahhan, M.P. Dudukovic, and W. Nicol, *Effect of operating pressure on the extent of hysteresis in a trickle bed reactor.* Industrial & Engineering Chemistry Research, 2008. **47**(20): p. 7593-7599.

241. van Houwelingen, A.J., C. Sandrock, and W. Nicol, *Particle wetting distribution in trickle-bed reactors.* AIChE Journal, 2006. **52**(10): p. 3532-3542.

242. Saroha, A.K. and I. Nandi, *Pressure drop hysteresis in trickle bed reactors.* Chemical Engineering Science, 2008. **63**(12): p. 3114-3119.

243. Maiti, R., A. Atta, and K. Nigam, *Effect of particle porosity on hysteresis in trickle-bed reactors.* Industrial & Engineering Chemistry Research, 2008. **47**(21): p. 8126-8135.

244. Bose, S.K., *Numerical Methods of Mathematics Implemented in Fortran*. First ed. 2019, Singapore: Springer.

245. Martín, M.M., *Introduction to Software for Chemical Engineers*. First ed. 2014, USA: CRC Press.

246. Versteeg, H.K. and W. Malalasekera, *An Introduction to Computational Fluid Dynamics: The Finite Volume Method*. Second ed. 2007, England: Pearson Education.

247. Cundall, P.A. and O.D. Strack, *A discrete numerical model for granular assemblies.* Geotechnique, 1979. **29**(1): p. 47-65.

248. Process Systems Enterprise Limited. *gPROMS ProcessBuilder* 2020 [cited 2020 April 08, 2020]; Available from: https://www.psenterprise.com/products/gproms/processbuilder.

249. Andrei, N., *Nonlinear Optimization Applications Using the GAMS Technology*. 2013, Romania: Springer.

250. Wood, S.N., *Generalized Additive Models: An Introduction with R*. Second ed. 2017, USA: CRC Press.

251. AthenaVisual. *AthenaVisual Studio is a unique software*. 2020 [cited 2020 2020 November 28]; Available from: https://athenavisual.com/about/.

252. Montgomery, D.C., *Design and Analysis of Experiments*. 2017, USA: John Wiley & Sons.

253. Gen, M. and R. Cheng, *Genetic Algorithms and Engineering Optimization*. First ed. 2000, USA: John Wiley & Sons Inc.

254. Al-Dalama, K. and A. Stanislaus, *Comparison between deactivation pattern of catalysts in fixed-bed and ebullating-bed residue hydroprocessing units.* Chemical Engineering Journal, 2006. **120**(1): p. 33-42.

255. Alvarez, A. and J. Ancheyta, *Modeling residue hydroprocessing in a multi-fixed-bed reactor system.* Applied Catalysis A: General, 2008. **351**(2): p. 148-158.

256. Elizalde, I. and J. Ancheyta, *Modeling the deactivation by metal deposition of heavy oil hydrotreating catalyst.* Catalysis Today, 2014. **220**: p. 221-227.

257. Torres-Mancera, P., P. Rayo, J. Ancheyta, G. Marroquín, G. Centeno, and F. Alonso, *Characterization of spent and regenerated catalysts recovered from a residue hydrotreating bench-scale reactor.* Fuel, 2015. **149**: p. 143-148.

258. Guo, J. and M. Al-Dahhan, *A sequential approach to modeling catalytic reactions in packed-bed reactors.* Chemical Engineering Science, 2004. **59**(10): p. 2023-2037.

259. Shahrokhi, M. and G. Baghmisheh, *Modeling, simulation and control of a methanol synthesis fixed-bed reactor.* Chemical Engineering Science, 2005. **60**(15): p. 4275-4286.

260. Sandelin, F., P. Oinas, T. Salmi, J. Paloniemi, and H. Haario, *Dynamic modelling of catalytic liquid-phase reactions in fixed beds—kinetics and catalyst deactivation in the recovery of anthraquinones.* Chemical Engineering Science, 2006. **61**(14): p. 4528-4539.

261. Zahedi, G., H. Yaqubi, and M. Ba-Shammakh, *Dynamic modeling and simulation of heavy paraffin dehydrogenation reactor for selective olefin production in linear alkyl benzene production plant.* Applied Catalysis A: General, 2009. **358**(1): p. 1-6.

262. Toukoniitty, E., J. Wärnå, D.Y. Murzin, and T. Salmi, *Modelling of transient kinetics in catalytic three-phase reactors: Enantioselective hydrogenation.* Chemical Engineering Science, 2010. **65**(3): p. 1076-1087.

263. Azarpour, A. and G. Zahedi, *Performance analysis of crude terephthalic acid hydropurification in an industrial trickle-bed reactor experiencing catalyst deactivation.* Chemical Engineering Journal, 2012. **209**: p. 180-193.

264. Alvarez, A. and J. Ancheyta, *Transient behavior of residual oil front-end hydrodemetallization in a trickle-bed reactor.* Chemical Engineering Journal, 2012. **197**(Supplement C): p. 204-214.

265. Aksikas, I., L. Mohammadi, J. Forbes, Y. Belhamadia, and S. Dubljevic, *Optimal control of an advection-dominated catalytic fixed-bed reactor with catalyst deactivation.* Journal of Process Control, 2013. **23**(10): p. 1508-1514.

266. Farsi, M. and A. Jahanmiri, *Dynamic modeling and operability analysis of a dual-membrane fixed bed reactor to produce methanol considering catalyst deactivation.* Journal of Industrial and Engineering Chemistry, 2014. **20**(5): p. 2927-2933.

267. Li, Z., W. Zhong, X. Wang, N. Luo, and F. Qian, *Control structure design of an industrial crude terephthalic acid hydropurification process with catalyst deactivation.* Computers & Chemical Engineering, 2016. **88**: p. 1-12.

268. Izadi, N., A.M. Rashidi, A. Izadi, S. Emami, V. Samimi, and H. Varmazyar, *Selective hydrogenation of 4-carboxybenzaldehyde over palladium catalysts supported with different structural organization.* International Journal of Hydrogen Energy, 2017. **42**(5): p. 2970-2983.

269. Zhou, J.-H., G.-Z. Shen, J. Zhu, and W.-K. Yuan, *Terephthalic acid hydropurification over Pd/C catalyst.* Studies in Surface Science and Catalysis, 2006: p. 293-296.

270. Rotunno, F., et al., *Preparation of Pd/C catalysts: from the Pd-precursor solution to the final systems.* Studies in Surface Science and Catalysis, 2006. **162**: p. 721-728.

271. Azarpour, A., T. Nejad Ghaffar Borhani, S.R. Wan Alwi, Z. Abdul Manan, and M. Madooli Behbehani, *Prediction of Pd/C catalyst deactivation rate and assessment of optimal operating conditions of industrial hydropurification process.* Industrial & Engineering Chemistry Research, 2015. **54**(28): p. 7067-7082.

272. Shevchenko, V., L. Kurochkina, L. Repina, and V. Malykh, *Synthesis of polyethylene terephthalate in the presence of 4-carboxybenzaldehyde.* Fibre Chemistry, 1984. **15**(4): p. 241-244.

273. Shaogang, Z., Z. Jinghong, and Y. Weikang, *Mathematical simulation of hydrorefining reactor for terephthalic acid.* Chemical Reaction Engineering and Technology, 2008. **24**(1): p. 54-60.

274. Butt, J.B., *Reaction Kinetics and Reactor Design*. 2000, New York: CRC Press.

275. Davis, M.E. and R.J. Davis, *Fundamentals of Chemical Reaction Engineering*. 2012, New York: McGraw-Hill Higher Education.

276. Chu, C. and K. Ng, *Flow in packed tubes with a small tube to particle diameter ratio.* AIChE Journal, 1989. **35**(1): p. 148-158.

277. Carberry, J. and D. White, *On the role of transport phenomena in catalytic reactor behavior.* Industrial & Engineering Chemistry, 1969. **61**(7): p. 27-35.

278. Ergun, S., *Fluid flow through packed columns.* Chemical Engineering Progress, 1952. **48**: p. 89-94.

279. He, Y., *Studies on a 2D Pseudo-homogeneous Reactor Model*. 2000, University of Kansas, Chemical and Petroleum Engineering.

280. Levenspiel, O., *Chemical Reaction Engineering*. Third ed. 1999, New York: John Wiley & Sons.

281. Roberts, G.W., *Chemical Reactions and Chemical Reactors*. 2009: John Wiley & Sons Hoboken, NJ.

282. Midoux, N., M. Favier, and J.-C. Charpentier, *Flow pattern, pressure loss and liquid holdup data in gas-liquid downflow packed beds with foaming and nonfoaming hydrocarbons.* Journal of Chemical Engineering of Japan, 1976. **9**(5): p. 350-356.

283. Bart, J.C., *Polymer Additive Analytics: Industrial Practice and Case Studies*. Vol. 14. 2006, Italy: Firenze University Press.

284. Shaogang, Z., Z. Jinghong, X. Xiaochun, S. Zhijun, Z. Xinggui, and Y. Woikang, *Apparent kinetics of 4-CBA tandem hydrogenation over Pd/C Catalyst.* Chemical Reaction Engineering and Technology, 2008. **24**(6): p. 509-515.

285. Zhou, J.-h., T. Zhang, Z.-j. Sui, P. Li, and W.-k. Yuan, *Hydropurification of Terephthalic Acid over Pd/AC I. Thermodynamics and Feature Analysis.* Journal of East China University of Science and Technology, 2006. **32**(4): p. 374-380.

286. Agency, E.P. *Chemical properties*. 2018 [cited 2018 05-Jan-2018]; Available from: https://comptox.epa.gov.

287. Iliuta, I., F. Larachi, and M.H. Al-Dahhan, *Multiple-zone model for partially wetted trickle flow hydrodynamics.* Chemical Engineering Research and Design, 2000. **78**(7): p. 982-990.

288. Xiao, Q., Z. Cheng, Z. Jiang, A. Anter, and W. Yuan, *Hydrodynamic behavior of a trickle bed reactor under "forced" pulsing flow.* Chemical Engineering Science, 2001. **56**(3): p. 1189-1195.

289. Iliuta, I., F. Larachi, and B. Grandjean, *Fines deposition dynamics in gas–liquid trickle-flow reactors.* AIChE Journal, 2003. **49**(2): p. 485-495.

290. Sales, F., L. Maranhão, J. Pereira, and C. Abreu, *Experimental dynamic evaluation of three-phase reactors.* Brazilian Journal of Chemical Engineering, 2005. **22**(3): p. 443-452.

291. Iliuta, I. and F. Larachi, *Deposition and aggregation of Brownian particles in trickle-bed reactors.* AIChE Journal, 2006. **52**(12): p. 4167-4180.

292. Tukač, V., et al., *The behavior of pilot trickle-bed reactor under periodic operation.* Chemical Engineering Science, 2007. **62**(18-20): p. 4891-4895.

293. van der Merwe, W., W. Nicol, and M.H. Al-Dahhan, *Effect of hydrodynamic multiplicity on trickle bed reactor performance.* AIChE Journal, 2008. **54**(1): p. 249-257.

294. Lopes, R.J. and R.M. Quinta-Ferreira, *Numerical simulation of trickle-bed reactor hydrodynamics with RANS-based models using a volume of fluid technique.* Industrial & Engineering Chemistry Research, 2009. **48**(4): p. 1740-1748.

295. Prokešová, A., V. Tukač, and M. Zbuzek, *Hydrodynamics characteristics of HDS trickle bed test reactor.* Procedia Engineering, 2012. **42**: p. 885-891.

296. Salimi, M., S.H. Hashemabadi, S. Noroozi, A. Heidari, and M. Bazmi, *Numerical and Experimental Study of Catalyst Loading and Body Effects on a Gas-Liquid Trickle-Flow Bed.* Chemical Engineering & Technology, 2013. **36**(1): p. 43-52.

297. Homma, T. and T. Kitaoka, *Multiphase catalytic oxidation of alcohols over paper-structured catalysts with micrometer-size pores.* Applied Catalysis A: General, 2014. **486**: p. 201-209.

298. Su, W.-B., T.-K. Chang, J.-H. Hwang, and H.-Y. Huang, *Applying reactor model parameters to estimate pygas selective hydrogenation catalyst activity during operation cycle.* Journal of the Taiwan Institute of Chemical Engineers, 2015. **56**: p. 28-33.

299. Rabbani, S., T. Sahmim, and M. Sassi, *Numerical Modelling and Simulation of Gas-Liquid Trickle Flow in Trickle Bed Reactor Using an Improved Phenomenological Model.* Energy Procedia, 2017. **105**: p. 4140-4145.

300. Guo, Y., C. Dai, and Z. Lei, *Hydrodynamics and mass transfer in multiphase monolithic reactors with different distributors: An experimental and modeling study.* Chemical Engineering and Processing-Process Intensification, 2018. **125**: p. 234-245.

301. Biardi, G. and G. Baldi, *Three-phase catalytic reactors.* Catalysis Today, 1999. **52**(2-3): p. 223-234.

302. Kapteijn, F., J.J. Heiszwolf, T.v. Nijhuis, and J.A. Moulijn, *Monoliths in multiphase catalytic processes: aspects and prospects.* Cattech, 1999. **3**(1): p. 24-41.

303. Charpentier, J.C. and M. Favier, *Some liquid holdup experimental data in trickle-bed reactors for foaming and nonfoaming hydrocarbons.* AIChE Journal, 1975. **21**(6): p. 1213-1218.

304. Dudukovic, M.P. and P. Mills, *Contacting and hydrodynamics in trickle-bed reactors.* Encyclopedia of Fluid Mechanics, 1986. **3**: p. 969.

305. Spiegel, L. and W. Meier, *Distillation columns with structured packings in the next decade.* Chemical Engineering Research and Design, 2003. **81**(1): p. 39-47.

306. Laso, M., M.H. de Brito, P. Bomio, and U. Von Stockar, *Liquid-side mass transfer characteristics of a structured packing.* The Chemical Engineering Journal and the Biochemical Engineering Journal, 1995. **58**(3): p. 251-258.

307. Kapteijn, F., T. Nijhuis, J. Heiszwolf, and J. Moulijn, *New non-traditional multiphase catalytic reactors based on monolithic structures.* Catalysis Today, 2001. **66**(2-4): p. 133-144.

308. Cybulski, A. and J.A. Moulijn, *Monoliths in heterogeneous catalysis.* Catalysis Reviews—Science and Engineering, 1994. **36**(2): p. 179-270.

309. Nijhuis, T., F. Kapteijn, and J. Moulijn, *Monolithic catalysts as more efficient reactors in three-phase applications*, in *Studies in Surface Science and Catalysis*. 2000, Elsevier. p. 2735-2740.

310. Kreutzer, M.T., F. Kapteijn, and J.A. Moulijn, *Shouldn't catalysts shape up?: Structured reactors in general and gas–liquid monolith reactors in particular.* Catalysis Today, 2006. **111**(1-2): p. 111-118.

311. Moulijn, J., M. Kreutzer, and F. Kapteijn, *A little structure works wonders.* Chemical Engineer, 2005. **768**: p. 32.

312. Azarpour, A., S.R.W. Alwi, G. Zahedi, M. Madooli, and G.J. Millar, *Catalytic activity evaluation of industrial Pd/C catalyst via gray-box dynamic modeling and simulation of hydropurification reactor.* Applied Catalysis A: General, 2015. **489**: p. 262-271.

313. Azarpour, A. and S. Zendehboudi, *A dynamic heterogeneous dispersion model evaluates performance of industrial catalytic hydrotreating systems.* Industrial & Engineering Chemistry Research, 2018. **57**(24): p. 8267-8282.

314. Iliuta, I., A. Ortiz-Arroyo, F.ç. Larachi, B.P. Grandjean, and G. Wild, *Hydrodynamics and mass transfer in trickle-bed reactors: an overview.* Chemical Engineering Science, 1999. **54**(21): p. 5329-5337.

315. Turpin, J.L. and R. Huntington, *Prediction of pressure drop for two-phase, two-component concurrent flow in packed beds.* AIChE Journal, 1967. **13**(6): p. 1196-1202.

316. Larkins, R.P., R. White, and D. Jeffrey, *Two-phase concurrent flow in packed beds.* AIChE Journal, 1961. **7**(2): p. 231-239.

317. Dudukovic, M.P., F. Larachi, and P.L. Mills, *Multiphase reactors–revisited.* Chemical Engineering Science, 1999. **54**(13-14): p. 1975-1995.

318. Iliuta, I., F. Larachi, and B.P. Grandjean, *Pressure drop and liquid holdup in trickle flow reactors: improved Ergun constants and slip correlations for the slit model.* Industrial & Engineering Chemistry Research, 1998. **37**(12): p. 4542-4550.

319. Krishna, R. and S. Sie, *Strategies for multiphase reactor selection.* Chemical Engineering Science, 1994. **49**(24): p. 4029-4065.

320. Larachi, F., I. Iliuta, M. Al-Dahhan, and M. Dudukovic, *Discriminating trickle-flow hydrodynamic models: some recommendations.* Industrial & Engineering Chemistry Research, 2000. **39**(2): p. 554-556.

321. Silveston, P. and J. Hanika, *Challenges for the periodic operation of trickle-bed catalytic reactors.* Chemical Engineering Science, 2002. **57**(16): p. 3373-3385.

322. Burghardt, A., A.S. Koodziej, and M.w. Jaroszyński, *Experimental studies of liquid—solid wetting efficiency in trickle-bed cocurrent reactors.* Chemical Engineering and Processing, 1990. **28**(1): p. 35-49.

323. Colombo, A., G. Baldi, and S. Sicardi, *Solid-liquid contacting effectiveness in trickle bed reactors*. Chemical Engineering Science, 1976. **31**(12): p. 1101-1108.

324. Gladden, L., M. Lim, M. Mantle, A. Sederman, and E. Stitt, *MRI visualisation of two-phase flow in structured supports and trickle-bed reactors.* Catalysis Today, 2003. **79**: p. 203-210.

325. Speccia, V., G. Baldi, and A. Gianetto, *Solid-liquid mass transfer in concurrent two-phase flow through packed beds.* Industrial & Engineering Chemistry Process Design and Development, 1978. **17**(3): p. 362-367.

326. Al-Dahhan, M.H. and M.P. Duduković, *Catalyst bed dilution for improving catalyst wetting in laboratory trickle-bed reactors.* AIChE Journal, 1996. **42**(9): p. 2594-2606.

327. Gladden, L., L. Anadon, M. Lim, A. Sederman, and E. Stitt, *Insights into the mechanism of the trickle-to-pulse transition in trickle-bed reactors.* Industrial & Engineering Chemistry Research, 2005. **44**(16): p. 6320-6331.

328. Al-Dahhan, M., W. Highfill, and M. Friedman, *Assessment of the effects of high-pressure operation on the liquid-solid mass-transfer coefficient in trickle-bed reactors.* Industrial & Engineering Chemistry Research, 1997. **36**(10): p. 4421-4426.

329. Rao, V.G. and A. Drinkenburg, *Solid-liquid mass transfer in packed beds with cocurrent gas-liquid downflow.* AIChE Journal, 1985. **31**(7): p. 1059-1068.

330. Hirose, T., Y. Mori, and Y. Sato, *Liquid-to-particle mass transfer in fixed bed reactor with cocurrent gas-liquid downflow*. Journal of Chemical Engineering of Japan, 1976. **9**(3): p. 220-225.

331. Mann, R., I. Sambi, and K. Khulbe, *Hydrofining of heavy gas oil on zeolite-alumina supported nickel-molybdenum catalyst.* Industrial & Engineering Chemistry Research, 1988. **27**(10): p. 1788-1792.

332. Mann, R.S., I.S. Sambi, and K.C. Khulbe, *Catalytic hydrofining of heavy gas oil*. Industrial & Engineering Chemistry Research, 1987. **26**(3): p. 410-414.

333. Mapiour, M.L., *Kinetics and effects of H2 partial pressure on hydrotreating of heavy gas oil*. 2009, University of Saskatchewan.

334. Nagy, G., G. Pölczmann, D. Kalló, and J. Hancsók, *Investigation of hydrodearomatization of gas oils on noble metal/support catalysts.* Chemical Engineering Journal, 2009. **154**(1-3): p. 307-314.

335. Vogelaar, B.M., S. Eijsbouts, J.A. Bergwerff, and J.J. Heiszwolf, *Hydroprocessing catalyst deactivation in commercial practice.* Catalysis Today, 2010. **154**(3-4): p. 256-263.

336. Ramírez-Castelán, C.E., A. Hidalgo-Vivas, J. Brix, A.D. Jensen, and J.K. Huusom, *Mathematical Modelling and Simulation of a Trickle-Bed Reactor for Hydrotreating of Petroleum Feedstock.* International Journal of Chemical Reactor Engineering, 2019. **17**(7).

337. Taulamet, M.J., N.J. Mariani, G.F. Barreto, and O.M. Martínez, *Prediction of thermal behavior of trickle bed reactors: The effect of the pellet shape and size.* Fuel, 2017. **202**: p. 631-640.

338. Jarullah, A.T., I.M. Mujtaba, and A.S. Wood, *Improving fuel quality by whole crude oil hydrotreating: A kinetic model for hydrodeasphaltenization in a trickle bed reactor.* Applied Energy, 2012. **94**: p. 182-191.

339. Alonso, F., J. Ancheyta, G. Centeno, G. Marroquín, P. Rayo, and R. Silva-Rodrigo, *Effect of Reactor Configuration on the Hydrotreating of Atmospheric Residue.* Energy & Fuels, 2019. **33**(2): p. 1649-1658.

340. Galiasso Tailleur, R. and Y. Davila, *Optimal hydrogen production through revamping a naphtha-reforming unit: catalyst deactivation.* Energy & Fuels, 2008. **22**(5): p. 2892-2901.

341. Xu, M., H. Liu, S. Ji, and C. Li, *Intensification of deep hydrodesulfurization through a two-stage combination of monolith and trickle bed reactors.* Chinese Journal of Chemical Engineering, 2014. **22**(8): p. 888-897.

342. Jiménez, F., V. Kafarov, and M. Nuñez, *Computer-aided modeling for hydrodesulfurization, hydrodenitrogenation and hydrodearomatization simultaneous reactions in a hydrotreating industrial process*, in *Computer Aided Chemical Engineering*. 2006, Elsevier. p. 651-657.

343. Elizalde, I. and J. Ancheyta, *Application of a three-stage approach for modeling the complete period of catalyst deactivation during hydrotreating of heavy oil.* Fuel, 2014. **138**: p. 45-51.

344. Pant, H. and V. Sharma, *Investigation of flow dynamics of liquid phase in a pilot-scale trickle bed reactor using radiotracer technique.* Applied Radiation and Isotopes, 2016. **116**: p. 163-173.

345. Cotta, R.M., M. Wolf-Maciel, and R. Maciel Filho, *A cape of HDT industrial reactor for middle distillates.* Computers & Chemical Engineering, 2000. **24**(2-7): p. 1731-1735.

346. Oyama, S., X. Wang, Y.-K. Lee, K. Bando, and F. Requejo, *Effect of phosphorus content in nickel phosphide catalysts studied by XAFS and other techniques.* Journal of Catalysis, 2002. **210**(1): p. 207-217.

347. Lopes, R.J. and R.M. Quinta-Ferreira, *Hydrodynamic simulation of pulsing-flow regime in high-pressure trickle-bed reactors.* Industrial & Engineering Chemistry Research, 2010. **49**(3): p. 1105-1112.

348. Holland, D., *Applications of tomography in bubble column and trickle bed reactors*, in *Industrial Tomography*. 2015, Elsevier. p. 477-507.

349. Boelhouwer, J.G., H.W. Piepers, and B.A. Drinkenburg, *Advantages of forced non-steady operated trickle-bed reactors.* Chemical Engineering and Technology, 2002. **25**(6): p. 647-650.

350. Nawaf, A.T., S.A. Gheni, A.T. Jarullah, and I.M. Mujtaba, *Improvement of fuel quality by oxidative desulfurization: Design of synthetic catalyst for the process.* Fuel Processing Technology, 2015. **138**: p. 337-343.

351. Hita, I., R. Palos, J.M. Arandes, J.M. Hill, and P. Castaño, *Petcoke-derived functionalized activated carbon as support in a bifunctional catalyst for tire oil hydroprocessing.* Fuel Processing Technology, 2016. **144**: p. 239-247.

352. Feng, X., D. Li, J. Chen, M. Niu, X. Liu, L.L.T. Chan, and W. Li, *Kinetic parameter estimation and simulation of trickle-bed reactor for hydrodesulfurization of whole fraction low-temperature coal tar.* Fuel, 2018. **230**: p. 113-125.

353. da Silva, J.I. and A.R. Secchi, *Model predective control for production of ultra-low sulfur diesel in a hydrotreating process.* Brazilian Journal of Chemical Engineering, 2019. **36**(1): p. 439-452.

354. Bannatham, P., S. Teeraboonchaikul, T. Patirupanon, W. Arkardvipart, S. Limtrakul, T. Vatanatham, and P.A. Ramachandran, *Kinetic evaluation for hydrodesulfurization via*

lumped model in a trickle-bed reactor. Industrial & Engineering Chemistry Research, 2016. **55**(17): p. 4878-4886.

355. Janecki, D., A. Burghardt, and G. Bartelmus, *Parametric sensitivity of a CFD model concerning the hydrodynamics of trickle-bed reactor (TBR).* Chemical and Process Engineering, 2016. **37**(1): p. 97-107.

356. Sbaaei, E.S. and T.S. Ahmed, *Predictive modeling and optimization for an industrial Coker Complex Hydrotreating unit–development and a case study*. Fuel, 2018. **212**: p. 61-76.

357. Li, K.-T. and S.-W. Li, *CoBr2-MnBr2 containing catalysts for catalytic oxidation of p-xylene to terephthalic acid.* Applied Catalysis A: General, 2008. **340**(2): p. 271-277.

358. Fadzil, N.A.M., M.H.A. Rahim, and G.P. Maniam, *A brief review of para-xylene oxidation to terephthalic acid as a model of primary C–H bond activation.* Chinese Journal of Catalysis, 2014. **35**(10): p. 1641-1652.

359. Shang, J., W. Sun, L. Zhao, and W.-K. Yuan, *Modeling of* CO_2*-assisted liquid phase oxidation of para-xylene catalyzed by transition metals/bromide.* Chemical Engineering Science, 2015. **127**: p. 52-59.

360. *Purified Terephthalic Acid (PTA) Properties, Production, Price, and Market*. 2020 (accessed 22 April 2020), https://www.plasticsinsight.com/resin-intelligence/resin-prices/purified-terephthalic-acid-pta/ [cited accessed 22 April 2020 April 22, 2020]; Available from: https://www.plasticsinsight.com/resin-intelligence/resin-prices/purified-terephthalic-acid-pta/.

361. Geng, Z., J. Dong, J. Chen, and Y. Han, *A new Self-Organizing Extreme Learning Machine soft sensor model and its applications in complicated chemical processes.* Engineering Applications of Artificial Intelligence, 2017. **62**: p. 38-50.

362. Geng, Z., H. Li, Q. Zhu, and Y. Han, *Production prediction and energy-saving model based on Extreme Learning Machine integrated ISM-AHP: Application in complex chemical processes.* Energy, 2018. **160**: p. 898-909.

363. Li, Z., W. Zhong, Y. Liu, N. Luo, and F. Qian, *Dynamic modeling and control of industrial crude terephthalic acid hydropurification process.* Korean Journal of Chemical Engineering, 2015. **32**(4): p. 597-608.

364. Zhang, X.-H., Q.-X. Zhu, Y.-L. He, and Y. Xu, *Energy modeling using an effective latent variable based functional link learning machine.* Energy, 2018. **162**: p. 883-891.

365. Cheng, Y., X. Li, Q. Wang, and L. Wang, *Effects of guanidine on the liquid-phase catalytic oxidation of p-xylene to terephthalic acid.* Industrial & Engineering Chemistry Research, 2005. **44**(20): p. 7756-7760.

366. Wang, Q., Y. Cheng, L. Wang, H. Xu, and X. Li, *Isothermal seeded semicontinuous reactive crystallization of crude terephthalic acid crystals.* Industrial & Engineering Chemistry Research, 2008. **47**(16): p. 5861-5870.

367. Wang, Q., Y. Cheng, L. Wang, and X. Li, *Semicontinuous studies on the reaction mechanism and kinetics for the liquid-phase oxidation of p-xylene to terephthalic acid.* Industrial & Engineering Chemistry Research, 2007. **46**(26): p. 8980-8992.

368. Cheng, Y., P. Ge, W. Lijun, and L. Xi, *Kinetics of burning side reaction in the liquid-phase oxidation of p-xylene.* Chinese Journal of Chemical Engineering, 2009. **17**(2): p. 181-188.

369. Jing-hong, Z., S. Guang-zho, L. Ping, D. Ying-chun, and Y. Wei-kang, *Hydropurification of terephthalic acid over Pd/Ac-apparent kinetics of 4-CBA hydrogenation on catalysts of different sizes.* Journal of East China University of Science and Technology, 2006. **32**: p. 503-507.

370. Takebayashi, Y., K. Sue, S. Yoda, Y. Hakuta, and T. Furuya, *Solubility of terephthalic acid in subcritical water.* Journal of Chemical & Engineering Data, 2012. **57**(6): p. 1810-1816.

371. Peiguo, G., Z. Lijin, Y. Jiyong, and Z. Chongyu, *Deactivation of Pd/C Catalyst for Purification of Terephthalic Acid.* Petroleum Processing and Petrochemicals, 2005. **36**(8): p. 5-9.

372. da Rocha Novaes, L., M.E. Pacheco, V.M.M. Salim, and N.S. de Resende, *Accelerated deactivation studies of hydrotreating catalysts in pilot unit.* Applied Catalysis A: General, 2017. **548**: p. 114-121.

373. Trinh, T.-K.-H., J.-C. de Hemptinne, R. Lugo, N. Ferrando, and J.-P. Passarello, *Hydrogen solubility in hydrocarbon and oxygenated organic compounds.* Journal of Chemical & Engineering Data, 2015. **61**(1): p. 19-34.

374. Goodman, J.B. and N.W. Krase, *Solubility of nitrogen in water at high pressures and temperatures.* Industrial & Engineering Chemistry, 1931. **23**(4): p. 401-404.

375. Herskowitz, M., J. Wisniak, and L. Skladman, *Hydrogen solubility in organic liquids.* Journal of Chemical and Engineering Data, 1983. **28**(2): p. 164-166.

376. Lijin, Z., W. Zhenxin, and Z. Chongyu, *Mathematical model of reactor for hydrorefining of terephthalic acid and its calculation.* Petrochemical Technology, 2005. **34**(11): p. 1068-1072.

377. Lin, R., R.S. O'meadhra, and R.B. Sheppard, *Process for the production of purified terephthalic acid*, in *European Patent Office*. 2002.

378. Bartholomew, C.H., *Sintering kinetics of supported metals: perspectives from a generalized power law approach*, in *Studies in Surface Science and Catalysis*. 1994, Elsevier. p. 1-18.

379. Partenheimer, W., *The effect of zirconium in metal/bromide catalysts on the autoxidation of p-xylene: Part II. Alternative metals to zirconium and the effect of zirconium on manganese (IV) dioxide formation and precipitation with pyromellitic acid.* Journal of Molecular Catalysis A: Chemical, 2003. **206**(1-2): p. 131-144.

380. Yavari, I. and E. Karimi, *N-hydroxyphthalimide-catalyzed oxidative production of phthalic acids from xylenes using O2/HNO3 in an ionic liquid.* Synthetic Communications®, 2009. **39**(19): p. 3420-3427.

381. Chavan, S., D. Srinivas, and P. Ratnasamy, *Selective oxidation of para-xylene to terephthalic acid by μ3-oxo-bridged Co/Mn cluster complexes encapsulated in zeolite–Y.* Journal of Catalysis, 2001. **204**(2): p. 409-419.

382. Karapekmez, A. and I. Dincer, *Comparative efficiency and environmental impact assessments of a solar-assisted combined cycle with various fuels.* Applied Thermal Engineering, 2020. **164**: p. 114409.

383. Ghritlahre, H.K. and P.K. Sahu, *A comprehensive review on energy and exergy analysis of solar air heaters.* Archives of Thermodynamics, 2020. **41**: p. 183-222.

384. Ding, S. and Y. Liu, *Adsorption of CO_2 from flue gas by novel seaweed-based KOH-activated porous biochars.* Fuel, 2020. **260**: p. 116382.

385. Mohamadi-Baghmolaei, M., A. Hajizadeh, P. Zahedizadeh, R. Azin, and S. Zendehboudi, *Evaluation of hybridized performance of amine scrubbing plant based on exergy, energy,*

environmental, and economic prospects: A gas sweetening plant case study. Energy, 2021. **214**: p. 118715.

386. Koc, Y., M. Aksar, and H. Yagli, *First and second law-based thermal optimisation of the Kalina cycle integrated into an existing burner-based cogeneration system using waste chips as fuel.* International Journal of Exergy, 2020. **33**(2): p. 165-182.

387. Mohebbi, M., M. Reyhanian, I. Ghofrani, A.A. Aziz, and V. Hosseini, *Availability analysis on combustion of n-heptane and isooctane blends in a reactivity controlled compression ignition engine.* Proceedings of the Institution of Mechanical Engineers, Part D: Journal of Automobile Engineering, 2018. **232**(11): p. 1501-1515.

388. Abdelaziz, E., R. Saidur, and S. Mekhilef, *A review on energy saving strategies in industrial sector.* Renewable and Sustainable Energy Reviews, 2011. **15**(1): p. 150-168.

389. BoroumandJazi, G., B. Rismanchi, and R. Saidur, *A review on exergy analysis of industrial sector.* Renewable and Sustainable Energy Reviews, 2013. **27**: p. 198-203.

390. Shekarchian, M., F. Zarifi, M. Moghavvemi, F. Motasemi, and T. Mahlia, *Energy, exergy, environmental and economic analysis of industrial fired heaters based on heat recovery and preheating techniques.* Energy Conversion and Management, 2013. **71**: p. 51-61.

391. Christopher, K. and R. Dimitrios, *A review on exergy comparison of hydrogen production methods from renewable energy sources.* Energy & Environmental Science, 2012. **5**(5): p. 6640-6651.

392. Saidur, R., G. BoroumandJazi, S. Mekhilef, and H. Mohammed, *A review on exergy analysis of biomass based fuels.* Renewable and Sustainable Energy Reviews, 2012. **16**(2): p. 1217-1222.

393. Xu, B., R. Qi, W. Zhong, W. Du, and F. Qian, *Optimization of p-xylene oxidation reaction process based on self-adaptive multi-objective differential evolution.* Chemometrics and Intelligent Laboratory Systems, 2013. **127**: p. 55-62.

394. Huang, X., J. Wang, and Z. Li, *Analysis of Dynamic Characteristics and Control Strategies of a Solvent Dehydration Distillation Column in a Purified Terephthalic Acid Plant.* Processes, 2020. **8**(1): p. 125.

395. Garg, K.K. and B. Prasad, *Removal of para-toulic acid (p-TA) from purified terephthalic acid (PTA) waste water by electrocoagulation process.* Journal of Environmental Chemical Engineering, 2015. **3**(3): p. 1731-1739.

396. Geng, Z., X. Yang, Y. Han, and Q. Zhu, *Energy optimization and analysis modeling based on extreme learning machine integrated index decomposition analysis: application to complex chemical processes.* Energy, 2017. **120**: p. 67-78.

397. Han, Y., H. Wu, M. Jia, Z. Geng, and Y. Zhong, *Production capacity analysis and energy optimization of complex petrochemical industries using novel extreme learning machine integrating affinity propagation.* Energy Conversion and Management, 2019. **180**: p. 240-249.

398. Gong, H.-F., Z.-S. Chen, Q.-X. Zhu, and Y.-L. He, *A Monte Carlo and PSO based virtual sample generation method for enhancing the energy prediction and energy optimization on small data problem: An empirical study of petrochemical industries.* Applied Energy, 2017. **197**: p. 405-415.

399. Eslami, S. and M.S. Sekhavatjou, *Introducing an application method for industries air pollutants emission control planning by preparing environmental flow diagram maps.* Journal of Cleaner Production, 2018. **178**: p. 768-775.

400. Chen, K., et al., *Energy efficiency assessment and resource optimization using novel DEA model: evidence from complex chemical processes.* Energy Efficiency, 2020. **13**(7): p. 1427-1439.

401. Song, C., et al., *Research on energy efficiency evaluation based on indicators for industry sectors in China.* Applied Energy, 2014. **134**: p. 550-562.

402. Chan, D.Y.-L., C.-F. Huang, W.-C. Lin, and G.-B. Hong, *Energy efficiency benchmarking of energy-intensive industries in Taiwan.* Energy Conversion and Management, 2014. **77**: p. 216-220.

403. Utlu, Z. and A. Hepbasli, *A review and assessment of the energy utilization efficiency in the Turkish industrial sector using energy and exergy analysis method.* Renewable and Sustainable Energy Reviews, 2007. **11**(7): p. 1438-1459.

404. James, C., T.Y. Kim, and R. Jane, *A Review of Exergy Based Optimization and Control.* Processes, 2020. **8**(3): p. 364.

405. Kumar, A., M. Sharma, P. Thakur, V.K. Thakur, S.S. Rahatekar, and R. Kumar, *A review on exergy analysis of solar parabolic collectors.* Solar Energy, 2020. **197**: p. 411-432.

406. Mohamadi-Baghmolaei, M., F. Tabkhi, and J. Sargolzaei, *Exergetic approach to investigate the arrangement of compressors of a pipeline boosting station.* Energy Technology, 2014. **2**(8): p. 732-741.

407. Ghannadzadeh, A. and M. Sadeqzadeh, *Cleaner production of purified terephthalic and isophthalic acids through exergy analysis.* International Journal of Exergy, 2020. **31**(4): p. 303-329.

408. Mingyan, S., W. Lijun, C. Youwei, and L. Xi, *Exergy Analysis of Two Typical Pure Terephthalic Acid Process.* Petrochemical Technology, 2012. **4**: p. 10.

409. Braimakis, K., D. Magiri-Skouloudi, D. Grimekis, and S. Karellas, *Energy-exergy analysis of ultra-supercritical biomass-fuelled steam power plants for industrial CHP, district heating and cooling.* Renewable Energy, 2020. **154**: p. 252-269.

410. Yuan, B., Y. Zhang, W. Du, M. Wang, and F. Qian, *Assessment of energy saving potential of an industrial ethylene cracking furnace using advanced exergy analysis.* Applied Energy, 2019. **254**: p. 113583.

411. Zhang, Q., H. Yi, Z. Yu, J. Gao, X. Wang, H. Lin, and B. Shen, *Energy-exergy analysis and energy efficiency improvement of coal-fired industrial boilers based on thermal test data.* Applied Thermal Engineering, 2018. **144**: p. 614-627.

412. Soufiyan, M.M. and M. Aghbashlo, *Application of exergy analysis to the dairy industry: A case study of yogurt drink production plant.* Food and Bioproducts Processing, 2017. **101**: p. 118-131.

413. Wu, J., R. Wang, G. Pu, and H. Qi, *Integrated assessment of exergy, energy and carbon dioxide emissions in an iron and steel industrial network.* Applied Energy, 2016. **183**: p. 430-444.

414. Sarker, M.S.H., M.N. Ibrahim, N.A. Aziz, and M.S. Punan, *Energy and exergy analysis of industrial fluidized bed drying of paddy.* Energy, 2015. **84**: p. 131-138.

415. Alpay, T., B. Karabey, N. Azbar, and G. Ozdemir, *Purified terephthalic acid wastewater treatment using modified two-stage UASB bioreactor systems.* Current Microbiology, 2020: p. 1-8.

416. Gujarathi, A.M. and B. Babu, *Improved multiobjective differential evolution (MODE) approach for purified terephthalic acid (PTA) oxidation process.* Materials and Manufacturing Processes, 2009. **24**(3): p. 303-319.

417. Kleerebezem, R. and G. Lettinga, *High-rate anaerobic treatment of purified terephthalic acid wastewater.* Water Science and Technology, 2000. **42**(5-6): p. 259-268.

418. Li, Q., W. Guan, L. Wang, H. Wan, and G. Guan, *Dynamic simulation and control of a complete industrial acetic acid solvent dehydration system in purified terephthalic acid production.* Industrial & Engineering Chemistry Research, 2015. **54**(45): p. 11330-11343.

419. Mu, S., H. Su, Y. Gu, and J. Chu, *Multi-objective optimization of industrial purified terephthalic acid oxidation process.* Chinese Journal of Chemical Engineering, 2003. **11**(5): p. 536-541.

420. Mu, S., H. Su, T. Jia, Y. Gu, and J. Chu, *Scalable multi-objective optimization of industrial purified terephthalic acid (PTA) oxidation process.* Computers & Chemical Engineering, 2004. **28**(11): p. 2219-2231.

421. Zhang, X.-x., et al., *Purified terephthalic acid wastewater biodegradation and toxicity.* Journal of Environmental Sciences, 2005. **17**(5): p. 876-880.

422. Han, I.-S., et al., *Application of partial least squares methods to a terephthalic acid manufacturing process for product quality control.* Korean Journal of Chemical Engineering, 2003. **20**(6): p. 977-984.

423. Chengfei, L., *Dynamic Simulation and Analysis of Industrial Purified Terephthalic Acid Solvent Dehydration Process.* Chinese Journal of Chemical Engineering, 2011. **19**(1): p. 89-96.

424. Huang, X., W. Zhong, W. Du, and F. Qian, *Thermodynamic analysis and process simulation of an industrial acetic acid dehydration system via heterogeneous azeotropic distillation.* Industrial & Engineering Chemistry Research, 2013. **52**(8): p. 2944-2957.

425. Geng, Z., L. Qin, Y. Han, and Q. Zhu, *Energy saving and prediction modeling of petrochemical industries: A novel ELM based on FAHP.* Energy, 2017. **122**: p. 350-362.

426. Xu, Y., M. Zhang, L. Ye, Q. Zhu, Z. Geng, Y.-L. He, and Y. Han, *A novel prediction intervals method integrating an error & self-feedback extreme learning machine with*

particle swarm optimization for energy consumption robust prediction. Energy, 2018. **164**: p. 137-146.

427. Han, Y., C. Fan, M. Xu, Z. Geng, and Y. Zhong, *Production capacity analysis and energy saving of complex chemical processes using LSTM based on attention mechanism.* Applied Thermal Engineering, 2019. **160**: p. 114072.

428. Zhong, W., C. Jiang, X. Peng, Z. Li, and F. Qian, *Online quality prediction of industrial terephthalic acid hydropurification process using modified regularized slow-feature analysis*. Industrial & Engineering Chemistry Research, 2018. **57**(29): p. 9604-9614.

429. Ma, X.-c., X.-k. Li, X.-w. Wang, G.-g. Liu, J.-l. Zuo, S.-t. Wang, and K. Wang, *Impact of salinity on anaerobic microbial community structure in high organic loading purified terephthalic acid wastewater treatment system.* Journal of Hazardous materials, 2020. **383**: p. 121132.

430. Taheri, K., R. Gadow, and A. Killinger, *Exergy analysis as a developed concept of energy efficiency optimized processes: The case of thermal spray processes.* Procedia CIRP, 2014. **17**(Complete): p. 511-516.

431. Fitzsimons, L., B. Corcoran, P. Young, and G. Foley, *Exergy analysis of water purification and desalination: a study of exergy model approaches.* Desalination, 2015. **359**: p. 212-224.

432. Joybari, M.M., M.S. Hatamipour, A. Rahimi, and F.G. Modarres, *Exergy analysis and optimization of R600a as a replacement of R134a in a domestic refrigerator system.* International Journal of Refrigeration, 2013. **36**(4): p. 1233-1242.

433. Etghani, M.M. and S.A.H. Baboli, *Numerical investigation and optimization of heat transfer and exergy loss in shell and helical tube heat exchanger.* Applied Thermal Engineering, 2017. **121**: p. 294-301.

434. Taguchi, G., *System of Experimental Design: Engineering Methods to Optimize Quality and Minimize Costs*. 1987, USA: UNIPUB.

435. Mohamadi-Baghmolaei, M., R. Azin, S. Osfouri, and S. Zendehboudi, *Evaluation of mass transfer coefficient for gas condensates in porous systems: Experimental and modeling.* Fuel, 2019. **255**: p. 115507.

436. Lawrence, A., P. Thollander, M. Andrei, and M. Karlsson, *Specific energy consumption/use (SEC) in energy management for improving energy efficiency in industry: Meaning, usage and differences.* Energies, 2019. **12**(2): p. 247.

437. Stepanov, V.S., *Analysis of energy efficiency of industrial processes*. 2012: Springer Science & Business Media.

438. Hajizadeh, A., M. Mohamadi-Baghmolaei, R. Azin, S. Osfouri, and I. Heydari, *Technical and economic evaluation of flare gas recovery in a giant gas refinery.* Chemical Engineering Research and Design, 2018. **131**: p. 506-519.

439. Congressional Budget Office. *Impose a Tax on Emissions of Greenhouse Gases*. 2018 23-December-2020]; Available from: https://www.cbo.gov/budget-options/54821.

440. Lijin, Z., W. Zhenxin, and Z. Chongyu, *Mathematical Model of Reactor for Hydrorefining of Terephthalic Acid and Its Calculation.* Petrochemical Technology, 2005. **34**: p. 1068-1072.